

13589

NATIONAL LIBRARY  
OTTAWA



BIBLIOTHÈQUE NATIONALE  
OTTAWA

NAME OF AUTHOR..... SHAM SUNDER.....  
TITLE OF THESIS..... The Vibrational Spectra  
..... of t-Butyl Bromide  
.....  
UNIVERSITY..... of Alberta, EDMONTON  
DEGREE FOR WHICH THESIS WAS PRESENTED..... Ph.D.....  
YEAR THIS DEGREE GRANTED..... 1972.....

Permission is hereby granted to THE NATIONAL LIBRARY  
OF CANADA to microfilm this thesis and to lend or sell copies  
of the film.

The author reserves other publication rights, and  
neither the thesis nor extensive extracts from it may be  
printed or otherwise reproduced without the author's  
written permission.

(Signed)..... Sham Sunder.....

PERMANENT ADDRESS:

Chemistry Dept.  
University of Alberta  
EDMONTON (Alberta)

DATED... July 21... 1971

THE UNIVERSITY OF ALBERTA

THE VIBRATIONAL SPECTRA OF t-BUTYL BROMIDE

by

© SHAM SUNDER

A THESIS

SUBMITTED TO THE FACULTY OF GRADUATE STUDIES AND RESEARCH  
IN PARTIAL FULFILMENT OF THE REQUIREMENTS FOR THE DEGREE

OF

DOCTOR OF PHILOSOPHY

DEPARTMENT OF CHEMISTRY

EDMONTON, ALBERTA

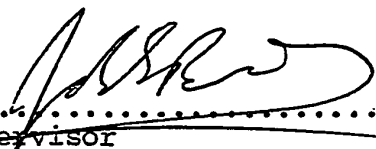
FALL 1972

THE UNIVERSITY OF ALBERTA  
FACULTY OF GRADUATE STUDIES AND RESEARCH

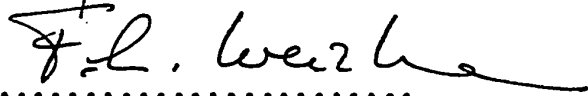
The undersigned certify that they have read, and recommend to the Faculty of Graduate Studies and Research for acceptance, a thesis entitled

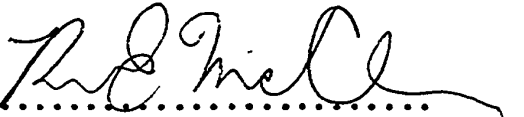
"THE VIBRATIONAL SPECTRA OF T-BUTYL BROMIDE"

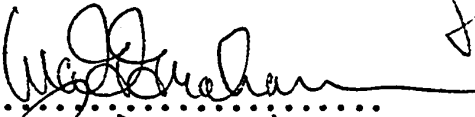
submitted by SHAM SUNDER in partial fulfilment of the requirements for the degree of Doctor of Philosophy.

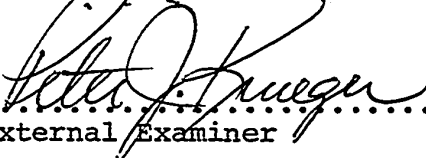
  
.....  
Supervisor

  
.....

  
.....

  
.....

  
.....

  
.....  
External Examiner

Date..... July 18, 1972 .....

ABSTRACT

The vibrational spectra of t-butyl bromide- $h_9$  and t-butyl bromide- $d_9$  in the gas, liquid and three solid phases have been studied between 4000 and  $10\text{ cm}^{-1}$ . A new assignment for the methyl stretching, deformation and torsional modes of t-butyl bromide- $h_9$ , and a complete, new assignment for t-butyl bromide- $d_9$ , are presented. Complete normal coordinate calculations are presented to verify the compatibility of the assignments for the two isotopic molecules. The thermodynamic properties of t-butyl bromide- $h_9$  and - $d_9$  have been calculated for the ideal gas state at a variety of temperatures.

The far-infrared spectra of the liquid and the plastic crystal phases show a broad band, and the frequency of the maximum absorption increases with decreasing temperature. This far-infrared absorption is discussed with reference to the current theories, and it is argued that both rotational and translational vibrations, as well as relaxation processes, contribute to it. However, the frequency of maximum absorption is determined by the intermolecular vibrations, rather than by a relaxation process.

The spectra of the liquid and plastic crystal phases show broad bands due to the intramolecular modes. The halfwidths of these bands decrease slowly in the liquid

iv.

and plastic phases with decreasing temperature, but decreases sharply at the low temperature transition.

The halfwidths of the bands in the liquid and plastic phases are attributed to three effects: intermolecular vibrational coupling, the distribution in the local fields experienced by the molecules, and the rapid molecular reorientation. These factors contribute about 4.5, 2.5, and 2.5  $\text{cm}^{-1}$ , respectively, to the 9.5  $\text{cm}^{-1}$  halfwidth of the infrared absorption band due to the  $A_1$  skeleton deformation mode in phase II of t-butyl bromide- $\text{h}_9$ . The decrease in halfwidth with decreasing temperature is shown to be mainly due to a decrease in the contribution from the molecular reorientation.

The study of the infrared spectra at various temperatures in phase III, the low temperature solid phase, shows that, while the C-Br bonds are fixed in an ordered manner in this phase, the atomic arrangement about the C-Br bonds is ordered only at the lower temperatures. The powder X-ray pattern at 120°K has been indexed on a primitive orthorhombic unit cell, containing eight molecules, with the following lattice parameters:  $a = 11.832 \pm 0.014 \text{ \AA}$ ,  $b = 10.801 \pm 0.012 \text{ \AA}$ , and  $c = 9.460 \pm 0.012 \text{ \AA}$ . The infrared and the Raman spectra of the pure solid and the infrared spectra of the isotopically dilute solutions, at 90°K, are analyzed to determine the factor group splittings and

the site group splittings. The bands in the far-infrared spectra at 90°K are assigned to the different lattice modes. Consideration of the X-ray data, molecular packing, and the spectroscopic evidence suggests that, at about 100°K, phase III of t-butyl bromide crystallizes in the space group  $P222-D_2^1$ , with molecules on two non-equivalent sets of general positions.

ACKNOWLEDGEMENTS

I would like to thank Dr. J. E. Bertie for his guidance, help, and encouragement. His interest and thoroughness were a constant source of inspiration.

I am thankful to the various members of the Chemistry Department who have helped in this project, particularly to the staff in the electronic and machine workshops for their competent technical assistance and to the members of Dr. Bertie's research group for their cooperation.

I am indebted to Miss Mary Fairhurst for reading and correcting the manuscript and typing a rough draft.

I am grateful to the Killam Estate (Ottawa) and the University of Alberta for financial support during the course of this work.

Sham Sunder

Sham Sunder

TABLE OF CONTENTS

	<u>Page</u>
ABSTRACT . . . . .	iii
ACKNOWLEDGEMENTS . . . . .	vi
LIST OF TABLES . . . . .	x
LIST OF FIGURES . . . . .	xiii
1. INTRODUCTION . . . . .	1
1.1 Plastic Crystals . . . . .	1
1.2 Vibrational Spectroscopy . . . . .	4
1.2.1 Vibrational Spectra of Isolated Molecules . . . . .	4
1.2.2 Vibrational Spectra of Ordered Molecular Crystals . . . . .	15
1.2.3 Vibrational Spectra of Disordered Solids and Plastic Crystals . . . . .	34
1.3 Resumé of Previous Studies of <u>t</u> -Butyl Bromide . . . . .	52
1.3.1 Vibrational Spectroscopy . . . . .	52
1.3.2 Properties of the Solid State . . . . .	58
2. FOURIER SPECTROSCOPY IN THE FAR-INFRARED . . . . .	64
3. EXPERIMENTAL . . . . .	75
3.1 Preparation and Purification of Chemicals. . . . .	75
3.2 Infrared Spectroscopy . . . . .	76
3.3 Raman Spectroscopy . . . . .	81
3.4 X-Ray Powder Photography . . . . .	82
4. THE INTRAMOLECULAR VIBRATIONS OF <u>t</u> -BUTYL BROMIDE- h <sub>9</sub> AND -d <sub>9</sub> . . . . .	85



	<u>Page</u>
4.1 Structural Considerations . . . . .	85
4.2 Results for <u>t</u> -Butyl Bromide-h <sub>9</sub> . . . . .	91
4.3 Assignment of the Infrared and Raman Spectra of T-Butyl Bromide-h <sub>9</sub> . . . . .	102
4.4 Results for T-Butyl Bromide-d <sub>9</sub> . . . . .	114
4.5 Assignment of the Infrared and Raman Spectra of T-Butyl Bromide-d <sub>9</sub> . . . . .	123
5. NORMAL COORDINATE ANALYSIS OF <u>t</u> -BUTYL BROMIDE. . . . .	133
5.1 Coordinates and Computer Programs . . . . .	134
5.2 Calculations and Results . . . . .	144
5.3 Thermodynamic Functions . . . . .	160
6. THE SOLID PHASES OF <u>t</u> -BUTYL BROMIDE . . . . .	164
6.1 Results	
6.1.1 The Vibrational Spectra of the Plastic Phases . . . . .	164
6.1.2 Spectra of Phase III . . . . .	184
6.1.3 X-Ray Measurements on Phase III . . . . .	221
6.2 Discussion of the Spectra of the Plastic Phases . . . . .	227
6.2.1 Intramolecular Modes . . . . .	227
6.2.2 Far-Infrared . . . . .	234
6.3 Discussion of the Spectra and Structure of Phase III . . . . .	239
6.3.1 General . . . . .	239
6.3.2 X-Ray Results . . . . .	244
6.3.3 Vibrational Spectra at 90°K . . . . .	246
6.3.4 Structure of Phase III at 90°K . . . . .	257
REFERENCES . . . . .	265

	<u>Page</u>
APPENDIX I: G Matrices . . . . .	281
APPENDIX II: Eigenvectors . . . . .	289
APPENDIX III: F Matrices . . . . .	301

LIST OF TABLES

<u>Table</u>		<u>Page</u>
I	Features seen in the infrared spectra of solid benzene for the three modes shown in Figures 4 to 6.	32
II	The assignments of the fundamental vibration frequencies of t-butyl bromide-h <sub>9</sub> .	55
III	The assignments of the fundamental vibration frequencies of t-butyl bromide-d <sub>9</sub> .	59
IV	Vibrational representation of t-butyl bromide.	86
V	Moments of inertia of t-butyl bromide-h <sub>9</sub> and t-butyl bromide-d <sub>9</sub> .	88
VI	Frequencies and assignment of the features observed in the infrared and the Raman spectra of t-butyl bromide-h <sub>9</sub> in the gas and liquid phases for the region 4000-100 cm <sup>-1</sup> .	94
VII	Frequencies and assignment of the features observed in the infrared and the Raman spectra of t-butyl bromide-d <sub>9</sub> in the gas and liquid phases for the region 4000-100 cm <sup>-1</sup> .	117
VIII	C-D <sub>3</sub> stretch and CD <sub>3</sub> deformation frequencies in some of the related molecules.	125
IX	Internal coordinates for t-butyl bromide.	135
X	Symmetry coordinates for t-butyl bromide.	139
XI	Force constants for t-butyl bromide	146
XII	Comparison of the calculated and observed frequencies for the fundamental vibrations of t-butyl bromide-h <sub>9</sub> .	149
XIII	Comparison of the calculated and observed frequencies for the fundamental vibrations of t-butyl bromide-d <sub>9</sub> .	150

<u>Table</u>		<u>Page</u>
XIV	Distribution of the potential energy for each normal mode of t-butyl bromide-h <sub>9</sub> among the force constants of force field I.	151
XV	Distribution of the potential energy for each normal mode of t-butyl bromide-d <sub>9</sub> among the force constants of force field I.	153
XVI	Distribution of the potential energy for each normal mode of t-butyl bromide-h <sub>9</sub> among the force constants of force field II.	156
XVII	Distribution of the potential energy for each normal mode of t-butyl bromide-h <sub>9</sub> among the force constants of force field II.	158
XVIII	Thermodynamic functions for t-butyl bromide-h <sub>9</sub> at 1 atm pressure and for the ideal gaseous state.	161
XIX	Thermodynamic functions for t-butyl bromide-d <sub>9</sub> at 1 atm pressure and for the ideal gaseous state.	162
XX	Frequencies and assignment of the features observed in the infrared and Raman spectra of t-butyl bromide-h <sub>9</sub> in the solid phases I and II.	167
XXI	Frequencies and assignment of the features observed in the infrared spectra of t-butyl bromide-d <sub>9</sub> in the solid phases I and II.	169
XXII	Halfwidths of some of the infrared bands of t-butyl bromide-h <sub>9</sub> in the liquid and plastic solids.	171
XXIII	Halfwidths of some of the infrared bands of t-butyl bromide-d <sub>9</sub> in the liquid and plastic solid phases.	177
XXIV	Far-infrared spectra of t-butyl bromide-h <sub>9</sub> and -d <sub>9</sub> in the condensed phases.	182
XXV	Frequencies and assignments of the features observed in the infrared and Raman spectra of t-butyl bromide-h <sub>9</sub> in the solid phase III.	207

<u>Table</u>		<u>Page</u>
XXVI	Frequencies and assignment of the features observed in the infrared and Raman spectra of t-butyl bromide-d <sub>9</sub> in the solid phase III.	212
XXVII	Observed and calculated d-spacings for the first 28 lines of the X-ray pattern of t-butyl bromide in phase III at 120°K.	223
XXVIII	Site group and factor group analysis for phase III of t-butyl bromide.	259

LIST OF FIGURES

<u>Figure</u>		<u>Page</u>
1	Dispersion curve diagram.	17
2	Cl-CI stretching vibrations in a chlorine crystal.	18
3	Correlation diagram for benzene.	24
4	Infrared spectra of $B_{1u}$ ( $\nu_{12}$ ) fundamental of benzene.	29
5	Infrared spectra of $B_{2u}$ ( $\nu_{15}$ ) fundamental of benzene.	30
6	Infrared spectra of $E_{1u}$ fundamental of benzene.	31
7	Far-infrared spectra of ice II and ice V.	45
8	Far-infrared spectra of solid acetylene.	46
9	A block diagram of the Michelson interferometer.	67
10	A typical interferogram.	70
11	The low temperature cell used for recording the infrared spectra.	77
12	A schematic diagram of the set up used for recording the low temperature X-ray photographs.	84
13	Calculated infrared band shapes for molecules of type 34 of Ueda and Shimanouchi's classification.	90
14	Infrared spectra of t-butyl bromide- $h_g$ in the gas <sub>1</sub> and liquid phases between 4000 and 1600 $cm^{-1}$ .	92
15	Infrared spectra of t-butyl bromide- $h_g$ in the gas <sub>1</sub> and liquid phases between 1600 and 200 $cm^{-1}$ .	93

<u>Figure</u>		<u>Page</u>
16	The intense bands in the infrared spectrum of gaseous t-butyl bromide-h <sub>9</sub> .	99
17	Raman spectrum of liquid t-butyl bromide-h <sub>9</sub> and t-butyl bromide-d <sub>9</sub> .	101
18	Infrared spectrum of t-butyl bromide-d <sub>9</sub> in the gas and liquid phases.	115
19	The intense bands in the infrared spectrum of gaseous t-butyl bromide-d <sub>9</sub> .	116
20	The atom-numbering system used to describe the internal coordinates of t-butyl bromide.	138
21	Infrared spectra of t-butyl bromide-h <sub>9</sub> in solid phases I and II.	165
22	Infrared spectra of t-butyl bromide-d <sub>9</sub> in solid phases I and II.	166
23	Graph, Halfwidth vs Temperature for $\nu_{18}$ band of t-butyl bromide-h <sub>9</sub> in the infrared spectrum of pure solid.	173
24	Graph, Halfwidth vs Temperature for $\nu_3$ and $\nu_6$ bands of t-butyl bromide-d <sub>9</sub> in the infrared spectrum of pure solid.	174
25	Infrared absorption by t-butyl bromide-d <sub>9</sub> and t-butyl bromide-h <sub>9</sub> in phase I as pure solid and isotopically mixed crystal.	176
26	Infrared absorption by t-butyl bromide-h <sub>9</sub> in phase II as pure solid and isotopically mixed crystals.	177
27	Infrared absorption by t-butyl bromide-d <sub>9</sub> in phase II as pure solid and isotopically mixed crystals.	178
28	Raman scattering by the $\nu_7$ and $\nu_8$ modes of t-butyl bromide-h <sub>9</sub> in the liquid and solid phase II.	179

<u>Figure</u>	<u>Page</u>
29 Far-infrared spectra of t-butyl bromide-h <sub>9</sub> and -d <sub>9</sub> in solid phase II at 228°K and phase I at 245° and in the liquid at 273°K.	181
30 Infrared spectra of t-butyl bromide-h <sub>9</sub> in the solid phase III at 195°K and at 90°K.	185
31 Infrared spectra of t-butyl bromide-d <sub>9</sub> in the solid phase III at 195°K and at 90°K.	186
32 Infrared and Raman spectra of phase III of t-butyl bromide-h <sub>9</sub> for the region 320-260 cm <sup>-1</sup> .	187
33 Infrared and Raman spectra of t-butyl bromide-h <sub>9</sub> in phase III for the region 1160-1100 cm <sup>-1</sup> .	188
34 Infrared and Raman spectra of ν <sub>19</sub> (E) fundamental of t-butyl bromide-h <sub>9</sub> in phase III.	189.
35 Infrared and Raman spectra of t-butyl bromide-h <sub>9</sub> in phase III for the region 1380-1350 cm <sup>-1</sup> .	190
36 Infrared and Raman spectra of t-butyl bromide-h <sub>9</sub> in phase III for the region 1490-1400 cm <sup>-1</sup> .	191
37 Infrared and Raman spectra of t-butyl bromide-d <sub>9</sub> in phase III for the region 480-420 cm <sup>-1</sup> .	192
38 Infrared and Raman spectra of t-butyl bromide-d <sub>9</sub> in phase III for the region 720-680 cm <sup>-1</sup> .	193
39 Infrared and Raman spectra of t-butyl bromide-d <sub>9</sub> in phase III for the region 1100-980 cm <sup>-1</sup> .	194
40 Infrared spectra of t-butyl bromide-d <sub>9</sub> in phase III for the region 1130-1100 cm <sup>-1</sup> .	195
41 Infrared spectra of the ν <sub>16</sub> (E) fundamental of t-butyl bromide-d <sub>9</sub> in phase III.	196



<u>Figure</u>		<u>Page</u>
42	Infrared and Raman spectra of t-butyl bromide-d <sub>9</sub> for the region 2250-2190 cm <sup>-1</sup> .	197
43	Infrared and Raman spectra of t-butyl bromide-h <sub>9</sub> in phase III for the region 530-490 cm <sup>-1</sup> .	198
44	Infrared and Raman spectra of t-butyl bromide-h <sub>9</sub> in phase III for the region 830-780 cm <sup>-1</sup> .	199
45	Infrared and Raman spectra of the $\nu_{20}$ (E) fundamental of t-butyl bromide-h <sub>9</sub> in phase III.	200
46	Infrared and Raman spectra of t-butyl bromide-h <sub>9</sub> in phase III for the region 3000-2800 cm <sup>-1</sup> .	201
47	Infrared and Raman spectra of t-butyl bromide-d <sub>9</sub> in phase III for the region 290-230 cm <sup>-1</sup> .	202
48	Infrared spectra of the $\nu_{20}$ (E) fundamental of t-butyl bromide-d <sub>9</sub> in phase III.	203
49	Infrared spectra of t-butyl bromide-d <sub>9</sub> in phase III for the region 2170-2030 cm <sup>-1</sup> .	204
50	Raman spectrum of $\nu_{21}$ (E) and $\nu_{22}$ (E) fundamentals of t-butyl bromide-h <sub>9</sub> in phase III.	205
51	Far-infrared spectra of t-butyl bromide-h <sub>9</sub> and -d <sub>9</sub> in phase III.	219
52	The correlation diagram for the six possible combinations of the space groups and site groups indicated by X-ray data.	

## 1. INTRODUCTION

This thesis deals with the vibrational spectra of t-butyl bromide- $h_9$  and  $-d_9$  in the gas, liquid, and the three solid phases. The two high temperature solid phases are known as plastic phases. Therefore it seems appropriate to introduce the subject of plastic crystals in the first section of this chapter. The second section introduces the theory underlying vibrational spectroscopy with particular reference to ordered and disordered solids. The third section of this chapter reviews the previous works on the vibrational spectra and the solid state of t-butyl bromide.

### 1.1 PLASTIC CRYSTALS

Molecules having globular, almost spherical, shapes exhibit anomalously low entropies of melting, relatively high melting points and more than one solid phase. The high temperature solid phases are soft and show high mobility when subjected to pressure, and consequently are called plastic crystals (1).

These plastic crystals invariably show a diffraction symmetry which is much higher than can be accounted for by the number of molecules per unit cell and the inherent symmetry of the molecules, which indicates that the molecules are situated at sites of symmetry higher than

the molecular symmetry. This is only possible if there is dynamic or static disorder in the crystals. The diffraction symmetry of the plastic crystals is generally cubic. At low temperatures the crystals undergo transitions to systems of lower symmetry (2).

The dielectric constant of a plastic crystal is approximately equal to that of its liquid phase. The drop in dielectric constant of a polar substance, normally associated with solidification, is observed instead at one of the phase transitions in the solid state. This indicates that in plastic crystals the molecules are able to reorient in response to an oscillating electric field. It does not mean that the molecules are rotating freely, as in a gas, but merely that they have sufficient energy to permit frequent passage over the potential barriers hindering rotation (3). Information about the height of these barriers can be obtained from the study of the dielectric loss as a function of frequency and temperature (4).

Plastic crystals show much narrower Nuclear Magnetic Resonance linewidths than do crystals with rigid lattices (5). In a rigid crystalline solid, the absorption line in the NMR spectrum is very broad because the nuclei experience random local fields, primarily due to

magnetic dipole-dipole coupling, that depend on their position in the lattice. The larger the variation in these fields, the wider the NMR line. If the molecules have mobility, as in a liquid, motion of the molecules averages out these fields and the NMR line is narrowed (2). The narrow NMR line indicates the presence of rapid molecular motions in plastic crystals. A study of the line widths can give information about the type of molecular motions in the solid and a study of spin-lattice relaxation times ( $T_1$ ) can give information about the rates of these motions (5-7).

The subject of plastic crystals has been reviewed several times in recent years (2, 8-11) and has been the subject of many symposia (12-14). But there has been no detailed review on the vibrational spectra of plastic crystals and, in fact, very few studies have been made on this subject. The work that has been done will be discussed in a later section of this chapter. Before presenting this discussion, the fundamentals of the vibrational spectroscopy of the gas, and rigid, ordered solids will be given.

angles, and so on. These correlations and the studies leading to them play an important part in aiding the assignment of the spectra of new molecules. In general, however, the assignment of a spectrum is more complicated than is suggested by these simple correlations. The problem is simplified by the presence of molecular symmetry and is greatly aided by studies of isotopic substitution effects. A knowledge of the polarization of the Raman lines of liquid or solid samples (15) and the shapes of the infrared band contours of gaseous samples (21) are also useful. Extremely careful use of normal coordinate calculations can aid the assignment of the spectrum and can confirm that the assignment is reasonable. The influence of symmetry and the principles underlying normal coordinate calculations are discussed in the next two parts of this section. Following this a very qualitative and brief discussion of the molecular vibrations is given in terms of quantum mechanical principles.

(A) Applications of Symmetry

The symmetry operations that transform a molecule into itself form the point group of the molecule (22). Each normal vibration of the molecule must transform under the symmetry operations in the same manner as one of the irreducible representations of the point group. For brev-

## 1.2 VIBRATIONAL SPECTROSCOPY

This section gives a qualitative introduction to the theory of the vibrational spectra of the molecules and their condensed phases.

### 1.2.1 VIBRATIONAL SPECTRA OF ISOLATED MOLECULES

Before discussing the vibrational spectra of solids, it is helpful to consider the vibrational spectra of single isolated molecules. There is a large literature on molecular vibrational spectra (15, 16) and only a few important points are discussed here.

A nonlinear polyatomic molecule consisting of  $n$  atoms has  $3n-6$  vibrational degrees of freedom, while a linear molecule has  $3n-5$ . Any arbitrary vibrational motion of the molecule can be expressed as a linear combination of the  $3n-6$  ( $3n-5$ ) normal or fundamental vibrations (15). The first problem in spectroscopy is to relate the frequencies of the observed spectral bands to the atomic displacements causing them, that is, to assign the spectrum. It has been found that useful correlations exist between the frequencies of the bands observed in the spectra and the chemical groups present in the molecule (17-20). Hence vibrations can often be assigned, for example to an O-H stretching vibration, or a C-H stretching vibration of a methyl or methylene group, or the changes in the H-C-C

ity, it is usually said that a vibration has a certain symmetry or that it belongs to a certain symmetry species or irreducible representation. In molecules with high symmetry the classification of the vibrations into various irreducible representations will aid calculations, and it will indicate which vibrations are infrared or Raman active. This classification will also indicate the polarization properties associated with the vibration and aid in determining the gas phase band shapes.

The use of symmetry in vibrational spectroscopy will be illustrated by considering the selection rules for vibrational transitions. Those vibrations which belong to the irreducible representations to which the translational vectors  $T_x$ ,  $T_y$ ,  $T_z$  belong, yield infrared-active fundamental transitions, while the vibrations which transform in the same way as the elements of the polarizability tensor yield Raman-active fundamental transitions (16). These selection rules result from consideration of the transition moment integral,  $[M]^{if}$ , defined as (15)

$$[M]^{if} = \int \Psi_f \cdot M \cdot \Psi_i d\tau \quad 1$$

which must be nonzero for an allowed transition between states  $i$  and  $f$ . Here  $\Psi_f$  and  $\Psi_i$  are the wavefunctions representing the final and initial states of the molecule,

respectively,  $M$  is either a dipole moment operator  $\mu_x$ ,  $\mu_y$  or  $\mu_z$  or a polarizability operator  $\alpha_{gg}$ , and  $d\tau$  is the volume element of  $3n-6$  ( $3n-5$ ) dimensional space. The integral can be nonzero only if the integrand transforms as the totally symmetric irreducible representation in the molecular point group. This is only possible if  $M$  and  $\Psi_f \cdot \Psi_i$  belong to the same irreducible representation. If the initial state is totally symmetric, as the ground vibrational state of a molecule is, the above condition reduces to the requirement that  $\Psi_f$  and  $M$  must belong to the same irreducible representation. For a fundamental transition,  $\Psi_f$  is a wave function describing a state in which only one of the normal vibrations of the molecules is excited. In the harmonic oscillator approximation  $\Psi_f$  is proportional to  $Q$ , the normal coordinate of the vibration. Thus the symmetry of the excited state wave function for a fundamental transition is simply that of the corresponding classical vibration. For transitions to overtones or combination levels, the symmetry of the excited state wave function is obtained from the direct product of the irreducible representations of the vibrations involved (16). Symmetry properties are also helpful in normal coordinate calculations as will be indicated in the following section.



(B) Vibrational Calculations

The purpose of vibrational calculations for a molecule is to determine the frequencies, or eigenvalues, and the atomic displacements, or eigenvectors or assignments, for the normal vibrations. The input into these calculations consists of the molecular geometric parameters and an assumed force field. The force field represents forces between the atoms of a molecule and usually many approximations are necessary in describing the assumed force field. The most common approximation is the harmonic approximation in which the potential energy expression contains only terms which are bilinear in the displacement coordinates. If this approximation is made, classical mechanics can be used to calculate the normal vibrations and the corresponding quantum mechanical problem reduces (23) to a series of simple harmonic oscillator wave equations, one for each normal vibration. This will be discussed in more detail in part C of this section.

In classical mechanics, the harmonic approximation means that one can express the kinetic energy  $T$  and the potential energy  $V$  by equations which are homogeneously quadratic in the displacement coordinates,  $q_i$ , of the atoms and their time derivatives  $\dot{q}_i$ . That is

9.

$$2T = \sum_{ij} T_{ij} \dot{q}_i \dot{q}_j \quad 2$$

$$2V = \sum_{ij} F_{ij} q_i q_j \quad 3$$

where  $T_{ij}$  is a constant for a given  $i$  and  $j$  and represents the change in kinetic energy with unit change in  $\dot{q}_i$  and  $\dot{q}_j$  and is a function of atomic masses. Similarly  $F_{ij}$  is also a constant for a given  $i$  and  $j$  and represents the change in potential energy with unit change in  $q_i$  and  $q_j$  and is a function of interatomic forces. This is a good approximation provided that the amplitude of the displacements is extremely small (16, 23). The above equations can be written in matrix notation as

$$2T = \dot{\mathbf{q}}^{\dagger} \mathbf{T} \dot{\mathbf{q}} \quad 4$$

and

$$2V = \mathbf{q}^{\dagger} \mathbf{F} \mathbf{q} \quad 5$$

where  $\mathbf{q}$  and  $\dot{\mathbf{q}}$  are column matrices and  $\mathbf{F}$  and  $\mathbf{T}$  are symmetric matrices with elements  $F_{ij}$  and  $T_{ij}$ .  $\mathbf{q}^{\dagger}$  is the transpose of  $\mathbf{q}$  (16).

The vibrational calculations involve the determination of the normal coordinates,  $Q_k$ , in which the kinetic and potential energies can be written as

$$2T = \sum_k \dot{Q}_k^2 \quad 6$$

and

$$2V = \sum_k \lambda_k Q_k^2 \quad 7$$

where  $\dot{Q}_k$  is the time derivative of the kth normal coordinate  $Q_k$ , and  $\lambda_k = 4\pi^2\nu_k^2$ , where  $\nu_k$  is the vibrational frequency of the kth normal mode. In other words, the transformation of coordinates from  $\{q_i\}$  to  $\{Q_k\}$  which simultaneously diagonalizes the matrices  $\mathcal{T}$  and  $\mathcal{F}$  must be determined. The transformation matrix  $L$  is defined as

$$\underset{\sim}{q} = \underset{\sim}{L} Q \quad 8$$

Thus one has from equations 4, 6 and 8

$$2T = \dot{Q}^\dagger (\underset{\sim}{L}^\dagger \underset{\sim}{\mathcal{T}} \underset{\sim}{L}) \dot{Q} = \dot{Q}^\dagger \underset{\sim}{E} \dot{Q} \quad 9$$

and from equations 5, 7 and 8

$$2V = Q^\dagger (\underset{\sim}{L}^\dagger \underset{\sim}{\mathcal{F}} \underset{\sim}{L}) Q = Q^\dagger \underset{\sim}{\lambda} Q \quad 10$$

where  $Q$  is a column matrix,  $\underset{\sim}{E}$  is an identity matrix and  $\underset{\sim}{\lambda}$  is a diagonal matrix of eigenvalues.

Thus  $\underset{\sim}{L}$  must satisfy the conditions:

$$\underset{\sim}{E} = \underset{\sim}{L}^\dagger \underset{\sim}{\mathcal{T}} \underset{\sim}{L} \quad 11$$

$$\underset{\sim}{\lambda} = \underset{\sim}{L}^\dagger \underset{\sim}{\mathcal{F}} \underset{\sim}{L} \quad 12$$

From equation (11),

$$\underset{\sim}{L}^\dagger = \underset{\sim}{L}^{-1} \underset{\sim}{\mathcal{T}}^{-1} \quad 13$$

Therefore equation (12) can be rewritten as

$$\lambda_k = L_k^{-1} (F_k^{-1} F_k) L_k \quad 14$$

In short, the solution of the vibrational problem involves the determination of the transformation matrix  $L_k$  which diagonalizes the product matrix  $F_k^{-1} F_k$  to give the eigen values  $\lambda_k$ , and hence the frequencies, of the normal vibrations. The assignments for the vibrations, that is, the relative displacements of the initial coordinates,  $q_i$ , during the normal vibration  $Q_k$ , are given by the  $k$ th column of the  $L_k$  matrix. Since the inverse of the  $L_k$  matrix gives the normal coordinates  $Q_k$ , as linear combinations of the starting coordinates,  $q_i$ , these calculations are often called normal coordinate calculations.

Any set of displacement coordinates can be used to set up the vibrational problem. It can be the set of cartesian displacement coordinates, but usually the so-called internal coordinates are used. These represent changes in the bond lengths and interbond angles in the molecule. When these coordinates are used, the elements of the  $F_k$  matrix are the valence force constants, which express the resistance of the bonds and angles in the molecule to deformation. The matrix  $F_k$  in equation 4 for kinetic energy is given the special symbol  $G_k^{-1}$  when internal

coordinates are used (16). Equation 14 then can be written as

$$\lambda = L^{-1} (G F) L \quad 15$$

It is often more convenient to use linear combinations of the internal coordinates as a basis for the vibrational calculations. These linear combinations are called symmetry coordinates if they transform as the irreducible representations of the molecular point group (16). The use of symmetry coordinates allows factorization of the  $G$  and  $F$  matrices, and this makes the diagonalization of the product matrix,  $GF$ , easier and the vibrational calculations can be performed more rapidly (16, 24).

The above discussion implies that one has a knowledge of the interatomic forces, i.e. the  $F$  matrix. In practice, it is usually the frequencies (eigenvalues) which are known and the  $F$  matrix elements which are unknown. The calculation is begun by using an assumed  $F$  matrix to calculate the frequencies and eigenvectors. The calculated frequencies are compared with the observed frequencies, the force constants are adjusted, and the calculation is repeated until successive iterations bring the calculated frequencies and eigenvectors into satisfactory agreement with the experimental frequencies and assignments.

Generally the number of observed frequencies for a molecule is much smaller than the number of distinct elements in its  $F_v$  matrix. To overcome this problem, some of the force constants must be set to zero. In many molecules, this can be done with a high degree of confidence, but in some molecules it is a severe limitation on the utility of the method (16, 25).

(C) Quantum Mechanics and Molecular Vibrations

In terms of the normal coordinates  $Q$ , the vibrational wave equation has the form (16)

$$\frac{-h^2}{8\pi^2} \sum_{k=1}^{3n-6} \frac{\delta^2 \Psi_V}{\delta Q_k^2} + \frac{1}{2} \sum_{k=1}^{3n-6} \lambda_k Q_k^2 \Psi_V = W_V \Psi_V \quad 16$$

where  $W_V$  is the vibrational energy and  $h$  is Planck's constant. Furthermore, if

$$W_V = W(1) + W(2) + \dots + W(3n-6) \quad 17$$

and  $\Psi_V = \psi(Q_1) \psi(Q_2) \dots \psi(Q_{3n-6}) \quad 18$

then the wave equation 16, can be broken into  $3n-6$  equations of the form (16)

$$\frac{-h^2}{8\pi^2} \frac{\delta^2 \psi(Q_k)}{\delta Q_k^2} + \frac{1}{2} \lambda_k Q_k^2 \psi(Q_k) = W(k) \psi(Q_k) \quad 19$$

$$k = 1, 2 \dots, 3n-6$$

Each of the above equations is a simple harmonic oscillator wave equation in the coordinate  $Q_k$ . The wave functions are the Hermite orthogonal functions of  $Q_k$ , and the energy  $W_k$  equals  $(\sigma_k + 1/2) h\nu_k$ , where  $\sigma_k$  is the vibrational quantum number,  $\nu_k$  is the classical vibration frequency.

In quantum mechanics the probability of infrared absorption or Raman scattering, in which a molecule goes from initial state  $\Psi_i$  to final state  $\Psi_f$ , is directly proportional to the square of the transition moment integral,  $[M]^{if}$  (see Part A of this section). For the transition moment to be nonzero the two states  $\Psi_i$  and  $\Psi_f$  should have only one quantum number different by  $\pm 1$  under the harmonic approximation. Thus only fundamental transitions should appear in the vibrational spectrum. All fundamentals are not allowed, but only those which are allowed by symmetry (Part A). Experimentally, it is found that the bands due to fundamental transitions are usually the most intense, but other transitions, in which the above selection rule is not obeyed, also appear. This, along with other observations, such as the convergence of the energy levels associated with one normal coordinate, indicates that the harmonic oscillator model for a vibrating molecule is not perfect, although it is a good first approximation.

### 1.2.2 VIBRATIONAL SPECTRA OF ORDERED MOLECULAR CRYSTALS

The theory of vibrations in crystals has been discussed in detail in the literature (26, 27). Here, those aspects of the theory which are needed to understand the vibrational spectra of molecular crystals will be discussed. The theory was developed for infinite crystals, but it can be applied to finite crystals by assuming Born and Von Karman's cyclic boundary conditions (28). Recently, effects due to the finitude of crystals have been discussed (29), but these are unimportant in the present discussion.

A crystal is made up of a small repeating unit called the unit cell (30). This translational symmetry is basic to the understanding of the properties of crystals. If a crystal contains  $N$  unit cells with  $S$  atoms per unit cell, then there are  $3S$  degrees of freedom per unit cell and  $3SN$  degrees of freedom altogether. These degrees of freedom, or vibrations, are represented in classical mechanics as displacement waves which propagate through the crystal. Each normal vibration or wave is characterized by a frequency,  $\nu$ , and a wave vector,  $\underline{k}$ , whose magnitude is the reciprocal of the wavelength of the vibration and whose direction is the direction of propagation. For each value of the wave vector,  $\underline{k}$ , there are  $3S$  distinct vibrations and therefore  $3S$  frequencies. A plot of frequency,



$\nu$ , versus wave vector,  $\underline{k}$ , yields curves of the form shown in Figure 1. These curves are called dispersion curves and show all of the frequencies that can occur for vibrations propagating in the chosen direction. The wave vector  $\underline{k}$  varies in magnitude from zero (infinite vibrational wavelength) to  $1/2a$ , where  $a$  is the length of the primitive translation in the direction of  $\underline{k}$ . The individual curves in such diagrams are called branches.

If a crystal contains  $p$   $m$ -atomic molecules per unit cell, i.e.  $S = pm$ , each of the  $3m-6$  ( $3m-5$  for linear molecules) intramolecular vibrations of one molecule will generate  $p$  branches of dispersion curves. For example, in the chlorine crystal in which there are two  $\text{Cl}_2$  molecules ( $m = 2$ ) per primitive unit cell (31), ( $p = 2$ ), there are 12 branches of dispersion curves, 2 of which represent Cl-Cl stretches. In a crystal containing  $N$  unit cells there are  $2N$  Cl-Cl stretching vibrations which differ from each other by the phase relationship between the displacement of the Cl-Cl bond in different molecules. The extreme cases are shown for example in Figure 2. The frequencies of all  $2N$  Cl-Cl stretching modes are similar but not identical. They are primarily determined by the strong intramolecular forces, but are influenced by the intermolecular forces through the static crystal field at the occupied

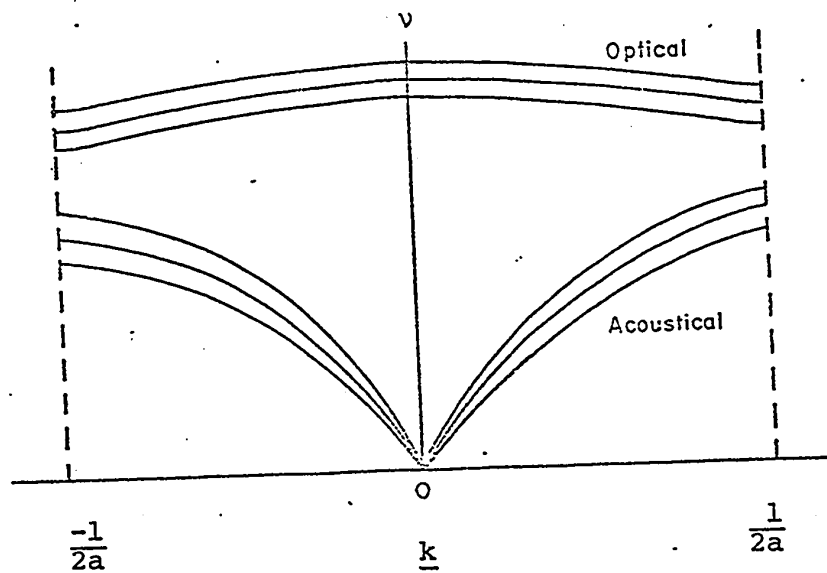


Figure 1

A Dispersion Curve Diagram

site and the intermolecular vibrational coupling. This coupling depends on the relative displacements in different molecules and is, therefore, wave-vector dependent. Therefore the branches corresponding to the Cl-Cl stretching modes are almost flat.

In the general case,  $p(3m-6)$  branches have their origin in the intramolecular vibrations of the molecules, and their frequencies are not strongly dependent on  $\underline{k}$ . The remaining  $6p$  ( $5p$  for linear molecules) branches arise from the translational and rotational motions of the molecules as rigid bodies and are known as lattice modes. These lattice mode branches usually exhibit a strong  $\underline{k}$ -dependence. The vibrations differ from each other because each one involves different intermolecular displacements from each other one. The frequency of these vibrations is completely determined by the intermolecular forces, and hence the greater the intermolecular displacements during a vibration the higher the frequency. It is common for lattice mode branches to contain frequencies differing by 50 to  $150 \text{ cm}^{-1}$ , while the frequencies in a branch due to intramolecular modes rarely differ by more than  $10 \text{ cm}^{-1}$ . In three of the  $6p$  lattice mode branches the frequency approaches zero as the wave vector approaches zero. These are called acoustical branches. At  $|\underline{k}| = 0$ , the three

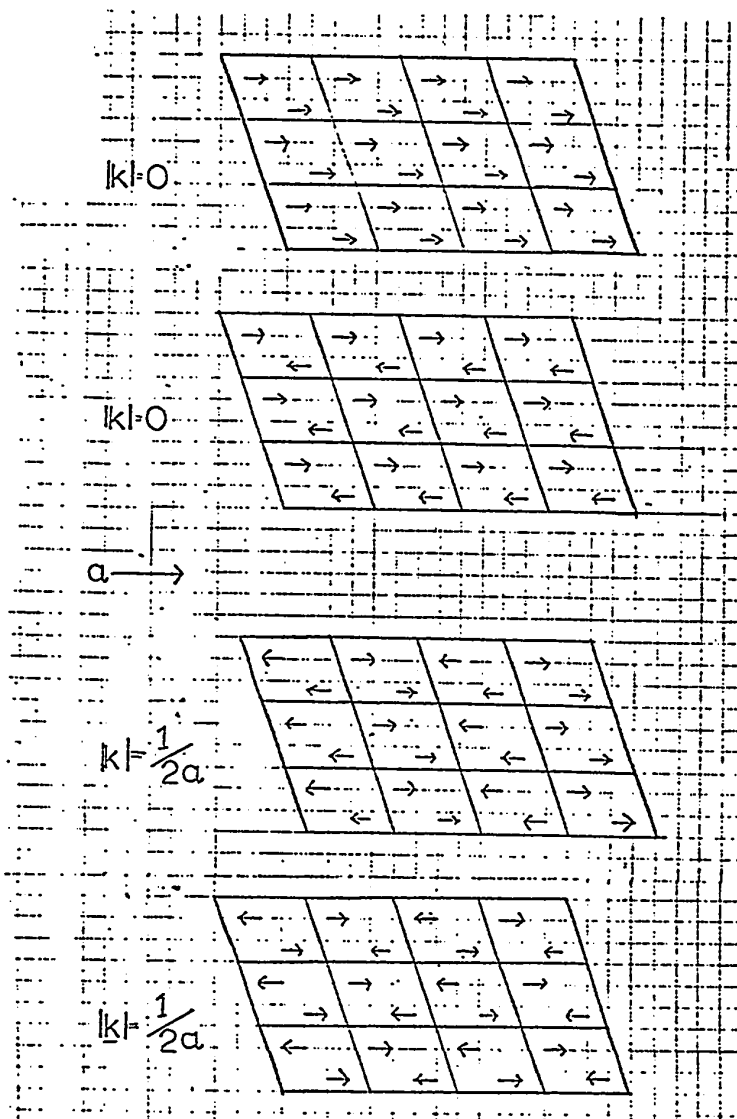


Figure 2

Cl-Cl stretching vibrations in a chlorine crystal. Arrows represent the relative phases of the stretching vibrations on different molecules. Thus if the arrow to left represents a stretched Cl-Cl bond then the arrow to right represents a contracted bond.

acoustical modes correspond to the three translations of the whole crystal. Some of the acoustical modes correspond to sound waves in the crystal and none of them absorb electromagnetic radiation. The remaining 3s-3 branches are called optical branches because certain vibrations in them may absorb electromagnetic radiation or produce Raman scattering.

Simple theory (32-34) shows that the only vibrations in an ordered crystal which will absorb radiation are those whose wave lengths equal that of the radiation. For infrared radiation this corresponds to wave lengths in the range  $10^{-4}$  to 1 cm, which are much larger than the unit cell dimensions. For a crystal with only short range intermolecular forces, a vibration with a wavelength of the order of  $10^{-4}$  cm has essentially the same frequency as one with infinite wavelength ( $\underline{k} = 0$ ). Thus for these crystals, the infrared spectrum can be predicted by considering only  $|\underline{k}| = 0$  modes. To understand these modes, only one unit cell need be considered, because the displacements in one unit cell are duplicated in all other cells.

The same result is obtained for Raman spectroscopy, for which the rigorous selection rule is

$$\underline{k} = \underline{K}_i - \underline{K}_s$$

where  $\underline{k}$  is the wave vector of the vibration and  $\underline{K}_i$  and  $\underline{K}_s$  are the wave vectors of the incident and the scattered light respectively. For visible light  $\underline{K}_i$  and  $\underline{K}_s$  are both about  $5 \times 10^{-5}$  cm and their difference is very small. Again, for crystals with short range intermolecular forces only, the selection rule is approximately  $\underline{k} = 0$ .

A crystal with  $S$  atoms per unit cell can have  $3S-3$  infrared and Raman active modes under the  $|\underline{k}| = 0$  selection rule. The number of modes which are actually active in the infrared and Raman spectra is further governed by the symmetry elements present in each unit cell. Since Bhagavantam and Venkatarayudu first applied symmetry considerations, using group theory, to obtain selection rules for the spectra of crystals (35), many articles have appeared on this topic (36-45). The following paragraphs give a brief discussion of the main points of the theory.

In order to examine the effects of symmetry on the vibrational modes in solids, it is convenient to define four groups, the space group, the factor group, the unit cell group, and the site group. All crystals belong to one of the 230 possible space groups (30, 46, 47). The space group is the group formed by all of the symmetry elements present in the crystal. It includes all combinations

of the primitive translations and the proper and improper rotations. The space group is the product of an invariant subgroup, consisting of the translation symmetry elements, and a 'factor group'. The elements of the factor group are the cosets of the translation subgroup in the space group (44, 46). The unit cell group consists of the elements of the space group modulo primitive translations (41). There is a one-to-one correspondence between its elements and the coset elements of the factor group, and the two groups are isomorphous with one another and also with one of the 32 crystallographic point groups. Any point in a crystal is said to be a site. The group formed by symmetry elements which pass through a site and leave it invariant is the site group. The site group is always a subgroup of the unit cell group and, hence, of the space group. The site group of a point occupied by a molecule is also always a subgroup of the molecular point group in an ordered crystal.

The symmetry of a molecule in a crystal may be less than the symmetry of the isolated molecule, and consequently some vibrational modes which are inactive in the gas phase may become active in the crystal. The degenerate modes of the isolated molecule may split into more than one component in the solid. These changes in the

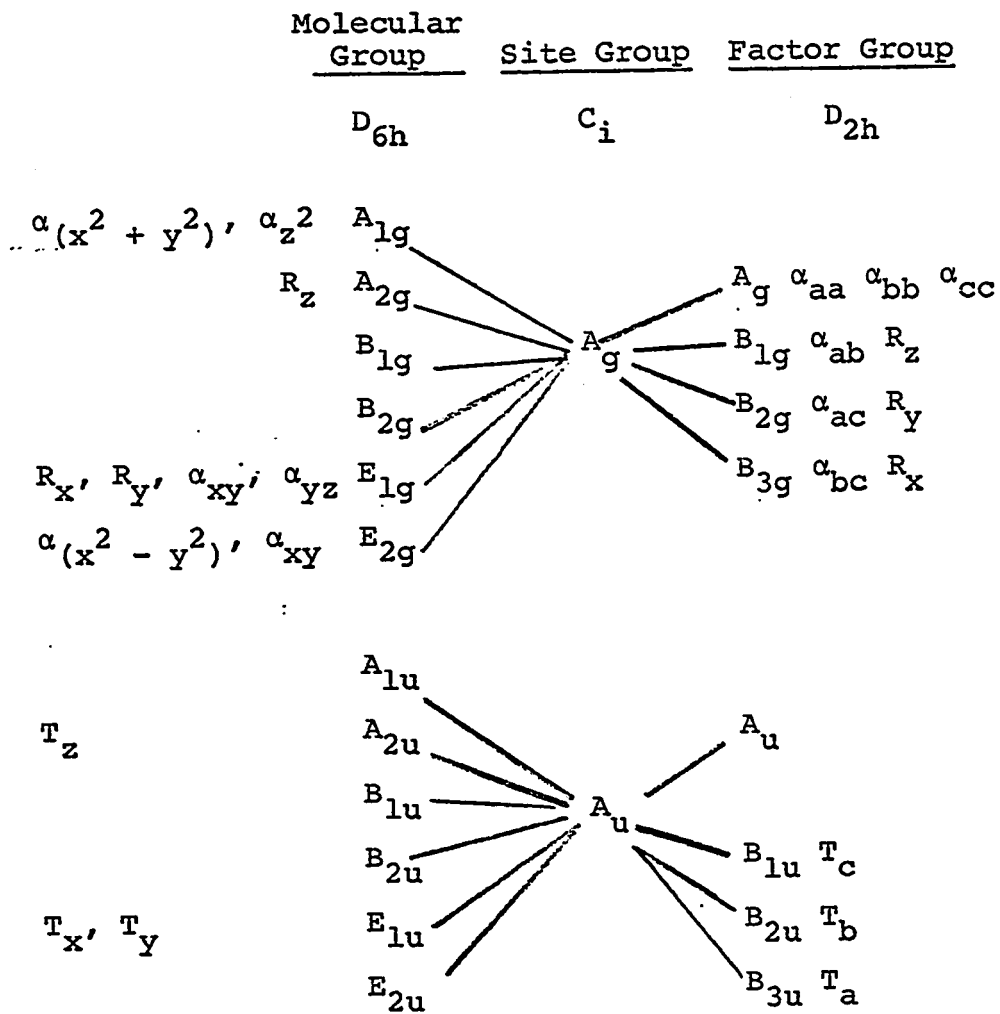


Figure 3

Correlation Diagram for Benzene



vibrational spectra due to the lower symmetry of the molecule in a crystal are called site group effects. Site group analysis, which is the symmetry analysis of the molecular vibrations under the site group, predicts these splittings but does not take into account the coupling which may occur between the different molecules in the crystal. This coupling can further split the different absorptions allowed under the site group. Because of the  $|\underline{k}| = 0$  selection rule, it is sufficient to consider the molecules and symmetry in a single unit cell in order to study the effects of intermolecular coupling. The unit cell group contains the symmetry elements associated with a single unit cell and hence a unit cell group analysis (also called factor group analysis) of a single unit cell is used to predict these unit cell group splittings (36-45). For a unimolecular unit cell, these splittings do not occur.

The above discussion can be illustrated by considering the example of solid benzene. Benzene has the molecular point group  $D_{6h}$  and crystallizes in the space group  $Pbca-D_{2h}^{15}$  with four molecules per unit cell (48). The molecules are situated at sites of symmetry  $C_i$ . The unit cell group is isomorphous with the point group of the crystal class,  $D_{2h}$ . Figure 3 shows the correlation

diagram for benzene which relates the irreducible representations of the molecular point group  $D_{6h}$  to those under the site group  $C_i$  and the unit cell group  $D_{2h}$ . The site group is always used to correlate the molecular point group with the unit cell group. Figure 3 also contains the symmetry species of the translations, T, along the x, y and z axes of the molecule and along the a, b, and c crystal axes, and of the various components of the polarizability,  $\alpha$ , and of the molecular rotations, R.

The site group,  $C_i$ , has only two irreducible representations,  $A_u$  and  $A_g$ . All the translations of the molecule are  $A_u$  while all the components of polarizability and all rotations are  $A_g$  under this group. Thus all infrared and Raman active modes of the isolated molecule retain their activity in the solid. Modes of symmetry  $A_{2g}$ ,  $B_{1g}$ ,  $B_{2g}$ ,  $A_{1u}$ ,  $B_{1u}$ ,  $B_{2u}$  and  $E_{2u}$  are inactive in the infrared and Raman spectra of the gas. In the solid, the  $A_{2g}$ ,  $B_{1g}$ , and  $B_{2g}$  modes of the molecule correspond to  $A_g$  modes of the site group and hence are Raman active. Similarly  $A_{1u}$ ,  $B_{1u}$ ,  $B_{2u}$  and  $E_{2u}$  modes of the molecule correspond to  $A_u$  modes of the site group and are infrared active in the solid. Thus the spectrum of solid benzene shows fundamentals which are absent in the gas phase spectrum. The degeneracy of all of the doubly degenerate E modes is lifted

under the site group. In the gas phase, the  $E_{2u}$  modes are inactive, but each pair of  $E_{1u}$  modes yields one band in the infrared spectrum, and each pair of  $E_{1g}$  or  $E_{2g}$  modes yields one band in the Raman spectrum. Under the site group, each pair of degenerate E modes is predicted to yield two bands in the appropriate spectrum. In this way, site group analysis predicts the site group splittings, and the changes in activity of the vibrations between the gas and the solid state.

Since the unit cell of benzene contains 4 molecules, there are four  $\underline{k} = 0$  vibrations corresponding to each non-degenerate intramolecular vibration. The correlation diagram (Figure 3) is used to determine how many of these are infrared or Raman active. Both  $A_u$  and  $A_g$  modes of the site group are related to four different modes, each with a different symmetry under the unit cell group. Thus one  $A_{2u}$  mode of the molecule generates four different  $\underline{k} = 0$  modes of symmetry  $A_u$ ,  $B_{1u}$ ,  $B_{2u}$ , and  $B_{3u}$  in the crystal; only the last three are infrared active. The first mode,  $A_u$ , is inactive in both the infrared and the Raman spectra of the crystal. Thus, a single band in the infrared spectrum of gaseous benzene, arising from an  $A_{2u}$  mode, splits into three lines in the infrared spectrum of the crystal. The three lines are all observed to lie

within about  $10 \text{ cm}^{-1}$  of each other. This splitting is the unit cell group splitting and arises from the dynamic coupling between the molecules. A degenerate molecular mode say an  $E_{1u}$  mode splits in a more complicated manner in the crystal spectrum. As a specific illustration, the  $E_{1u}$  modes arising from C-C-H angle deformations may be considered. These modes yield a single band in the gas phase infrared spectrum. In the crystal, the degeneracy is lifted under the site group and two infrared active  $A_u$  modes result, due to the site group splitting. Each of these  $A_u$  components splits further under the unit cell group into  $A_u$ ,  $B_{1u}$ ,  $B_{2u}$ , and  $B_{3u}$  modes, the last three being infrared active. Thus, in the crystal, the one molecular  $E_{1u}$  C-C-H angle deformation mode yields six lines in the crystal spectrum. Like the lines arising from the  $A_{2u}$  vibrations, those arising from the  $E_{1u}$  mode lie close together, within  $15 \text{ cm}^{-1}$  in this case.

In the spectrum of an isotopically pure sample the factor group splitting is observed. One may observe the site splittings by recording the spectrum of a 'mixed crystal' (49-52). In a true mixed crystal, the crystal structure of the host component must be essentially the same as that of the pure guest compound, and the two molecules must be essentially the same size. Then, if the guest

molecule concentration is low (of the order of a few percent) so that guest molecules are far apart in the crystal, and if the guest molecule vibrations have quite different frequencies from those of the host molecule, so that the two do not couple, the spectrum of the guest molecule shows site splitting but no unit cell splitting. This is a particularly useful technique when the guest molecule is a deuterated isotope of the host or vice versa (50).

The various splittings of spectral bands are demonstrated in the infrared spectrum of solid benzene, as reported by Bernstein et al (53). Figures 4a, 5a, and 6a show the infrared spectrum of normal benzene crystals for the  $B_{1u}$  ( $\nu_{12}$ ),  $B_{2u}$  ( $\nu_{15}$ ) and  $E_{1u}$  ( $\nu_{18}$ ) fundamentals respectively. Figures 4b, 5b and 6b show the infrared spectrum for the same fundamentals in a mixed crystal of 1% benzene- $h_6$  plus 99% benzene- $d_6$ . The frequencies of the different features in these bands are given in Table I. The site group analysis predicts that the mixed crystal spectrum will show a single peak for each of the non-degenerate  $B_{1u}$  and  $B_{2u}$  modes, and a doublet for the degenerate  $E_{1u}$  molecular mode. The pure crystal spectrum shows the additional effect of the unit cell group splitting. It contains 3 peaks each for the  $B_{1u}$  and  $B_{2u}$  modes while the  $E_{1u}$  mode

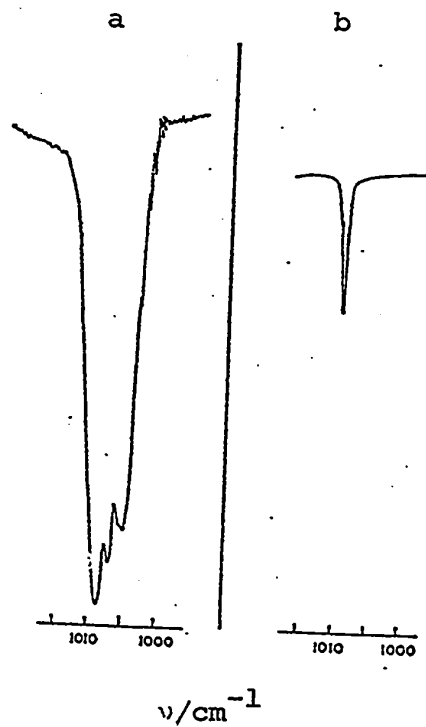


Figure 4

Infrared spectra of the B<sub>1u</sub> (ν<sub>12</sub>) fundamental of, (a) neat C<sub>6</sub>H<sub>6</sub>, and (b) 1% C<sub>6</sub>H<sub>6</sub> in C<sub>6</sub>D<sub>6</sub> at 77°K. This figure is from reference (53).

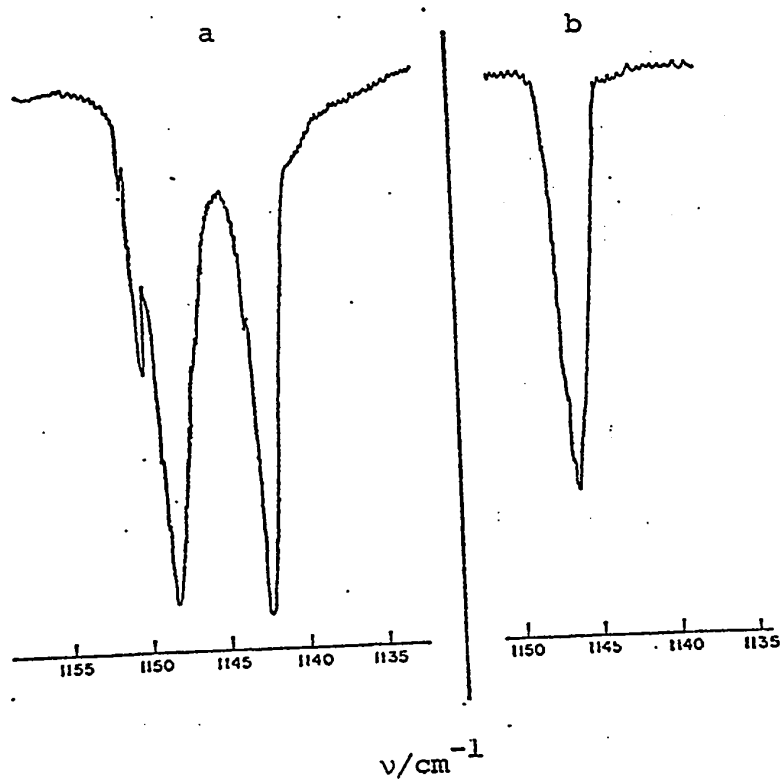


Figure 5

Infrared spectra of the B<sub>2u</sub> (ν<sub>15</sub>) fundamental of (a) neat C<sub>6</sub>H<sub>6</sub>, and (b) 1% C<sub>6</sub>H<sub>6</sub> in C<sub>6</sub>D<sub>6</sub> at 77°K. This figure is from reference (53).

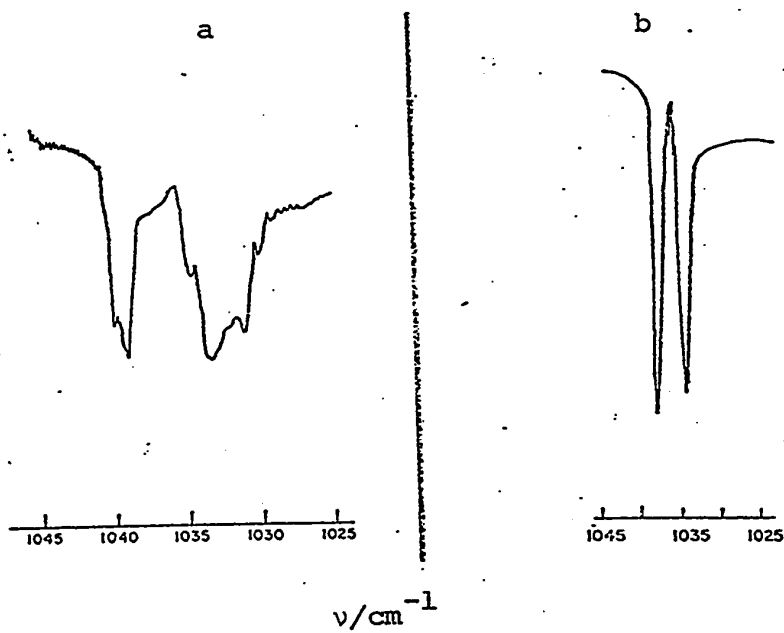


Figure 6

Infrared spectra of the  $E_{1u}$  ( $\nu_{18}$ ) fundamental of (a) neat  $C_6H_6$ , and (b) 1%  $C_6H_6$  in  $C_6D_6$  at 4.2°K. This figure is from reference (53).



Table I

Features seen in the infrared spectra of solid benzene for the three modes shown in Figures 4 to 6

Mode	Symmetry	$C_6H_6$ in $C_6D_6$	Pure $C_6H_6$
		$cm^{-1}$	$cm^{-1}$
$\nu_{12}$	$B_{1u}$	1011.3	1006.9
			1008.6
			1009.7
$\nu_{15}$	$B_{2u}$	1146.9	1142.5
			1148.6
			1150.3
$\nu_{18}$	$E_{1u}$	1034.8 1038.6	1030.0
			1032.5
			1033.3
			1034.6
			1038.9
			1039.8

Above data is from reference (53).

clearly splits in a more complicated manner, and the expected six features have been identified (Table I).

In the above discussion the crystal structure was known from crystallographic studies (48) and it was used to interpret the infrared spectrum. Frequently the splittings observed in the infrared and Raman spectra of pure and mixed crystals are used to obtain information about the crystal symmetry of solids whose structures are not known. This work is not too definitive unless some knowledge of the size of the unit cell is available. It has been used to obtain information on the hydrogen atom positions in the solid hydrogen halides (54-56) because these were not provided by X-ray analysis. In other cases (57-62), this method has been used to obtain information on solids which are difficult to handle by single-crystal X-ray methods because, for example, they may be extremely difficult to obtain in single crystal form. In these cases, the combination of powder X-ray diffraction methods, which can yield the unit cell size and the lattice symmetry (59), and vibrational spectroscopy provides a potentially useful way of obtaining information on the crystal structure.

The spectra of the lattice modes can also be predicted from symmetry considerations, and hence can also

provide information on the unit cell size and symmetry. The pure translations of a benzene molecule fall in the  $A_{2u}$  and  $E_{1u}$  representations of  $D_{6h}$  (Figure 3). These degrees of freedom yield  $3 A_u + 3 B_{1u} + 3 B_{2u} + 3 B_{3u}$  crystal modes. Thus  $2B_{1u}$ ,  $2B_{2u}$  and  $2B_{3u}$  translational lattice vibrations are predicted to be infrared active and Raman inactive. Similarly the three rotational degrees of freedom of a benzene molecule fall into the  $A_{2g}$  and  $E_{1g}$  representations of  $D_{6h}$ , and yield altogether  $3A_g + 3B_{1g} + 3B_{2g} + 3B_{3g}$  rotational lattice vibrations in the solid. All of them are Raman active and infrared inactive. The lattice modes have been detected in solid benzene below  $140 \text{ cm}^{-1}$  (63-65).

### 1.2.3 THE VIBRATIONAL SPECTRA OF DISORDERED SOLIDS AND PLASTIC CRYSTALS

An ordered solid is characterized by the translational symmetry of its lattice, as discussed in section 1.2.2. When a solid does not possess translational symmetry it is called a disordered solid (66). Disorder in solids can be divided into three general types. The first type is substitutional disorder and is caused by the presence of foreign moieties in the solid lattice. The effects of this type of disorder on the vibrational spectra have been discussed in the literature (66, 67), but are not of dir-

ect importance to the work reported in this thesis. The second type is orientational disorder (68), which means that the molecular centres are on, or very near to, regular lattice sites, but the orientation of the molecules, or of parts of the molecules, varies in an irregular manner from site to site. The third type of disorder is translational disorder, in which the centres of gravity of the molecules are not on regular lattice sites. The third type of disorder leads to solids that are non-crystalline and are usually called amorphous or vitreous solids, or glasses.

Plastic crystals are orientationally disordered solids formed by covalent molecules, in which the molecules reorient at very high speeds (Section 1.1). The vibrational spectra of orientationally disordered solids and plastic crystals are discussed in this section. For the sake of convenience the discussion is divided into two parts. The first part deals with the vibrational spectra due to intramolecular modes, which occur in the mid-infrared region of the spectrum, while the second part deals with the far-infrared spectra due to intermolecular modes.

(A) Intramolecular Vibration Spectra

In the previous section it was shown that each

intramolecular vibration of a molecule in an ordered solid causes only a very small number of sharp absorption lines in the spectrum of the solid, in spite of there being a very large number of crystal vibrations arising from that mode. This arises because of the very strict selection rules concerning the wave vector of the vibrations, which, in turn, arise from the translational symmetry in the ordered solid. In an orientationally-disordered solid there is no rigorous translational symmetry, and therefore the wave vector selection rules do not apply in general, and all vibrations in the crystal are infrared and Raman active. Hence one finds broad bands in the vibrational spectra of disordered solids (69-70). There is usually one band for every molecular vibrational mode and the factor group and site group splittings observed in the ordered solids are absent. Therefore, the spectra of any compound in its disordered solid phase look simpler than those of its ordered solid phase, if one overlooks the large bandwidths observed in the former.

Three factors which contribute to the width of a band in orientationally disordered crystals can readily be identified. They are the intermolecular vibrational coupling (intermolecular coupling), the actual non-equivalence of diffraction-equivalent sites (site effects),

and the reorientational motion of the molecules. A further factor which is important at high temperatures is the anharmonic coupling with other crystal modes. This factor however affects the spectra of ordered and disordered solids alike and will not be discussed specifically.

The intermolecular distances in a disordered crystal are nearly the same as in the ordered phase of the same species, and therefore the intermolecular vibrational coupling is of the same order in the two phases. In the ordered phase the intermolecular coupling causes the factor group splittings, and hence the magnitude of these splittings may be used to estimate the influence of this coupling upon the band widths of the disordered phase.

In an ordered crystal the static crystal field is identical at each diffraction-equivalent site, and therefore the vibrational frequencies of the molecules on these sites are identical from site to site, if one neglects intermolecular vibrational coupling. In an orientationally disordered crystal this is not the case, and the static crystal field, and hence the molecular vibration frequencies, vary from one site to its diffraction-equivalent sites. The influence of this factor on the bandwidths in disordered crystals can be estimated from

the magnitude of the site splittings in the ordered phase, if they occur. Hence a band of frequencies is expected for every intramolecular vibrational mode even if the intermolecular coupling is totally absent. If the intermolecular coupling is present it contributes further to the observed bandwidths, in addition to the site effects. These two factors were first recognized by Hornig (71) in 1948 and have been reiterated more recently (72). In spite of this, recent papers on the spectra of the disordered phase of sodium borofluoride (70), and of the plastic phases of adamantane (73) and cyclohexane (74-76), have included either the use of factor group analysis to interpret the spectra, or the specific statement that "the spectra are compatible with the high diffraction symmetry" (73). It is clear that the spectra of disordered solids cannot be interpreted correctly using these ideas, although they may appear to be valid phenomenologically.

The third factor which can contribute to the band widths in the spectra of orientationally disordered solids is rapid molecular reorientation (77). In perfectly ordered solids, and in some disordered solids, molecular reorientation does not occur, but, in many orientationally disordered solids, such as plastic crystals and ammonium salts, the molecules reorient at rates of the order of  $10^{10}$

$\text{sec}^{-1}$  in addition to executing the vibrational motions. An appreciable fraction of the width of the absorption by intramolecular modes in such solids has been attributed to this rapid reorientation.

The theory employed to determine the contribution of molecular reorientations to the broadening of the intramolecular vibrational bands is based on the Heisenberg picture of spectroscopy, rather than the more usual Schrödinger picture (77).

In the Schrödinger picture of spectroscopy one's attention is concentrated on the distinct energy states of the system. The Heisenberg picture, on the other hand, emphasizes the importance of the time-dependence of the energies of the molecules in determining the shape of the spectral band. For example, one might describe an infrared absorption peak in the Schrödinger picture as arising from transitions between two vibrational states of the molecules. If the molecules also have rotational degrees of freedom which are more 'rotation-like' than 'vibration-like' in the solid, the Schrödinger picture would represent the observed spectral band as the overlapping of many vibration-rotation lines. It has been pointed out (77), however, that the rate at which the molecules in the solid rotate can have a considerable influence on the actual



shape of the spectral band. The Heisenberg picture brings this feature out since it expresses the bandshape as the Fourier transform of a reorientational autocorrelation function (77). This autocorrelation function describes the 'memory' of the transition dipole moment, associated with the spectral band of interest. If the transition dipole has a long 'memory' (does not reorient very rapidly), the spectral line will be narrow, but if the transition dipole has a very short memory the line will be broad. These qualitative statements deal only with the limit of motional narrowing which is the case in liquids and solids. The Schrödinger approach works well for the interpretation of the spectra of ordered solids or isolated molecules, and enables one to understand the broadening of spectral bands by the first two factors discussed above. It is more difficult to understand the broadening caused by the reorientational motion of the molecules using the Schrödinger picture. The Heisenberg formulation, on the other hand, provides a relatively clear understanding of the contribution to the bandwidth from molecular rotation in condensed phases.

The analysis of spectral bandshapes, corrected for the instrumental slit width, using the Heisenberg approach has been attempted mainly for liquids (77-81).

Gordon (77) studied the vibrational bands of certain linear molecules in their condensed phases using the assumption that the observed band widths were completely determined by molecular reorientations. Other workers (78, 79, 81, 82) have pointed out that the observed bandwidth is not entirely due to molecular reorientation. Some of them (78, 79, 82) considered that the observed width was the simple sum of the orientational width and the 'intrinsic width' where the intrinsic width is caused by factors other than molecular reorientations. In the light of the earlier discussion, it will include the width caused by intermolecular coupling, and site-effects. Recently Bartoli and Litovitz (81) have pointed out that the observed width is not a simple sum of these widths, it is obtained by convolution of the intrinsic line shape with the rotational line shape. They have also suggested methods for separating the orientational width from the intrinsic width.

Knowing the orientational halfwidth, one can obtain information about the molecular reorientations using the Heisenberg formalism. One assumes a physical model and calculates the correlation function (77, 80, 81) for its reorientational motions. From the correlation function one can obtain different spectral properties, like the orientational halfwidth (81), and the spectral moments

(77). Agreement between the properties calculated from the model and those obtained from the experimental observations is a measure of the correctness of the model.

The vibrational spectra of only three plastic crystals, CO (77), CCl<sub>4</sub> (81), and cyclohexane (81), have been partially analyzed using the Heisenberg formalism. Gordon (77) concluded that the rotational motion of CO is strongly hindered in its solid, as well as in its liquid and compressed gas phases. Bartoli and Litovitz (81) concluded that the molecular reorientation in the plastic phases of cyclohexane and carbon tetrachloride is best described as collision-limited free diffusion, wherein the molecules are free to rotate until they collide with the neighbouring molecules, when the direction of rotation changes. The above rotation takes place in very small steps and the average time between successive 'collisions' is of the order of  $10^{-13}$  second.

The remaining literature on the vibrational spectra of intramolecular modes in plastic crystals contains very qualitative, and often very vague, discussions of the spectra. These will be summarized briefly after a brief review of the main experimental results.

The vibrational spectra of plastic phases are very similar to those of liquids (83-89). The spectra can

often be analyzed in terms of the gas phase selection rules, but in some cases, modes which are inactive in the gas do appear weakly in the spectrum of a plastic phase (87). The bandwidth decreases slowly with decreasing temperature in the plastic phases, but usually shows a sharp drop at the disorder-order transition (86). Different explanations have been offered for the observed breadths of the spectral features. One group of workers considered that it is due to the disorder present in the plastic solid phases (90), and not due to molecular reorientation, while another group of workers considered that it is due only to the molecular reorientation, and intermolecular coupling and site-effects are not important (77, 84), and a third group suggested that both disorder and molecular reorientation contribute to the bandwidth (89). In some cases, the spectra of plastic phases have been analyzed on the basis of the high diffraction symmetry (Section 1.1), without making any comment about the shape of the spectral features (73). In most of the published literature, the factors which can be expected to influence the spectra have not been considered systematically.

(B) Far-Infrared Region

The far-infrared spectra of ordered solids generally show well-defined, sharp features (63-65, 91, 92)

which arise from the rotational and translational lattice modes. But the spectra of disordered solids generally show broad bands, as shown for the disordered ice (91) and acetylene (92) in Figures 7 and 8. Although both ice and acetylene show a broad band in the far-infrared spectrum of their disordered phases, there is a notable difference between them. The broad band in the spectrum of ice shows definite features while the spectrum of the plastic phase of acetylene is featureless except for a very broad maximum. These spectra are typical of those seen for plastic crystals (89, 92-96) and for the disordered ice phases (91, 97). It is known that molecules in plastic crystals reorient rapidly (Section 1.1) while the molecules in the ices are essentially static at 100°K (98). The available evidence, therefore, indicates that very rapid molecular reorientation causes the loss of all of the structure observed in the far-infrared spectra of orientationally disordered phases in which the molecules reorient very slowly.

Again, two approaches can be used to interpret the far-infrared spectra, the Schrödinger approach and the Heisenberg approach. There are only two models based on the Schrödinger approach that have been applied to explain the far-infrared spectra of disordered solids.

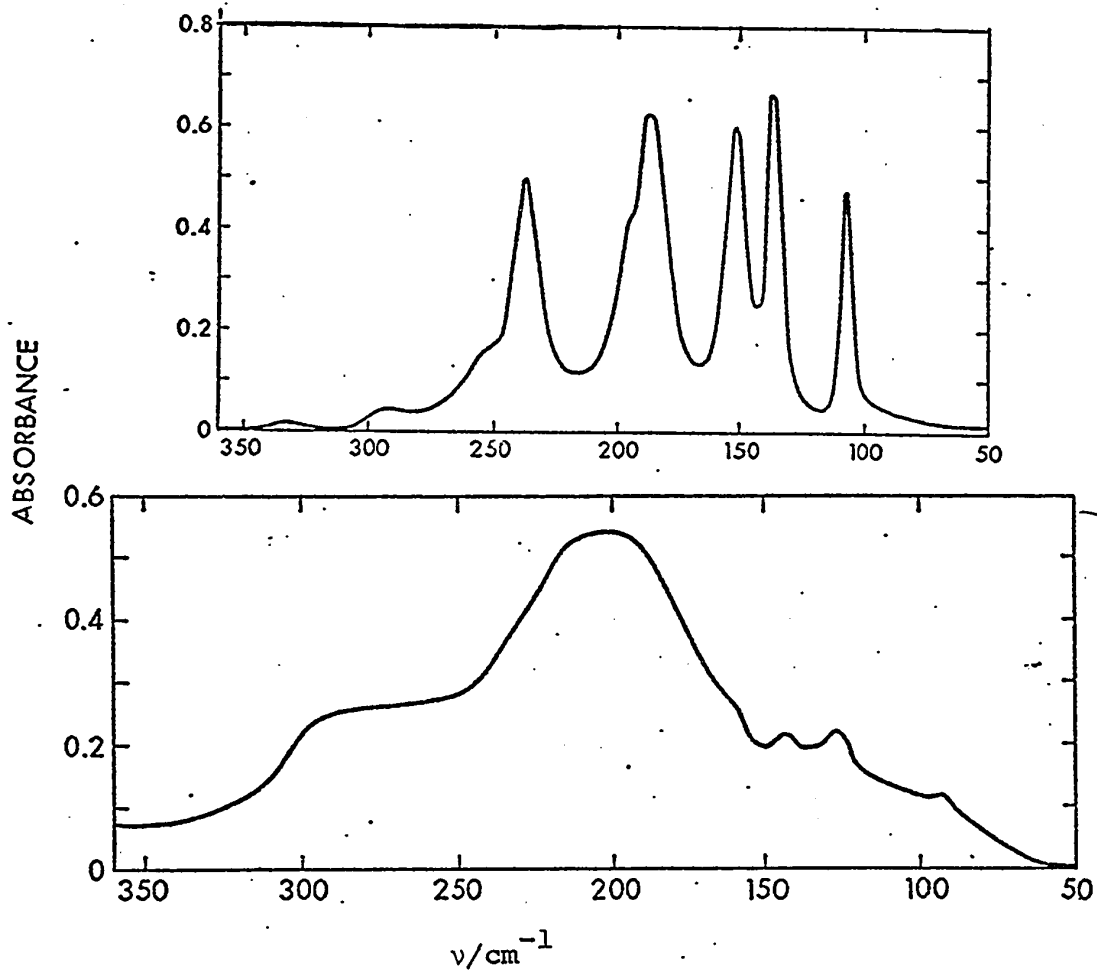


Figure 7

Far-infrared spectra of ice II, an ordered solid (upper box);  
and ice V, an orientationally disordered solid (lower box).  
These figures are from reference (91).

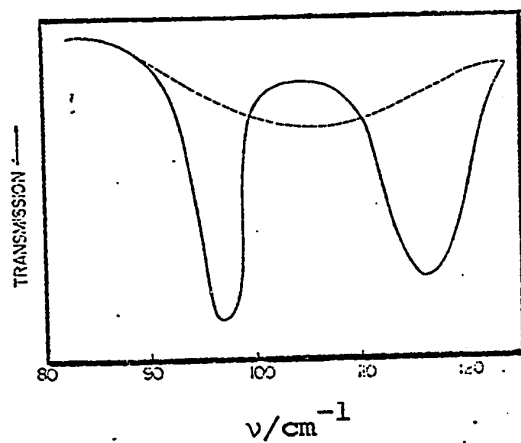


Figure 8

Far-infrared spectra of solid acetylene above and below the temperature of phase transition; ---, 134°K, plastic crystal phase; — 132°K. This figure is from reference (92).

The first one was suggested by Whalley and Bertie (68) to explain the far-infrared absorption due to the translational vibrations of molecules in orientationally disordered solids in which the molecules do not reorient rapidly. It does not deal with the rotational vibrations in these solids. Hence it is useful in solids where the translational and rotational vibrations are distinct because they occur in different regions of the spectrum, as in the ices (97). The second model, by Pourprix, Abbar, and Decoster (96), was suggested for systems where the far-infrared absorption is mainly due to the rotational vibrations of the molecules and the translational vibrations can be ignored. Here the two models will be discussed briefly and qualitatively.

Whalley and Bertie consider an orientationally disordered solid to be mechanically regular as far as the 'translational vibrations' of the molecules are concerned, provided they can be separated from the rotational vibrations. The translational vibrations of the molecules in such a system can be approximately represented by those of the corresponding ordered solid obtained by replacing the molecules with spheres which have the same mass as the molecules and the same intermolecular forces. The system is electrically irregular because the dipole moment deri-



vative with respect to translation of a molecule varies in direction and magnitude from one site to its diffraction equivalents, in a random way depending on the orientations of the neighbouring molecules. The electrical irregularity ensures that there are no rigorous selection rules for the interaction of the translational vibrations with light. The dipole moment derivative with respect to translation of the individual molecules is considered in two parts. One part is the average of the derivatives over all diffraction equivalent translations of equivalent molecules in the crystal. This part has the diffraction symmetry of the crystal. The second part is the deviation of the actual derivative for each translation of each molecule from the appropriate average part. It varies in an irregular manner from site to equivalent site.

The results of this theory that are relevant to the present discussion are: (a) No selection rules apply because of the disorder and therefore all vibrations are infrared active. (b) The average part of the dipole moment derivative leads to absorption by vibrations allowed by the diffraction symmetry. There are very few such vibrations compared to the number of disorder-allowed ones, and the spectrum is expected to consist of broad absorption with the diffraction-symmetry-allowed transitions appearing

as sharp features on this broad absorption. (c) The broad absorption also shows features which correspond to features in the density of states curve for the translational vibrations.

This model was suggested originally to explain the absorption by the translational vibrations in orientationally disordered solids and successfully explained the complex far-infrared spectra of the ices (97). The general conclusions can also be qualitatively applied to other vibrations of static, orientationally-disordered solids, and have been used to explain the spectra of the ammonium halides (99) and the methyl ammonium halides (100).

Pourprix, Abbar, and Decoster (96) assumed that the far-infrared absorption in the plastic solid and liquid phases of  $\text{CH}_3\text{CCl}_3$  is unaffected by the translational vibrations, because it does not change sharply at the melting point. They separated the far-infrared and microwave absorption into two parts. The lower-frequency part was assigned to the orientational relaxation of the molecules, while the higher frequency part was assigned to the rotational vibrations of the molecules in potential wells. The height of the potential well was determined from the variation of the critical relaxation frequency with temperature. They calculated the vibrational frequencies

assuming the potential well to be harmonic and, subsequently, anharmonic. The mean frequency, calculated assuming the potential wells to be anharmonic, agreed rather well with the experimental frequencies of the band maximum for  $-45^{\circ}\text{C}$ ,  $-20^{\circ}\text{C}$ , and  $+20^{\circ}\text{C}$ . The far-infrared bandwidth was estimated from the range of transition frequencies calculated for the anharmonic potential well, but was found to be too small to account for the experimental width. The authors concluded that it was necessary to consider the distribution of barrier heights and, perhaps, the fluctuation of the barrier heights with time, in order to obtain a more reasonable model.

There is only one model based on the Heisenberg picture which has been applied to the far-infrared and microwave absorption in plastic crystals. It was proposed by Lassier and Brot (101) and is applicable to both plastic crystals and liquids with quasicrystalline structures. In this model it is assumed that the molecules can occupy only a discrete number of orientations. These different orientations are separated by potential barriers greater than  $kT$ , where  $k$  is Boltzmann's constant and  $T$  is the absolute temperature of the system. Molecules can jump from one orientation to another but these jumps take a finite time which depends upon the moment of inertia of the mole-

cules. In between jumps, the molecules undergo rotational vibrations in a potential well. Lassier and Brot calculated the far-infrared absorption in the plastic phase of t-butyl chloride (102) using their model. The agreement between the observed and calculated absorption is excellent in the microwave region, but in the far-infrared region the calculated absorption is weaker than that observed.

Several other models have been suggested to explain the far-infrared spectra of liquids, but none have been applied to plastic crystals (103-108). The far-infrared spectra of other plastic crystals have been explained only qualitatively. For methane (95), monosilane, (89) and acetylene (92) the absorption was assigned to rotational motion of the molecules. For HCl and DBr (93) the absorption was attributed to torsional motion of the molecules with the broad and smooth shape of the band due to the disorder in the plastic crystal phase.

### 1.3 RESUMÉ OF PREVIOUS STUDIES OF t-BUTYL BROMIDE

The previous studies of the vibrational spectra and the solid state of t-butyl bromide are summarized in this section.

#### 1.3.1 VIBRATIONAL SPECTROSCOPY

The earliest published work on the vibrational spectrum of t-butyl bromide-h<sub>9</sub> dealt with the Raman spectrum of the liquid. Harkins and Bowers (109) in 1931 published the frequencies of the features in the Raman spectrum. Soon afterwards, Dadiou, Pongratz and Kohlrausch (110) published the frequencies and relative intensities of the Raman bands, and in 1940 Wagner (111) published the frequencies, relative intensities and depolarization ratios. The agreement between the frequencies reported by these workers is better than  $10 \text{ cm}^{-1}$  for strong bands but there were large discrepancies for weak features. Wagner's data has been used by most of the subsequent authors. More recently Zeil et al (112) published a partial Raman spectrum of the liquid, without depolarization data, and Durig et al (113) reported the Raman spectrum of the solid between  $-61^{\circ}\text{C}$  and  $-190^{\circ}\text{C}$  for the region below  $100 \text{ cm}^{-1}$  only.

The infrared spectrum of liquid t-butyl bromide-

$h_9$  was first reported by Mortimer et al (114) in 1947 who studied only the 800 to 500  $\text{cm}^{-1}$  region. Sheppard (115) studied the infrared spectrum of the liquid between 3500 and 450  $\text{cm}^{-1}$ . His work suffers only from the low resolution available in 1950. More recently Zeil et al (112) reported the spectrum of the liquid between 1500 and 1000  $\text{cm}^{-1}$ , and Bentley and coworkers (116, 117) studied the region between 670 and 100  $\text{cm}^{-1}$ . Huttner and Zeil (118) in 1966 reported the gas phase frequencies for the bands which they assigned to fundamental transitions. Moller et al (119) studied the spectrum of gaseous t-butyl bromide in the region 350 to 40  $\text{cm}^{-1}$  in 1967. The most recent published work relevant to the assignment of the intramolecular modes of t-butyl bromide is by Durig et al (113) who studied the infrared spectrum of the solid between 300 and 33  $\text{cm}^{-1}$  in 1970. Thus, the infrared spectrum of liquid t-butyl bromide- $h_9$  is well documented in the literature, but no complete gas phase spectrum has been published. Furthermore, the only Raman polarization data for the liquid dates from 1940.

The assignment of the spectrum of t-butyl bromide- $h_9$  has been the subject of much debate, mainly over the bands between 1400 and 800  $\text{cm}^{-1}$  (115, 120-123). Sheppard (115) published the first assignment that was com-

plete except for the methyl torsion modes, which have been assigned only recently (113). His assignment for the bands below  $800\text{ cm}^{-1}$  has not been seriously challenged by subsequent authors. An alternate assignment of the bands below  $400\text{ cm}^{-1}$  was proposed (117) but it appears to be based on a misinterpretation of the Raman polarization data, and is certainly incorrect. Various assignments of the remainder of the bands have been reported. Tobin (120) in 1952 and Mann et al (121) in 1958 proposed alternate assignments using Sheppard's infrared data and Wagner's (111) Raman data. Hayashi (122) in 1958 reported a partial calculation for the normal vibrations of t-butyl bromide- $\text{h}_9$ . Hirschmann and Kniseley (123) proposed an alternate assignment for the bands between  $800$  and  $1250\text{ cm}^{-1}$  using Sheppard's data. Huttner and Zeil (118) used new data, which differs significantly from the earlier results, and also reported normal coordinate calculations. These various assignments of the spectra of t-butyl bromide- $\text{h}_9$  are summarized in Table II.

Most of the debate over the assignment arose because the only experimental evidence available, other than the frequencies of the bands, was Wagner's Raman polarization data, and because the spectrum of t-butyl bromide- $\text{d}_9$  was not available to indicate the hydrogen iso-

Table II

The Assignments of the Fundamental Vibration Frequencies of t-Butyl Bromide-h<sub>9</sub><sup>a</sup>

Symmetry	Mode	Sheppard		Tobin		Mann et al		Huttner and Zeil		This Work		
		IR	Raman	IR	Raman	IR	Raman	IR	Raman	Gas	Liquid	
A <sub>1</sub>	1	--	2918 C-H <sub>3</sub> Asym. St.	2982 CH <sub>3</sub> Asym. St.	2918 C-H <sub>3</sub> St. Asym.	2954 C-H <sub>3</sub> St. Asym.	2977	2970	CH <sub>3</sub> St. Asym.			
	2	--	2870 C-H <sub>3</sub> Sym. St.	2918 CH <sub>3</sub> Sym. St.	2918 C-H <sub>3</sub> St. Sym.	2935 C-H <sub>3</sub> St. Sym.	2934	2925	CH <sub>3</sub> St. Sym.			
	3	--	1445 CH <sub>3</sub> Asym. Def.	1358 CH <sub>3</sub> Asym. Def.	1358 CH <sub>3</sub> Asym. Def.	1454 CH <sub>3</sub> Def. Def. Asym.	1476 CH <sub>3</sub> Def. Asym.	1480	1475	CH <sub>3</sub> Def. Asym.		
	4	--	1358 CH <sub>3</sub> Sym. Def.	1235 CH <sub>3</sub> Sym. Def.	1235 CH <sub>3</sub> Sym. Def.	1358 CH <sub>3</sub> Def. Def. Sym.	1374 CH <sub>3</sub> Def. Sym.	1397	1393	CH <sub>3</sub> Def. Sym.		
	5	1145	1142 C-C St.	1142 CH <sub>3</sub> Rock.	1142 CH <sub>3</sub> Rock.	1142 CH <sub>3</sub> Rock.	1150 CH <sub>3</sub> Rock.	1153	1144	CH <sub>3</sub> Rock.		
	6	802	805 CH <sub>3</sub> Wag.	805 C-C St.	805 C-C St.	805 C-C St.	806 C-C St.	808	804	C-C St.		
	7	514	515 C-Br St.	515 C-Br St.	515 C-Br St.	515 C-Br St.	520 C-Br St.	524	518	C-Br St.		
	8	--	303 Skeletal Def.	303 Skeletal Def.	303 Skeletal Def.	303 C-C Def. Skeletal Def.	303 Skeletal Def.	304	303	Skeletal Def.		
A <sub>2</sub>	9			2982 CH <sub>3</sub> Asym. St.			2978 <sup>b</sup>		CH <sub>3</sub> St.		51	
	10			1454 CH <sub>3</sub> Asym. Def.			1456 <sup>b</sup>		CH <sub>3</sub> Def.		51	



Table II - cont'd.

11		1026	CH <sub>3</sub> Rock.							1021 <sup>b</sup>	CH <sub>3</sub> Rock.	
12		--	CH <sub>3</sub> Torsion							267 <sup>b</sup>	CH <sub>3</sub> Torsion	
E 13	2970	2982	C-H <sub>3</sub> St. Asym.	2982	CH <sub>3</sub> Asym. St.	2970	C-H <sub>3</sub> St. Asym.	2992	CH <sub>3</sub> St. Asym.	2985	CH <sub>3</sub> St. Asym.	
14	--	2960	C-H <sub>3</sub> St. Asym.	2982	CH <sub>3</sub> Asym. St.	2970	C-H <sub>3</sub> St. Asym.	2977	CH <sub>3</sub> St. Asym.	2970	CH <sub>3</sub> St. Asym.	
15	2890	2890	C-H <sub>3</sub> St. Sym.	2960	CH <sub>3</sub> Sym. St.	2970	C-H <sub>3</sub> St. Sym.	2953	CH <sub>3</sub> St. Sym.	2945	CH <sub>3</sub> St. Sym.	
16	1455	1454	CH <sub>3</sub> Def. Asym.	1454	CH <sub>3</sub> Asym. Def.	1454	CH <sub>3</sub> Def. Asym.	1467	CH <sub>3</sub> Asym. Def.	1457	CH <sub>3</sub> Def. Asym.	
17	--	1445	CH <sub>3</sub> Def. Asym.	1454	CH <sub>3</sub> Asym. Def.	1454	CH <sub>3</sub> Def. Asym.	1460	CH <sub>3</sub> Asym. Def.	--	1449	CH <sub>3</sub> Def. Asym.
18	1370	--	CH <sub>3</sub> Def. Sym.	1235	CH <sub>3</sub> Sym. Def.	1358	CH <sub>3</sub> Def. Sym.	1420	CH <sub>3</sub> Sym. Def.	1375	1371	CH <sub>3</sub> Def. Sym.
19	1237	1235	C-C St. Rock.	1029	CH <sub>3</sub> Rock.	1235	C-C St. Rock.	1235	C-C St. + CH <sub>3</sub> Rock.	1238	1238	C-C St.
20	1034	1029	CH <sub>3</sub> Wag. Rock.	1029	CH <sub>3</sub> Rock.	1029	CH <sub>3</sub> Rock.	1033	CH <sub>3</sub> Rock.	1033	1031	CH <sub>3</sub> Rock.
21	--	932	CH <sub>3</sub> Wag. Rock.	932	C-C St. Rock.	932	CH <sub>3</sub> Rock.	931	CH <sub>3</sub> Rock.	--	930	CH <sub>3</sub> Rock.
22	--	398	Skeletal Deformation	398	C-C <sub>3</sub> Bend Def.	398	C-C-C Def.	398	C-C Def.	396	394	C-C Def.

Table II - cont'd.

23	--	268	Skeletal Deformation	268	Skeletal Rocking	268	C-C-Br Def.	268	C-Br Def.	285	CH <sub>3</sub> Torsion
24	--	--	--	--	--	--	--	--	--	272	C-C-Br

<sup>a</sup>Frequencies have the units cm<sup>-1</sup>.

<sup>b</sup>Calculated values from force field I, Chapter 5.

tope shifts.

There is only one published report of the vibrational spectrum of t-butyl bromide- $d_9$ , that of Zeil et al (112). They studied the infrared spectrum of the liquid in the sodium chloride region and proposed a partial assignment. In a subsequent paper (118), the same authors realized that this assignment was incorrect, but did not correct it. Their assignment is given for reference in Table III along with the one proposed in this thesis.

### 1.3.2 PROPERTIES OF THE SOLID STATE

A t-butyl bromide molecule has three methyl groups and one bromine atom attached to the central carbon atom. The sum of the carbon-bromine bond length and the van der Waal radius of bromine is close to the sum of the C-C bond length and the methyl group van der Waal radius (124). Also the C-C-C and C-C-Br angles are close to tetrahedral (125-128). Thus t-butyl bromide molecules are globular (1) and form more than one solid phase. In fact three solid phases exist and first order phase transitions occur at 231.6°K and 208.6°K (2). No uniform phase designation exists, and in this thesis the phase stable between the melting point (256.2°K) and 231.6°K is designated phase I, the intermediate phase is phase II, and the phase stable below 208.6°K is called phase III.

Table III

The Assignments of the Fundamental Vibration Frequencies of t-Butyl Bromide-d<sub>9</sub><sup>a</sup>

Symmetry	Mode	Zeil et al		This Work		
		IR Liquid		IR Gas	IR Liquid	
A <sub>1</sub>	1	2220	C-D <sub>3</sub> Asym. Stretch.	2221	2217	C-D <sub>3</sub> Asym. Stretch.
	2	2220	C-D <sub>3</sub> Sym. Stretch.	--	2118	C-D <sub>3</sub> Sym. Stretch.
	3	1286	CD <sub>3</sub> Asym. Deformation	1118	1114	CD <sub>3</sub> Sym. Deformation
	4	1206	CD <sub>3</sub> Sym. Deformation	--	1062	CD <sub>3</sub> Asym. Deformation
	5	1000	CD <sub>3</sub> Rock.	1011	1000	CD <sub>3</sub> Rock.
	6	700	C-C Stretch.	706	704	C-C Stretch.
	7	--		463	454	C-Br Stretch.
	8	--		274	273	Skeletal Deformation
A <sub>2</sub>	9	--		2221 <sup>b</sup>		C-D Stretch.
	10	--		1045 <sup>b</sup>		CD <sub>3</sub> Deformation
	11	--		772 <sup>b</sup>		CD <sub>3</sub> Rock.
	12	--		189 <sup>b</sup>		C-C Stretch.

. . . cont'd.

Table III - cont'd.

Symmetry	Mode	Zeil et al		This Work		
		IR		IR		
		Liquid		Gas	Liquid	
E	13	2242	C-D <sub>3</sub> Asym. Stretch.	2246	2240	C-D <sub>3</sub> Asym. Stretch.
	14	2242	C-D <sub>3</sub> Asym. Stretch.	2229	2217	C-D <sub>3</sub> Asym. Stretch.
	15	2242	C-D <sub>3</sub> Sym. Stretch.	2124	--	C-D <sub>3</sub> Sym. Stretch.
	16	1307	CD <sub>3</sub> Asym. Deformation	1214	1214	C-C Stretch.
	17	1307	CD <sub>3</sub> Asym. Deformation	1052	1049	CD <sub>3</sub> Asym. Deformation
	18	1206	CD <sub>3</sub> Sym. Deformation	1040	1039	CD <sub>3</sub> Asym. Deformation
	19	1117	C-C Stretch.	1040	1038	CD <sub>3</sub> Sym. Deformation
	20	1050	CD <sub>3</sub> Rock.	824	822	CD <sub>3</sub> Rock.
	21	820	CD <sub>3</sub> Rock.	742	738	CD <sub>3</sub> Rock.
	22			335	335	C-C-C Deformation
	23			239	242	C-C-Br Deformation
	24			--	206	CD <sub>3</sub> Torsion

<sup>a</sup>Frequencies have the units cm<sup>-1</sup>.

<sup>b</sup>Calculated values from force field I, Chapter 5.

Smyth and coworkers have studied the solid phases of t-butyl bromide-h<sub>9</sub> using optical, calorimetric and dielectric techniques (4, 129-130). They have shown that phases I and II are optically isotropic and phase III is anisotropic (130). Their calorimetric studies (129) showed that the entropy change at the III to II transition is 6.5 e.u./mole, while those for the II to I and I to the liquid are 1.1 e.u./mole and 1.8 e.u./mole respectively. They determined the dielectric constant at a frequency of  $5 \times 10^4 \text{ sec}^{-1}$  (129) and found it to be 11.6, 12.8, 9.5 and 2.4 for the liquid and the solid phases I, II, and III respectively. Later studies (4) showed essentially the same values of the dielectric constants at  $9.32 \times 10^9 \text{ sec}^{-1}$ . They also measured (4) the dielectric loss at the latter frequency and concluded that t-butyl bromide molecules can reorient at frequencies greater than  $9.32 \times 10^9 \text{ sec}^{-1}$  in the solid phases I and II and in the liquid.

Proton magnetic resonance (PMR) studies (5) in the temperature range 0°C to -196°C showed a sharp increase in the linewidth at the II to III transition, indicating a sudden decrease in the molecular mobility at this transition. The dielectric constant values indicate that the molecular dipoles cannot reorient in phase III. However, the width of the PMR lines just below the II to III transi-

tion is too small to indicate that the molecules are completely rigid, and rotation of the methyl groups about the C-C bonds and rotation of the molecule about the C-Br bond must be postulated to explain this width. These rotational motions become quenched out as the temperature is lowered, and at about 77°K the solid behaves like a rigid lattice. At temperatures above the III to II transition the linewidth is very small, similar to that found for t-butyl chloride in its plastic phases (4). For t-butyl chloride, this width has been explained (6) in terms of molecular rotation about all three inertial axes and translational diffusion, and a similar explanation presumably applies to t-butyl bromide in phases I and II.

Single crystal X-ray diffraction studies (131) indicate that phase I of t-butyl bromide has a face-centered cubic structure with 4 molecules per unit cell. The molecules occupy sites of cubic symmetry, while the molecular symmetry is only  $C_{3v}$ . Molecules can occupy sites of diffraction symmetry higher than the molecular symmetry only if the crystal is disordered or if the molecules are undergoing rapid reorientation. The distance between the neighbouring molecular centres is 6.2 Å, smaller than the 7.5 Å diameter of the sphere swept by a freely rotating molecule, and therefore the molecular reori-

## 2. FOURIER SPECTROSCOPY IN THE FAR-INFRARED

The far-infrared spectra reported in this thesis were obtained using the relatively new technique of Fourier spectroscopy. This chapter gives a brief introduction to the technique and the principles underlying it. The experimental details are given in Section 2 of the next chapter.

The major difficulties in far-infrared spectroscopy are the low intensity of the sources and the low sensitivity of the detectors used in this part of the spectrum (133). In the normal dispersion spectrometers (prism or grating) these problems are compounded by the fact that, at any given instant, the detector receives light from only a small fraction of the spectrum to be studied. Also the beam size is limited by the slit opening which must be kept very small for good resolution. Thus the detector receives only a very small part of the far-infrared radiation produced by the source, resulting in a low signal to noise ratio. Fourier spectroscopy reduces this problem by simultaneously looking at all frequencies in the spectrum to be studied. This has been called the ' Fellgett advantage ' or ' multiplex advantage ' (134). Also the resolution is not a function of the beam size and hence no slits are



required to limit the aperture of the incident beam. Thus one can use the whole beam generated by the source. This is known as the 'Jacquinot advantage' or 'throughput advantage' (134).

The use of Fourier infrared spectroscopy has greatly increased in the last twenty years. Although Fourier spectrometers are still not very common in chemical laboratories, they have been extensively used in the study of extra-terrestrial infrared sources in astrophysics. Four international conferences have been organized on this subject (135). There is a growing volume of literature in this field and here reference is given to a few review articles only (135-140).

The underlying principle of Fourier spectroscopy is that, knowing the intensity of a light beam formed by the combination of two light beams as a function of the phase difference of the constituent beams, one can express the intensity of the resultant beam as a function of its component frequencies. Since this involves interference between the two light beams, the instruments used for Fourier spectroscopy in the infrared are called 'interferometers'. There are several types of interferometer described in the literature, for example, Michelson, Lamellar grating, and Fabry-Perot interferometers (135,

entation must be subject to steric restriction.

Higgins et al (132) measured the density of t-butyl bromide at different temperatures in phase I. They found good agreement between their values of the molecular volume and those from X-ray data, and therefore concluded that phase I does not contain a large number of vacant sites.

Durig et al (113) reported the Raman spectra of the solid between 30 and  $100\text{ cm}^{-1}$ , for sample temperatures between  $-60$  and  $-190^\circ\text{C}$ , and also reported the far-infrared spectrum of the solid at  $-190^\circ\text{C}$  between 300 and  $33\text{ cm}^{-1}$  (Section 1.3.1). They observed two lattice modes below  $100\text{ cm}^{-1}$  and made tentative assignments.

All of the above literature deals with the solid phases of t-butyl bromide- $\text{h}_9$  only. There appears to be no published work on the solid state of t-butyl bromide- $\text{d}_9$ .

141). The Michelson interferometer is the most commonly used for the infrared region and was also used in this work. The basic principles involved in the Michelson interferometer are discussed below.

Figure 9 shows a block diagram of a typical Michelson interferometer. The entire optical system is enclosed and can be evacuated to a pressure of less than 0.1 torr to avoid absorption by atmospheric water vapour. The light coming from the source S, which is usually a quartz-jacketed high-pressure mercury lamp for the far-infrared region, is collimated by an off-axis paraboloid mirror,  $P_1$ . This parallel beam of radiation meets the beam splitter BS at an angle of  $45^\circ$ . The beam splitter consists of a sheet of material which partly reflects the beam and partly transmits it and, ideally, does not absorb in the spectral region of interest. Mylar, polyethylene terephthalate, is normally used in far-infrared interferometers. The beam-splitter divides the incident beam into two parts at right angles to each other. These two beams are reflected back by the mirrors  $M_1$  and  $M_2$ .  $M_1$  is a moving mirror and  $M_2$  is a stationary mirror. The two beams reflected by the mirrors  $M_1$  and  $M_2$  meet at the beam-splitter and are again reflected or transmitted. The interference between these two beams depends upon the fre-

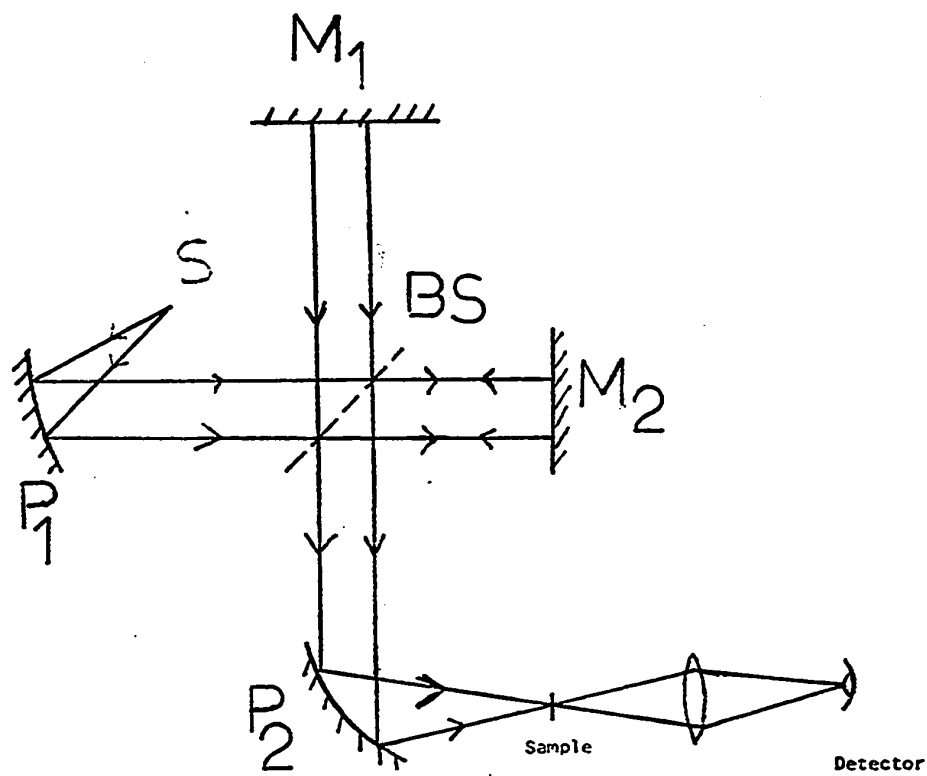


Figure 9

A block diagram of the Michelson interferometer.

quency of the radiation and the difference between the optical paths travelled by the two beams  $BM_1B$  and  $BM_2B$ . After the second passage through the beam splitter, two beams are again obtained, one returning to the source and the second one travelling to the sample and detector. The second beam is focussed by a second off-axis paraboloid mirror  $P_2$ , and the sample is placed at the focal point. The beam passes through the sample and is focussed on the detector via a polythene lens and a conical light pipe. A Golay detector is usually used for the far-infrared region. The high frequency radiation is prevented from reaching the detector by placing suitable filters in the beam.

The intensity of the radiation received by the detector is a function of the optical path difference,  $x$ . When there is no path difference,  $x = 0$ , all the radiation reflected by mirrors  $M_1$  and  $M_2$  interferes constructively, irrespective of its frequency. At any other value of  $x$ , light at some of the frequencies contained in the beam interferes destructively and thus a lower signal than at  $x = 0$  must result.

If the interfering beams consist of monochromatic radiation of wavelength  $\lambda$ , then the intensity of the light incident on the detector is given by

$$I'(x) = A(1 + \cos 2\pi\nu x) \quad 21$$

where  $\nu = 1/\lambda$  and is the wave number of the radiation and  $A$  is a constant (142). If the radiation is polychromatic one must integrate the right hand side of equation 21 over all frequencies.

$$\text{Thus,} \quad I'(x) = \int_{-\infty}^{+\infty} I(\nu) d\nu + \int_{-\infty}^{+\infty} I(\nu) \cos(2\pi\nu x) \cdot d\nu$$

$$\text{or} \quad I'(x) = I'(\infty) + \int_{-\infty}^{+\infty} I(\nu) \cos(2\pi\nu x) d\nu \quad 22$$

where  $I'(\infty)$  is the signal at infinite path difference and can be obtained from the asymptotic value of  $I'(x)$ . A plot of  $I'(x)$  against  $x$  is called an 'interferogram'. Figure 10 shows an interferogram for light of frequencies between 0 and  $230 \text{ cm}^{-1}$  with water vapour in the light path. Rearranging equation 22 one has

$$F(x) = I'(x) - I'(\infty) = \int_{-\infty}^{+\infty} I(\nu) \cos(2\pi\nu x) d\nu \quad 23$$

where  $F(x)$  is called the 'interferogram function'. Equation 23 is a Fourier integral and its Fourier transform is

$$I(\nu) = \int_{-\infty}^{+\infty} F(x) \cos(2\pi\nu x) dx \quad 24$$

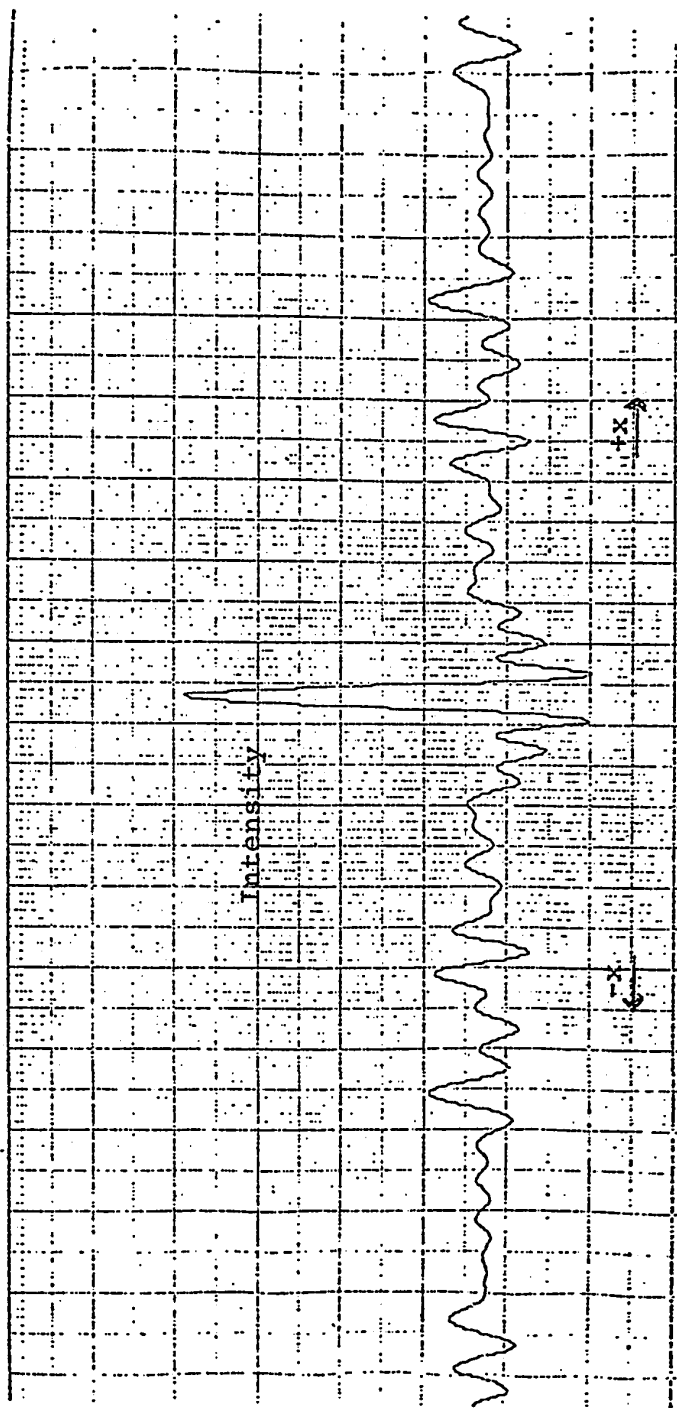


Figure 10

A typical interferogram. This one was recorded for light of frequencies  
0-230  $\text{cm}^{-1}$  with water vapour in the light path.

The line is not smooth because the step drive was used.

In practice  $F(x)$  can be determined only over a finite interval  $-x$  to  $+x$  so that the calculated spectrum  $I(\nu)$  is given by a truncated integral

$$I(\nu) = \int_{-x}^{+x} F(x) \cos(2\pi\nu x) dx \quad 25$$

The effect of using a truncated integral is to introduce side bands around any peak in the spectrum. These effects can be minimized by multiplying the interferogram function  $F(x)$  by a suitable function  $A(x)$ . This process is called apodization and various apodization functions are discussed in the literature (143, 144). In this work a triangular apodization function was used, that is  $A(x)$  was  $(1 - \frac{x}{x_{\max}})$ . In calculating the spectrum, the Fourier cosine integral is approximated by a summation.

$$I(\nu) = \sum_{-x}^{+x} F(x) \cos(2\pi\nu x) \Delta x \quad 26$$

The above calculations require precise knowledge of the optical path difference  $x$ . In practice there is always some error in the experimental value of  $x$  and it introduces 'phase error' into the calculations. Various procedures have been described to overcome this problem (145-147). In the far-infrared region, for moderate resolution, the number of sample points is of the order of a



thousand and the problem of the phase error can be eliminated by using equal numbers of points with positive and negative optical path differences, and replacing the simple cosine function in equation 21 with an exponential function. Equation 21 thus becomes

$$I'(x) = A[1 + \exp(2\pi i\nu x)] \quad 27$$

Then equation 26 is replaced by

$$I(\nu) = [c^2 + s^2]^{\frac{1}{2}} \quad 28$$

where

$$c = \sum_{-x}^{+x} F(x) \cos(2\pi\nu x) \Delta x \quad 29$$

and

$$s = \sum_{-x}^x F(x) \sin(2\pi\nu x) \Delta x \quad 30$$

Information theory (148) shows that in order to obtain all the information in the spectral range 0 to  $\nu_{\max}$ , it is essential to sample points from the interferogram at intervals of

$$\Delta x = \frac{1}{2\nu_{\max}} \quad 31$$

For the spectral range 0 to  $500 \text{ cm}^{-1}$  one must, therefore, sample points at intervals equal to or less than  $\frac{1}{2 \times 500}$  cm or 10 microns.

The theoretical resolution  $\Delta\nu$ , of the spectrum

advantages, particularly with its high resolution capability, than instrumental disadvantages over grating spectroscopy. It is expected that its use in chemical laboratories will increase with the availability of faster and cheaper computers.

obtained from an interferometer is determined by the maximum optical path difference  $x$  of the interfering beams and is given by (149)

$$\Delta\nu = \frac{1}{x} \quad . \quad 32$$

Thus, for a resolution of  $0.3 \text{ cm}^{-1}$  one has to sample points up to a path difference of  $\frac{1}{0.3} = 3.33 \text{ cm}$ , which is not very difficult. Thus one can readily achieve high resolution which is very difficult to obtain using conventional far-infrared spectrometers (150).

The main disadvantage of Fourier spectroscopy is that one does not see the spectrum until the computer has completed the calculations. This introduces a time lag between the experiment and the reception of the results. Thus one cannot detect any immediate changes in the sample. This problem can be minimized by the use of a fast scanning interferometer directly connected to a bench computer (151).

Most interferometers are single beam instruments. This results in the appearance of extra bands in the spectrum due to absorption by the cell windows and beam splitter. These effects can be eliminated by dividing the spectrum of the cell plus sample by the spectrum of the empty cell (152). Fourier spectroscopy offers more fundamental

### 3. EXPERIMENTAL

#### 3.1 PREPARATION AND PURIFICATION OF CHEMICALS

tertiary butyl bromide- $h_9$  was obtained from Matheson Coleman and Bell and was of research grade. It was washed twice with a 10% aqueous solution of sodium bicarbonate and then with distilled water until it was free from alkali. It was then dried overnight over anhydrous calcium chloride and was distilled through a 'Teflon spinning band column'. The fraction boiling at  $346.3 \pm 0.5^\circ K$  was collected, literature b.p.  $346.4^\circ K$  (130). No impurity lines were detected in its proton magnetic resonance spectrum or in its mass spectrum.

t-butyl bromide- $d_9$  was prepared by reacting deuterium bromide with t-butyl alcohol- $d_9$ , obtained from Merck, Sharp and Dohme of Canada. 5 gm of t-butyl alcohol- $d_9$  was added to 50 ml of an azeotropic solution of DBr in  $D_2O$ , and stirred for about 2 hours at room temperature. The product separated as a lighter layer and was washed twice with a 10% solution of sodium carbonate in  $D_2O$ . It was then washed with heavy water until it was free from alkali, and was dried and distilled as described for the light compound. The fraction boiling at  $346.3 \pm 1^\circ K$  was collected. Its purity was checked by mass spectroscopic analysis. The only impurities detected were less than 7%

of t-butyl bromide- $d_8$  and less than 1% of the  $-d_7$  isotope. The product was kept in sealed, light-proof containers in the refrigerator until required.

### 3.2 INFRARED SPECTROSCOPY

Gaseous samples were contained in conventional 10 cm path length cells, fitted with cesium iodide windows for the region  $4000-200\text{ cm}^{-1}$  and with polyethylene windows for the region  $400-10\text{ cm}^{-1}$ . The sample temperature was about  $303^\circ\text{K}$  for the mid-infrared region and about  $298^\circ\text{K}$  for the far-infrared region.

In the early stages of this work the liquid and solid samples were contained in a FH-01 liquid cell, mounted in a VLT-2 variable low temperature cell, both purchased from Beckman-R.I.I.C. Later an improved version of this cell was designed and constructed in the chemistry department workshop. This is shown in Figure 11. A small cell, containing the liquid sample, was inserted into the copper block, which was in direct contact with liquid nitrogen. The sample temperature was measured with an iron-constantan thermocouple inserted through the metal of the liquid cell to touch the window. The thermocouple indicated a temperature of  $78^\circ\text{K}$  with liquid nitrogen in the reservoir. Higher temperatures could be obtained by passing an electric current through heaters attached to the sides of the copper

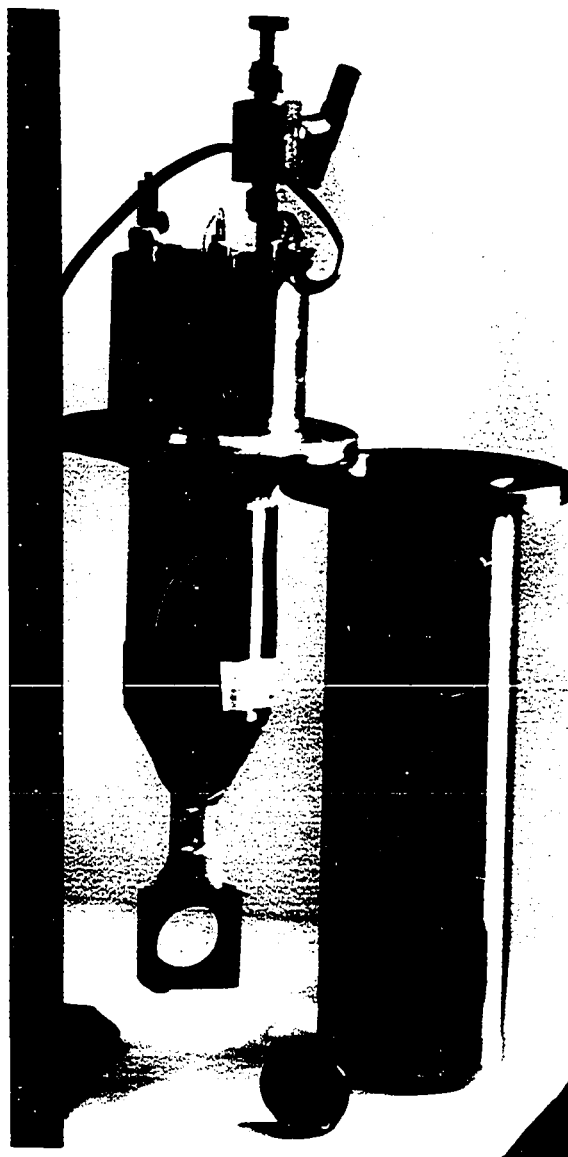


Figure 11

The low temperature cell used for recording the infrared spectra.

block. The current was regulated by a 'thermo-electric-temperature controller' which uses a copper-constantan thermocouple to sense the temperature of the copper block, and regulates according to the difference between the actual and the desired temperature. The temperature of the sample-cell windows could be controlled to  $\pm 1^\circ\text{K}$  in the range of  $300^\circ\text{K}$  to  $78^\circ\text{K}$ . The temperature of the sample was shown to be within  $3^\circ\text{K}$  of the measured temperature by the numerous studies of the III to II transition of t-butyl bromide at  $231.6^\circ\text{K}$  (2) and of propane freezing at  $83.4^\circ\text{K}$  (153). Polyethylene or cesium iodide windows were used for both the sample cell and the vacuum jacket. These windows tend to deform and hence, even though the sample-cell windows were held apart by a teflon spacer of known thickness, the sample thickness is not known precisely. The polyethylene windows were bevelled on the outside to remove the interference fringes arising from them in the far-infrared region.

A Beckman IR-12 spectrometer was used to record the infrared spectra between 200 and  $4000\text{ cm}^{-1}$ . This instrument was fitted with the Beckman Fiducial Marker accessory which was calibrated using standard gases (154). The frequency accuracy of the spectrometer is about  $\pm 0.5\text{ cm}^{-1}$  below  $2000\text{ cm}^{-1}$  and about  $1\text{ cm}^{-1}$  above  $2000\text{ cm}^{-1}$ .

The far-infrared spectra were mainly obtained using the Beckman-R.I.I.C. model FS-720 Michelson interferometer. The principles of the method have been discussed earlier, in Chapter 2, and only the practical details are described here. The signal from the Golay detector of the interferometer was amplified and recorded, both as an interferogram on a strip chart recorder and as digital data using an IBM model-026 card punch. Interferometric data was recorded with both positive and negative path differences. The digital data so obtained was processed using the program BOBS (155). This program calculates the intensity of the radiation reaching the detector after transmission through the sample,  $I_t$ , as a function of frequency. Two interferograms are needed to determine the absorbance,  $\log_e I_0/I_t$ , of the sample as a function of frequency. One, in which the cell plus sample is placed just in front of the detector, yields  $I_t$ , while the second, in which the cell with no sample is used, yields  $I_0$ , both as a function of frequency. An option in the program permits the acceptance of these two interferograms and the calculation of absorbance. The results are obtained both as printed output and as a plotted spectrum of intensity or absorbance against wavenumber. The interferogram is used only to show obvious machine failures.



agreement between the results obtained from the different instruments was good.

### 3.3 RAMAN SPECTROSCOPY

The Raman spectrometer consisted of a Carson Laboratories model 10SP Ar<sup>+</sup>/Kr<sup>+</sup> laser, a SPEX sample illumination chamber, a SPEX model 1401 monochromator, a FW-130 photomultiplier operated at -25°C, photon counting electronics and a strip-chart recorder. The Raman spectra were obtained using the yellow 5682 Å line or the red 6471 Å line, both of Kr<sup>+</sup> and each with a power of about 120 mW at the laser and about 40 mW at the sample, as exciting radiation. The exciting lines were polarized and the analyzer was placed between the sample and the monochromator. The liquid samples were sealed in pyrex melting point capillaries, with internal and external diameters of 1 mm and 1.5 mm respectively. The spectra were recorded using a 90° scattering geometry. The frequency accuracy of the monochromator was checked by the spectra of carbon tetrachloride (15), benzene (15), and indene (157) and was found to be better than 1 cm<sup>-1</sup>. The spectrometer was calibrated by recording the symmetric C-Cl stretching mode band of carbon tetrachloride every time it was used.

The Raman samples were maintained at low tem-

perature by placing the capillary containing the sample in a cylindrical, unsilvered, glass dewar, open at both ends, through which was passed a continuous flow of cold nitrogen gas obtained by boiling liquid nitrogen. The temperature was recorded on a strip chart recorder, using an iron-constantan thermocouple placed next to the sample. The temperature could be controlled to  $\pm 3^\circ\text{K}$ , between room temperature and  $90^\circ\text{K}$ , by controlling the voltage applied to the heater in the liquid nitrogen.

#### 3.4 X-RAY POWDER PHOTOGRAPHY

A Jarrel-Ash precession camera was used as a flat-plate powder camera. Two X-ray lines,  $\text{Cu K}_\alpha$  and  $\text{Co K}_\alpha$  with wavelengths of  $1.541 \text{ \AA}$  and  $1.792 \text{ \AA}$  respectively (153), were used. The X-ray films used were obtained from Ilford Ltd. of England and were of Industrial G quality. The camera was calibrated by recording the powder photographs of sodium chloride at  $295^\circ\text{K}$  and at  $120^\circ\text{K}$  (158).

The samples were contained in Lindemann glass capillaries with an internal diameter of 0.3 mm and wall thickness of 0.01 mm. The capillary was attached to the goniometer head of the camera by a teflon adapter. The set-up shown in Figure 12 was used to maintain the X-ray samples at low temperatures (159). The samples were cooled

The calibration of the interferometer was checked using the pure rotational spectrum of water vapour (156) and was found accurate to better than  $\pm 0.2 \text{ cm}^{-1}$ . The accuracy of the frequencies in the far-infrared region reported in this thesis is limited by the width of the corresponding spectral feature. The resolution of the interferometer was checked by recording the pure rotation spectrum of methyl chloride and was found to be as expected from theory (see Chapter 2).

A continuous, Moiré drive or a discontinuous, step drive was used for the moving mirror. The agreement between the spectra obtained from the drives was excellent below  $200 \text{ cm}^{-1}$ . Above  $200 \text{ cm}^{-1}$  the step drive was completely inaccurate and only the Moiré drive was used. The interferometer was used to obtain the spectra between 350 and  $10 \text{ cm}^{-1}$ . However, five different interferograms run with different combinations of beam splitter, filter, and sampling interval are required to cover this range with optimum performance. The spectra from these interferograms overlap extensively and excellent agreement was obtained in the overlap regions.

The spectra of the gaseous and the liquid samples between 500 and  $100 \text{ cm}^{-1}$  were also recorded using a Beckman IR-11 spectrometer, calibrated with water vapour. The

by a stream of cold nitrogen gas obtained by boiling liquid nitrogen.

A continuous stream of warm and dry nitrogen, surrounding the cold stream, Figure 12, prevented the condensation of atmospheric water vapour on the sample. The powder photographs did not show any diffraction which could be attributed to ice. The temperature of the sample was measured by placing an iron-constantan thermocouple near the sample but not in the path of the incident X-rays. It was possible to maintain the sample temperature between room temperature and  $120 \pm 10^\circ\text{K}$  for periods of 24 hours or less. The  $10^\circ\text{K}$  uncertainty in the temperature arises from the relative positions of the sample and the thermocouple, and the fluctuations observed in the temperature indicated by the thermocouple were less than  $3^\circ\text{K}$ . The X-ray photographs were taken at a temperature of  $120 \pm 10^\circ\text{K}$  with exposure times varying from 2 hours to 12 hours. The sample-to-film distance was  $6.00 \pm 0.03$  cm.

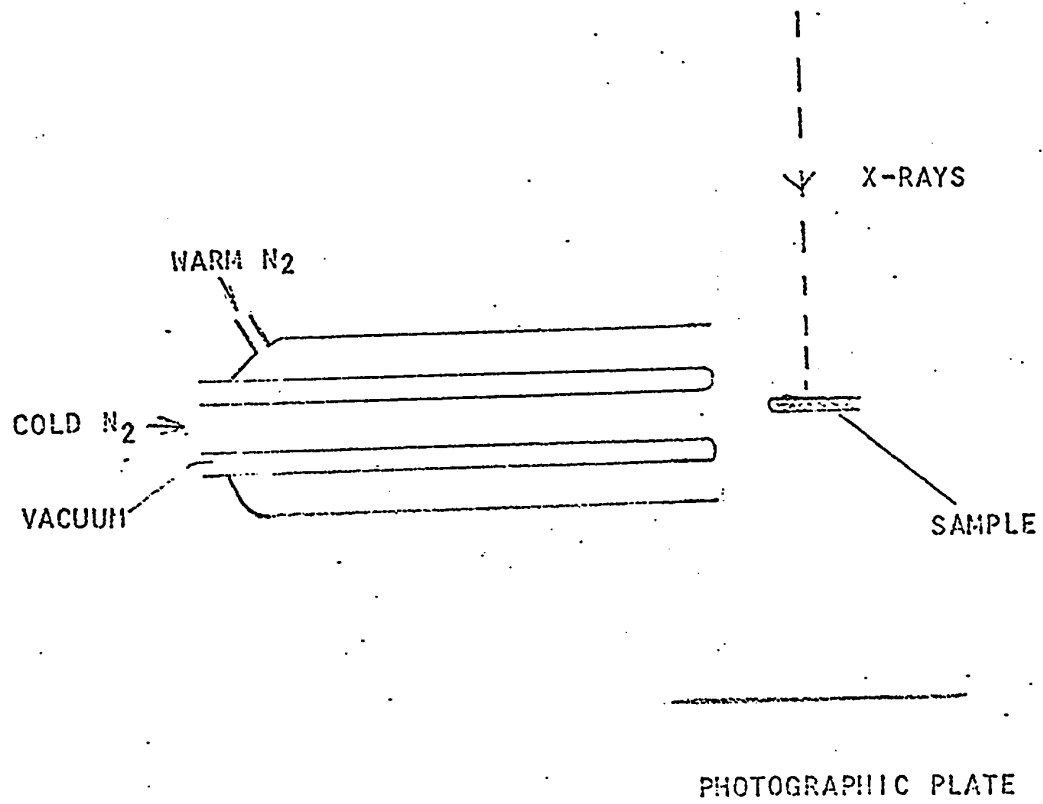


Figure 12

A schematic diagram of the set up used for recording the low temperature X-Ray photographs.

#### 4. THE INTRAMOLECULAR VIBRATIONS OF t-BUTYL BROMIDE- $h_9$ AND $d_9$

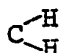
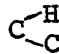
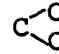
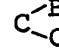
The infrared spectra of the gas and liquid phases of the two isotopes of t-butyl bromide and the Raman spectra of their liquid phases are presented in this chapter. The observed spectral features are assigned to the intramolecular vibrational modes of the molecules.

##### 4.1 STRUCTURAL CONSIDERATIONS

The interpretation of electron diffraction (125-127) and microwave (128) measurements on t-butyl bromide- $h_9$  confirms the expected  $C_{3v}$  symmetry for the heavy atom skeleton of the molecule. These measurements have not yielded any information about the position of the hydrogen atoms. There is no similar work available for t-butyl bromide- $d_9$ . The vibrational representation shown in Table IV is based on the assumption of  $C_{3v}$  symmetry for both molecules including the hydrogen (or deuterium) atoms. The  $4A_2$  modes are inactive in both the infrared and the Raman spectra, while  $8A_1$  and  $12E$  modes are active in both types of spectra. These group theoretical predictions are only strictly valid for molecules in the gas phase. The  $A_2$  modes may appear in the spectra of the liquid because the molecular symmetry is lowered by the intermolecular force field, but these

Table IV

Vibrational representation of t-butyl bromide.

Types of Vibration	Symmetry Species		
	A <sub>1</sub>	A <sub>2</sub>	E
C-H stretches	2	1	3
 C-H bends	2	1	3
 C-H bends	1	1	2
C-C stretches	1	0	1
C-Br stretch	1	0	0
 C-C bends	1	0	1
 C-Br bends	1	0	1
CH <sub>3</sub> torsion	0	1	1
Total	8	4	12
Activity	Raman + IR	Inactive	Raman + IR

absorptions are expected to be weak.

Williams et al (128) report the moment of inertia of t-butyl bromide- $h_9$  about the axes perpendicular to the molecular symmetry axis. There is no report of measurement or calculation of the moments of inertia for t-butyl bromide- $d_9$ . The principal moments of inertia of t-butyl bromide- $h_9$  and - $d_9$ , calculated from estimated bond lengths (124, 128) and tetrahedral bond angles, are given in Table V together with the experimental values for the - $h_9$  compound. These calculated values are about 1.5% larger than the corresponding experimental values, which were, however, felt to be sufficiently good to yield reliable estimates of the band contours. The molecules are 'prolate' symmetric-top rotors, because the moment of inertia about the symmetry axis is less than that about any axis perpendicular to it.

Ueda and Shimanouchi (160) have defined two parameters  $x$  and  $y$ , which are determined by the molecular moments of inertia, to predict the shapes of the infrared absorption bands of asymmetric top molecules in the gas phase. The value of  $x$  equals 2 for symmetric top molecules while  $y$  is -0.44 for the light compound and -0.49 for the heavy compound. The asymmetric molecule, whose  $x$



Table V

Moments of inertia of t-butyl bromide-h<sub>9</sub> and t-butyl bromide-d<sub>9</sub>.

Molecule	Moments of Inertia (gm cm <sup>2</sup> )			
	I <sub>A</sub>		I <sub>B</sub>	
	Observed	Calculated	Observed <sup>a</sup>	Calculated <sup>b</sup>
C <sub>4</sub> H <sub>9</sub> <sup>79</sup> Br	--	183.5 x 10 <sup>-40</sup>	410.5 x 10 <sup>-40</sup>	416.37 x 10 <sup>-40</sup>
C <sub>4</sub> H <sub>9</sub> <sup>81</sup> Br	--	183.5 x 10 <sup>-40</sup>	413.7 x 10 <sup>-40</sup>	419.8 x 10 <sup>-40</sup>
C <sub>4</sub> D <sub>9</sub> <sup>79</sup> Br	--	240.8 x 10 <sup>-40</sup>	--	487.9 x 10 <sup>-40</sup>
C <sub>4</sub> D <sub>9</sub> <sup>81</sup> Br	--	240.8 x 10 <sup>-40</sup>	--	492.1 x 10 <sup>-40</sup>

<sup>a</sup>Reference 128.

<sup>b</sup>Calculated assuming all bond angles to be tetrahedral and the following band lengths: R<sub>C-H</sub> = 1.093 Å, R<sub>C-C</sub> = 1.54 Å and R<sub>C-Br</sub> = 1.96 Å [References (124, 128)].

and  $\gamma$  parameters are nearest to the above values for t-butyl bromide, is of type 34 in Ueda and Shimanouchi's classification (160). The band shapes predicted by Ueda and Shimanouchi's classification are shown in Figure 13. Parallel bands of t-butyl bromide, due to  $A_1$  vibrations, should resemble the A type bands while perpendicular bands, due to degenerate vibrations, should have shapes intermediate between those of the B and C type bands. Thus parallel bands should have clearly defined maxima in the P and R branch envelopes, well separated from a prominent Q branch, while the perpendicular bands do not have well pronounced maxima in the P, Q, or R branches. A similar description of the parallel and perpendicular bands is obtained from calculations based on the ' $\beta$ ' parameter of Gerhard and Dennison (161).

Here it must be mentioned that both band shape calculations employ simplified models which neglect Coriolis coupling, centrifugal distortion, and the change in moments of inertia with vibrational state (162). Therefore one can take the above predictions only as a guide, and should consider all other evidence, such as Raman polarization data for the liquid state, before assigning any particular band to an  $A_1$  or an E vibrational mode.

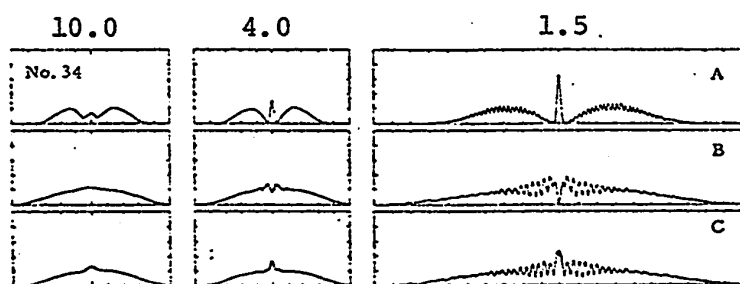


Figure 13

Calculated infrared band shapes for molecules of type 34 of Ueda and Shimanouchi's classification (63). The numbers on the top refer to the halfwidth of the slit function, in  $\text{cm}^{-1}$ , used in calculating the band shape.

#### 4.2 RESULTS FOR t-BUTYL BROMIDE-h<sub>9</sub>

The infrared spectrum of gaseous t-butyl bromide-h<sub>9</sub> is shown in Figures 14 and 15 for the region 4000-200 cm<sup>-1</sup>. The frequencies of the different features, accurate to ±1 cm<sup>-1</sup> for the sharp features, are listed in Table VI along with the relative intensities. The spectra were recorded at 1 cm<sup>-1</sup> resolution, using gas pressures of 8.0 and 1.0 cm of mercury. The strong bands were further studied at a resolution of about 0.5 cm<sup>-1</sup> and are shown on an expanded scale in Figure 16. The bands at 304, 524, 808, and 1153 cm<sup>-1</sup> are clearly parallel bands with the 1153 cm<sup>-1</sup> band showing 3Q branches. The band at 1375 cm<sup>-1</sup> has a sharp Q branch but no separate maxima for the P or R envelopes and seems to be a perpendicular band. The band at 1238 cm<sup>-1</sup> has the shape of a distorted parallel band. There is a very broad band between 1430 and 1500 cm<sup>-1</sup> showing the Q branch of a parallel band at 1480 cm<sup>-1</sup>. The associated P envelope merges with a broad band with maximum absorption at about 1457 cm<sup>-1</sup>. The only other strong bands are between 2840 and 3020 cm<sup>-1</sup>, and have complex shapes, presumably due to the overlap of the rotational envelopes of several bands. The only band which can be easily characterized in this region is a parallel band with its Q branch at 2934 cm<sup>-1</sup>.

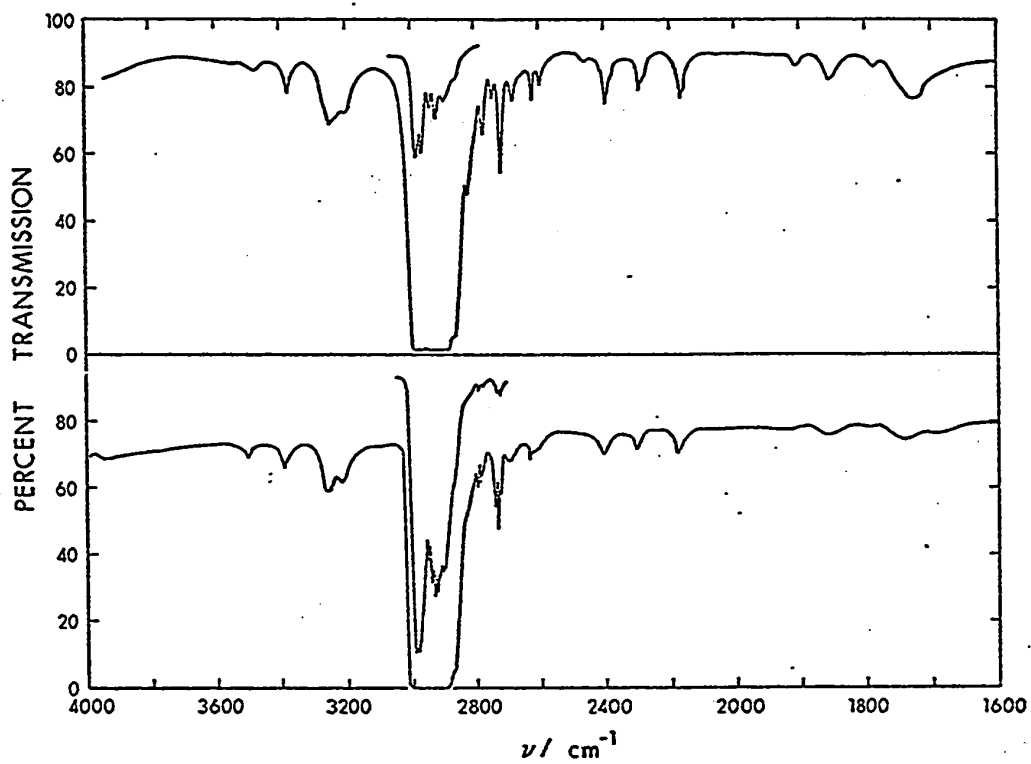


Figure 14

Infrared spectra of t-butyl bromide- $\text{h}_9$  in the gas (lower box) and liquid (upper box) phases, between 4000 and 1600  $\text{cm}^{-1}$ .

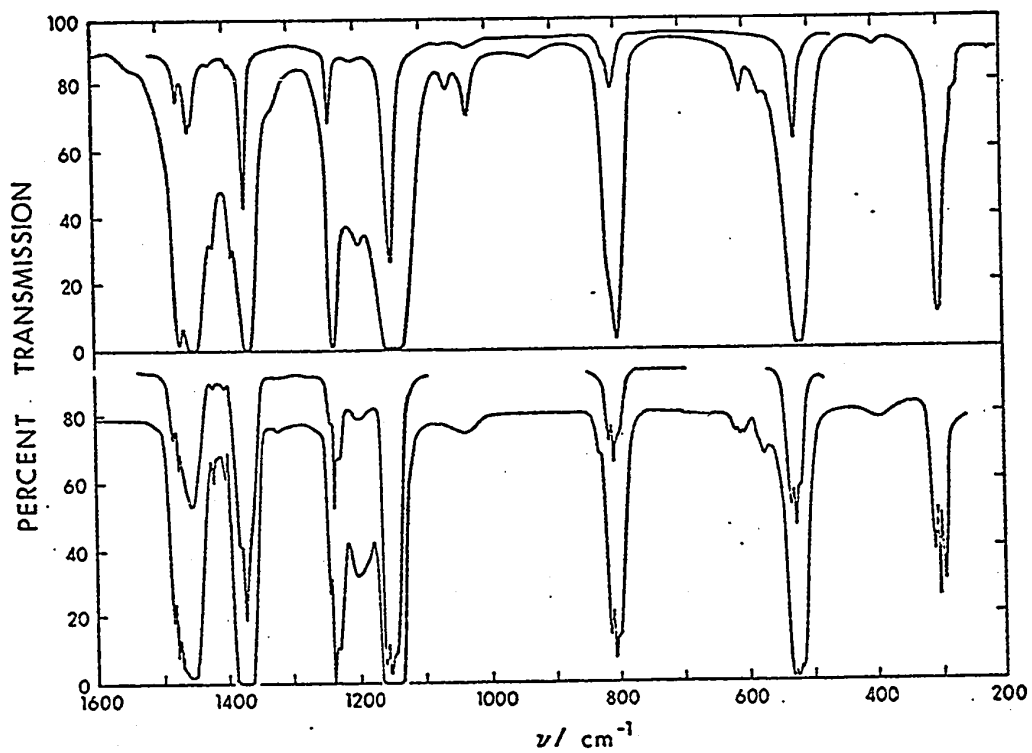


Figure 15

Infrared spectra of t-butyl bromide- $\text{h}_9$  in the gas (lower box) and liquid (upper box) phases between 1600 and 200  $\text{cm}^{-1}$ .



Table VI - cont'd.

Infrared			Raman			Assignment
Gas	Liquid		Liquid		Depolarization Ratio	
$\nu$ -l cm <sup>-1</sup>	Inten- sity	$\nu$ -l cm <sup>-1</sup>	Inten- sity	$\Delta\nu$ -l cm <sup>-1</sup>		Inten- sity
2875		2870	sh	2850	sh	$\nu_3 + \nu_4$
2800	w	2827	w			$\nu_4 + \nu_{16}$
2790	w	2782	w	2783	w	$\nu_{16} + \nu_{18}$
2733	w	2754	vW	2726	s	$\nu_{17} + \nu_{18}$
2695	vW	2689	vW			$2\nu_4 + \nu_{18}$
2634	w	2629	w			$\nu_4 + \nu_{19}$
		2604	vW			$\nu_4 + \nu_{19}$
		2471	vW			$\nu_{18} + \nu_{19}$
2404	w	2399	w			$2\nu_{19}$
2302	w	2298	w			$\nu_{18} + \nu_{20}$
2182	w	2171	w			$2\nu_5, \nu_{18} + \nu_{21}$
		1911	vW			$\nu_6 + \nu_{18}$
						$\nu_4 + \nu_7$
						... cont'd.



Table VI - cont'd.

Infrared			Raman			Assignment
Gas	Liquid		Liquid		Depolarization Ratio	
$\nu$ -l cm <sup>-1</sup>	Inten- sity	$\nu$ -l cm <sup>-1</sup>	Inten- sity	$\Delta\nu$ -l cm <sup>-1</sup>		Inten- sity
1859	vw b	1859	w			$\nu_3 + \nu_{22}$
		1791	vw b			$\nu_3 + \nu_8$
1734	w	1731	w			$\nu_6 + \nu_{21}$
1480	s	1475	s			$\nu_3$
1457	s	1457	s	1459	m	$\nu_{16}$
		1449	sh	1447	sh	$\nu_{17}$
1423	w	1423	w	1425	sh	$\nu_{20} + \nu_{22}$
1406	w					$\nu_6 + 2\nu_8$
1397	sh	1393	w	1395	w	$\nu_4$
1375	vs	1371	vs	1372	w	$\nu_{18}$
		1324	sh			$\nu_8 + \nu_{20}$
1238	s	1238	w	1236	w	$\nu_{19}$
1203	w	1198	w			$\nu_{21} + \nu_{24}$
1153	vs	1144	vs	1142	vs	$\nu_5$
						.. cont'd.

Table VI - cont'd.

Infrared			Raman			Assignment
Gas	Liquid		Liquid			
$\nu_{-1}$ cm <sup>-1</sup>	Inten- sity	$\nu_{-1}$ cm <sup>-1</sup>	Inten- sity	$\Delta\nu_{-1}$ cm <sup>-1</sup>	Inten- sity	Depolarization Ratio
1033	vw b	1059	w	1031	w	0.75
		1031	w			
		930	vw	931	w	0.8
		813	sh	815	sh	0.5
808	s	804	s	805	s	0.5
				643	w	0.1
608	w	604	w	604	w	0.1
571	w	571	sh	571	sh	0.1
524	s	518	s	516	vs	0.1
396	vw	394	w	396	w	0.8
304	s	303	s	301	vs	0.15
		285	sh	285	sh	DP
		272	sh	271	sh	0.7
		214	vw	215	w	0.15
				187	w	0.15

Table VI - cont'd.

<sup>a</sup>Symbols in the above table are as follows:

vs = very strong

s = strong

m = medium

w = weak

vw = very weak

sh = shoulder

DP = depolarized

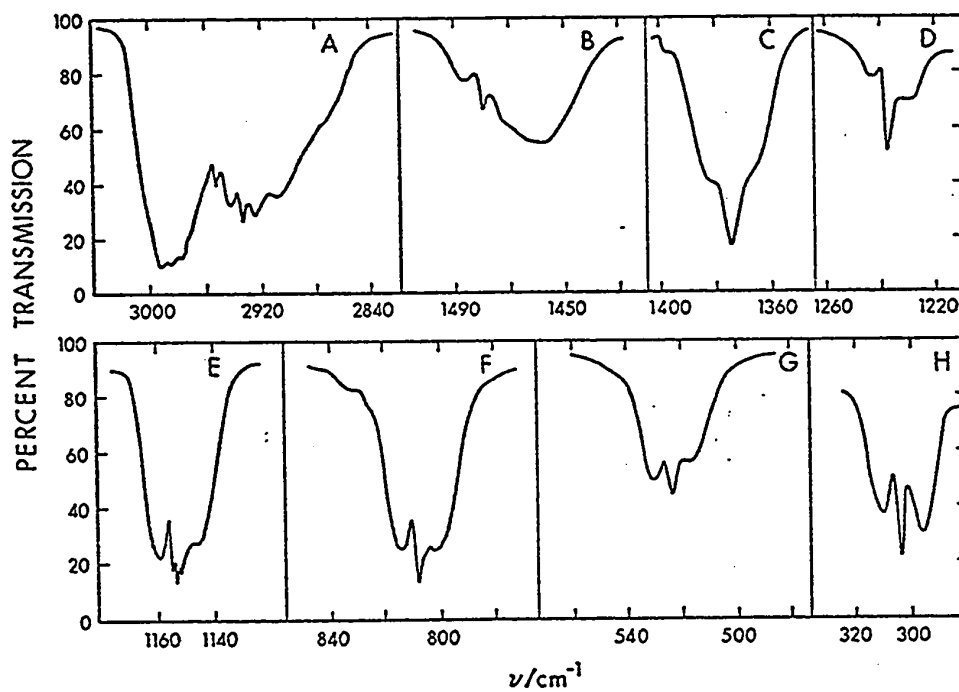


Figure 16

The intense bands in the infrared spectrum of gaseous t-butyl bromide-h<sub>9</sub>.

The infrared spectrum of the liquid at room temperature is also shown in Figures 14 and 15 for the region 4000 to 200  $\text{cm}^{-1}$ . The spectrum was recorded at a resolution of about 1  $\text{cm}^{-1}$  for the region above 650  $\text{cm}^{-1}$  and about 2  $\text{cm}^{-1}$  for the region below 650  $\text{cm}^{-1}$ . The nominal sample thickness was about 0.02 and 0.2 mm for the thin and the thick samples, respectively. The frequencies of the features are reported in Table VI with an accuracy of  $\pm 1 \text{ cm}^{-1}$ . The liquid phase bands are, of course, much narrower than their gas phase counterparts, and this enables more detail to be seen in regions containing overlapping bands. There are two well-defined peaks and a shoulder in the region between 1430 and 1500  $\text{cm}^{-1}$  instead of the broad band observed in the spectrum of the gas phase. Between 3000 and 2880  $\text{cm}^{-1}$  there are five well-defined peaks which are also difficult to characterize in the gas phase. Many features that are weak or missing in the spectrum of the gas phase are well defined in that of the liquid phase, such as the bands at 272, 930, 1031, 1059, 1731 and 1859  $\text{cm}^{-1}$ .

The Raman spectrum of liquid t-butyl bromide- $\text{h}_9$  is shown in Figure 17 and the frequencies are listed in Table VI along with the qualitative intensities and the depolarization ratios. The resolution used was about 1

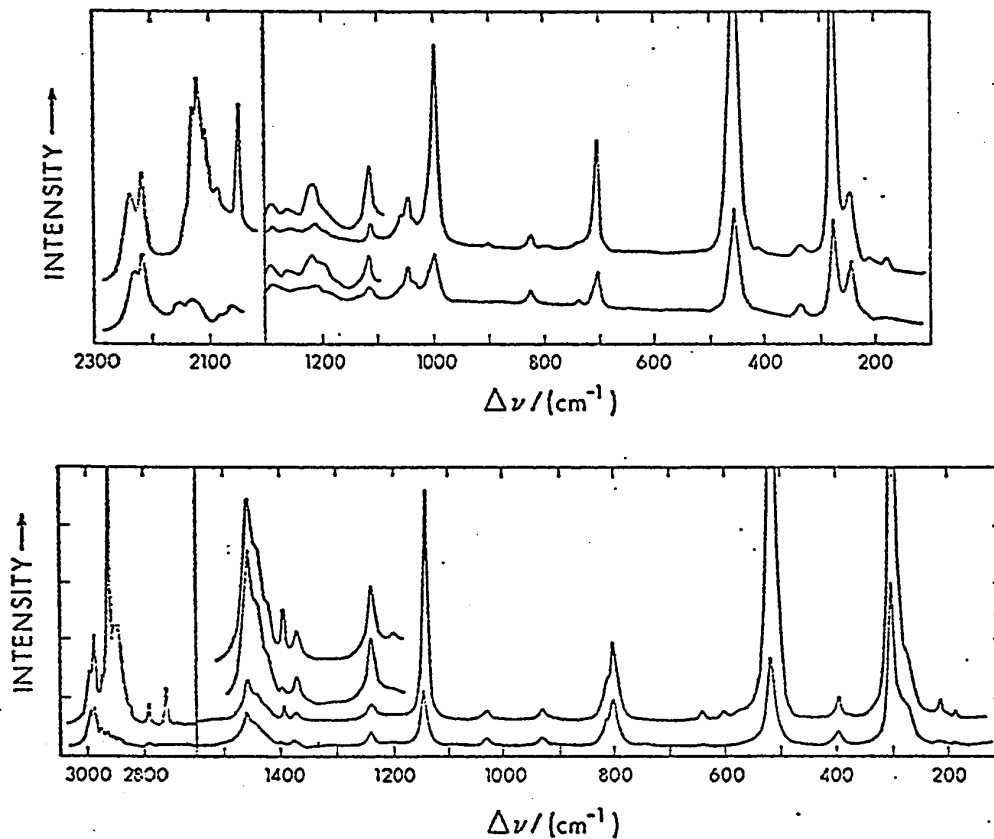


Figure 17

Raman spectrum of liquid t-butyl bromide- $\text{h}_9$  (lower box) and t-butyl bromide- $\text{d}_9$  (upper box). In each figure the upper full curve shows the spectrum under parallel polarization and the lower full curve shows that under perpendicular polarization. The partial spectra near  $1200 \text{ cm}^{-1}$  in both figures show the weaker features recorded at higher gain, again with the spectrum under parallel polarization lying above that under perpendicular polarization.

$\text{cm}^{-1}$  and the frequencies are accurate to about  $\pm 1 \text{ cm}^{-1}$ . Except for the bands at 2890, 2850, 643, and  $187 \text{ cm}^{-1}$ , all of the features appearing in the Raman spectrum of the liquid were also seen in the infrared spectrum. The frequencies observed in the Raman and infrared spectra of the liquid are the same within the combined errors of measurement and are slightly lower in most cases than the frequencies observed in the gas phase. Depolarization ratios were determined by measuring the peak height relative to the base line around the peak. They were reproducible to within  $\pm 0.15$  for the medium to strong bands and for the well-separated weak bands.

#### 4.3 ASSIGNMENT OF THE INFRARED AND RAMAN SPECTRA OF t-BUTYL BROMIDE-h<sub>9</sub>

Four groups of workers have previously assigned the spectra of t-butyl bromide-h<sub>9</sub>, as discussed in Chapter 1. Their assignments are presented in Table II along with the one proposed in this work. The main basis for the proposed assignment is the information obtained from the infrared spectrum of the gas and the Raman spectrum of the liquid. The infrared spectrum of the liquid and the assignments available in the literature for related compounds (163-166) have also been considered. In the fol-

lowing presentation, assignments of the different vibrations occurring in the same frequency regions are discussed together in order of decreasing frequency.

The numbering of the vibrational modes is according to the convention suggested by Herzberg (15). In this numbering scheme the  $A_1$  modes are numbered first followed by the  $A_2$  modes and the E modes. In each symmetry species the modes are numbered in decreasing order of their frequencies. Thus for t-butyl bromide the  $A_1$  modes are from  $\nu_1$  to  $\nu_8$ , the  $A_2$  modes are from  $\nu_9$  to  $\nu_{12}$  and the E modes are from  $\nu_{13}$  to  $\nu_{24}$  (see Tables II, III and IV).

(A) C-H Stretching Modes

From the vibrational analysis (Table IV) five C-H stretching modes,  $2A_1$  and  $3E$ , are active in both the infrared and the Raman. The sixth,  $A_2$ , mode is inactive in the gas and is possibly too weak to be observed in the liquid spectrum. All of these modes are expected to occur in the region  $3100-2800 \text{ cm}^{-1}$  (15, 17). It is a useful first approximation to consider the C-H stretching modes as being derived from the symmetric and asymmetric stretching modes of a methyl group of  $C_{3v}$  symmetry. Deviations from the predictions made on this basis can be expected, because the site symmetry of the methyl groups in t-butyl



bromide is, at best,  $C_s$ , but the approximation is helpful for predicting the approximate frequencies of these modes. In this approximation, the C-H stretching modes of t-butyl bromide can be described as symmetric or asymmetric depending on the relative displacements of the atoms within each methyl group rather than in the molecule as a whole. The symmetric modes form the representation  $A_1 + E$ , and the asymmetric modes form  $A_1 + A_2 + 2E$ , under the  $C_{3v}$  point group of the entire molecule. The asymmetric modes are expected to occur at higher frequencies than the symmetric modes because of the kinetic coupling within each methyl group through the carbon atom. For example, in methyl bromide the asymmetric C-H stretches occur at  $3055.9 \text{ cm}^{-1}$  and the symmetric C-H stretch is at  $2878.8 \text{ cm}^{-1}$  (15).

The utility of this approach can be demonstrated by the following arguments. The spectrum of gaseous t-butyl bromide- $d_9$  shows a parallel-type band at  $2925 \text{ cm}^{-1}$  and a perpendicular-type band at  $2971 \text{ cm}^{-1}$ , (Figure 19). These almost certainly arise from the t-butyl bromide- $d_8$  ( $C_4HD_8Br$ ) impurity. The parallel band can be assigned to the unique C-H bond trans to the C-Br bond, while the perpendicular type band can be assigned to the two equivalent C-H bonds, gauche to the C-Br bond. The difference between these frequencies agrees with values found by McKean (163)

in compounds containing the  $\text{CD}_2\text{H}$  group and O or N atoms. One can calculate the force constants for the two types of C-H bonds using these two frequencies for  $\text{C}_4\text{D}_8\text{HBr}$ . If these force constants are used, without an interaction constant, to calculate the vibrational frequencies of a  $\text{CH}_3$ , or  $\text{CD}_3$ , group of symmetry  $\text{C}_s$ , it is found that the eigenvectors approximate those of a methyl group of  $\text{C}_{3v}$  symmetry, as do the frequencies, although of course the two higher frequency modes differ by about  $20 \text{ cm}^{-1}$  in the  $\text{C}_s$  model, and are degenerate in the  $\text{C}_{3v}$  model. In any event, the approximation discussed above remains useful, and in t-butyl bromide one can expect the asymmetric methyl stretches to occur at higher frequencies than the symmetric methyl stretches.

The infrared spectrum of the gas for the methyl stretching region is shown in Figures 14 and 16. There are two regions of strong absorption, one between 2965 and  $3010 \text{ cm}^{-1}$  and another between 2900 and  $2955 \text{ cm}^{-1}$ . The peak at  $2977 \text{ cm}^{-1}$  appears to be the Q branch of a parallel band, and the assignment of this feature to the  $\text{A}_1$  asymmetric stretching mode,  $\nu_1$ , is supported by the strong, partially polarized, Raman band at  $2971 \text{ cm}^{-1}$  (Figure 17) and a strong peak in the infrared spectrum of the liquid at  $2970 \text{ cm}^{-1}$ . The broad peak in the infrared spectrum of

the gas, at  $2992\text{ cm}^{-1}$  can be assigned to an E mode,  $\nu_{13}$ , which is also derived from asymmetric methyl stretches. The second E mode derived from asymmetric methyl stretches,  $\nu_{14}$ , is expected to occur close to the  $A_1$  and E modes already assigned. This requires a brief justification because two modes of the same symmetry may be expected to interact and move apart. However, the two E modes in question, although having the same symmetry under the  $C_{3v}$  point group of the molecule, belong to different irreducible representations of the  $C_s$  subgroup of individual methyl groups. Therefore, intra-methyl-group interaction cannot occur, and only the much weaker inter-methyl-group interaction could cause the two E modes to interact. Here the second E mode,  $\nu_{14}$ , is assigned as coincident with the  $A_1$  mode at  $2977\text{ cm}^{-1}$ , mainly because the corresponding Raman band at  $2971\text{ cm}^{-1}$  is only partially polarized.

The  $A_1$  symmetric C-H stretch,  $\nu_2$ , is assigned to the parallel band with its Q branch at  $2934\text{ cm}^{-1}$  in the infrared spectrum of the gas, and to the strong, polarized band at  $2924\text{ cm}^{-1}$  in the Raman spectrum of the liquid. This assignment is supported by the presence of a strong band in the infrared spectrum of the liquid at  $2925\text{ cm}^{-1}$ . The E symmetric C-H stretching mode,  $\nu_{15}$ , is assigned to the band at  $2953\text{ cm}^{-1}$  in the infrared spectrum of the gas

and to the depolarized band at  $2944 \text{ cm}^{-1}$  in the Raman spectrum of the liquid. The gas-phase band at  $2953 \text{ cm}^{-1}$  looks rather like a Q branch, which might be interpreted as part of a parallel band, but other E modes in this molecule have been found to yield Q branches in their gas phase bands, as discussed in Part C of this section. An alternative assignment of this mode is to the broad maximum at  $2910 \text{ cm}^{-1}$  in the infrared spectrum of the gas, with the corresponding band at  $2903 \text{ cm}^{-1}$  in the liquid. However, the corresponding Raman band is strongly polarized and either rules out this assignment or indicates the coincidence of an  $A_1$  combination or overtone.

(B) CH<sub>3</sub> Deformation Modes

The vibrational analysis (Table IV), yields five infrared and Raman active modes, two  $A_1$  and three E, arising from the deformations of the H-C-H angles. They are expected to occur in the region  $1500\text{-}1300 \text{ cm}^{-1}$  (15, 17). One can again use the concept of symmetric and asymmetric deformations of the individual methyl groups to classify these modes into two groups: two E modes and one  $A_1$  mode arising from the asymmetric methyl deformations, and one  $A_1$  mode and one E mode arising from the symmetric methyl deformations. The asymmetric deformations

should occur at higher frequencies than the symmetric deformations (164-166).

There are two groups of bands in the 1500-1300  $\text{cm}^{-1}$  region in the spectra of the gas and the liquid. One group is below and the other is above 1400  $\text{cm}^{-1}$  (see Figures 15 and 16). The Raman spectrum shows a depolarized band at 1372  $\text{cm}^{-1}$ , corresponding to the perpendicular band at 1375  $\text{cm}^{-1}$  in the infrared spectra of the liquid. This band is assigned to the E symmetric  $\text{CH}_3$  deformation,  $\nu_{18}$ . The polarized Raman band at 1397  $\text{cm}^{-1}$  and the weak infrared feature at 1397  $\text{cm}^{-1}$  and 1395  $\text{cm}^{-1}$  in the gas and liquid, respectively are assigned to the  $A_1$  symmetric deformation,  $\nu_4$ .

The infrared spectrum of the gas phase shows a broad band with its maximum at 1457  $\text{cm}^{-1}$ , and a Q branch of a parallel band at 1480  $\text{cm}^{-1}$ , (Figures 15 and 16). This Q branch and the corresponding band at 1475  $\text{cm}^{-1}$  in the infrared spectrum of the liquid are assigned to the  $A_1$  asymmetric methyl deformation,  $\nu_3$ . There is no corresponding band in the Raman spectrum of the liquid. Between 1500 and 1400  $\text{cm}^{-1}$ , the Raman spectrum shows only a medium-strong depolarized band at 1459  $\text{cm}^{-1}$  and two shoulders at 1447  $\text{cm}^{-1}$  and 1425  $\text{cm}^{-1}$ . However the Raman spectrum of the solid at 90°K does show a weak band at 1475

$\text{cm}^{-1}$  (see Chapter 6). The nonappearance of this mode in the Raman spectra of the liquid has also been observed for t-butyl chloride (164).

The depolarized bands at  $1459 \text{ cm}^{-1}$  and  $1447 \text{ cm}^{-1}$  in the Raman spectrum of liquid t-butyl bromide- $h_9$  are assigned to the two E modes derived from the asymmetric methyl deformations,  $\nu_{16}$  and  $\nu_{17}$ . The broad featureless absorption peaking at  $1457 \text{ cm}^{-1}$  in the infrared spectrum of the gas is consistent with this assignment and corresponding bands appear at  $1457$  and  $1449 \text{ cm}^{-1}$  in the infrared spectrum of the liquid. The weak, depolarized band at  $1425 \text{ cm}^{-1}$ , in the Raman spectrum, is assigned to the combination  $\nu_{20} + \nu_{22}$ .

#### (C) C-C Stretching and Methyl Rocking Modes

The vibrational modes arising from the C-C stretching and methyl rocking motions are expected to occur between  $650$  and  $1300 \text{ cm}^{-1}$  (15, 164-166). One expects two E modes and one  $A_1$  mode from the methyl rocking motions and one  $A_1$  mode and one E mode from the C-C stretching motions to be infrared and Raman active (Table IV).

The infrared spectrum of the gas shows a very strong parallel band at  $1153 \text{ cm}^{-1}$  (Figures 15 and 16).

The corresponding band at  $1142\text{ cm}^{-1}$  in the Raman spectrum of the liquid is highly polarized. Therefore this feature must be assigned to one of the  $A_1$  fundamentals expected in this region and, because  $1153\text{ cm}^{-1}$  is too high for a symmetric C-C stretch (123), it is assigned to the  $A_1$  methyl rock,  $\nu_5$ . The infrared spectrum of the gas phase shows a parallel band at  $808\text{ cm}^{-1}$  while the band at  $1238\text{ cm}^{-1}$  could be a highly distorted parallel band. The corresponding bands in the Raman spectrum of the liquid are at  $804\text{ cm}^{-1}$  and  $1236\text{ cm}^{-1}$ , and are partially polarized and depolarized respectively. The  $A_1$  C-C stretching mode,  $\nu_6$ , is therefore assigned at  $808\text{ cm}^{-1}$  in the gas and  $804\text{ cm}^{-1}$  in the liquid.

The Raman spectrum of the liquid shows depolarized bands at  $931$ ,  $1031$ , and  $1236\text{ cm}^{-1}$ , while the infrared spectrum of the gas shows perpendicular bands at  $1033$  and  $1203\text{ cm}^{-1}$ ; only. The  $1203\text{ cm}^{-1}$  band has weak counterparts in the liquid, but the Raman line is polarized and, hence, cannot arise from an E mode. The three E fundamentals,  $\nu_{19}$ ,  $\nu_{20}$ , and  $\nu_{21}$ , are assigned to the three depolarized bands in the Raman spectrum of the liquid, at  $1236$ ,  $1031$ , and  $931\text{ cm}^{-1}$ . A simple calculation on the  $(\text{CH}_3)_3\text{C}$  unit treating the  $\text{CH}_3$  groups as points of mass 15, and neglecting interaction constants, shows that if the  $A_1$  C-C

$\text{cm}^{-1}$  (Figure 17). The corresponding bands in the infrared spectrum of the gas, at  $524 \text{ cm}^{-1}$  and  $304 \text{ cm}^{-1}$ , are strong, parallel bands, and these two features clearly arise from the two  $A_1$  modes,  $\nu_7$  and  $\nu_8$ . The C-Br stretch occurs at  $611 \text{ cm}^{-1}$ ,  $559 \text{ cm}^{-1}$  and  $535 \text{ cm}^{-1}$  in methyl bromide (15), ethyl bromide (116) and isopropyl bromide (116) respectively. Therefore it is logical to assign the C-Br stretching mode,  $\nu_7$ , at  $524 \text{ cm}^{-1}$  rather than at  $304 \text{ cm}^{-1}$ . The  $A_1$  skeleton deformation mode,  $\nu_8$ , is assigned at  $304 \text{ cm}^{-1}$ .

There are three depolarized features in the Raman spectrum of the liquid below  $650 \text{ cm}^{-1}$ , at  $396 \text{ cm}^{-1}$ ,  $285 \text{ cm}^{-1}$ , and  $271 \text{ cm}^{-1}$  (Figure 17), and are assigned to the three E fundamentals expected in this region. Methyl torsion vibrations are found to absorb below  $300 \text{ cm}^{-1}$  in related compounds, such as t-butyl chloride (164) and t-butyl fluoride (122). Hence it is reasonable to assume that the methyl torsions are not responsible for the band at  $396 \text{ cm}^{-1}$ . The C-C-C deformation does not involve motion of the heavy bromine atom to as great an extent as the C-C-Br deformation does, and is therefore assigned to the higher frequency  $396 \text{ cm}^{-1}$ . It is, however, expected that this normal mode,  $\nu_{22}$ , does involve some C-C-Br deformation. The E mode,  $\nu_{24}$ , arising mainly from C-C-Br deformations



stretch is at  $808\text{ cm}^{-1}$ , the E C-C stretch is expected at about  $1105\text{ cm}^{-1}$ . Therefore the  $1236\text{ cm}^{-1}$  depolarized band is assigned to an E fundamental,  $\nu_{19}$ , mainly derived from the C-C stretches, but heavily coupled to the  $\text{CH}_3$  rocking motion. The infrared gas phase band contour does not support this assignment and might argue against it. The assignment is, however, consistent with the assignment for  $\text{C}_4\text{D}_9\text{Br}$  (Section 4.5), for which the evidence is less confused, and it therefore appears necessary to describe the gas-phase band as a highly distorted perpendicular band. The 1031 and 931 bands are assigned to the E methyl rock,  $\nu_{20}$ , and a mixture of E methyl rock and E C-C stretch,  $\nu_{21}$ .

(D) C-Br Stretching, Skeleton Deformations and Methyl Torsion Modes

There are two E modes and one  $A_1$  mode derived from the deformations of the molecular skeleton, that is changes in the C-C-Br and C-C-C angles. One  $A_1$  mode is derived from the C-Br stretch and one E and one  $A_2$  mode arise from the torsional motions of the methyl group (Table IV). All of these are expected to occur below  $650\text{ cm}^{-1}$  (15, 164, 168).

There are two strong and highly polarized bands in this region of the Raman spectrum, at  $516\text{ cm}^{-1}$  and  $301$

concluded that they were coincident.

#### 4.4 RESULTS FOR T-BUTYL BROMIDE-d<sub>9</sub>

The infrared spectrum of gaseous t-butyl bromide-d<sub>9</sub> is shown in Figure 18 and the strong bands are shown on an expanded scale in Figure 19. The spectrum was recorded at 1 cm<sup>-1</sup> resolution, with the sample at room temperature in a 10 cm cell at a pressure of 5.0 and 0.5 cm of Hg. The frequencies of the features observed between 4000 and 200 cm<sup>-1</sup> are given in Table VII, accurate to ±1 cm<sup>-1</sup>. The bands at 274, 463, 537, 706, 1011 and 1118 cm<sup>-1</sup> have the sharp Q branches and well-defined P and R branch envelopes characteristic of parallel bands. The bands at 1052, 1214, and 1291 cm<sup>-1</sup> have neither sharp Q branches nor well-defined P and R branch envelopes and hence are perpendicular bands. In the 2300-2000 cm<sup>-1</sup> region, there are two groups of strong bands. The lower frequency group between 2190-2040 cm<sup>-1</sup> has a very complex shape presumably due to the overlapping of many bands. The second group, between 2270-2200 cm<sup>-1</sup>, is more intense and shows the Q branch of a parallel band at 2221 cm<sup>-1</sup>.

The infrared spectrum of the liquid is also shown in Figure 19 and the frequencies of the observed features are given in Table VII with an accuracy of ±1 cm<sup>-1</sup>. The

could be assigned to the feature at  $285\text{ cm}^{-1}$  or at  $272\text{ cm}^{-1}$ . It is assigned to the  $272\text{ cm}^{-1}$  feature, and the  $285\text{ cm}^{-1}$  feature is assigned to the methyl torsion mode,  $\nu_{23}$ . This assignment is preferred because in t-butyl fluoride and t-butyl chloride, the methyl torsion is assigned at  $298$  and  $290\text{ cm}^{-1}$  respectively.

(E) Summary

The assignment presented above is identical to the most recent assignment in the literature between  $300$  and  $1300\text{ cm}^{-1}$ . However the present analysis, coupled with the results for  $\text{C}_4\text{D}_9\text{Br}$  (Sections 4.4 and 4.5) puts the assignment on a much firmer experimental basis, although anomalies in the evidence do exist. The new assignments for the C-H stretching and methyl deformation modes result in part from the improved experimental evidence. In particular, the assignments of  $\nu_4$  and  $\nu_{18}$  are required by the Raman spectrum. The assignment of the C-H stretching modes is still not as definitive as would be desirable, except for  $\nu_2$  whose assignment is clear from the infrared spectrum of the gas. A new feature has been detected in the spectra of the liquid below  $300\text{ cm}^{-1}$ , and has allowed the methyl torsion and C-C-Br deformation modes to be assigned distinct frequencies. Previous authors (113) had

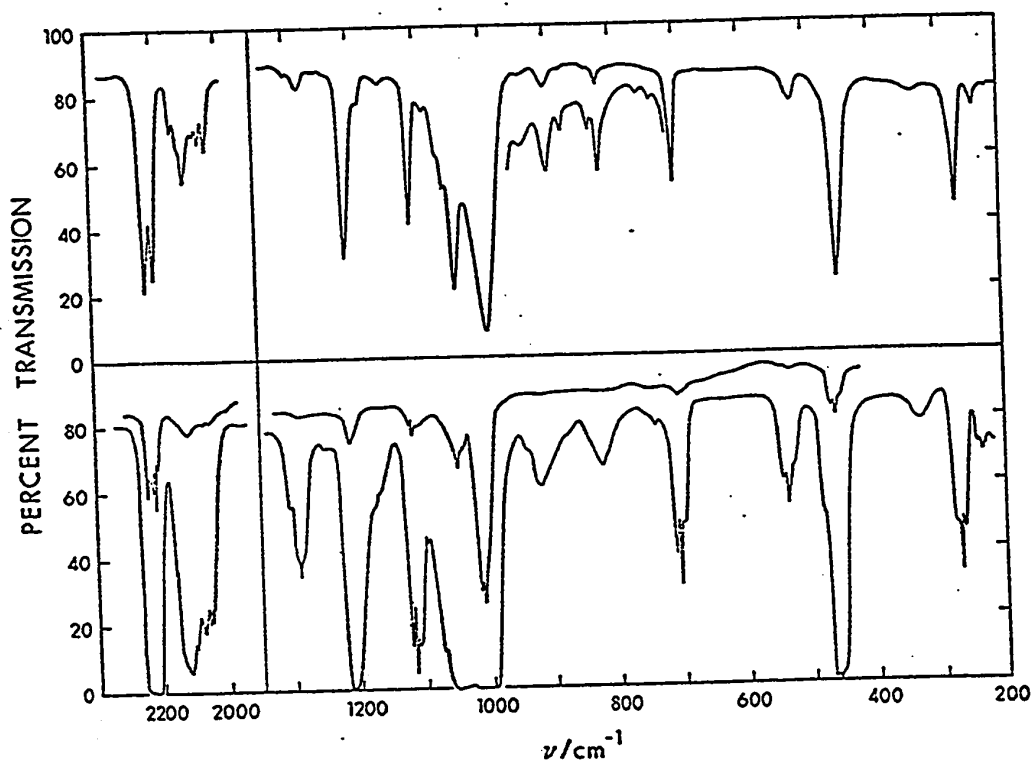


Figure 18

Infrared spectrum of t-butyl bromide- $\text{d}_9$  in the gas  
(lower box) and liquid (upper box) phases.

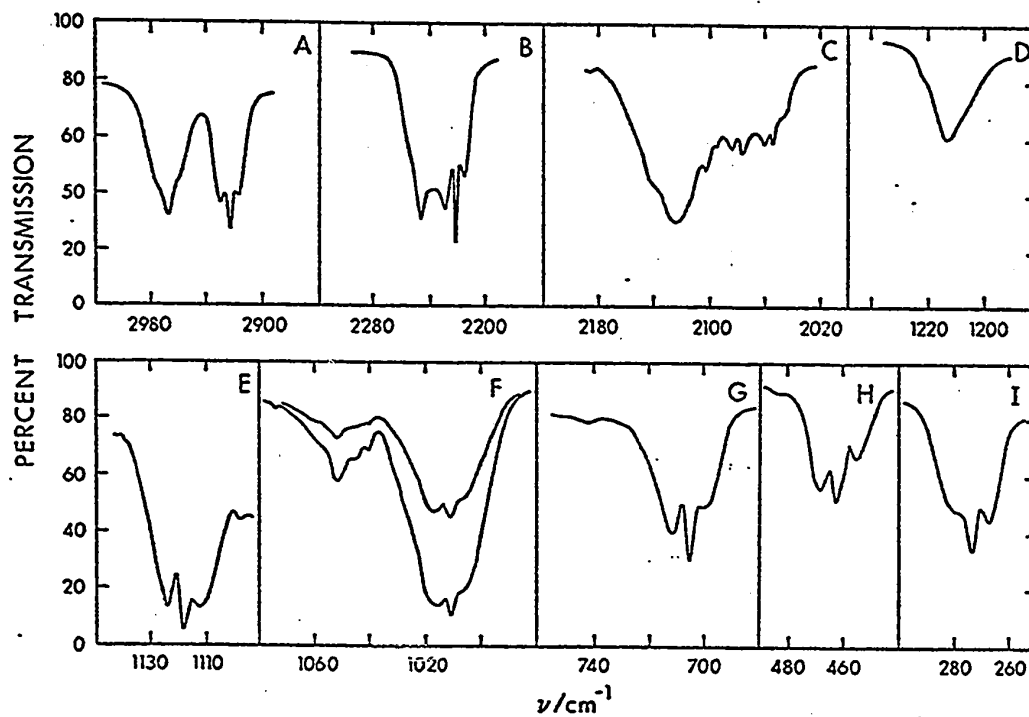


Figure 19

The intense bands in the infrared spectrum of gaseous t-butyl bromide- $d_9$ . Figure A is due to t-butyl bromide- $d_8$  impurity.

Table VII  
 Frequencies and assignment of the features observed in the infrared and the  
 Raman spectra of t-butyl bromide-d<sub>9</sub> in the gas and liquid phases for the  
 region 4000 - 100 cm<sup>-1</sup>. a

IR		Raman			Assignment
Gas	Liquid	Intensity	Δν <sub>-1</sub> cm	Depolarization Ratio	
ν <sub>-1</sub> cm	ν <sub>-1</sub> cm	Intensity	Δν <sub>-1</sub> cm	Intensity	Depolarization Ratio
--	3271	VW			ν <sub>1</sub> + ν <sub>17</sub>
--	3243	VW			ν <sub>2</sub> + ν <sub>3</sub>
2971	2963	W			C <sub>4</sub> D <sub>8</sub> HBr impurity
2925	2922	W			ν <sub>13</sub> + ν <sub>22</sub>
2570	2561	VW			ν <sub>2</sub> ν <sub>22</sub>
	2460	VW			ν <sub>13</sub>
2246	2240	VS	2240	S	ν <sub>14</sub>
2229		S			ν <sub>1</sub>
2221	2217	VS	2216	S	ν <sub>3</sub> + ν <sub>17</sub>
2145	2150	sh	2148	W	... cont'd.

Table VII - cont'd.

		IR			Raman			Assignment
Gas		Liquid			Liquid			
$\nu$ -l cm	Inten- sity	$\nu$ -l cm	Inten- sity	$\Delta\nu$ -l cm	Inten- sity	Depolarization Ratio		
2124		2131	sh	2130	s	P	$2\nu_4$ $\nu_{15}$	
2104		2117	s	2118	vs	0.15	$\nu_2$	
2084	m	2084	m	2107	m	0.2	$2\nu_{17}$	
2076	m	2070	m	2086	m	0.3	$\nu_{17} + \nu_{18}$	
2060	m						$2\nu_{18}$	
2053	m	2048	m	2046	s	0.15	$\nu_5 + \nu_{17}$	
1742	w	1734	w				$\nu_4 + \nu_5$	
1447	w	1443	w				$\nu_5 + \nu_{21}$	
1307	w	1303	w				$\nu_3 + \nu_{22}$	
1291	m	1285	m	1288	VW	DP	$\nu_3 + \nu_{24}$	
				1257	VW	DP	$\nu_4 + \nu_{23}$	
1214	s	1214	s	1215	w	DP	$\nu_5 + \nu_{23}$	
				1200	sh w	DP?	$\nu_{16} + \nu_{24}$	
							$\nu_5 + \nu_{24}$	
							...	

118.

... cont'd.

Table VII - cont'd.

		IR			Raman			Assignment
Gas		Liquid			Liquid			
$\nu$ -1 cm	Inten- sity	$\nu$ -1 cm	Inten- sity	$\Delta\nu$ -1 cm	Inten- sity	Depolarization Ratio		
1175	sh	1190	sh				$\nu_7 + \nu_{21}$	
1168	sh	1158	w				$\nu_6 + \nu_7$	
1118	s	1114	s	1115	m	0.3	$\nu_{20} + \nu_{22}$	
1097	w	1092	w				$\nu_3$	
1072	sh	1071	sh				$\nu_8 + \nu_{20}$	
		1062	w	1062		0.55	$\nu_{21} + \nu_{22}$	
1052	s	1049	s	1048		0.6	$\nu_4$	
1040	w	1039	sh w	1038	w	DP	$\nu_{17}$	
1011	ws	1000	vs	1001	s	0.2	$\nu_{18}, \nu_{19}$	
940	sh,w	939	vw				$\nu_5$	
923	w	903	w	901	vw	0.8	$\nu_6 + \nu_{23}$	
		880	vw				$2\nu_7$	
		837	vw				$\nu_6 + \nu_{12}$	
824	w	822	w	823	w	0.8	$\nu_8 + \nu_{22} + \nu_{23}$	
							$\nu_{20}$	



Table VII - cont'd.

IR			Raman				Assignment
Gas		Liquid		Liquid		Depolarization Ratio	
$\nu$ -1 cm	Intensity	$\nu$ -1 cm	Intensity	$\Delta\nu$ -1 cm	Intensity		
742	vw	758	vw	739	vw	DP?	$\nu_{11}, \nu_7 + \nu_{22}$
706	s	738	w	705	s	0.3	$\nu_{21}$ $\nu_6$
537	m	703	s				$2\nu_8$
484	sh	521	m				$\nu_8 + \nu_{24}$
463	vs	480	sh	454	vvs	0.15	$\nu_7$
		454	s	411	vw	P	$2\nu_{24}$
335	w	335	w	337	vvs	0.75	$\nu_{22}$
274	s	273	s	274	vvs	0.15	$\nu_8$
239	w	241	w	243	m	0.85	$\nu_{23}$
		206	vw	207	vw	0.80	$\nu_{24}$
		181		181	w	0.25	$\nu_7 - \nu_8$

The symbols are as given under Table IV, plus:

P = polarized Raman feature; PP = partially polarized Raman feature;

ized or depolarized. In the C-D stretch region, the polarization properties of the bands at 2221 and 2238  $\text{cm}^{-1}$  are not certain, except that they are not strongly polarized, and the details of the residual bands in the perpendicular spectrum between 2050 and 2200  $\text{cm}^{-1}$  are not certain. The Figure 17 and Table VII provide our best estimate of these features but experimental difficulties prevented us from obtaining definitive results. The Raman scattering by the heavy compound appeared to be much weaker than that by the light compound, and the samples of  $\text{C}_4\text{D}_9\text{Br}$  showed much more intense fluorescence than those of the light compound.

Except for the features at 411, 1257, and 2107  $\text{cm}^{-1}$  all of the features seen in the Raman spectrum of the liquid were also observed in the infrared spectrum of the liquid. The frequencies of corresponding bands in the infrared and Raman spectra agree to within the combined experimental uncertainties, except in one case. The weak feature seen at 1285  $\text{cm}^{-1}$  in the infrared spectrum occurred at 1288  $\text{cm}^{-1}$  in the Raman but this difference is almost certainly not real. In general the bands appear in the spectra of the liquid at slightly lower frequencies than in that of the gas.

spectrum was recorded at  $1 \text{ cm}^{-1}$  resolution for the region above  $650 \text{ cm}^{-1}$ , and  $2 \text{ cm}^{-1}$  resolution for the region below  $650 \text{ cm}^{-1}$ . The sample was at room temperature in cells with a nominal thickness of 0.1 mm. The band widths have decreased in going from the gas to the liquid phases, and consequently overlapping bands are more distinct in the spectrum of the liquid. Features that are weak or missing in the gas phase spectrum are well-defined in the liquid phase spectrum, such as the bands at 758, 822, 837, 880, 903, 1062, 1190, 2131, 2460, 3243, and  $3271 \text{ cm}^{-1}$  (Table VII).

Figure 17 shows the Raman spectrum of the liquid under parallel and under perpendicular polarizations. The spectrum was recorded at a resolution of  $1.5 \text{ cm}^{-1}$  with the sample at room temperature. The frequencies and depolarization ratios of the observed features are listed in Table VII. The frequencies are accurate to about  $\pm 1 \text{ cm}^{-1}$  and the depolarization ratios, obtained by measuring the peak heights relative to the base lines around the bands, are reproducible to  $\pm 0.1$ , except for the following uncertainties. The existence, frequency and polarization of the  $207 \text{ cm}^{-1}$  and  $904 \text{ cm}^{-1}$  features are not certain. Similarly the details of the region  $1150$  to  $1300 \text{ cm}^{-1}$  are not certain; in particular the features could be partially polar-

#### 4.5 ASSIGNMENT OF THE INFRARED AND RAMAN SPECTRA OF t-BUTYL BROMIDE-d<sub>9</sub>

There is only one assignment of the vibrational spectrum of t-butyl bromide-d<sub>9</sub> in the literature (112). This assignment was based on the infrared spectrum of liquid t-butyl bromide-d<sub>9</sub> in the sodium chloride region only, and is therefore incomplete. It has also been recognized as incorrect (118) but remains uncorrected. The assignment given in this thesis is based on the infrared spectra of the gas and the liquid, and on the Raman spectra of the liquid under parallel and perpendicular polarizations. The present assignment is presented in Table III along with that of Zeil and coworkers (112). In the following sections, the vibrational assignment is presented in four parts, each part dealing with one frequency region. The order of presentation follows the ease with which the vibrational assignments of the bands can be made, rather than the order of decreasing frequencies adopted in Section 4.3.

##### (A) C-D Stretching Modes

One expects five infrared and Raman active C-D stretching modes of t-butyl bromide-d<sub>9</sub> (Table IV). One A<sub>1</sub> and two E modes arise from the asymmetric C-D stretch-

ing modes of the individual methyl groups, and one  $A_1$  and one E mode arise from the symmetric  $CD_3$  stretching modes (Section 4.3). The methyl- $d_3$  stretching frequencies for some related molecules are presented in Table VIII. The data in Table VIII show that the asymmetric stretching modes occur at higher frequencies than the symmetric stretching modes, and both occur in the region between 2300 and 2000  $cm^{-1}$ . The gas phase infrared spectrum in this region shows two distinct regions of absorption. The absorption above 2200  $cm^{-1}$  clearly arises from the asymmetric stretches while the symmetric stretches occur below 2200  $cm^{-1}$ . The asymmetric and symmetric stretches are, then, more separated than in the light compound, but this is to be expected from simple consideration of the kinetic coupling within each  $CD_3$  group.

The parallel band at 2221  $cm^{-1}$  (Figure 19) is clearly due to the  $A_1$  asymmetric methyl- $d_3$  stretch,  $\nu_1$ . Corresponding bands occur at 2217  $cm^{-1}$  and 2216  $cm^{-1}$  in the infrared and Raman spectra of the liquid, the latter being partially polarized. The broader maximum at 2246  $cm^{-1}$  in the gas is assigned to one of the E asymmetric stretches,  $\nu_{13}$ . Corresponding bands are found at 2240  $cm^{-1}$  in the liquid, the Raman band appearing to be depolarized. The gas phase peak at 2229  $cm^{-1}$  is too intense to be attrib-

Table VIII

C-D<sub>3</sub> stretch and CD<sub>3</sub> deformation frequencies in some of the related molecules.

Molecule	Reference	Methyl-d <sub>3</sub> Stretch		Methyl-d <sub>3</sub> Deformation	
		Asym.	Sym.	Asym.	Sym.
		cm <sup>-1</sup>	cm <sup>-1</sup>	cm <sup>-1</sup>	cm <sup>-1</sup>
CD <sub>3</sub> .Br	15	2293	2151	1053	987
CD <sub>3</sub> .Cl	15	2286	2161	1058	1029
CD <sub>3</sub> .CD <sub>2</sub> Cl	168	2234	2079	1052	1079
$\begin{array}{c} \text{O} \\ \parallel \\ \text{CD}_3 \cdot \text{C} \cdot \text{CD}_3 \end{array}$	169	2270	2114 2185	1053	1089 1005
$\begin{array}{c} \text{O} \\ \parallel \\ \text{CD}_3 \cdot \text{C} \cdot \text{H} \end{array}$	169	2265	2130	1045	1028
CD <sub>4</sub>	15	2258	2085		
CD <sub>3</sub> .CD <sub>3</sub>	15	2225	2083	1055	1158
CD <sub>3</sub> .CD <sub>2</sub> .CD <sub>3</sub>	166	2225	2081	1064	1130
CD <sub>3</sub> .CH <sub>2</sub> .CD <sub>3</sub>	166	2225	2090	1066	1085
(CD <sub>3</sub> ) <sub>2</sub> CD	167	2217 (E) 2216 (A)	2073	1117 1087	1068 1056
(CD <sub>3</sub> ) <sub>3</sub> CH	167	2219 (E) 2212 (A)	2076	1122 1102	1071 1052
(CD <sub>3</sub> ) <sub>3</sub> CCl	164	2244 (E) 2226 (A)	2124	1054	1016

stretching mode,  $\nu_{15}$ . The liquid phase frequency of this mode cannot be determined.

(B) C-Br Stretching, Skeleton Deformations and Methyl-d<sub>3</sub> Torsion Modes

These vibrations occur below  $530 \text{ cm}^{-1}$  in t-butyl bromide-h<sub>9</sub> (Section 4.3). The replacement of <sup>1</sup>H by <sup>2</sup>H can be expected to lower the frequencies of all of these vibrations even though the hydrogen atoms are only directly involved in the methyl-d<sub>3</sub> torsions (164). One A<sub>1</sub> mode arising from the C-Br stretch, one A<sub>1</sub> and two E modes due to skeleton deformations and one E mode from methyl-d<sub>3</sub> torsions are expected to be active in the infrared and Raman.

The A<sub>1</sub> C-Br stretch,  $\nu_7$ , is clearly indicated at  $463 \text{ cm}^{-1}$  in the gas and  $454 \text{ cm}^{-1}$  in the liquid, by the parallel gas phase band and strong polarized Raman line. The skeleton deformation mode,  $\nu_8$ , is assigned to the parallel band at  $274 \text{ cm}^{-1}$  in the infrared spectrum of the gas, and to the strong polarized Raman band at the same frequency in the spectrum of the liquid.

The E C-C-C deformation,  $\nu_{22}$ , is assigned at  $335 \text{ cm}^{-1}$  in both phases. Weak bands, depolarized in the Raman spectrum of the liquid and of perpendicular type in

utable to only the R branch of the parallel band at 2221  $\text{cm}^{-1}$ , and this could indicate that the second E mode is coincident with it, but a distinct feature is not resolved in the liquid spectrum. The second E mode arising from the asymmetric methyl- $\text{d}_3$  stretches,  $\nu_{14}$ , is assigned to this feature in the spectrum of the gas, and to the 2217  $\text{cm}^{-1}$  band in the liquid, coincident with  $\nu_1$ .

The assignment of the symmetric methyl- $\text{d}_3$  stretching modes is less clear than is desirable. The gas phase infrared spectrum shows perpendicular bands at 2124  $\text{cm}^{-1}$  and possibly 2145  $\text{cm}^{-1}$ . The only peak which has the appearance of a Q branch occurs at 2104  $\text{cm}^{-1}$  and is an  $A_1$  mode. The Raman spectrum of the liquid is dominated by a series of strong highly polarized lines which must indicate that several  $A_1$  overtones and combinations are in Fermi-resonance with the  $A_1$  fundamental. The  $A_1$  fundamental arising from the symmetric methyl- $\text{d}_3$  stretches,  $\nu_2$ , is assigned to the strongest, highly polarized Raman line, at 2118  $\text{cm}^{-1}$ . The infrared spectrum of the liquid shows a strong peak at 2118  $\text{cm}^{-1}$ , coincident with the Raman line, but the gas phase frequency for the mode cannot be determined since no parallel band occurs near this frequency. The intense perpendicular band at 2124  $\text{cm}^{-1}$  in the gas phase spectrum is assigned to the degenerate symmetric C-D



the infrared spectra of the gas, are present at this frequency. The second E,  $\nu_{23}$ , skeleton deformation mode, mainly due to C-C-Br bending motion, is assigned to the depolarized band at  $242 \text{ cm}^{-1}$  in the Raman spectrum of the liquid. The infrared spectra show absorption at about  $242 \text{ cm}^{-1}$  in the liquid and at about  $239 \text{ cm}^{-1}$  in the gas.

Only two features in the Raman spectrum in this region remain unassigned; a depolarized, very weak feature at  $207 \text{ cm}^{-1}$ , and a weak polarized band at  $181 \text{ cm}^{-1}$ . The remaining fundamental, the E methyl- $\text{d}_3$  torsion,  $\nu_{24}$ , is assigned to the weak feature at  $207 \text{ cm}^{-1}$ . This assignment gives a value of about 1.38 for the ratio of the frequencies of the  $\text{CH}_3$  and  $\text{CD}_3$  torsional modes in t-butyl bromide which agrees well with the theoretical value of 1.41.

#### (C) Carbon-Carbon Stretching Modes

In order to estimate the frequencies of the C-C stretching modes in  $\text{C}_4\text{D}_9\text{Br}$  from their frequencies in  $\text{C}_4\text{H}_9\text{Br}$ , a calculation was made for the  $\text{C}(\text{CD}_3)_3$  and  $\text{C}(\text{CH}_3)_3$  moieties, treating the  $\text{CD}_3$  and  $\text{CH}_3$  units as points of mass 18 and 15 respectively. The same force constant was used in the two cases, and interactions between different C-C bonds were neglected. The calculations showed that if the  $A_1$  and E modes in the  $\text{C}(\text{CH}_3)_3$  unit are at 808 and  $1105 \text{ cm}^{-1}$  respectively, then they occur at 750 and  $1150 \text{ cm}^{-1}$  respectively

in  $C(CD_3)_3$ . These calculations are extremely approximate because they neglect the interaction with other modes of vibration, but they do indicate the general region in which these vibrations must be sought in  $C_4D_9Br$ . The band at  $706\text{ cm}^{-1}$  in the spectrum of the gas is therefore assigned to the  $A_1$  stretching mode,  $\nu_6$ . The corresponding band in the spectrum of the liquid is at  $704 \pm 1\text{ cm}^{-1}$ . In contrast to the corresponding Raman band in the light compound which is only partially polarized, the  $704\text{ cm}^{-1}$  band in the heavy compound is more clearly polarized, with  $\rho = 0.3$ . The E C-C stretching mode,  $\nu_{16}$ , is assigned at  $1214\text{ cm}^{-1}$  in the gas and the liquid. The gas phase band is clearly a perpendicular band, in contrast to the band seen at  $1238\text{ cm}^{-1}$  in the light compound. Thus the above assignment of the C-C stretching modes firmly supports the assignment of these modes in the light compound for which the evidence is ambiguous.

(D) Methyl Deformation and Rocking Modes

Two  $A_1$  and three E modes derived from the methyl- $d_3$  deformations, and one  $A_1$  and two E modes derived from the methyl- $d_3$  rocks are active in both types of spectra. Table VIII contains the methyl  $d_3$  deformation frequencies for some related compounds and shows that they lie between  $1160$  and  $980\text{ cm}^{-1}$ . Methyl- $d_3$  rocking modes have been

assigned between 630 and 1220  $\text{cm}^{-1}$  for  $(\text{CD}_3)_3\text{CCl}$  (164),  $(\text{CD}_3)_3\text{CH}$  (167),  $(\text{CD}_3)_3\text{CD}$  (167), and  $(\text{CD}_3)_2\text{CD}_2$  (166).  $3A_1$  and  $5E$   $\text{CD}_3$  deformation and rocking modes must, therefore, be assigned to the bands between 600 and 1200  $\text{cm}^{-1}$ .

Parallel bands are seen in the infrared spectrum of the gas at 706, 1011 and 1118  $\text{cm}^{-1}$ . The 706  $\text{cm}^{-1}$  band has been assigned to the  $A_1$  C-C stretch. The Raman spectrum of the liquid shows polarized bands at 1000 and 1115  $\text{cm}^{-1}$  which are taken to correspond to the 1011 and 1118  $\text{cm}^{-1}$  gas-phase bands. The 1118  $\text{cm}^{-1}$  band is assigned to one of the  $A_1$   $\text{CD}_3$  deformations,  $\nu_3$ , and the 1011  $\text{cm}^{-1}$  band is assigned to the  $A_1$   $\text{CD}_3$  rocking mode,  $\nu_5$ . The third  $A_1$  mode, due to the other  $\text{CD}_3$  deformation,  $\nu_4$ , is assigned to the only remaining polarized Raman band, at 1062  $\text{cm}^{-1}$ . No corresponding band was seen in the gas phase. The assignment of  $\nu_4$  is reasonable, but must be regarded as tentative. It must be emphasized that, although the bands have been assigned to  $\text{CD}_3$  deformation and rocking modes, these two types of motion are so close in frequency that they probably interact strongly, so that the actual normal vibrations are mixtures of the two types of motion.

The two E rocking modes are assigned to the gas phase features at 824 and 742  $\text{cm}^{-1}$  with corresponding features, which are depolarized in the Raman spectrum, at

822 and 738  $\text{cm}^{-1}$  in the liquid. An alternative assignment for one of these modes is the gas phase perpendicular band at 923  $\text{cm}^{-1}$ , found at 902  $\text{cm}^{-1}$  (depolarized) in the liquid. This appears to be too high in frequency for an E methyl- $\text{d}_3$  rocking mode (164, 167) and too low for a methyl- $\text{d}_3$  deformation (Table VIII) and it is therefore assigned to a combination  $\nu_6 + \nu_{24}$  (Table VII).

The only modes still unassigned are the three E modes derived from the methyl- $\text{d}_3$  deformations. One of them is clearly to be assigned to the perpendicular band at 1052  $\text{cm}^{-1}$  in the gas, with corresponding band at 1048  $\text{cm}^{-1}$  in the liquid. The assignment of the remaining two E modes is unclear. The only other depolarized Raman feature in this region is at 1038  $\text{cm}^{-1}$ . The infrared spectra of the gas and liquid show weak features at 1040  $\text{cm}^{-1}$  and 1039  $\text{cm}^{-1}$  which presumably correspond to the Raman feature at 1038  $\text{cm}^{-1}$ . This is, therefore, tentatively assigned to the remaining two E modes derived from methyl- $\text{d}_3$  deformations,  $\nu_{18}$  and  $\nu_{19}$ . It is clear that the evidence for the assignment of  $\nu_4$  and of  $\nu_{18}$  and  $\nu_{19}$  is much less definitive than is desirable.

(E) Summary

A complete assignment has been presented for the infrared and Raman spectra of t-butyl bromide- $\text{d}_9$ . Most

of the assignments are clear from the experimental data, but some must be regarded as tentative. In particular the assignment of one of the degenerate asymmetric C-D stretching modes,  $\nu_{14}$  and of one  $A_1$  and two E  $CD_3$  deformation modes,  $\nu_4$ ,  $\nu_{18}$ , and  $\nu_{19}$ , are not as firmly based on experimental evidence as is desirable.

The compatibility of this assignment with that of the spectra of  $C_4H_9Br$  is demonstrated by the normal coordinate calculation reported in the next chapter.

5. NORMAL COORDINATE ANALYSIS OF t-BUTYL BROMIDE

Normal coordinate calculations have been made to fit the frequencies of the two isotopic molecules to the same force field, in order to check the mutual compatibility of the assignments for the two molecules suggested in the last chapter. Such calculations have been reported by Huttner and Zeil (118) for t-butyl bromide- $h_9$  but there is no such report for t-butyl bromide- $d_9$ . Also Huttner and Zeil ignored the methyl torsional modes in their calculations. The assignments proposed in this thesis indicate that the methyl torsional modes have frequencies comparable to those of the skeleton deformation modes, so that the torsional modes cannot properly be neglected in the calculations, and they are included in this work. A complete vibrational calculation gives the frequencies of all of the modes, including those which are inactive in the infrared or Raman spectra, as the  $A_2$  modes of t-butyl bromide are. When the frequencies of all of the vibrational modes of a molecule are known, its thermodynamic properties can be calculated (15). This chapter presents the normal coordinate calculations for t-butyl bromide- $h_9$  and - $d_9$ , followed by the calculated thermodynamic properties of the gaseous molecules.

### 5.1 COORDINATES AND COMPUTER PROGRAMS

The problem was set up in internal coordinates using a valence force field. The set of 40 internal coordinates used is given in Table IX. The various internal coordinates are described with reference to Figure 20. The normal coordinate analysis was carried out using Wilson's  $G\bar{F}$  matrix method (16). For each molecule the  $G$  matrix was calculated from the data given under Table V, and the atomic weights (153) using the programs CART and GMAT (24). Typical elements were checked by hand calculations using established methods (16). The  $G$  matrices for the two molecules are given in Appendix I.

Since the t-butyl bromide molecule has fourteen atoms, there are thirty-six normal vibrations and therefore thirty-six internal coordinates can completely define the vibrational problem for one molecule. Because symmetry coordinates were used, it was necessary to include symmetrically complete sets of coordinates and a total of forty coordinates resulted. Four of them were redundant coordinates and yielded zero frequencies when carried through the calculations. The symmetry coordinates are given in terms of the internal coordinates in Table X. A comparison of Table X with the representation formed by the cartesian displacement coordinates (Table IV) shows

Table IX  
Internal Coordinates for t-butyl bromide.<sup>a</sup>

Coordinate	No.	Description
R	1	$\nu(\text{C}_1\text{-Br})$
$s_1$	2	$\nu(\text{C}_1\text{-C}_2)$
$s_2$	3	$\nu(\text{C}_1\text{-C}_3)$
$s_3$	4	$\nu(\text{C}_1\text{-C}_4)$
$r_1$	5	$\nu(\text{C}_2\text{-H}_1)$
$r_2$	6	$\nu(\text{C}_2\text{-H}_2)$
$r_3$	7	$\nu(\text{C}_2\text{-H}_3)$
$r_4$	8	$\nu(\text{C}_3\text{-H}_4)$
$r_5$	9	$\nu(\text{C}_3\text{-H}_5)$
$r_6$	10	$\nu(\text{C}_3\text{-H}_6)$
$r_7$	11	$\nu(\text{C}_4\text{-H}_7)$
$r_8$	12	$\nu(\text{C}_4\text{-H}_8)$
$r_9$	13	$\nu(\text{C}_4\text{-H}_9)$
$\alpha_1$	14	$\delta(\text{C}_2\text{-C}_1\text{-Br})$
$\alpha_2$	15	$\delta(\text{C}_3\text{-C}_1\text{-Br})$
$\alpha_3$	16	$\delta(\text{C}_4\text{-C}_1\text{-Br})$
$\beta_1$	17	$\delta(\text{H}_2\text{-C}_2\text{-H}_3)$
$\beta_2$	18	$\delta(\text{H}_1\text{-C}_2\text{-H}_3)$
$\beta_3$	19	$\delta(\text{H}_1\text{-C}_2\text{-H}_2)$
$\beta_4$	20	$\delta(\text{H}_5\text{-C}_3\text{-H}_6)$
$\beta_5$	21	$\delta(\text{H}_4\text{-C}_3\text{-H}_6)$

. . . cont'd.



Table IX - cont'd.

Coordinate	No.	Description
$\beta_6$	20	$\delta(H_4-C_3-H_5)$
$\beta_7$	23	$\delta(H_8-C_4-H_9)$
$\beta_8$	24	$\delta(H_7-C_4-H_9)$
$\beta_9$	25	$\delta(H_7-C_4-H_8)$
$\gamma_1$	26	$\delta(H_1-C_2-C_1)$
$\gamma_2$	27	$\delta(H_2-C_2-C_1)$
$\gamma_3$	28	$\delta(H_3-C_2-C_1)$
$\gamma_4$	29	$\delta(H_4-C_3-C_1)$
$\gamma_5$	30	$\delta(H_5-C_3-C_1)$
$\gamma_6$	31	$\delta(H_6-C_3-C_1)$
$\gamma_7$	32	$\delta(H_7-C_4-C_1)$
$\gamma_8$	33	$\delta(H_8-C_4-C_1)$
$\gamma_9$	34	$\delta(H_9-C_4-C_1)$
$\epsilon_1$	35	$\delta(C_3-C_1-C_4)$
$\epsilon_2$	36	$\delta(C_2-C_1-C_4)$
$\epsilon_3$	37	$\delta(C_2-C_1-C_3)$
$\tau_1$	38	Torsional motion of methyl group at $C_2$
$\tau_2$	39	Torsional motion of methyl group at $C_3$

. . . cont'd.

Table IX - cont'd.

Coordinate	No.	Description
$\tau_3$	40	Torsional motion of methyl group at C <sub>4</sub> .

<sup>a</sup>These are described with reference to the Figure 20.

$\nu$  represents change in bond length

$\delta$  represents change in bond angles.

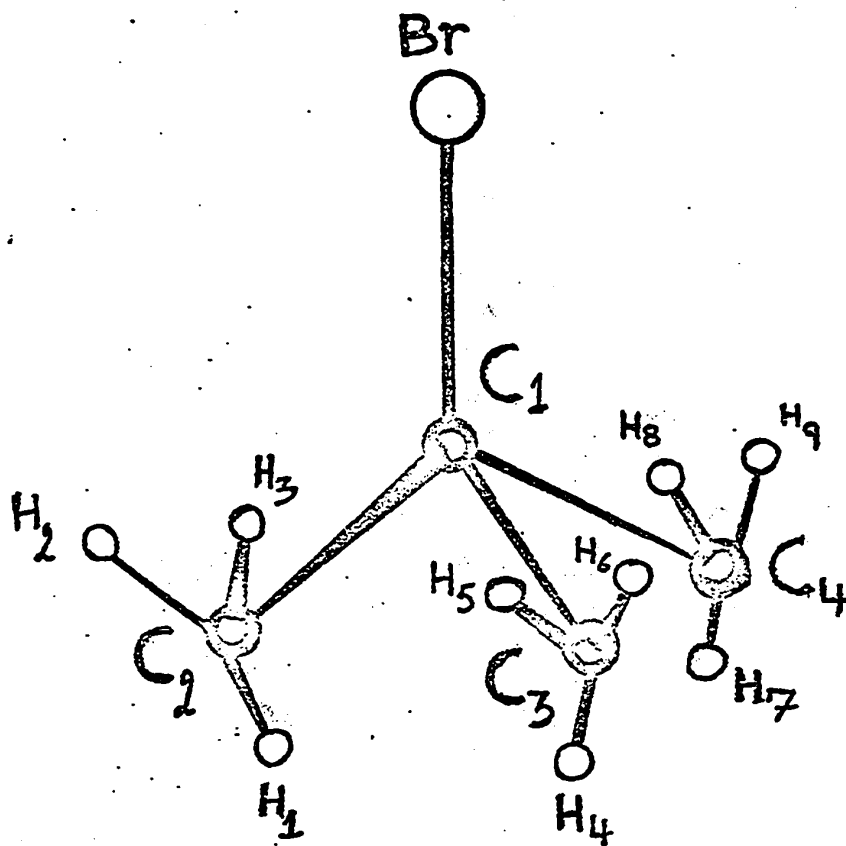


Figure 20

The atom-numbering system used to describe the internal coordinate of t-butyl bromide.

Table X  
Symmetry Coordinates for t-butyl bromide.<sup>a</sup>

Coordinate No.	Description	Symmetry
s <sub>1</sub>	$\frac{1}{\sqrt{3}}(r_1+r_4+r_7)$	A <sub>1</sub>
s <sub>2</sub>	$\frac{1}{\sqrt{6}}(r_2+r_3+r_5+r_6+r_8+r_9)$	A <sub>1</sub>
s <sub>3</sub>	$\frac{1}{\sqrt{3}}(s_1+s_2+s_3)$	A <sub>1</sub>
s <sub>4</sub>	R	A <sub>1</sub>
s <sub>5</sub>	$\frac{1}{\sqrt{3}}(\beta_1+\beta_4+\beta_7)$	A <sub>1</sub>
s <sub>6</sub>	$\frac{1}{\sqrt{6}}(\beta_2+\beta_3+\beta_5+\beta_6+\beta_8+\beta_9)$	A <sub>1</sub>
s <sub>7</sub>	$\frac{1}{\sqrt{3}}(\gamma_1+\gamma_4+\gamma_6)$	A <sub>1</sub>
s <sub>8</sub>	$\frac{1}{\sqrt{6}}(\gamma_2+\gamma_3+\gamma_5+\gamma_6+\gamma_8+\gamma_9)$	A
s <sub>9</sub>	$\frac{1}{\sqrt{3}}(\epsilon_1+\epsilon_2+\epsilon_3)$	A <sub>1</sub>
s <sub>10</sub>	$\frac{1}{\sqrt{3}}(\alpha_1+\alpha_2+\alpha_3)$	A <sub>1</sub>
s <sub>11</sub>	$\frac{1}{\sqrt{6}}(r_2-r_3+r_5-r_6+r_8-r_9)$	A <sub>2</sub>
s <sub>12</sub>	$\frac{1}{\sqrt{6}}(\beta_2-\beta_3+\beta_5-\beta_6+\beta_8-\beta_9)$	A <sub>2</sub>
s <sub>13</sub>	$\frac{1}{\sqrt{6}}(\gamma_2-\gamma_3+\gamma_5-\gamma_6+\gamma_8-\gamma_9)$	A <sub>2</sub>
s <sub>14</sub>	$\frac{1}{\sqrt{3}}(\tau_1+\tau_2+\tau_3)$	A <sub>2</sub>
s <sub>15</sub>	$\frac{1}{\sqrt{6}}(2r_1-r_4-r_7)$	E (a)
s <sub>16</sub>	$\frac{1}{\sqrt{12}}[2(r_2+r_3)-(r_5+r_6)-(r_8+r_9)]$	E (a)
s <sub>17</sub>	$\frac{1}{2}(r_5-r_6-r_8+r_9)$	E (a)

... cont'd.

Table X - cont'd.

Coordinate No.	Description	Symmetry
s <sub>18</sub>	$\frac{1}{\sqrt{6}}(2\beta_1 - \beta_2 - \beta_3)$	E (a)
s <sub>19</sub>	$\frac{1}{\sqrt{12}}(2\beta_2 + 2\beta_3 - \beta_5 - \beta_6 - \beta_8 - \beta_9)$	E (a)
s <sub>20</sub>	$\frac{1}{2}(\beta_5 - \beta_6 - \beta_8 + \beta_9)$	E (a)
s <sub>21</sub>	$\frac{1}{\sqrt{6}}(2\gamma_1 - \gamma_2 - \gamma_3)$	E (a)
s <sub>22</sub>	$\frac{1}{\sqrt{12}}(2\gamma_2 + 2\gamma_3 - \gamma_5 - \gamma_6 - \gamma_8 - \gamma_9)$	E (a)
s <sub>23</sub>	$\frac{1}{2}(\gamma_5 - \gamma_6 - \gamma_8 + \gamma_9)$	E (a)
s <sub>24</sub>	$\frac{1}{\sqrt{6}}(2s_1 - s_2 - s_3)$	E (a)
s <sub>25</sub>	$\frac{1}{\sqrt{6}}(2\varepsilon_1 - \varepsilon_2 - \varepsilon_3)$	E (a)
s <sub>26</sub>	$\frac{1}{\sqrt{6}}(2\alpha_1 - \alpha_2 - \alpha_3)$	E (a)
s <sub>27</sub>	$\frac{1}{\sqrt{2}}(\tau_1 - \tau_2)$	E (a)
s <sub>28</sub>	$\frac{1}{\sqrt{2}}(r_4 - r_7)$	E (b)
s <sub>29</sub>	$\frac{1}{\sqrt{12}}(2r_2 - 2r_3 - r_5 + r_6 - r_8 + r_9)$	E (b)
s <sub>30</sub>	$\frac{1}{2}(r_5 + r_6 - r_8 - r_9)$	E (b)
s <sub>31</sub>	$\frac{1}{\sqrt{2}}(\beta_4 - \beta_7)$	E (b)
s <sub>32</sub>	$\frac{1}{\sqrt{12}}(2\beta_2 - 2\beta_3 - \beta_5 + \beta_6 - \beta_8 + \beta_9)$	E (b)
s <sub>33</sub>	$\frac{1}{2}(\beta_5 + \beta_6 - \beta_8 - \beta_9)$	E (b)
s <sub>34</sub>	$\frac{1}{\sqrt{2}}(\gamma_4 - \gamma_7)$	E (b)
s <sub>35</sub>	$\frac{1}{\sqrt{12}}(2\gamma_2 - 2\gamma_3 - \gamma_5 + \gamma_6 - \gamma_8 + \gamma_9)$	E (b)

. . . cont'd.

Table X - cont'd.

Coordinate No.	Description	Symmetry
$s_{36}$	$\frac{1}{2}(\gamma_5 + \gamma_6 - \gamma_8 - \gamma_9)$	E (b)
$s_{37}$	$\frac{1}{\sqrt{2}}(s_2 - s_3)$	E (b)
$s_{38}$	$\frac{1}{\sqrt{2}}(\epsilon_2 - \epsilon_3)$	E (b)
$s_{39}$	$\frac{1}{\sqrt{2}}(\alpha_2 - \alpha_3)$	E (b)
$s_{40}$	$\frac{1}{\sqrt{6}}(2\tau_1 - \tau_2 - \tau_3)$	E (b)

<sup>a</sup>These are described in terms of the internal coordinates given in the Table IX.

that there are two redundant coordinates of symmetry  $A_1$  and two of symmetry E (an  $E_a$  and  $E_b$  pair corresponding to one doubly degenerate mode).

Two programs, VSEC and FPERT, written by Schachtschneider (24) and modified for use on the IBM 360/67 computer at the University of Alberta, were used to calculate the normal modes and their frequencies. Both programs were checked using the methyl fluoride data of Schachtschneider, and reproduced Schachtschneider's solutions exactly. They have also satisfactorily reproduced other published data, including that of Huttner and Zeil for *t*-butyl bromide- $h_9$ . VSEC simply calculates the frequencies and eigenvectors (normal coordinates) from a given G matrix and set of force constants, and was used for preliminary calculations. FPERT calculates the frequencies from the G matrices and force constants supplied, compares them with the observed frequencies, adjusts the force constants to improve the fit, and continues until a satisfactory solution is reached. If the G matrices and observed frequencies of two or more isotopic molecules are supplied, the same force field will be refined to simultaneously fit the frequencies of all of the molecules. It is necessary to carry out tests to check that the final force

field calculated by the program is the optimum force field. Several criteria are applied. First, the calculations are repeated starting from a different force field which must, of course, be reasonable. Secondly, the final force constants should have reasonable values. Thirdly, the determinant involved in the calculation of the correction to the force constants must not be singular or near singular (170). Fourth, the distribution of the potential energy of each vibration between the different force constants, and the description of the normal coordinates in terms of the internal coordinates, should be consistent with the experimental assignments for all normal modes.

The potential energy distribution was obtained by calculating the matrix  $P_{\nu}^E$  which is given by

$$P_{\nu}^E = \lambda_{\nu}^{-1} J_{\nu} Z_{\nu} \phi_{\nu} \quad 33$$

where  $\phi_{\nu}$  is a diagonal matrix, with the  $m$  force constants as its elements.  $Z_{\nu}$  is a rectangular matrix of order  $n \times m$ , where  $m$  is as defined above, and  $n$  is the number of elements in the force constant matrix,  $F_{\nu}$ . The elements of  $Z_{\nu}$  are given by

$$Z_{\nu} = F_{\nu} \phi_{\nu}^{-1} \quad 34$$



$J$  is a rectangular matrix, of order  $q \times n$ , with the elements  $J_{jk} = L_{ij} \cdot L_{ik}$  ( $i, j, k=1 \dots q$ );  $q$  is the number of internal coordinates, 40 in the present case.  $L_{ij}$  and  $L_{ik}$  are elements of the  $L$  matrix which relates internal coordinates to the normal coordinates by the relation (see Section 1.2.1)

$$R = LQ \quad 35$$

$\lambda^{-1}$  is the inverse of the diagonal matrix  $\lambda$  defined in Section 1.2.1. Each row of the  $PE$  matrix gives the potential energy distribution for one normal mode in terms of the  $m$  force constants.

## 5.2 CALCULATIONS AND RESULTS

In order to obtain a starting diagonal force field, two separate calculations were carried out for the light compound. One started with the diagonal force constants of the force field given by Evans and Lo for *t*-butyl chloride (164), and the second started with the diagonal elements of the force field given by Huttner and Zeil (118). The methyl torsional force constant was kept equal to zero for these preliminary calculations. Although these two force fields are quite different initially, they converged to the same set of values on refinement by

FPERT. The frequencies calculated from the refined diagonal force field differed considerably from the observed ones, but the assignments were correct, except for the  $A_1$  skeleton deformation and C-Br stretching modes, which were interchanged. When the methyl torsional force constant was allowed to vary, neither force field converged. Therefore, in all subsequent calculations, the methyl torsional force constant was constrained to a value which was adjusted from run to run to seek the optimum value.

In order to correct the assignment of the  $A_1$ , C-C-Br deformation and C-Br stretching modes, interaction constants between the C-Br stretch and C-C-Br angle deformation,  $F_{R\alpha}$  and between the C-Br stretch and the C-C stretches,  $F_{rs}$ , were introduced. In addition to these, the four other interaction constants shown in Table XI were necessary in order to obtain satisfactory agreement between the observed and the calculated frequencies. With these interaction constants included in the force field, it was found that the agreement between the calculated and observed frequencies was better if the C-Br stretching force constant was constrained to a suitable value than if it was allowed to refine during the calculation. The value to which it was constrained was selected from the results of a number of runs. Two such calculations, which resulted

Table XI

Force constants for t-butyl bromide.

No.	Symbol	Value <sup>a</sup>		Description
		Force Field I	Force Field II	
1	F <sub>R</sub>	2.560 <sup>b</sup>	1.85 <sup>b</sup>	C-Br Stretch
2	F <sub>S</sub>	4.0546	3.9047	C-C Stretch
3	F <sub>rr</sub>	4.8097	4.8099	C-H Stretch
4	F <sub>α</sub>	0.8800	0.9200 <sup>b</sup>	C-C-Br Bend
5	F <sub>β</sub>	0.5336	0.5358	H-C-H Bend
6	F <sub>Y</sub>	0.6823	0.6656	C-C-H Bend
7	F <sub>ε</sub>	1.1390	1.1400 <sup>b</sup>	C-C-C Bend
8	F <sub>T</sub>	0.0148 <sup>b</sup>	0.0159 <sup>b</sup>	Methyl torsion
9	F <sub>RS</sub>	0.7396	0.5000 <sup>b</sup>	C-Br stretch and C-C stretch interaction
10	F <sub>SS</sub>	0.5284	0.4162	C-C stretch and C-C stretch interaction
11	F <sub>rr</sub>	0.0946	0.0842	C-H stretch and C-H stretch interaction
12	F <sub>Rα</sub>	0.4753	0.2000 <sup>b</sup>	C-Br stretch and C-C-Br bend interaction
13	F <sub>YY</sub>	-0.0347	-0.0267	C-C-H and C-C-H interaction, common C-C
14	F <sub>SY</sub>	0.2196	0.2158	C-C stretch and C-C-H bend interaction, common C-C

146.

. . . cont'd.

## Table XI - cont'd.

a The force constants are in units of  $\text{mdyne } \text{Å}^{-1}$ ,  $\text{mdyne}$ , or  $\text{mdyne } \text{Å}$ , for constants of the type  $F_s$  and  $F_{ss}$ ,  $F_{sy}$  or  $F_\gamma$  and  $F_{\gamma\gamma}$  and  $F_\tau$  respectively.

b The force constants were constrained to the values shown.

in two distinct force fields, are described below.

The first force field was obtained by constraining only the methyl torsion and C-Br stretch force constants to the values shown in Table XI. This force field gave an average error of  $8 \text{ cm}^{-1}$  or 1.2% between the observed and calculated frequencies (Tables XII and XIII) which is regarded as good, in view of the neglect of anharmonic effects. But the distribution of the potential energy of the  $\nu_7$  and  $\nu_8$  modes included a very large contribution from the interaction constant between the C-Br stretch and C-C-Br deformations (Tables XIV and XV). This was felt to be undesirable and attempts were made to seek a force field that gave a satisfactory fit to the observed frequencies without this disadvantage. The second force field was obtained by constraining the C-Br stretch and the C-C-Br and C-C-C deformation force constants and the two interaction constants involving these coordinates,  $F_{rs}$  and  $F_{R\alpha}$ , to the values shown in Table XI. These values were selected as the best of many sets of values tried. The average error between the observed and calculated frequencies obtained after refining this force field was  $12.0 \text{ cm}^{-1}$  or 2.0%, Tables XII and XIII. It is not as good as that obtained with the first force field, particularly for the  $\nu_8$  mode, but the potential energy distribution (Tables

Table XIII

Comparison of the calculated and observed frequencies for the fundamental vibrations of t-butyl bromide-h<sub>9</sub>.<sup>a</sup>

Symmetry	Mode No.	Observed Frequencies	Calculated Frequencies	
			Force Field <sup>b</sup>	
			I	II
A <sub>1</sub>	1	2977	2981	2984
	2	2934	2947	2941
	3	1480	1464	1463
	4	1397	1394	1392
	5	1153	1169	1180
	6	808	809	805
	7	524	527	541
	8	304	300	259
A <sub>2</sub>	9		2978	2982
	10		1456	1457
	11		1021	1005
	12		267	276
E	13	2992	2982	2985
	14	2977	2979	2982
	15	2953	2946	2940
	16	1457 <sup>c</sup>	1462	1462
	17	1449 <sup>c</sup>	1457	1458
	18	1375	1378	1379
	19	1238	1257	1249
	20	1033	1031	1015
	21	930 <sup>c</sup>	930	920
	22	396 <sup>c</sup>	396	396
	23	285 <sup>c</sup>	283	290
	24	272 <sup>c</sup>	244	251

<sup>a</sup>All frequencies are in the units cm<sup>-1</sup>.

<sup>b</sup>The two force fields used in the calculations are given in Table XI.

<sup>c</sup>These frequencies are from the infrared spectrum of the liquid. All others are from the infrared spectrum of the gas.

Table XIII

Comparison of the calculated and observed frequencies for the fundamental vibrations of t-butyl bromide-d<sub>9</sub>.<sup>a</sup>

Symmetry	Mode No.	Observed Frequencies	Calculated Frequencies	
			Force Field <sup>b</sup>	
			I	II
A <sub>1</sub>	1	2221	2227	2230
	2	2118 <sup>c</sup>	2125	2120
	3	1118	1123	1122
	4	1062 <sup>c</sup>	1054	1054
	5	1011	1002	1026
	6	706	687	677
	7	463	467	469
	8	274	274	240
A <sub>2</sub>	9		2221	2223
	10		1045	1046
	11		772	759
	12		189	196
E	13	2246	2230	2232
	14	2229	2223	2226
	15	2124	2122	2118
	16	1214	1215	1210
	17	1052	1051	1052
	18	1040	1047	1048
	19	1040	1035	1035
	20	824	788	776
	21	742	736	727
	22	335	339	339
	23	239	242	247
	24	206 <sup>c</sup>	182	188

<sup>a</sup>All frequencies are in the units cm<sup>-1</sup>.

<sup>b</sup>The two force fields used in the calculations are given in Table XI.

<sup>c</sup>These frequencies are from the spectra of the liquid. All others are from the infrared spectrum of the gas.

Table XIV

Distribution of the potential energy for each normal mode of t-butyl bromide-h<sub>9</sub> among the force constants of force field I.<sup>a</sup>

Symmetry	Mode	Frequency/Potential energy distribution									
A <sub>1</sub>	1	FREQUENCY = 2980.6 CM <sup>-1</sup>	0.0000	0.0000	1.0131	0.0007	0.0031	0.0020	0.0009	0.0	-0.0000
		0.0000	-0.0199	-0.0001	0.0001	-0.0000					
		FREQUENCY = 2947.6 CM <sup>-1</sup>	0.0000	0.0023	0.9582	0.0000	0.0009	0.0012	0.0000	0.0	-0.0000
	2	0.0006	0.0377	-0.0000	-0.0001	-0.0008					
		FREQUENCY = 1463.7 CM <sup>-1</sup>	0.0024	0.0018	0.0013	0.0000	0.8732	0.1168	0.0001	0.0	-0.0017
		0.0005	-0.0000	-0.0003	0.0059	-0.0000					
	3	FREQUENCY = 1393.9 CM <sup>-1</sup>	0.0000	0.0681	0.0024	0.0000	0.4671	0.5973	0.0000	0.0	0.0003
		0.0178	0.0001	0.0000	-0.0007	-0.0923					
		FREQUENCY = 1168.6 CM <sup>-1</sup>	0.0780	0.0704	0.0049	0.0642	0.1071	0.6481	0.0831	0.0	-0.0652
	4	0.0204	-0.0001	-0.0777	0.0339	0.0018					
		FREQUENCY = 809.2 CM <sup>-1</sup>	0.0549	0.7592	0.0015	0.0145	0.0118	0.0557	0.0188	0.0	-0.1623
		0.1979	0.0000	-0.0310	0.0037	0.0354					
5	FREQUENCY = 526.8 CM <sup>-1</sup>	0.8462	0.0008	0.0001	0.2647	0.0104	0.0723	0.3426	0.0	-0.0200	
	0.0002	0.0000	-0.5192	0.0028	-0.0009						
	FREQUENCY = 300.4 CM <sup>-1</sup>	0.3693	0.0440	0.0006	0.1689	0.0037	0.0111	0.2186	0.0	-0.1014	
6	0.0115	-0.0000	0.2739	0.0005	-0.0026						
	FREQUENCY = 2978.2 CM <sup>-1</sup>	0.0	0.0	1.0151	0.0	0.0030	0.0018	0.0	0.0000	0.0	
	0.0	-0.0200	0.0	0.0001	0.0						
7	FREQUENCY = 1456.3 CM <sup>-1</sup>	0.0	0.0	0.0016	0.0	0.9128	0.0818	0.0	0.0000	0.0	
	0.0	-0.0000	0.0	0.0042	0.0						
	FREQUENCY = 1021.0 CM <sup>-1</sup>	0.0	0.0	0.0034	0.0	0.0844	0.8579	0.0	0.0002	0.0	
8	0.0	-0.0001	0.0	0.0441	0.0						
	FREQUENCY = 266.7 CM <sup>-1</sup>	0.0	0.0	0.0000	0.0	0.0001	0.0001	0.0	0.9998	0.0	
	0.0	-0.0000	0.0	0.0000	0.0						
9											
10											
11											
12											

. . . cont'd.



Table XIV - cont'd.

Symmetry	Mode	Frequency/Potential energy distribution
E	13	FREQUENCY = 2981.7 CM-1 0.0 0.0000 1.0124 0.0001 0.0031 0.0019 0.0023 0.0000 0.0 -0.0000 -0.0199 0.0 0.0001 -0.0000
	14	FREQUENCY = 2979.1 CM-1 0.0 0.0000 1.0144 0.0006 0.0030 0.0019 0.0000 0.0000 0.0 -0.0000 -0.0200 0.0 0.0001 -0.0000
	15	FREQUENCY = 2946.4 CM-1 0.0 0.0025 0.9590 0.0000 0.0009 0.0011 0.0000 0.0000 0.0 -0.0003 0.0377 0.0 -0.0001 -0.0008
	16	FREQUENCY = 1462.6 CM-1 0.0 0.0109 0.0013 0.0006 0.0686 0.1148 0.0000 0.0001 0.0 -0.0014 -0.0000 0.0 0.0058 -0.0005
	17	FREQUENCY = 1457.4 CM-1 0.0 0.0002 0.0016 0.0005 0.9129 0.0753 0.0013 0.0000 0.0 -0.0000 -0.0000 0.0 0.0040 -0.0000
	18	FREQUENCY = 1377.8 CM-1 0.0 0.0764 0.0020 0.0002 0.4795 0.6124 0.0005 0.0000 0.0 -0.0100 0.0001 0.0 -0.0622 -0.0999
	19	FREQUENCY = 1257.2 CM-1 0.0 0.4460 0.0042 0.0362 0.0849 0.3247 0.1170 0.0078 0.0 -0.0581 -0.0001 0.0 0.0160 0.0184
	20	FREQUENCY = 1030.5 CM-1 0.0 0.0019 0.0039 0.0106 0.0770 0.6545 0.0089 0.0000 0.0 -0.0002 -0.0001 0.0 0.0435 0.0000
	21	FREQUENCY = 929.6 CM-1 0.0 0.4823 0.0019 0.0129 0.0365 0.4875 0.0063 0.0026 0.0 -0.0628 -0.0000 0.0 0.0247 0.0062
	22	FREQUENCY = 395.8 CM-1 0.0 0.1398 0.0009 0.0174 0.0099 0.0318 0.7568 0.0590 0.0 -0.0182 -0.0000 0.0 0.0016 0.0011
	23	FREQUENCY = 282.6 CM-1 0.0 0.0171 0.0003 0.3931 0.0028 0.0063 0.1059 0.4762 0.0 -0.0022 -0.0000 0.0 0.0003 0.0001
	24	FREQUENCY = 244.4 CM-1 0.0 0.0158 0.0002 0.5249 0.0016 0.0043 0.0010 0.4542 0.0 -0.0020 -0.0000 0.0 0.0002 0.0001

The 14 entries after each frequency are in the order of the force constants in Table XI.

Table XV

Distribution of the potential energy for each normal mode of t-butyl bromide-d<sub>9</sub> among the force constants of force field I. a

Symmetry	Mode	Frequency/Potential energy distribution	
A <sub>1</sub>	1	FREQUENCY = 227.4 CM-1 0.0001 0.0000 0.9958 0.0028 0.0101 0.0073 0.0036 0.0 -0.0000 0.0000 -0.0198 -0.0005 0.0004 -0.0000	
	2	FREQUENCY = 2125.2 CM-1 0.0000 0.0112 0.9435 0.0000 0.0043 0.0055 0.0000 0.0 -0.0003 0.0029 0.0371 -0.0000 -0.0006 -0.0036	
	3	FREQUENCY = 1122.6 CM-1 0.0131 0.3133 0.0164 0.0075 0.3540 0.4814 0.0096 0.0 -0.0810 0.0817 0.0006 -0.0109 -0.0441 -0.1717	
	4	FREQUENCY = 1054.3 CM-1 0.0192 0.0026 0.0030 0.0028 0.8121 0.1612 0.0032 0.0 -0.0056 0.0007 -0.0001 -0.0076 0.0059 0.0029	
	5	FREQUENCY = 1001.8 CM-1 0.1523 0.0655 0.0178 0.1115 0.1998 0.4721 0.1444 0.0 -0.0794 0.0171 -0.0003 -0.1430 0.0167 0.0257	
	6	FREQUENCY = 687.2 CM-1 0.0223 0.5228 0.0039 0.0011 0.0658 0.2446 0.0014 0.0 -0.0858 0.1363 0.0001 -0.0054 0.0005 0.0927	
	7	FREQUENCY = 467.5 CM-1 0.9047 0.0049 0.0005 0.1739 0.0188 0.1575 0.2250 0.0 -0.0532 0.0013 0.0000 -0.4351 0.0056 -0.0040	
	8	FREQUENCY = 273.6 CM-1 0.2392 0.0343 0.0014 0.2138 0.0144 0.0348 0.2768 0.0 -0.0720 0.0089 -0.0000 0.2481 0.0017 -0.0014	
	A <sub>2</sub>	9	FREQUENCY = 2220.9 CM-1 0.0 0.0 1.0035 0.0 0.0098 0.0060 0.0 0.0000 0.0 0.0 -0.0197 0.0 0.0003 0.0
		10	FREQUENCY = 1044.9 CM-1 0.0 0.0 0.0067 0.0 0.9509 0.0404 0.0 0.0001 0.0 0.0 -0.0001 0.0 0.0021 0.0
		11	FREQUENCY = 772.2 CM-1 0.0 0.0 0.0098 0.0 0.0391 0.9048 0.0 0.0004 0.0 0.0 -0.0002 0.0 0.0460 0.0
		12	FREQUENCY = 189.1 CM-1 0.0 0.0 0.0000 0.0 0.0001 0.0003 0.0 0.9995 0.0 0.0 -0.0000 0.0 0.0000 0.0

. . . cont'd.

Table XV - cont'd.

Symmetry	Mode	Frequency/Potential energy distribution
E	13	FREQUENCY = 2230.1 CM-1 0.0 0.0002 0.9929 -0.0000 -0.0195 0.0
		FREQUENCY = 2223.3 CM-1 0.0 0.0001 1.0007 -0.0000 -0.0197 0.0
	14	FREQUENCY = 2122.0 CM-1 0.0 0.0131 0.9466 -0.0017 0.0372 0.0
		FREQUENCY = 1215.0 CM-1 0.0 0.7500 0.0164 -0.0977 0.0003 0.0
	15	FREQUENCY = 1050.5 CM-1 0.0 0.0000 0.0092 -0.0000 -0.0002 0.0
		FREQUENCY = 1047.3 CM-1 0.0 0.0027 0.0062 -0.0003 -0.0001 0.0
	16	FREQUENCY = 1034.8 CM-1 0.0 0.0000 0.0079 -0.0000 0.0000 0.0
		FREQUENCY = 788.4 CM-1 0.0 0.0089 0.0122 -0.0012 -0.0002 0.0
	17	FREQUENCY = 736.4 CM-1 0.0 0.2722 0.0074 -0.0355 -0.0001 0.0
		FREQUENCY = 338.6 CM-1 0.0 0.1173 0.0016 -0.0153 -0.0000 0.0
	18	FREQUENCY = 241.9 CM-1 0.0 0.0266 0.0011 -0.0035 -0.0000 0.0
		FREQUENCY = 181.7 CM-1 0.0 0.0015 0.0001 -0.0002 -0.0000 0.0
	19	0.0002 0.0103 0.0070 0.0085 0.0001 0.0 0.0004 -0.0000
		0.0022 0.0059 0.0064 0.0000 0.0000 0.0 0.0003 -0.0000
20	0.0000 0.0039 0.0050 0.0000 0.0000 0.0 -0.0005 -0.0037	
	0.432 0.0568 0.2232 0.1053 0.0082 0.0 0.0004 -0.1060	
21	0.0007 0.9470 0.0308 0.0110 0.0000 0.0 0.0015 -0.0001	
	0.0004 0.8814 0.1186 0.0013 0.0001 0.0 -0.0042 -0.0061	
22	0.0143 0.4610 0.5030 0.0343 0.0022 0.0 -0.0435 0.0008	
	0.0226 0.0246 0.8651 0.0230 0.0000 0.0 0.0439 0.0012	
23	0.0014 0.0337 0.6567 0.0021 0.0005 0.0 0.0309 0.0306	
	0.0313 0.0231 0.0785 0.7095 0.0429 0.0 0.0037 0.0074	
24	0.7363 0.0101 0.0237 0.0898 0.1132 0.0 0.0011 0.0016	
	0.1473 0.0008 0.0022 0.0162 0.8329 0.0 0.0001 -0.0001	

<sup>a</sup>The 14 entries after each frequency are in the order of the force constants in Table XI.

XVI and XVII) does contain much smaller contributions from the interaction constants than was found for the first force field. The eigenvectors (Section 1.2.1) obtained from the two force fields are very similar and are given in Appendix II. The F matrices describing the two force fields are given in Appendix III.

The choice between these two force fields depends on the acceptability of large contributions to the potential energy of a mode from an interaction constant. It was not found possible to fit the low frequency  $A_1$  modes well without this large contribution resulting, and it is noteworthy that Huttner and Zeil's force field (118) also gives such a large contribution. This appears to be a case where the approximations in the theory lead to results that seem to be out of keeping with the philosophy of a valence force field.

The assignment of the  $\nu_{15}$  mode of  $C_4H_9Br$  and the  $\nu_4$ ,  $\nu_{14}$ ,  $\nu_{18}$  and  $\nu_{19}$  modes of  $C_4D_9Br$  discussed in the last chapter was less clear than for the other modes.

Therefore, the frequencies of these modes were weighted only half as much as those of the remaining modes in the calculation (24). The calculated values, which agree reasonably well with the experimental ones, therefore lend some support to the assignment suggested for these modes.

Table XVI

Distribution of the potential energy for each normal mode of t-butyl bromide-h<sub>9</sub> among the force constants of force field II.<sup>a</sup>

Symmetry	Mode	Frequency/Potential energy distribution									
A <sub>1</sub>	1	FREQUENCY = 2984.0 CM-1	0.0000	0.0000	1.0109	0.0008	0.0031	0.0015	0.0010	0.0	-0.0000
		0.0000	-0.0177	-0.0000	0.0001	-0.0000					
	2	FREQUENCY = 2941.2 CM-1	0.0000	0.0022	0.9624	0.0000	0.0009	0.0011	0.0000	0.0	-0.0000
		0.0005	0.0337	-0.0000	-0.0001	-0.0007					
	3	FREQUENCY = 1463.3 CM-1	0.0015	0.0017	0.0014	0.0000	0.8865	0.1054	0.0000	0.0	-0.0011
		0.0004	-0.0000	-0.0001	0.0042	-0.0001					
	4	FREQUENCY = 1391.7 CM-1	0.0000	0.0650	0.0023	0.0000	0.4714	0.5655	0.0000	0.0	-0.0007
		0.0139	0.0001	-0.0000	-0.0470	-0.0905					
5	FREQUENCY = 1172.6 CM-1	0.0683	0.0099	0.0049	0.0751	0.0091	0.6206	0.0931	0.0	-0.0505	
	0.0192	-0.0001	-0.0381	0.0248	0.0035						
6	FREQUENCY = 804.5 CM-1	0.0597	0.6927	0.0013	0.0211	0.0139	0.1546	0.0262	0.0	-0.1310	
	0.1477	0.0000	-0.0109	0.0056	0.0270						
7	FREQUENCY = 541.5 CM-1	0.4243	0.0386	0.0003	0.2274	0.0115	0.0821	0.2818	0.0	0.0825	
	0.0082	0.0000	-0.1650	0.0029	0.0055						
8	FREQUENCY = 259.0 CM-1	0.5816	0.0402	0.0004	0.1381	0.0040	0.0067	0.1711	0.0	-0.0986	
	0.0986	-0.0000	0.1505	0.0002	-0.0027						
A <sub>2</sub>	9	FREQUENCY = 2981.5 CM-1	0.0	0.0	1.0129	0.0	0.0030	0.0017	0.0	0.0000	0.0
		0.0	-0.0177	0.0	0.0001	0.0					
	10	FREQUENCY = 1456.9 CM-1	0.0	0.0	0.0017	0.0	0.9208	0.0745	0.0	0.0000	0.0
		0.0	-0.0000	0.0	0.0030	0.0					
11	FREQUENCY = 1005.0 CM-1	0.0	0.0	0.0032	0.0	0.0761	0.8650	0.0	0.0002	0.0	
	0.0	-0.0001	0.0	0.0355	0.0						
12	FREQUENCY = 276.4 CM-1	0.0	0.0	0.0000	0.0	0.0001	0.0002	0.0	0.9998	0.0	
	0.0	-0.0000	0.0	0.0000	0.0						

. . . cont'd.

Table XVII

Distribution of the potential energy for each normal mode of t-butyl bromide-d<sub>9</sub> among the force constants of force field II. <sup>a</sup>

Symmetry	Mode	Frequency/Potential energy distribution											
A <sub>1</sub>	1	FREQUENCY = 2230.1 CM-1											
		0.0001	0.0001	0.9931	0.0030	0.0102	0.0072	0.0037	0.0	0.0000	0.0000	0.0000	0.0000
		0.0000	-0.0174	-0.0002	0.0003	-0.0000							
	2	FREQUENCY = 2120.0 CM-1											
		0.0000	0.0107	0.9484	0.0000	0.0042	0.0053	0.0000	0.0	-0.0002	0.0000	0.0000	0.0000
		0.0023	0.0332	-0.0000	-0.0004	-0.0035							
	3	FREQUENCY = 1122.2 CM-1											
		0.0266	0.3342	0.0161	0.0209	0.3117	0.4664	0.0259	0.0	-0.0606	0.0000	0.0000	0.0000
		0.0712	0.0005	-0.0125	-0.0279	-0.1663							
	4	FREQUENCY = 1053.6 CM-1											
		0.0142	0.0007	0.0030	0.0028	0.8089	0.1670	0.0035	0.0	-0.0020	0.0000	0.0000	0.0000
		0.0001	-0.0000	-0.0034	0.0031	0.0020							
5	FREQUENCY = 1026.3 CM-1												
	0.1020	0.0291	0.0170	0.1050	0.2577	0.4128	0.1302	0.0	-0.0351	0.0000	0.0000	0.0000	
	0.0062	-0.0003	-0.0550	0.0041	0.0254								
6	FREQUENCY = 676.9 CM-1												
	0.0228	0.5028	0.0040	0.0012	0.0540	0.2936	0.0015	0.0	-0.0689	0.0000	0.0000	0.0000	
	0.1072	0.0000	-0.0028	0.0047	0.0799								
7	FREQUENCY = 469.2 CM-1												
	0.4807	0.0152	0.0005	0.1636	0.0236	0.1914	0.2026	0.0	0.0551	0.0000	0.0000	0.0000	
	0.0032	0.0000	-0.1489	0.0060	0.0067								
8	FREQUENCY = 240.2 CM-1												
	0.4892	0.0377	0.0011	0.1660	0.0100	0.0203	0.2057	0.0	-0.0875	0.0000	0.0000	0.0000	
	0.0080	-0.0000	0.1513	0.0007	-0.0024								
A <sub>2</sub>	9	FREQUENCY = 2223.2 CM-1											
		0.0	0.0	1.0016	0.0	0.0099	0.0058	0.0	0.0000	0.0	0.0000	0.0000	0.0
		0.0	-0.0175	0.0	0.0002	0.0							
	10	FREQUENCY = 1046.3 CM-1											
		0.0	0.0	0.0070	0.0	0.9555	0.0361	0.0	0.0001	0.0	0.0000	0.0000	0.0
		0.0	-0.0001	0.0	0.0014	0.0							
	11	FREQUENCY = 759.5 CM-1											
		0.0	0.0	0.0093	0.0	0.0345	0.9191	0.0	0.0004	0.0	0.0000	0.0000	0.0
		0.0	-0.0002	0.0	0.0369	0.0							
	12	FREQUENCY = 196.0 CM-1											
		0.0	0.0	0.0000	0.0	0.0001	0.0004	0.0	0.9994	0.0	0.0000	0.0000	0.0
		0.0	-0.0000	0.0	0.0000	0.0							

. . . cont'd.

Table XVI - cont'd.

Symmetry	Mode	Frequency/Potential energy distribution
E	13	FREQUENCY = 2984.9 CM <sup>-1</sup> 0.0 0.000 1.0102 0.0001 0.0031 0.0019 0.0023 0.0000 0.0 -0.0000 -0.0177 0.0 0.0001 -0.0000
		FREQUENCY = 2982.4 CM <sup>-1</sup> 0.0 0.000 1.0122 0.0006 0.0030 0.0018 0.0000 0.0000 0.0 -0.0000 -0.0177 0.0 0.0001 -0.0000
14	15	FREQUENCY = 2940.3 CM <sup>-1</sup> 0.0 0.0024 0.9630 0.0000 0.0009 0.0011 0.0000 0.0000 0.0 -0.0003 0.0337 0.0 -0.0001 -0.0008
		FREQUENCY = 1462.4 CM <sup>-1</sup> 0.0 0.0081 0.0015 0.0005 0.8666 0.1006 0.0000 0.0001 0.0 -0.0009 -0.0000 0.0 0.0040 -0.0004
16	17	FREQUENCY = 1458.2 CM <sup>-1</sup> 0.0 0.0003 0.0019 0.0005 0.9206 0.0725 0.0013 0.0000 0.0 -0.0000 -0.0000 0.0 0.0029 -0.0000
		FREQUENCY = 1379.5 CM <sup>-1</sup> 0.0 0.0736 0.0020 0.0002 0.4803 0.5961 0.0005 0.0000 0.0 -0.0078 0.0001 0.0 -0.0478 -0.0371
18	19	FREQUENCY = 1248.8 CM <sup>-1</sup> 0.0 0.4511 0.0040 0.0428 0.0691 0.3216 0.1198 0.0088 0.0 -0.0481 -0.0000 0.0 0.0125 0.0185
		FREQUENCY = 1014.8 CM <sup>-1</sup> 0.0 0.0020 0.0038 0.0114 0.0688 0.6701 0.0093 0.0000 0.0 -0.0002 -0.0001 0.0 0.0349 0.0000
20	21	FREQUENCY = 919.7 CM <sup>-1</sup> 0.0 0.4494 0.0019 0.0125 0.0369 0.5128 0.0052 0.0027 0.0 -0.0479 -0.0000 0.0 0.0205 0.0060
		FREQUENCY = 366.6 CM <sup>-1</sup> 0.0 0.1404 0.0009 0.0155 0.0097 0.0332 0.7380 0.0709 0.0 -0.0150 -0.0000 0.0 0.0013 0.0012
22	23	FREQUENCY = 289.9 CM <sup>-1</sup> 0.0 0.0145 0.0003 0.3444 0.0028 0.0067 0.1231 0.5053 0.0 -0.0015 -0.0000 0.0 0.0003 0.0001
		FREQUENCY = 251.2 CM <sup>-1</sup> 0.0 0.0180 0.0002 0.6675 0.0019 0.0082 0.0006 0.4082 0.0 -0.0019 -0.0000 0.0 0.0002 0.0001
24		

The 14 entries after each frequency are in the order of the force constants in Table XI.

Table XVII - cont'd.

Symmetry	Mode	Frequency/Potential energy distribution
E	13	FREQUENCY = 2232.3 CM-1
		0.0 0.0002 0.9911 0.0002 0.0104 0.0068 0.0085 0.0001 0.0
14	14	0.0 0.0000 -0.0174 0.0
		FREQUENCY = 2225.7 CM-1
15	15	0.0 0.0001 0.9986 0.0023 0.0100 0.0062 0.0001 0.0000 0.0
		0.0 0.0000 -0.0175 0.0
16	16	FREQUENCY = 2117.7 CM-1
		0.0 0.0126 0.9565 0.0000 0.0039 0.0049 0.0000 0.0000 0.0
17	17	0.0 0.0013 0.0333 0.0
		FREQUENCY = 1210.3 CM-1
18	18	0.0 0.7318 0.0164 0.0453 0.0615 0.2182 0.1051 0.0088 0.0
		0.0 0.0780 0.0003 0.0
19	19	FREQUENCY = 1052.1 CM-1
		0.0 0.0000 0.0000 0.0098 0.0007 0.9510 0.0251 0.0125 0.0001 0.0
20	20	0.0 0.0000 -0.0002 0.0
		FREQUENCY = 1048.3 CM-1
21	21	0.0 0.0015 0.0067 0.0008 0.9123 0.0833 0.0004 0.0000 0.0
		0.0 0.0002 -0.0001 0.0
22	22	FREQUENCY = 1035.0 CM-1
		0.0 0.0159 0.4487 0.5200 0.0354 0.0026 0.0
23	23	0.0 0.0000 0.0001 0.0
		FREQUENCY = 776.4 CM-1
24	24	0.0 0.0094 0.0116 0.0242 0.0206 0.8746 0.0246 0.0000 0.0
		0.0 0.0010 -0.0002 0.0
25	25	FREQUENCY = 726.7 CM-1
		0.0 0.2584 0.0072 0.0010 0.0308 0.6732 0.0026 0.0005 0.0
26	26	0.0 0.0275 -0.0001 0.0
		FREQUENCY = 338.8 CM-1
27	27	0.0 0.1180 0.0015 0.0353 0.0227 0.0823 0.6930 0.0493 0.0
		0.0 0.0126 -0.0000 0.0
28	28	FREQUENCY = 246.8 CM-1
		0.0 0.0258 0.0011 0.7162 0.0107 0.0263 0.1015 0.1187 0.0
29	29	0.0 0.0027 -0.0000 0.0
		FREQUENCY = 187.8 CM-1
30	30	0.0 0.0019 0.0001 0.1581 0.0009 0.0027 0.0164 0.8199 0.0
		0.0 0.0002 -0.0000 0.0

The 14 entries after each frequency are in the order of the force constants in Table XI.



Thus two force fields, each consisting of 14 variables, are able to satisfy 40 observed frequencies with an average error of 1.2% and 2% respectively. One can, of course, improve the agreement between the observed and calculated frequencies by introducing more interaction constants, but it was considered that the agreement obtained is as good as can be expected in view of the approximations in the theory, and that further work was not justified. The frequencies of the  $A_2$  modes obtained from the two calculations are sufficiently close that they can be used to calculate the thermodynamic properties of t-butyl bromide.

### 5.3 THERMODYNAMIC FUNCTIONS

Thermodynamic functions for gaseous  $-h_9$  and  $-d_9$  were calculated, for the  $^{79}\text{Br}$  isotope only, using the calculated moments of inertia given in Table 50, the observed frequencies for the  $A_1$  and E modes, and the calculated frequencies for the  $A_2$  modes, Tables XII and XIII. A Fortran computer program was used to calculate the enthalpy function  $(H_0 - E_0^0)/T$ , the Gibbs free energy function  $(G_0 - E_0^0)/T$ , the entropy  $S_0$  and heat capacity  $C_p$  at different temperatures (171). The values of these functions calculated for the  $A_2$  mode frequencies obtained from force field I are shown in Tables XVIII for the light compound and XIX for

Table XIX

Thermodynamic functions for t-butyl bromide-d<sub>9</sub>  
at 1 atm pressure and for the ideal gaseous state.<sup>a</sup>

T (°K)	$(H_0 - E_0^0)/T$	$(G_0 - E_0^0)/T$	$S_0$	$C_p$
50	8.090	44.330	52.421	8.834
100	9.743	50.359	60.103	14.173
150	12.040	54.742	66.782	18.895
200	14.272	58.513	72.786	23.019
250	16.438	61.931	78.370	27.191
300	18.581	65.118	83.699	31.371
350	20.698	68.141	88.839	35.367
400	22.767	71.040	93.808	39.070
450	24.770	73.838	98.609	42.450
500	26.695	76.548	103.244	45.519

<sup>a</sup>Using the observed frequencies for the A<sub>1</sub> and E modes and the frequencies calculated with force field I for the A<sub>2</sub> mode; units are cal mole<sup>-1</sup>deg<sup>-1</sup>.

Table XVIII

Thermodynamic functions for t-butyl bromide-h<sub>9</sub>  
at 1 atm pressure and for the ideal gaseous state.<sup>a</sup>

T (°K)	(H <sub>0</sub> -E <sub>0</sub> <sup>0</sup> )/T	(G <sub>0</sub> -E <sub>0</sub> <sup>0</sup> )/T	S <sub>0</sub>	C <sub>p</sub>
50	7.976	43.533	51.510	8.199
100	8.899	49.265	58.164	12.000
150	10.707	53.202	63.910	16.485
200	12.614	56.545	69.159	20.065
250	14.430	59.556	73.986	23.297
300	16.176	62.342	78.519	26.517
350	17.885	64.964	82.850	29.746
400	19.567	67.462	87.030	32.901
450	21.218	69.862	91.081	35.904
500	22.829	72.181	95.011	38.714

<sup>a</sup>Using the observed frequencies for the A<sub>1</sub> and E modes and the frequencies calculated with force field I for the A<sub>2</sub> mode; units are cal mole<sup>-1</sup>deg<sup>-1</sup>.

## 6. THE SOLID PHASES OF t-BUTYL BROMIDE

The vibrational spectra of the three solid phases and the X-ray photographs of phase III of t-butyl bromide are presented and discussed in this chapter.

### 6.1 RESULTS

#### 6.1.1 The Vibrational Spectra of the Plastic Phases

The infrared spectra of the intramolecular modes of t-butyl bromide-h<sub>9</sub> in phase I at 245°K and phase II at 223°K are shown in Figures 21 and 22. The spectra were recorded with resolutions of about 1 cm<sup>-1</sup> above 650 cm<sup>-1</sup> and 2 cm<sup>-1</sup> below 650 cm<sup>-1</sup>. The nominal sample thickness was about 0.05 mm for the light compound and 0.1 mm for the heavy compound. The observed frequencies of the light and heavy compounds, respectively, are presented in Tables XX and XXI with an accuracy of ±1 cm<sup>-1</sup>. The vibrational frequencies of t-butyl bromide in the liquid and solid phases I and II are identical within experimental error (cf. Tables VI, VII, XX, and XXI). A small gradual decrease in the widths of the absorption lines in the solid phases is observed with decreasing temperature, Tables XXII and XXIII. Figures 23 and 24 show the variation of halfwidth with temperature for some typical bands in the liquid and solid phases. No abrupt changes in the

the heavy compound. If the  $A_2$  mode frequencies for force field II are used instead, the calculated thermodynamic functions are within 0.05% of the values shown.

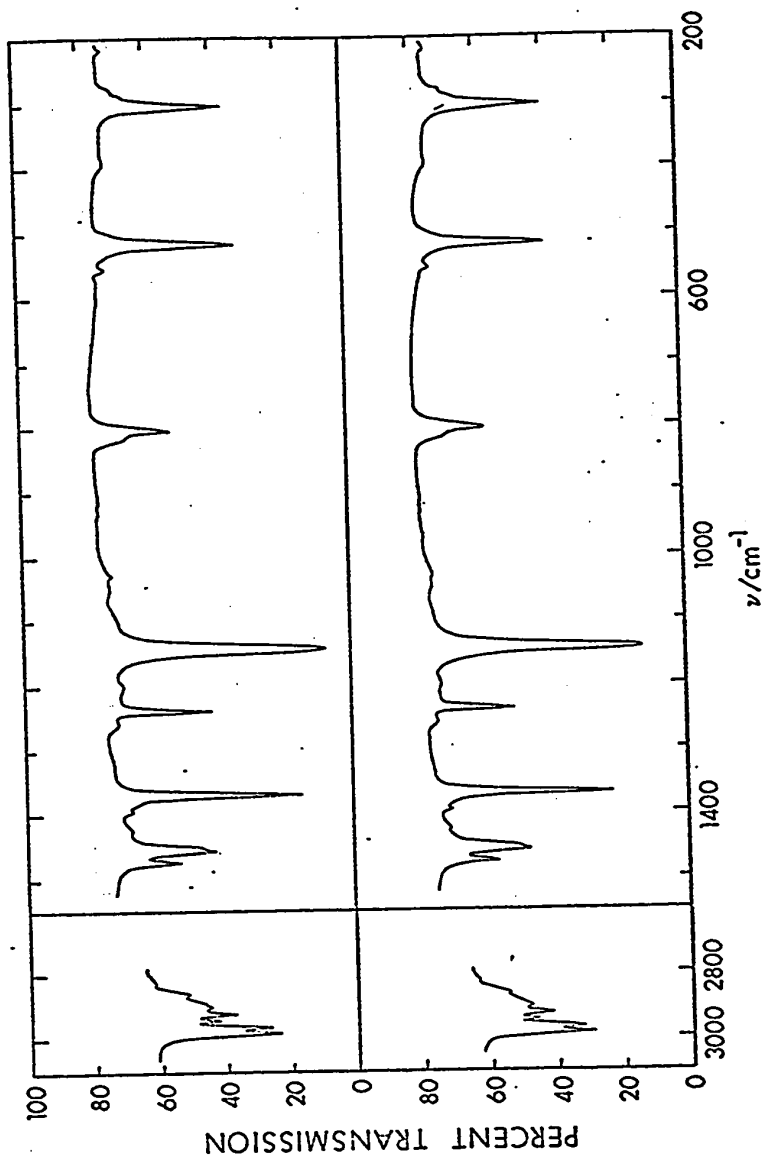


Figure 21

Infrared spectra of t-butyl bromide-h<sub>9</sub> in solid phases I  
at 245°K (lower box) and II at 223°K (upper box).

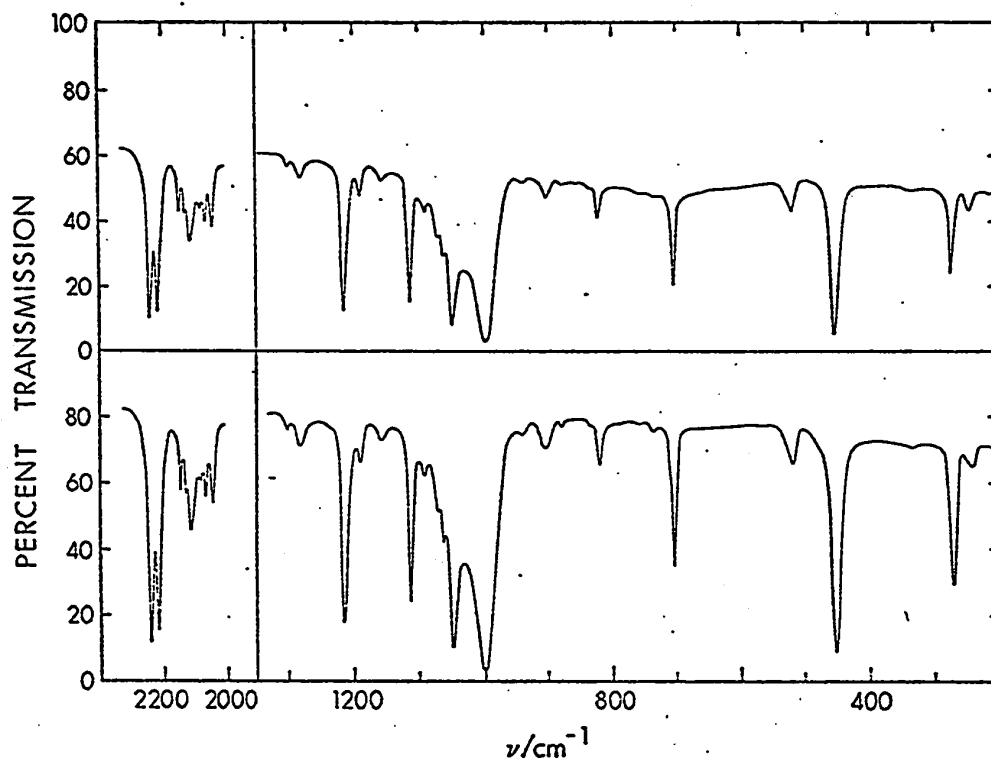


Figure 22

Infrared spectra of t-butyl bromide- $\text{d}_9$  in the solid phase I at 245°K (lower box) and II at 223°K (upper box).

Table XX - cont'd.

Phase I 245°K		Phase II 228°K				Assignment
IR		Pure Solid		Dilute <sup>b</sup> Solution		
		IR	Raman	IR		
$\nu_{-1}$ cm <sup>-1</sup>	Inten- sity	$\nu_{-1}$ cm <sup>-1</sup>	Inten- sity	$\Delta\nu_{-1}$ cm <sup>-1</sup>	$\nu_{-1}$ cm <sup>-1</sup>	
1144	vs	1144	vs	1142	1144	$\nu_5$
1060	vvw	1060	vw			$\nu_6 + \nu_{12}$
1031	w	1031	w			$\nu_{20}$
930	vvw	930	vvw			$\nu_{21}$
814	sh	814	sh			$\nu_7 + \nu_8$
804	m	804	m	804	804	$\nu_6$
604	vvw	604	vvw			$2\nu_8$
572	vw	574	vw			$2\nu_{23}$
553	w	554	w			$\nu_{23} + \nu_{24}$
517	s	517	s	516		$\nu_7$
396	vw	396				$\nu_{22}$
302	s	302	s	300		$\nu_8$
286	sh	287	sh			$\nu_{23}$
272	sh	272	sh			$\nu_{24}$
214	vw	214	vw			$\nu_7 - \nu_8$

<sup>a</sup>The symbols are as given under Table IV.

<sup>b</sup>5% of C<sub>4</sub>H<sub>9</sub>Br in C<sub>4</sub>D<sub>9</sub>Br.



Table XX

Frequencies and assignment of the features observed in the infrared and Raman spectra of t-butyl bromide-h<sub>9</sub> in the solid phases I and II.<sup>a</sup>

Phase I 245°K		Phase II 228°K			Assignment	
		Pure Solid		Dilute <sup>b</sup> Solution		
IR		IR	Raman	IR		
$\nu_{-1}$ cm <sup>-1</sup>	Inten- sity	$\nu_{-1}$ cm <sup>-1</sup>	Inten- sity	$\Delta\nu_1$ cm <sup>-1</sup>	$\nu_{-1}$ cm <sup>-1</sup>	
2985	s	2985	s		2986	$\nu_{13}$
2968	s	2968	s		2967	$\nu_{1'}$ , $\nu_{14}$
2945	m	2945	m		2943	$\nu_{15}$
2924	s	2924	s		2922	$\nu_2$
2903	m	2903	m		2903	$2\nu_{16}$
2892	sh	2891	sh			$2\nu_{17}$
2866	sh	2866	sh			$\nu_3 + \nu_4$
2826	vw	2827	vw			$\nu_{16} + \nu_{18}$
1474	m	1474	m		1474	$\nu_3$
1457	s	1456	s		1457	$\nu_{16}$
1449	sh	1449	sh		1450	$\nu_{17}$
1423	w	1423	w			$\nu_{20} + \nu_{22}$
1393	w	1393	w			$\nu_4$
1369	vs	1369	vs		1370	$\nu_{18}$
1324	vw	1324	vw			$\nu_8 + \nu_{20}$
1258	sh	1260	sh			$\nu_{11} + \nu_{12}$
1238	s	1238	s		1239	$\nu_{19}$
1200	vw	1201	vw			$\nu_{21} + \nu_{24}$
. . cont'd.						

Table XXI

Frequencies and assignment of the features observed in the infrared spectra of t-butyl bromide-d<sub>9</sub> in the solid phases I and II.

Phase I 245°K			Phase II 228°K			Assignment
Pure Solid		Dilute <sup>a</sup> Solution	Pure Solid		Dilute <sup>a</sup> Solution	
$\nu$ -1 cm <sup>-1</sup>	Inten- sity	$\nu$ -1 cm <sup>-1</sup>	$\nu$ -1 cm <sup>-1</sup>	Inten- sity	$\nu$ -1 cm <sup>-1</sup>	
2240	vs	2240	2240	vs	2240	$\nu_{13}$
2216	vs	2216	2216	vs	2215	$\nu_1, \nu_{14}$
2150	m		2150	m		$\nu_3 + \nu_{17}$
2130	w		2130	w		$2\nu_4$
2116	m		2116	m		$\nu_2, \nu_{15}$
2084	w		2084	w		$\nu_{17} + \nu_{18}$
2070	m		2070	m		$2\nu_{18}$
2051	sh		2051	sh		$2\nu_{19}$
2047	m		2047	m		$\nu_4 + \nu_5$
1303	vw		1303	vw		$\nu_3 + \nu_{24}$
1285	w		1284	w		$\nu_4 + \nu_{23}$
1215	s	1215	1215	s	1215	$\nu_{16}$
1190	w		1190	w		$\nu_7 + \nu_{31}$
1158	w		1158	w		$\nu_{20} + \nu_{22}$
1114	s		1114	s		$\nu_3$
1092	w		1092	w		$\nu_8 + \nu_{20}$
1072	w		1072	w		$\nu_{21} + \nu_{22}$
1063	w		1063	w		$\nu_4$
1049	s	1049	1049	s	1049	$\nu_{17}$
1038	sh		1037	sh		$\nu_{18}, \nu_{19}$

. . cont'd.

Table XXI - cont'd.

Phase I 245°K			Phase II 228°K			Assignment
Pure Solid		Dilute <sup>a</sup> Solution	Pure Solid		Dilute <sup>a</sup> Solution	
$\nu$ -1 cm	Inten- sity	$\nu$ -1 cm	$\nu$ -1 cm	Inten- sity	$\nu$ -1 cm	
1000	vs	1000	1000	vs	1000	$\nu_5$
939	vw		940	vw		$\nu_6 + \nu_{23}$
904	w		904	w		$\nu_6 + \nu_{24}$
880	vw		880	vw		$\nu_6 + 12$
837	sh, vw		837	sh, vw		$3\nu_8$
823	w		824	w		$\nu_{20}$
759	vw		759	vw		$\nu_{11} + \nu_{22}$ $\nu_7 + \nu_{22}$
738	vw		738	vw		$\nu_{21}$
709	sh		709	sh		$\nu_7 + \nu_8$
704	s	704	704		703	$\nu_6$
521	w		521	w		$2\nu_8$
480	sh		480	sh		$\nu_8 + \nu_{24}$
465	sh		465	sh		$\nu_{23} + \nu_{24}$
454	vs	454	454	s	454	$\nu_7$
336	vw		336	vw		$\nu_{22}$
274	s		274			$\nu_8$
242	w		242	w		$\nu_{23}$
210	vw		210	vw		$\nu_{24}$
181	vw		181	vw		$\nu_7 - \nu_8$

<sup>a</sup>5% of t-butyl bromide-d<sub>9</sub> in t-butyl bromide-h<sub>9</sub>.

Table XXII

Halfwidths of some of the infrared bands of t-butyl bromide-h<sub>9</sub> in the liquid and plastic solids.<sup>a</sup>

Band		Liquid	Solid I	Solid II	
Frequency	Mode	270°K	245°K	223°K	
		Pure	Pure	Pure	5% Solution
302	$\nu_8$	10.5	10.0	9.5	5.0
517	$\nu_7$	10.5	10.0	9.5	-- <sup>c</sup>
1144	$\nu_5$	12.5	12.0	11.5	6.5
1238	$\nu_{19}$	7.5	7.0	6.0	5.0
1370	$\nu_{18}$	7.5	7.0	6.0	4.0
1457	$\nu_{16} + \nu_{17}$ <sup>b</sup>	15.0	14.5	14.0	12.5
1474	$\nu_3$	8.0	7.5	7.0	5.0

<sup>a</sup>The frequencies and halfwidths have the units  $\text{cm}^{-1}$ .

<sup>b</sup>The observed halfwidth in the spectra of the pure phases shows a value of  $\nu_{16} - \nu_{17} + \frac{1}{2}(\Delta_{16} + \Delta_{17})$ , where  $\nu_i$  and  $\Delta_i$  represent the frequencies and halfwidths of the two modes. The decrease in halfwidth in going from the pure phase to the solution gives the change in  $\frac{1}{2}(\Delta_{16} + \Delta_{17})$ .

<sup>c</sup>Not measured due to interference with the  $521 \text{ cm}^{-1}$  band of  $\text{C}_4\text{D}_9\text{Br}$ .

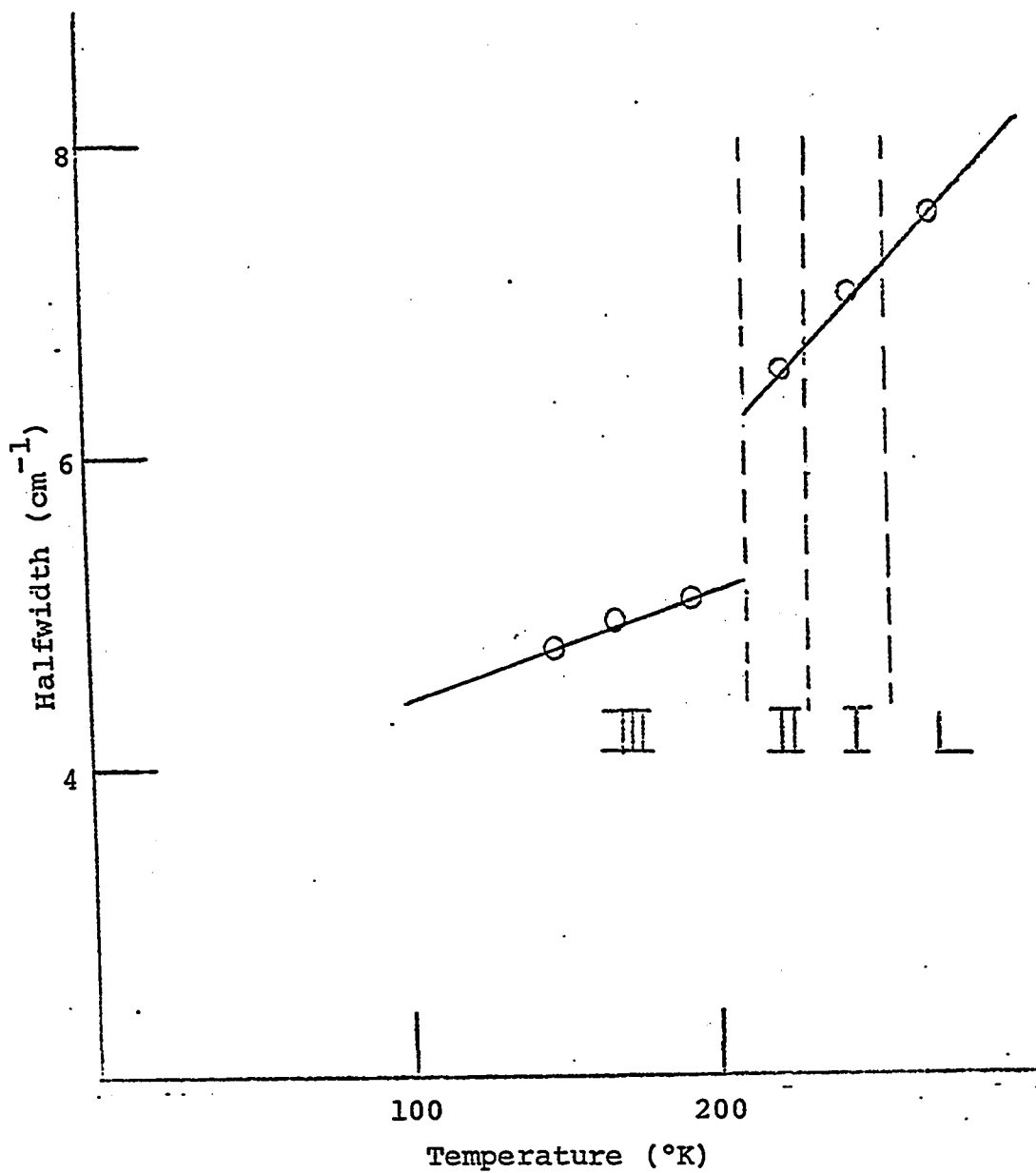


Figure 23

Graph, Halfwidth vs Temperature for  $\nu_{18}$  band of  $C_4H_9Br$  in the infrared spectrum of pure solid.

Table XXIII

Halfwidths of some of the infrared bands of t-butyl bromide-d<sub>9</sub> in the liquid and plastic solid phases.<sup>a</sup>

Band Frequency	Mode	Liquid 298°K		Solid I 245°K		Solid II 223°K	
		Pure	5% Solution	Pure	5% Solution	Pure	5% Solution
274	$\nu_8$	8.0	-- <sup>c</sup>	7.0	-- <sup>c</sup>	6.5	-- <sup>c</sup>
454	$\nu_7$	12.0	10	10.5	9.5	10.0	9.0
704	$\nu_6$	7.0	5	5.2	4.5	4.8	4.3
1113	$\nu_3$	7.0	-- <sup>c</sup>	5.1	-- <sup>c</sup>	4.6	-- <sup>c</sup>
1217	$\nu_{16}$	11.5		9.5		8.8	
2214	$\nu_1$	-- <sup>b</sup>	10	11.8	8	11.5	6.5
2240	$\nu_{13}$	-- <sup>b</sup>	12	13.5	10	13.0	9.0

<sup>a</sup>The frequencies and halfwidths have the units  $\text{cm}^{-1}$ .

<sup>b</sup>Not measured due to overlap between  $\nu_1$  and  $\nu_{13}$  at half absorption.

<sup>c</sup>Not measured due to the interference with the bands of  $\text{C}_4\text{H}_9\text{Br}$ .

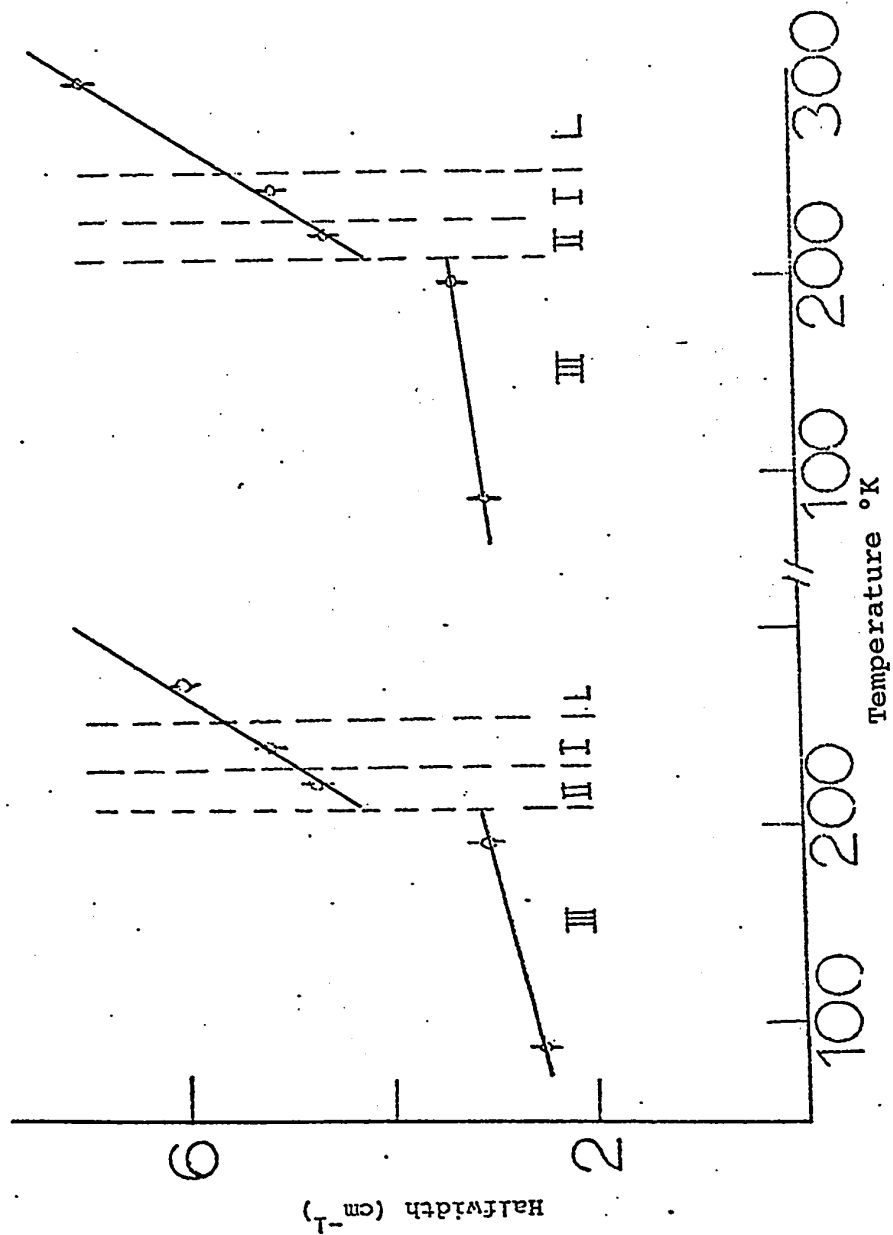


Figure 24. Graph, Halfwidth vs Temperature for  $\nu_3$  and  $\nu_6$  bands of  $C_4D_9Br$  in the infrared spectrum of pure solid.

halfwidths occur between the liquid, solid I and solid II phases, but the halfwidths do decrease significantly at the II to III transition.

The infrared spectra of phases I and II and the liquid made from a 5% solution of  $C_4H_9Br$  in  $C_4D_9Br$  and of  $C_4D_9Br$  in  $C_4H_9Br$  were recorded. Figures 25-27 show the comparison of the shapes of certain bands in the spectrum of the solute isotope in the 5% solutions with the shapes of the same bands in the spectrum of the pure isotope. Figure 25 shows the comparison in phase I for three bands of  $C_4D_9Br$  and one band of  $C_4H_9Br$ . Figures 26 and 27 show the results obtained for phase II. The frequencies of some of the bands of the solute isotope are given in Tables XX and XXI beside the frequencies of the corresponding features in the pure solid.

The partial Raman spectrum of the light compound in phase II at 228°K was recorded at  $1\text{ cm}^{-1}$  resolution. Only four strong bands,  $\nu_5$  to  $\nu_8$ , were studied and the observed frequencies are listed in Table XX with an accuracy of  $\pm 1\text{ cm}^{-1}$ . Two of these bands, due to  $\nu_7$  and  $\nu_8$ , are shown in Figure 28. The halfwidth of the  $\nu_7$  band is about  $9\text{ cm}^{-1}$  and that of the  $\nu_8$  band is about  $7\text{ cm}^{-1}$ . The corresponding bands in the infrared spectrum, in phase II have halfwidths of  $9.5\text{ cm}^{-1}$ .



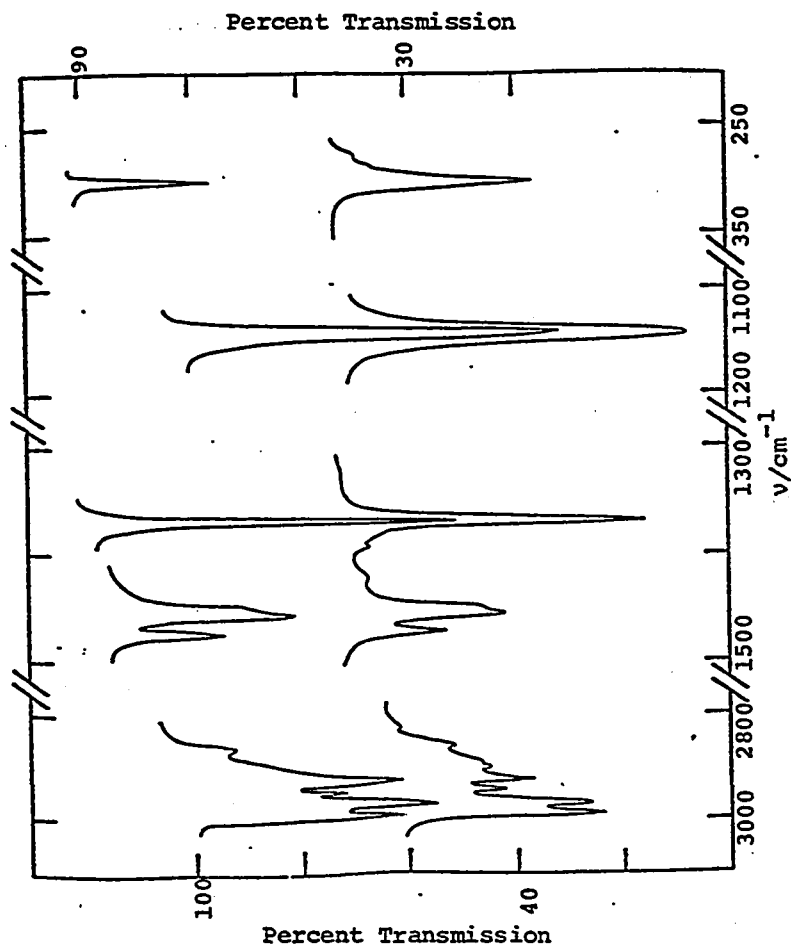


Figure 26. Infrared absorption by t-butyl bromide-h<sub>9</sub> in phase II at 223°K. The lower spectrum shows the absorption by the pure solid (L.H.S. transmission scale) while the upper spectrum indicates the absorption by 5% of C<sub>4</sub>H<sub>9</sub>Br (R.H.S. transmission scale).

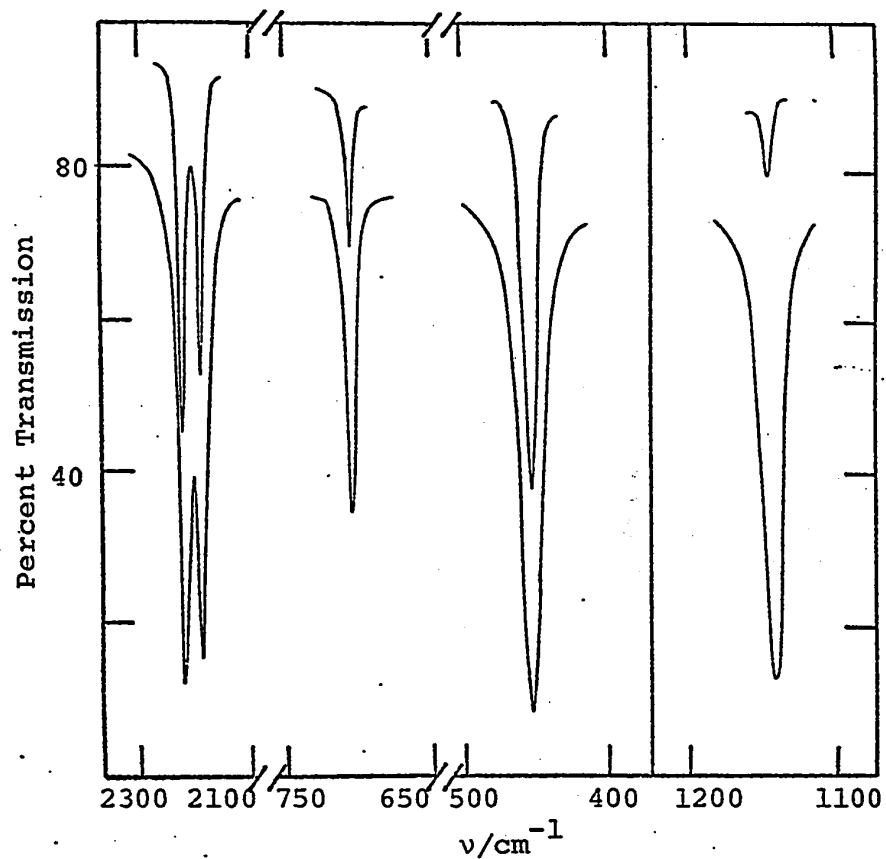


Figure 25

Infrared absorption by t-butyl bromide- $d_9$  (left box) and t-butyl bromide- $h_9$  (right box) in phase I at 245°K. The lower spectra indicate the absorption by the pure solid while the upper spectra show the absorption by 5%  $C_4D_9Br$  in  $C_4H_9Br$  (left box) and 5% of  $C_4H_9Br$  in  $C_4D_9Br$ .

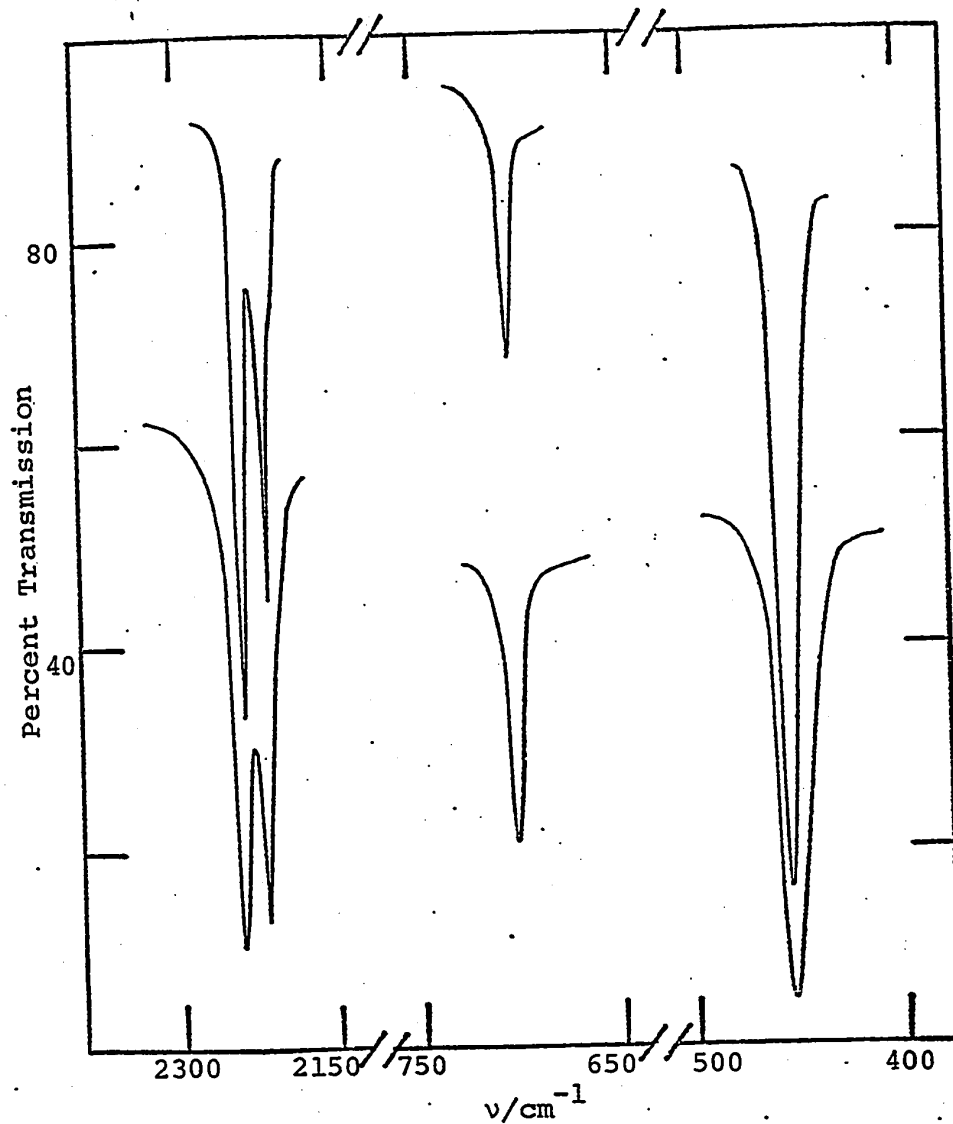


Figure 27

Infrared absorption by *t*-butyl bromide- $\text{d}_9$  in phase II at  $223^\circ\text{K}$ . The lower spectrum shows the absorption by the pure solid and the upper spectrum show the absorption by 5% of  $\text{C}_4\text{D}_9\text{Br}$  in  $\text{C}_4\text{H}_9\text{Br}$ .

The far-infrared spectra of t-butyl bromide-h<sub>9</sub> and -d<sub>9</sub> are shown in Figure 29, for the liquid and for solid phases I and II. Each spectrum was obtained by averaging at least 4 spectra, each obtained from a different sample, and by smoothing features on the averaged spectra that were clearly due to noise. The noise was only really significant in the region below 20 cm<sup>-1</sup>. Therefore the exact shape of the spectra below 20 cm<sup>-1</sup> is uncertain, but a clear trend towards lower absorption with decreasing frequency was observed. Noise can appear either as a spike or, more deceptively, as a sinusoidal variation on a spectrum obtained from an interferometer. This latter type of noise makes it very difficult to prove the existence of weak features on a broad absorption. No evidence was found that the bands shown in Figure 29 show any features. Therefore it is concluded that t-butyl bromide shows smooth broad absorption bands with rather broad maxima in the liquid and plastic solid phases. The frequencies of the maxima, with an accuracy of ±2 cm<sup>-1</sup>, are given in Table XXIV. The frequency of maximum absorption clearly shifts to high frequency with decreasing temperature. The samples were maintained at 273°K, 245°K, and 223°K, all controlled to ±3°K for the spectra of the liquid and solids I and II respectively. The spectrum of the light compound

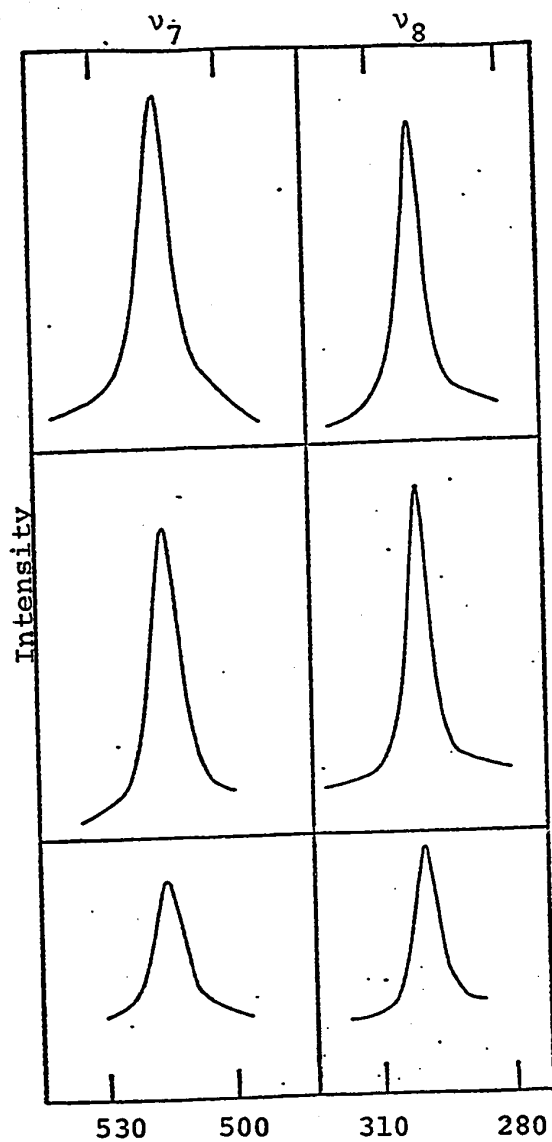


Figure 28

Raman scattering by the  $\nu_7$  (left) and  $\nu_8$  (right) modes of t-butyl bromide- $\text{h}_9$  in phase II (bottom), in the liquid phase under parallel polarization, (middle) and in the liquid phase without the analyzer (top).

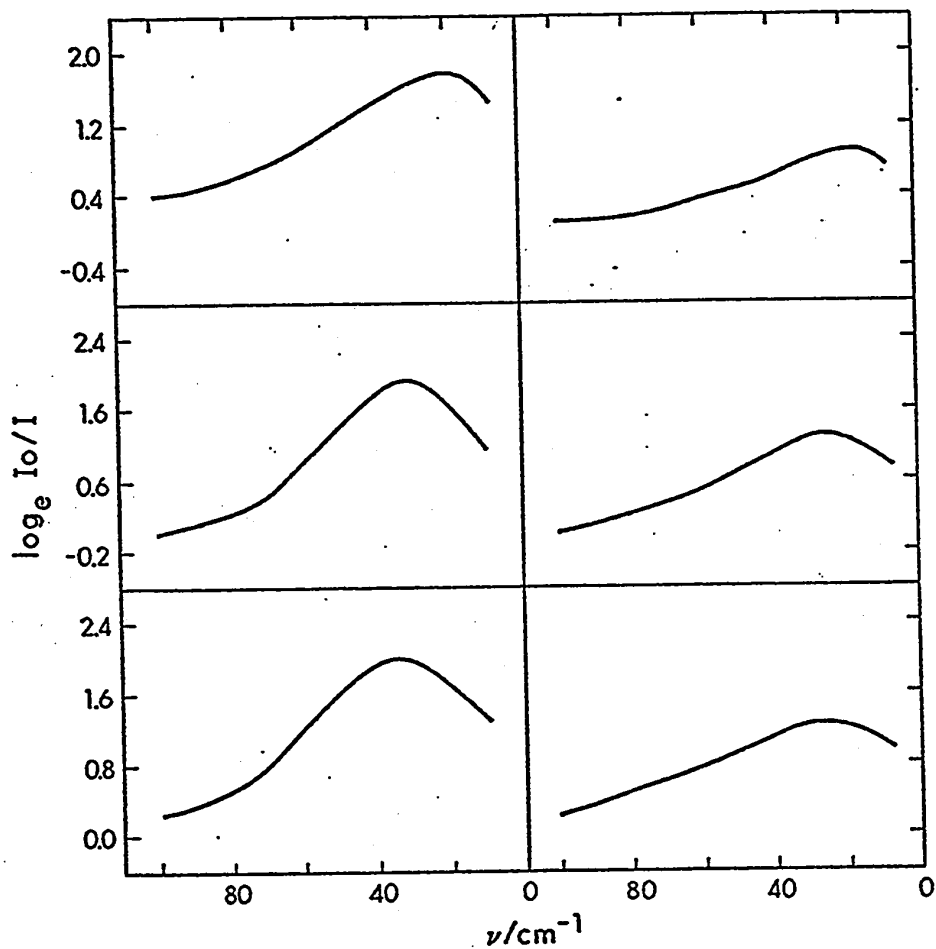


Figure 29

Far-infrared spectra of t-butyl bromide-h<sub>9</sub> (left boxes) and -d<sub>9</sub> (right boxes); in the solid phase II at 228°K (bottom boxes); and in phase I at 245°K (middle boxes); and in the liquid at 273°K (top boxes).

Table XXIV  
Far-infrared spectra of t-butyl bromide-h<sub>9</sub> and -d<sub>9</sub> in the condensed phases.

Phase	Temperature	Feature	Frequency (cm <sup>-1</sup> )		$\frac{\nu_H}{\nu_D}$	Assignment
			-h <sub>9</sub>	-d <sub>9</sub>		
Solid III	90°K	very weak peak	16.8±0.2	16.3±0.2	1.03	T
		weak peak	24.1±0.1	23.5±0.1	1.03	T
		shoulder	31.3±0.2	30.3±0.2	1.03	T + R
		m.s. peak	34.0±0.1	32.6±0.1	1.04	T + R
		v.s. peak	52.2±0.2	50.7±0.2	1.03	T
		shoulder	58.5±0.5	55.0±0.5	1.06	R ⊥
		s peak	68.5±0.2	62.1±0.2	1.10	R
		shoulder	73.5±0.5	69.6±0.5	1.06	R ⊥
		v. weak peak	17.0±1.0	15.0±1.0		
		medium peak	31.4±0.5	30.0±0.5		
Solid II	223°K	v.s. peak	47.5±0.4	47.3±0.5		
		shoulder	62.5±0.7	58.0±1.0		
			35 ±2	30 ±2		

... cont'd.

Table XXIV - cont'd.

Phase	Temperature	Feature	Frequency (cm <sup>-1</sup> )		$\frac{\nu_H}{\nu_D}$	Assignment
			-h <sub>9</sub>	-d <sub>9</sub>		
Solid I	245°K		30 ±2	25 ±2		
Liquid	273°K		20 ±2	15 ±2		



in the liquid phase is qualitatively consistent with that reported by Leroy and Constant (172).

#### 6.1.2 Spectra of Phase III

The infrared spectra of t-butyl bromide- $h_9$  and  $-d_9$  in phase III, at 195°K and 90°K, are shown in Figures 30 and 31 respectively. Each spectrum shown was obtained from the same sample over the whole frequency range, except for the spectrum of  $C_4H_9Br$  at 90°K, for which the 3000  $cm^{-1}$  region has been taken from the spectrum of a thicker sample than was used for the region below 1550  $cm^{-1}$ . The sample thickness was nominally 0.05 mm. However a large range of absorbances was obtained for the same band from different samples of the same nominal thickness, and therefore the exact thickness of each sample is unknown. Figures 32-50 show the intense bands on an expanded frequency scale. The curves shown in these Figures were selected for clear presentation of the fine structure and were not all obtained from a single sample of each isotope. The transition from phase II to phase III caused the samples to become powdered and the scattering of the infrared beam by these amorphous samples presented difficulties in spectral studies of phase III. Light scattering by the sample prevented the use of samples thicker than 0.1 mm. The

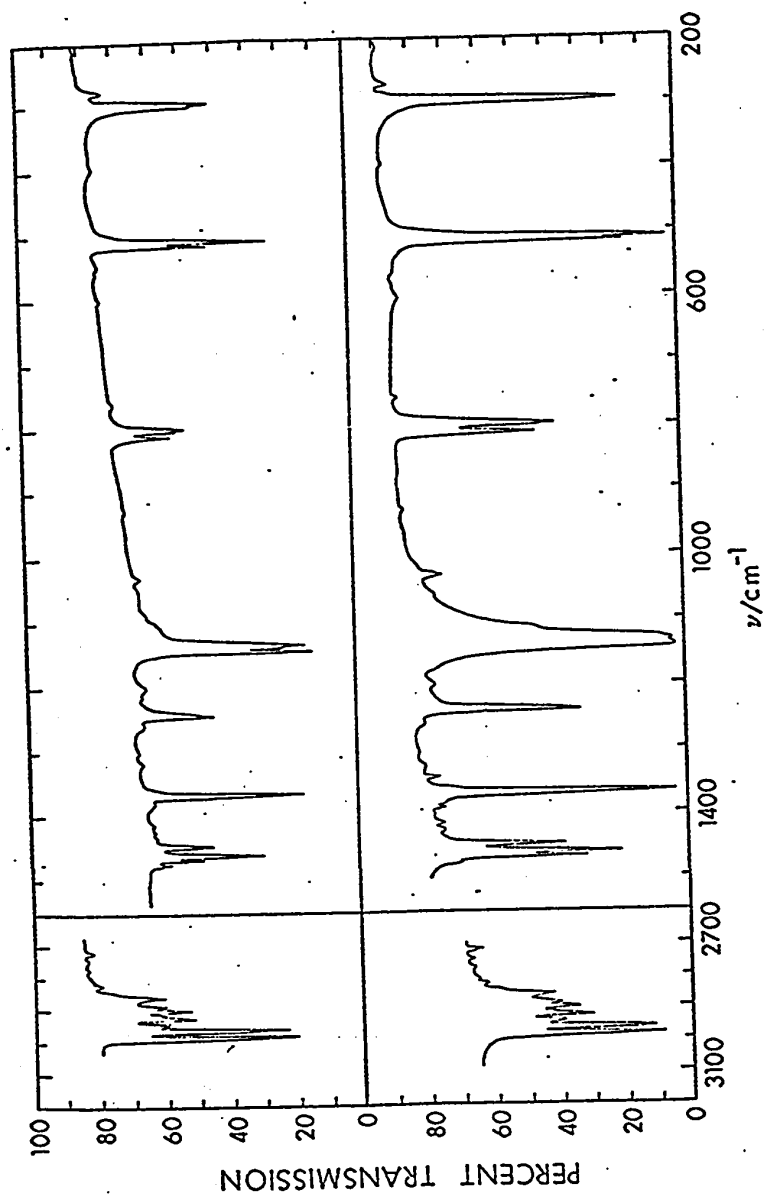


Figure 30

Infrared spectra of t-butyl bromide-h<sub>9</sub> in the solid phase III at 195°K (bottom box) and at 90°K (upper box).

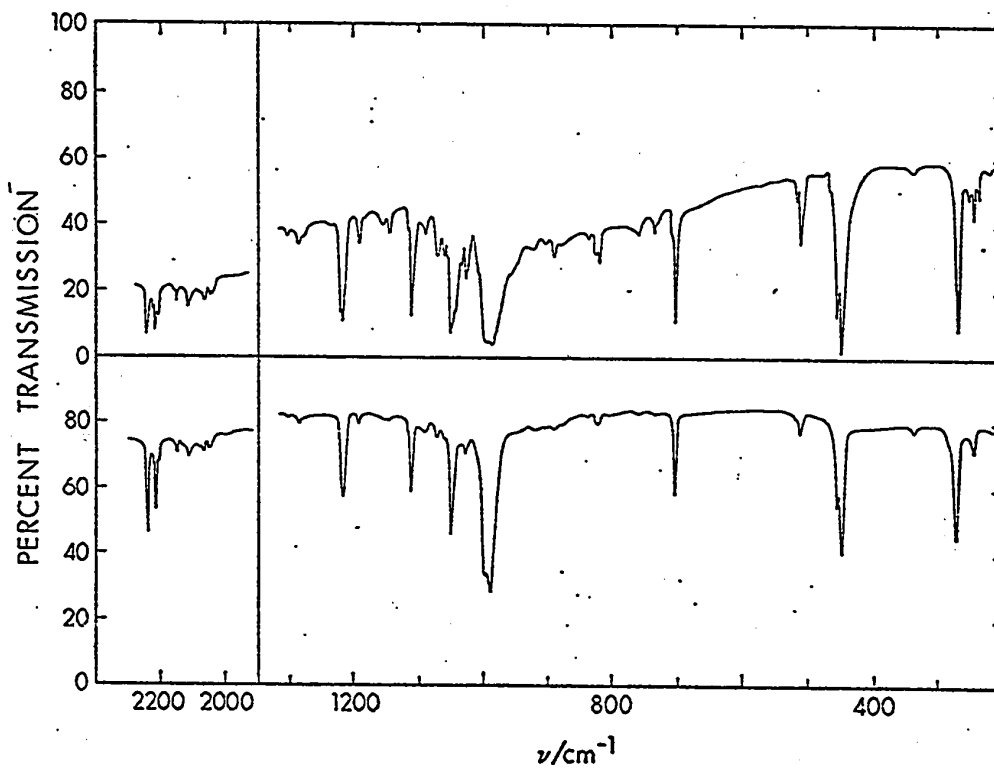


Figure 31

Infrared spectra of t-butyl bromide-d<sub>9</sub> in the solid phase III at 195°K (bottom box) and at 90°K (upper box).

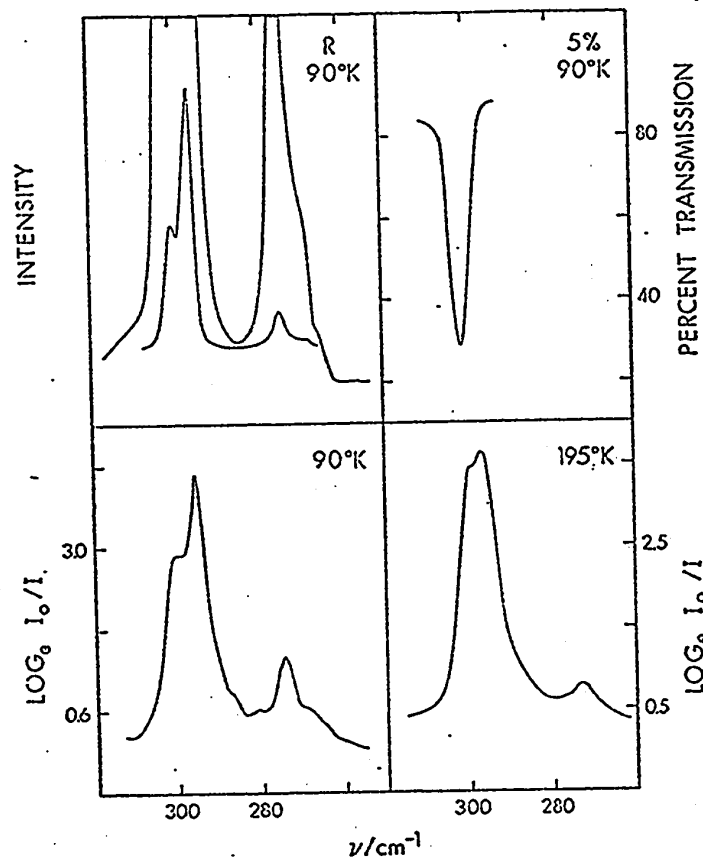


Figure 32

Infrared and Raman spectra of phase III of t-butyl bromide- $h_9$  for the region  $320-260\text{ cm}^{-1}$ . In figures 32-49 the symbols '90°K' and '195°K' denote the infrared spectra of the pure solid at 90°K and 195°K respectively while the symbol '5% 90°K' indicates the infrared spectrum of 5% solution of  $C_4H_9Br$  in  $C_4D_9Br$  or vice versa; and the symbol 'R 90°K' denotes the Raman spectrum of the pure solid at 90°K.

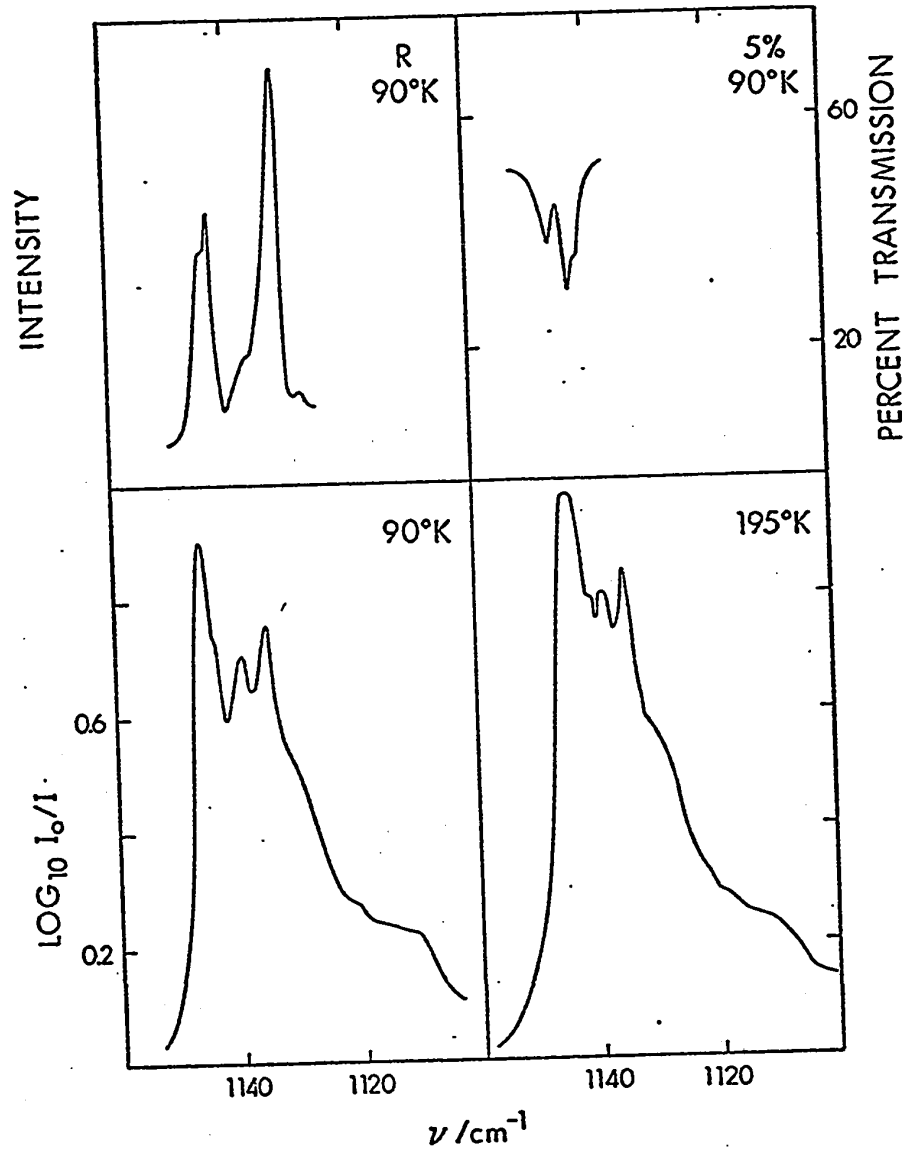


Figure 33

Infrared and Raman spectra of t-butyl bromide-h<sub>9</sub>  
in phase III for the region 1160 - 1100 cm<sup>-1</sup>.

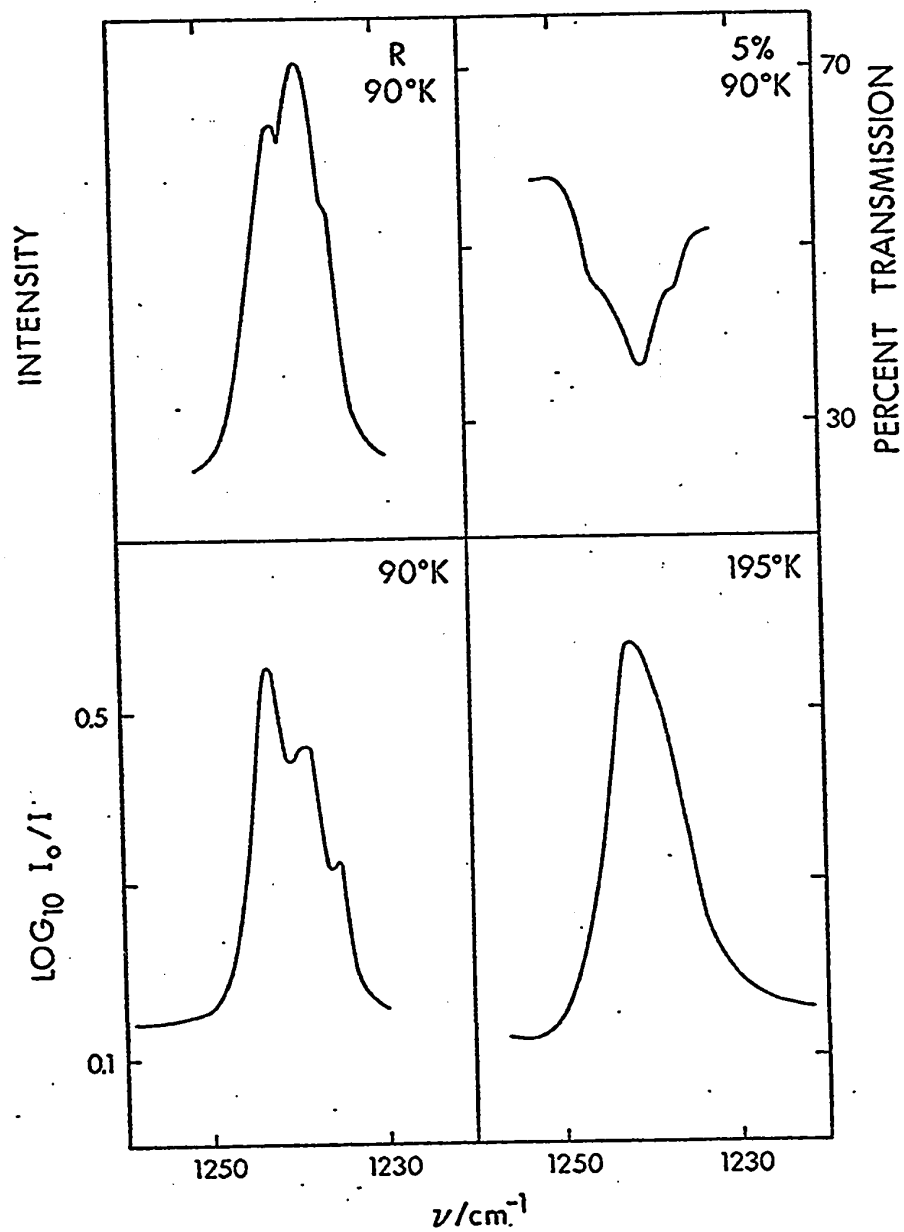


Figure 34

Infrared and Raman spectra of  $\nu_{19}$  (E) fundamental of t-butyl bromide- $h_9$  in phase III.

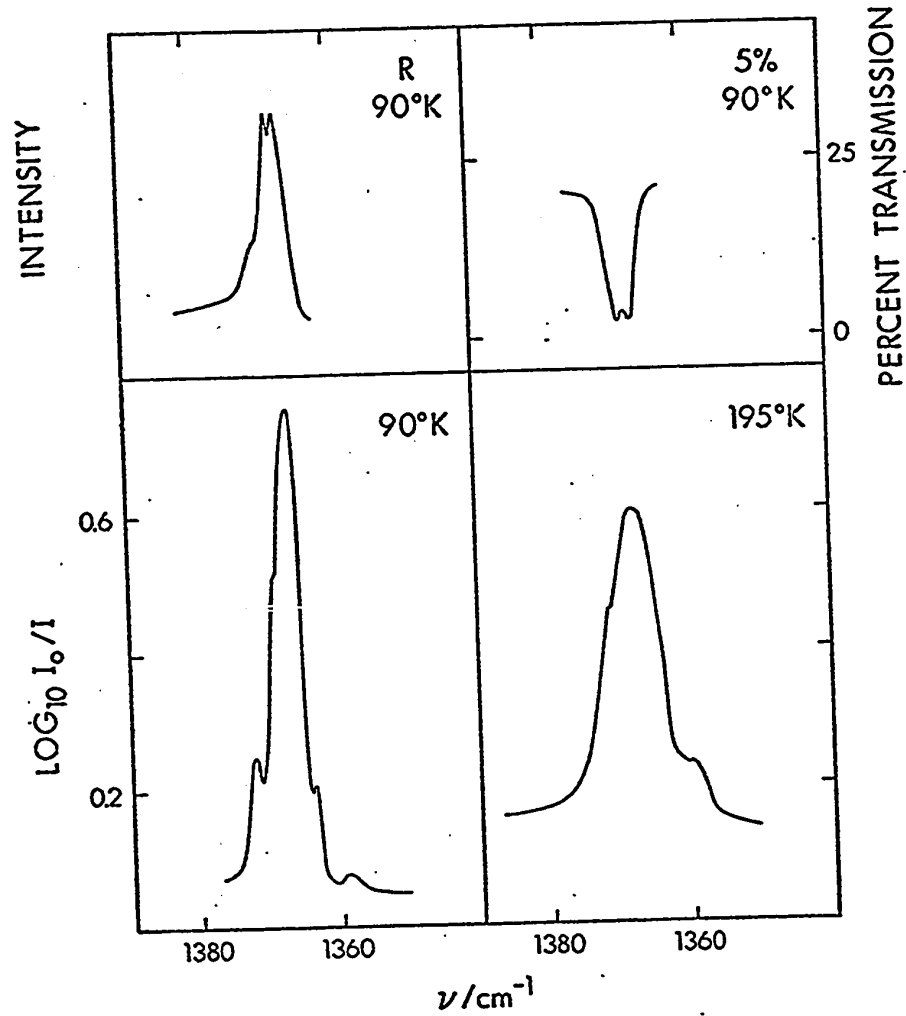


Figure 35

Infrared and Raman spectra of t-butyl bromide-h<sub>9</sub> in phase III for the region 1380 - 1350 cm<sup>-1</sup>.

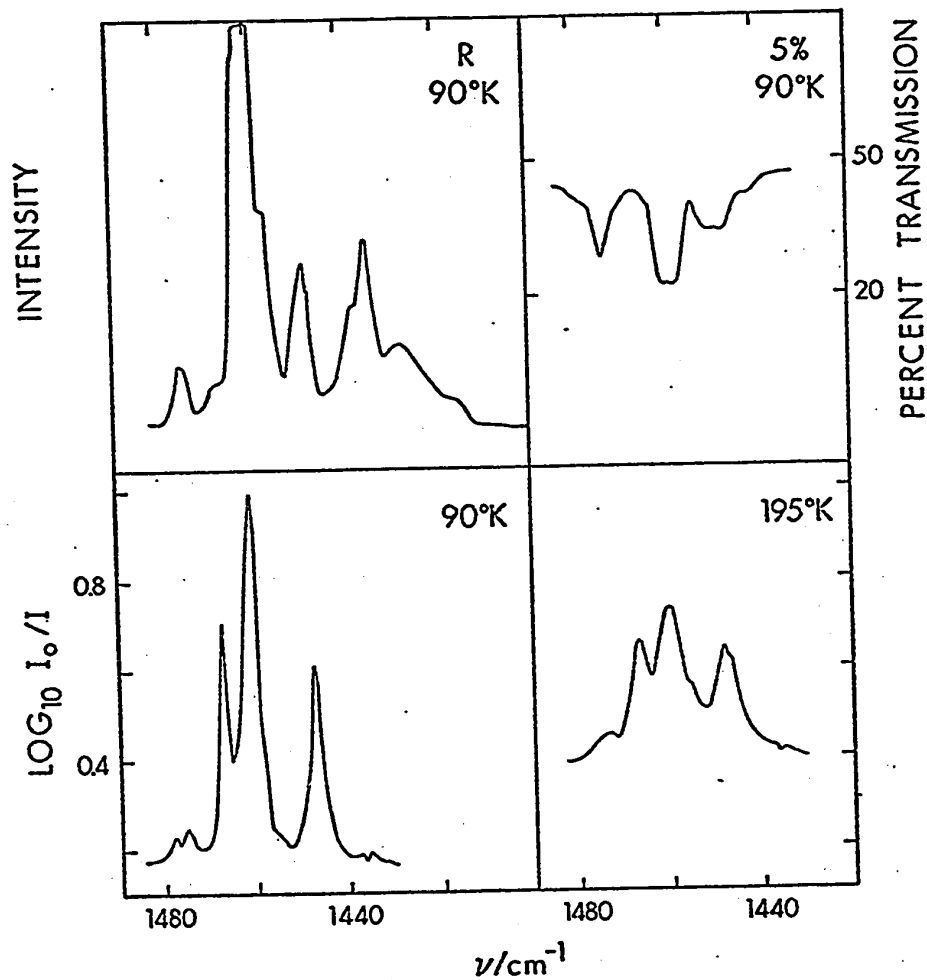


Figure 36

Infrared and Raman spectra of t-butyl bromide-h<sub>9</sub> in phase III for the region 1490 - 1400 cm<sup>-1</sup>.



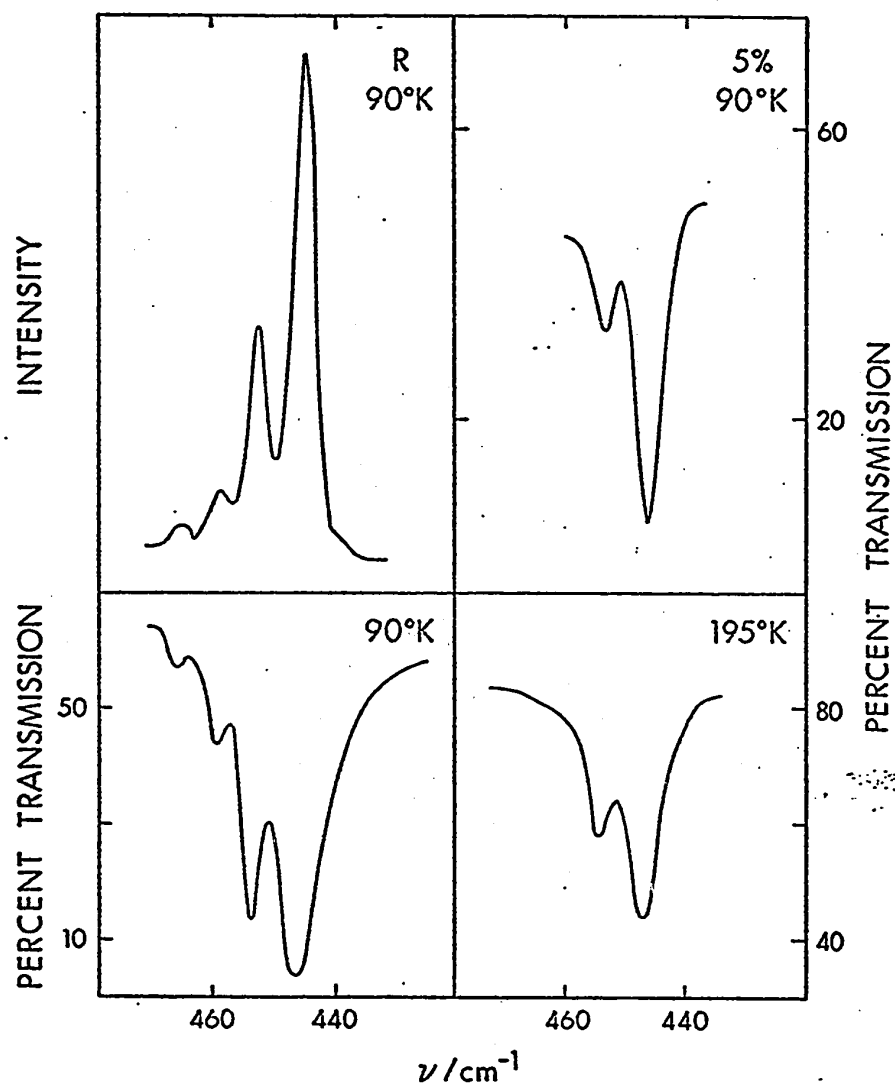


Figure 37

Infrared and Raman spectra of t-butyl bromide-d<sub>9</sub>  
in phase III for the region 480 - 420 cm<sup>-1</sup>.

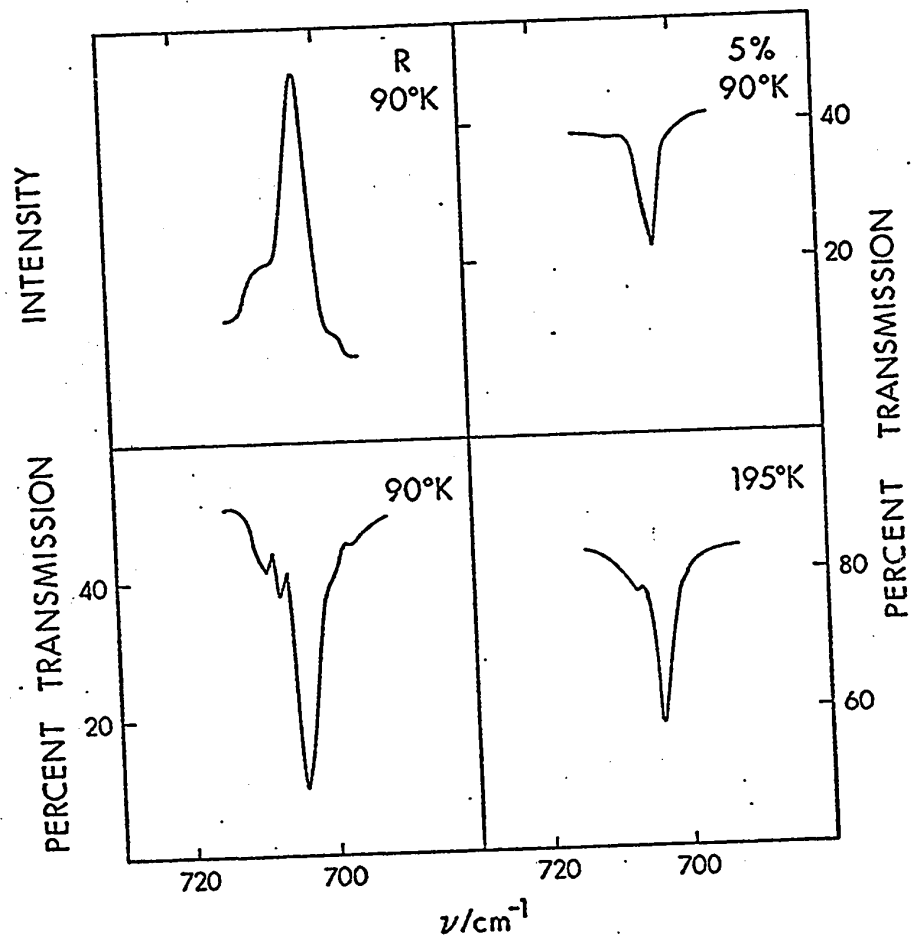
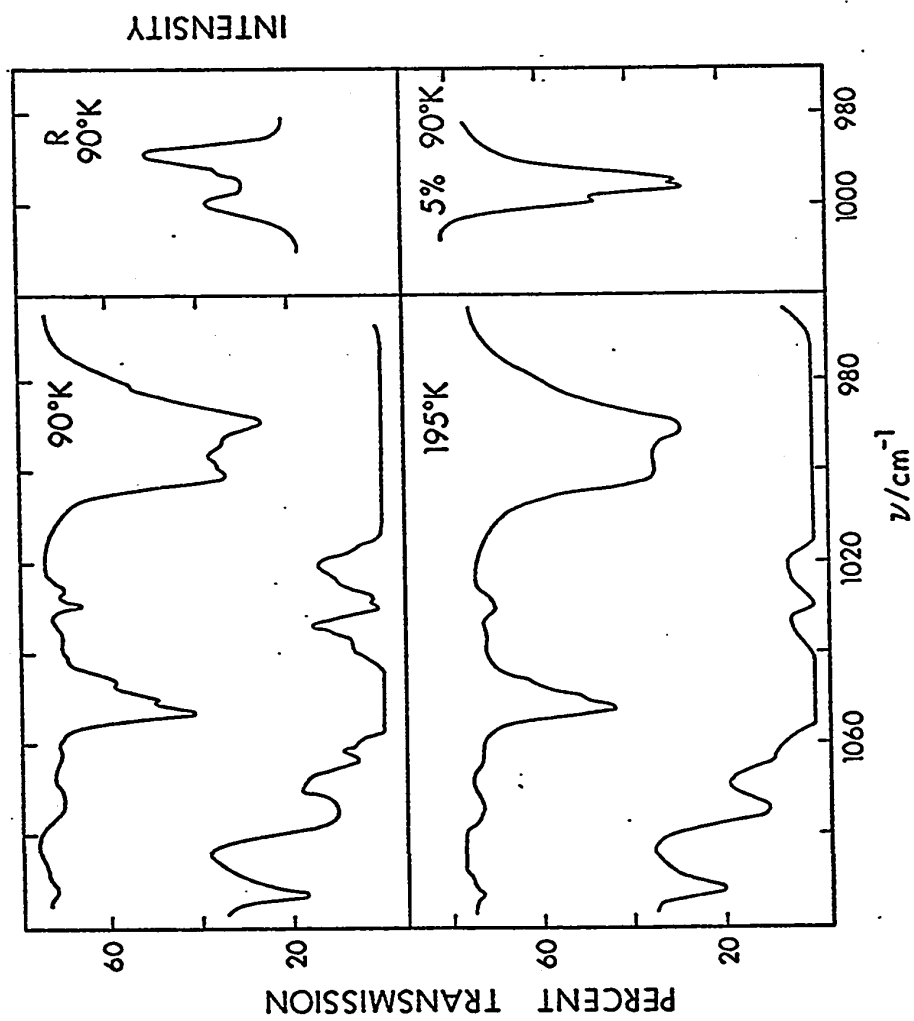


Figure 38

Infrared and Raman spectra of *t*-butyl bromide- $d_9$  in phase III for the region 720 - 680  $\text{cm}^{-1}$ .



**Figure 39** Infrared and Raman spectra of t-butyl bromide- $\text{d}_9$  in phase III for the region 1100 - 980  $\text{cm}^{-1}$ .

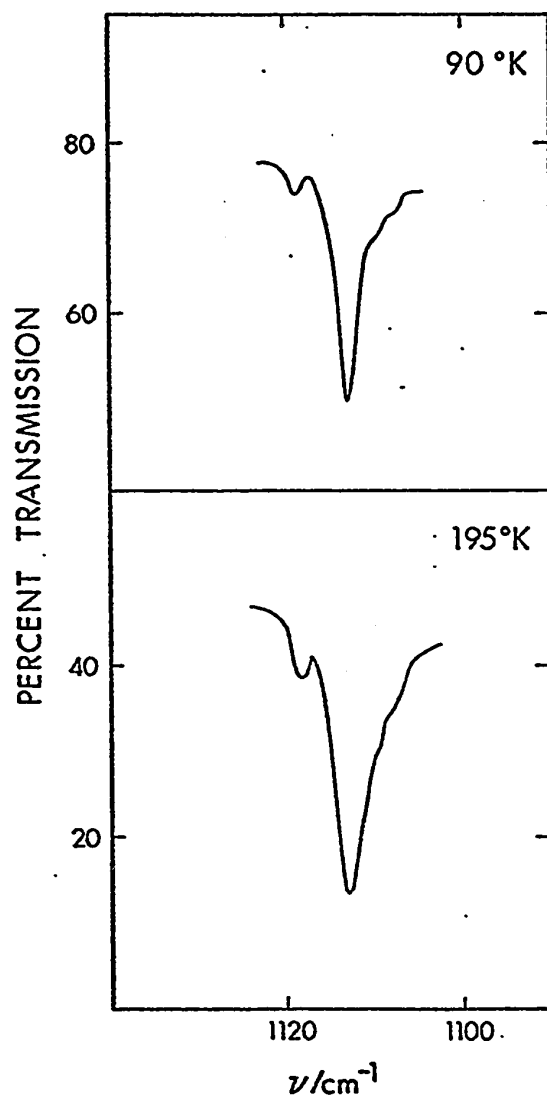


Figure 40

Infrared spectra of t-butyl bromide- $\text{d}_9$  in phase III  
for the region  $1130 - 1100 \text{ cm}^{-1}$ .

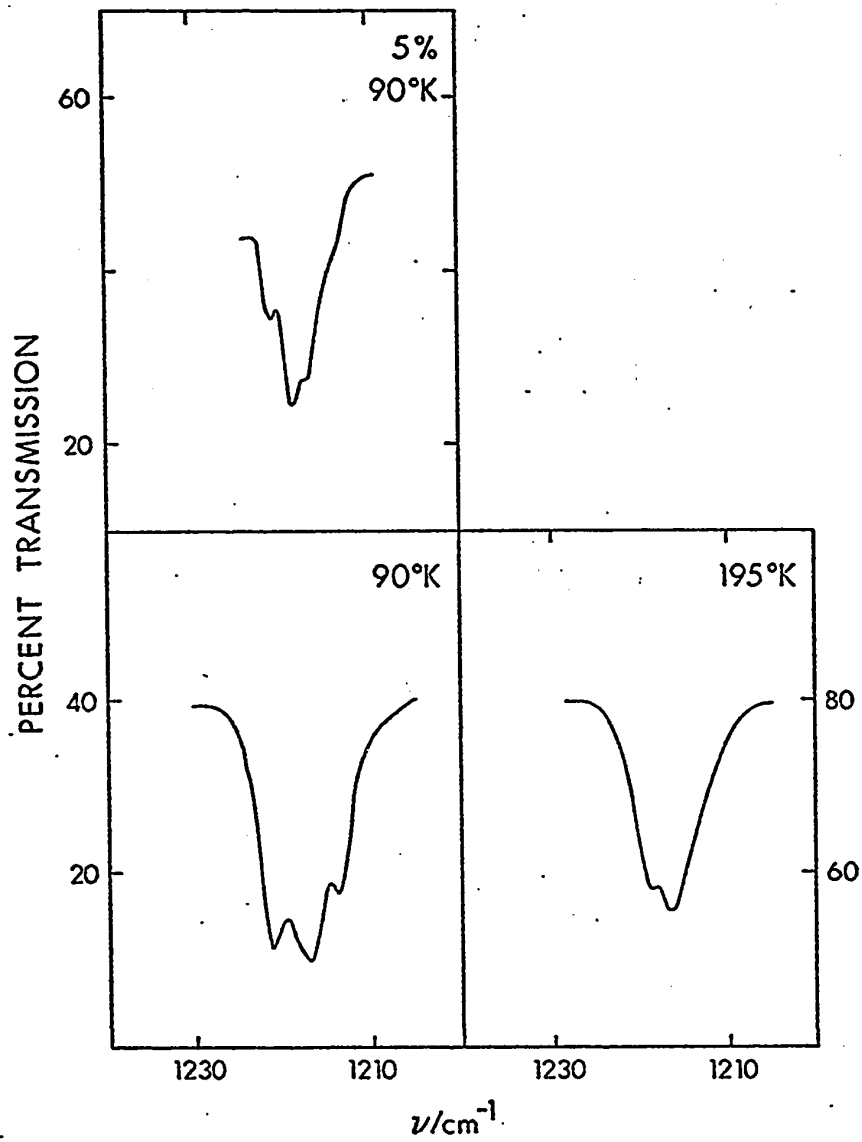


Figure 41

Infrared spectra of the  $\nu_{16}$  (E) fundamental of t-butyl bromide- $\text{d}_9$  in phase III.

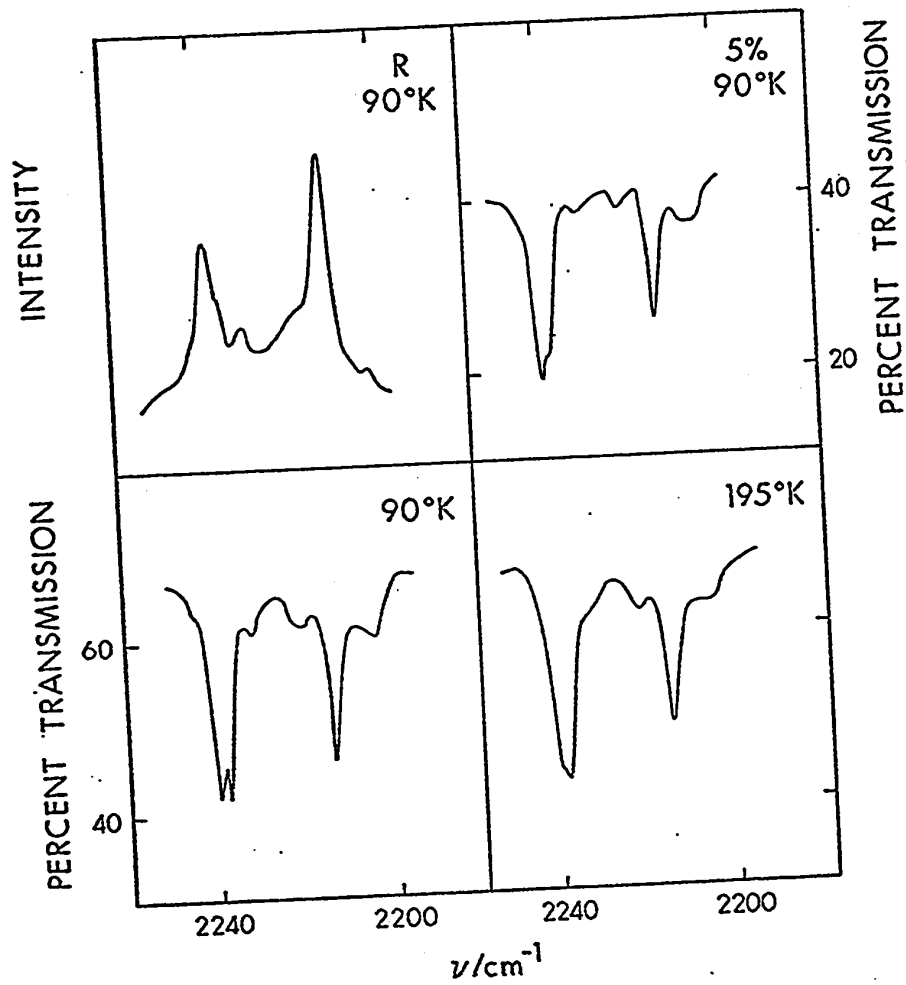


Figure 42

Infrared and Raman spectra of t-butyl bromide-d<sub>9</sub>  
for the region 2250 - 2190 cm<sup>-1</sup>.

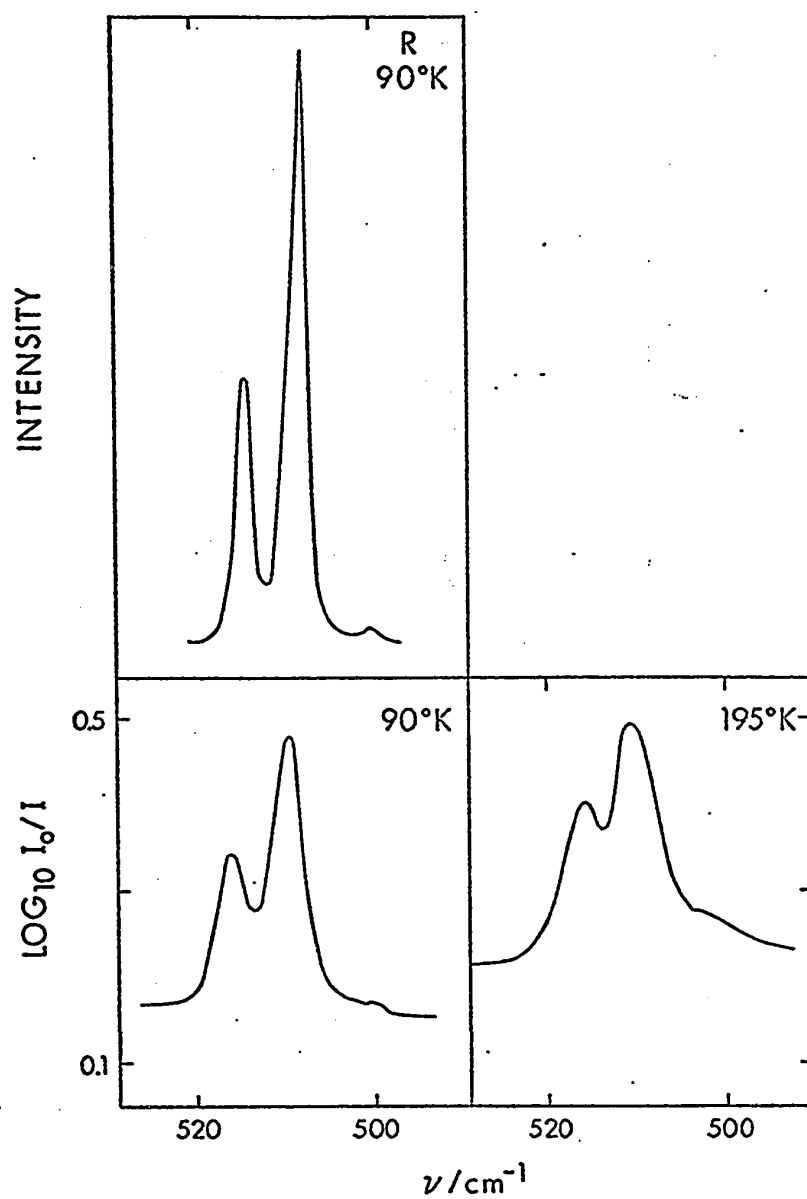


Figure 43

Infrared and Raman spectra of t-butyl bromide-h<sub>9</sub>  
in phase III for the region 530 - 490 cm<sup>-1</sup>.

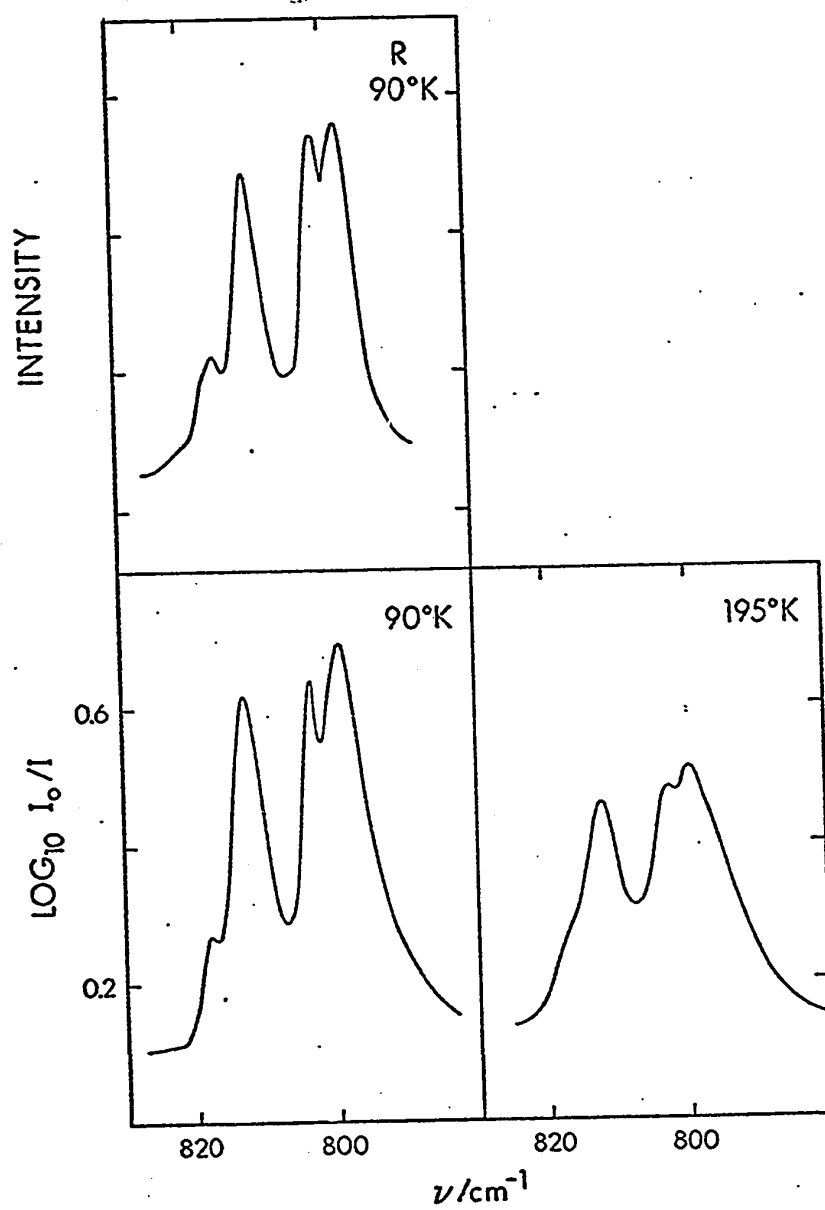


Figure 44

Infrared and Raman spectra of t-butyl bromide-h<sub>9</sub>  
in phase III for the region 830 - 780 cm<sup>-1</sup>.



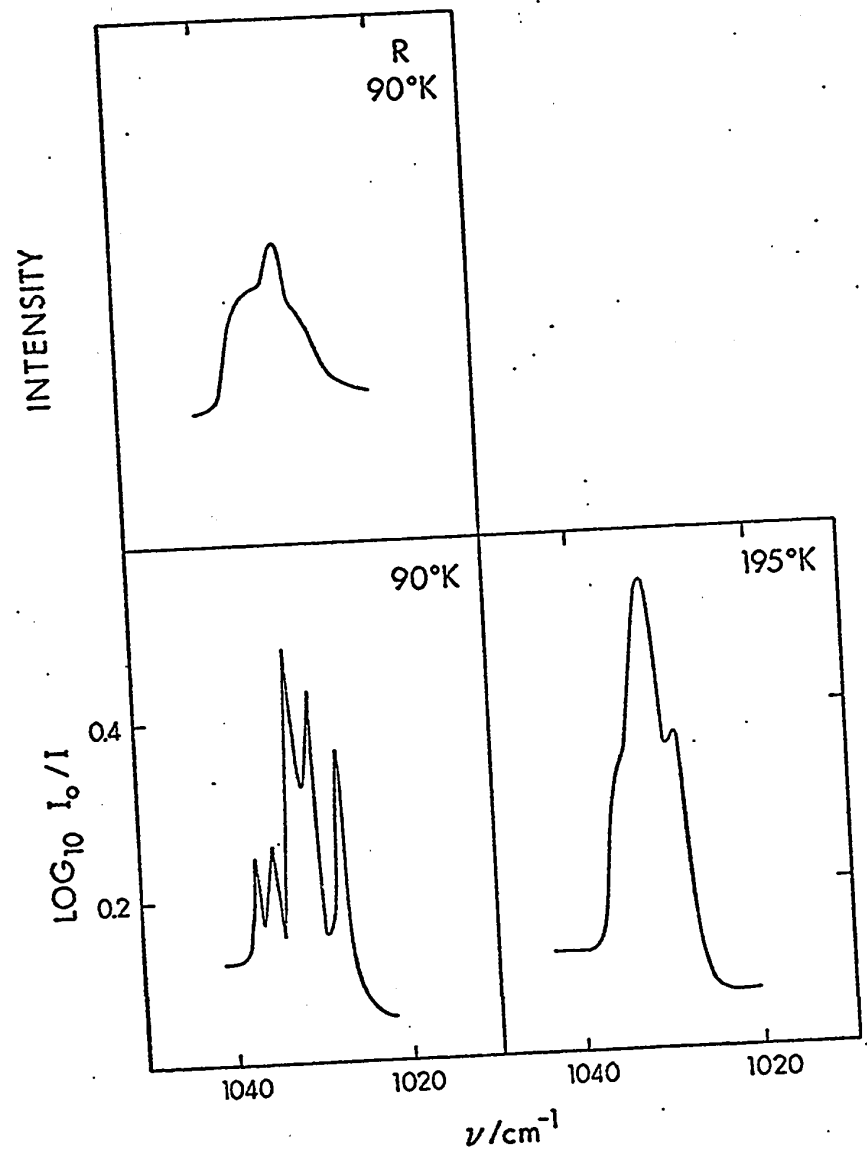


Figure 45

Infrared and Raman spectra of the  $\nu_{20}$  (E) fundamental of t-butyl bromide- $h_9$  in phase III.

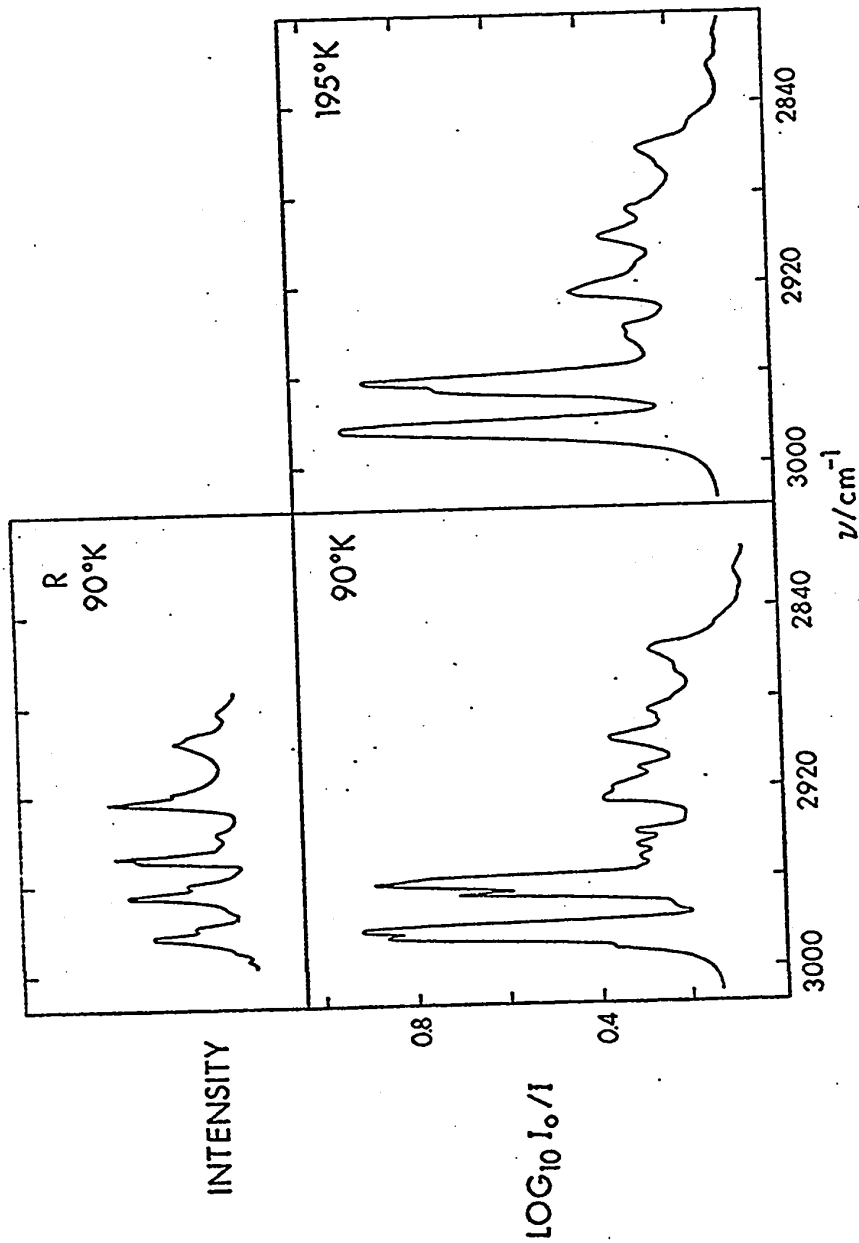


Figure 46

Infrared and Raman spectra of t-butyl bromide-h<sub>9</sub> in phase III for the region 3000 - 2800 cm<sup>-1</sup>.

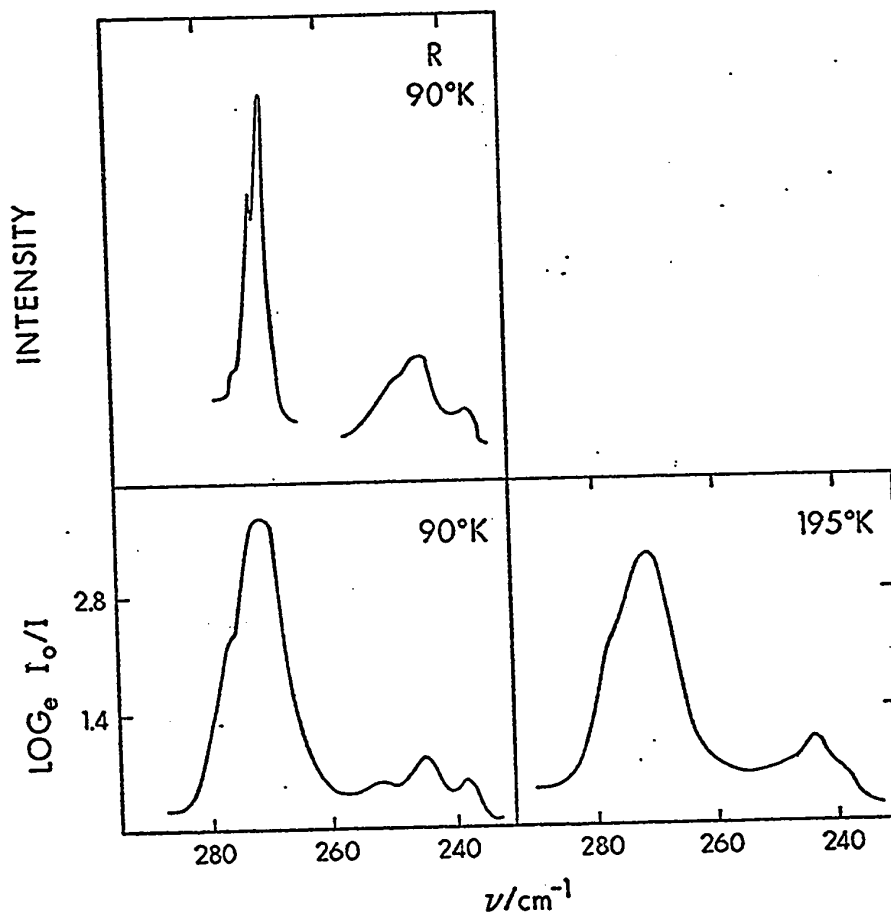


Figure 47

Infrared and Raman spectra of t-butyl bromide-d<sub>9</sub> in phase III for the region 290 - 230 cm<sup>-1</sup>.

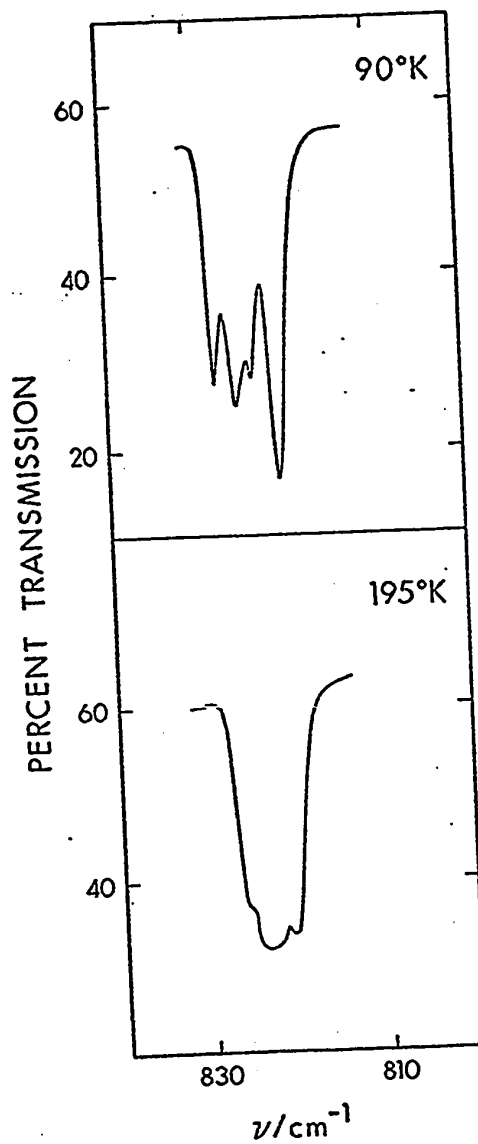


Figure 48

Infrared spectra of the  $\nu_{20}$  (E) fundamental of t-butyl bromide- $\text{d}_9$  in phase III.

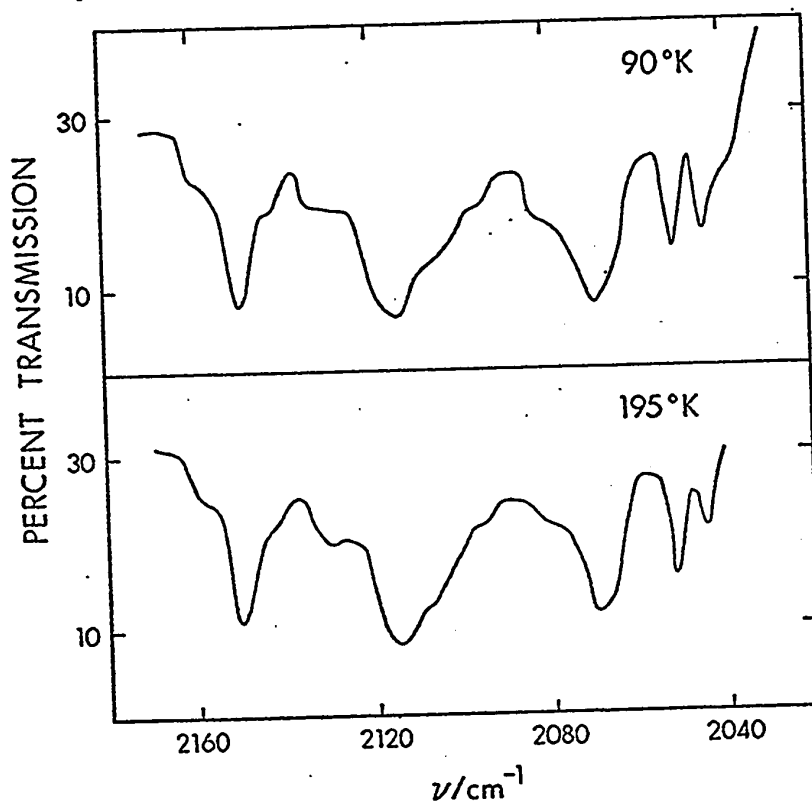


Figure 49

Infrared spectra of t-butyl bromide- $\text{d}_9$  in phase III for the region 2170 - 2030  $\text{cm}^{-1}$ .

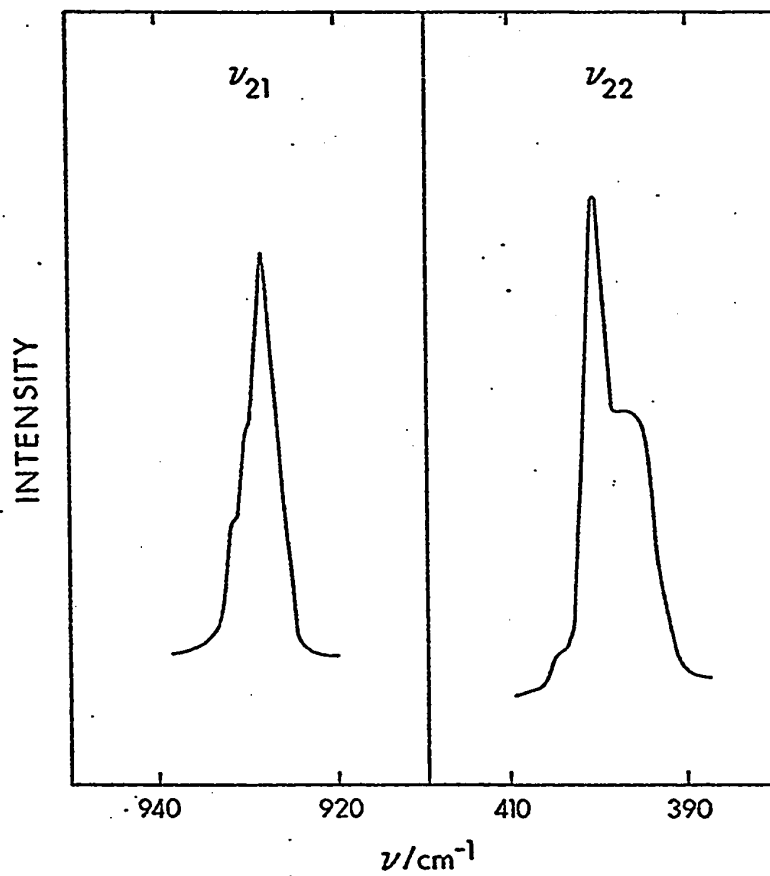


Figure 50

Raman spectrum of  $\nu_{21}$  (E) and  $\nu_{22}$  (E) fundamentals of t-butyl bromide- $\text{h}_9$  in phase III at  $90^\circ\text{K}$ .

intensity reduction caused by light scattering is apparent in the spectrum of  $C_4D_9Br$  at  $90^\circ K$  shown in Figure 31. The details of the very weak features could not be obtained reliably. The spectra shown in Figures 32-50 have been traced, smoothing the noise which was 1% or less. All of the features shown were obtained reproducibly. Some variations from sample to sample were observed in the relative intensities of the components of the band near  $1140\text{ cm}^{-1}$  in the spectrum of the light compound. This band is the most intense in the spectrum and the variations were probably due to reflection effects.

The infrared spectra of phase III were recorded using a resolution of about  $1\text{ cm}^{-1}$ . The frequencies of the features are tabulated in Tables XXV and XXVI for the light and heavy isotopes respectively. The frequency accuracy is better than  $1\text{ cm}^{-1}$  for the sharp features. The separation of close features could be measured to about  $\pm 0.1\text{ cm}^{-1}$ .

The spectra of phase III at  $90^\circ K$  contains a considerable amount of fine structure. At  $195^\circ K$  some of the fine structure has been lost, particularly in the bands due to the degenerate molecular modes, but the spectra are still much more detailed than those of solid phases I or II. The transition from phase II to III is slow, but com-

Table XXV  
 Frequencies and assignments of the features observed in the infrared and Raman spectra of t-butyl bromide-h<sub>9</sub> in the solid phase III.

195°K		90°K						Assignment
		Pure Solid			Dilute <sup>a</sup> Solution			
ν-l cm	Inten- sity	IR		Raman		IR		
		ν-l cm	Inten- sity	Δν-l cm	Inten- sity	ν-l cm		
2985	vs	2991 2985 2982	sh vs vs	2997 2991 2985 2981	vw sh s m	2997 2991 2985 2981	2ν <sub>18</sub> + ν <sub>24</sub>	
2967 2964	sh vs	2973 2967 2962	sh s vs	2972 2967 2962	sh s m	2972 2967 2962	ν <sub>13</sub> ν <sub>1</sub> , ν <sub>14</sub>	
2944 2940	sh w	2951 2945 2940	vw w w	2950 2948 2945 2939	sh s sh w	2950 2948 2945 2939	ν <sub>15</sub>	
2924	m	2925 2919	m sh	2925 2920	s m	2925 2920	ν <sub>2</sub>	

... cont'd.





Table XXV - cont'd.

1426 1415	w w	1426 1415	VW VW	1426 1415	w sh	1426 1415	v <sub>20</sub> + v <sub>22</sub>
1390	w	1389 1386	w w	1391	w	1391	v <sub>4</sub>
1372 1368	sh vs	1372 1369 1367 1364	w sh vs w	1372 1369 1367	sh m m	1369 1367	v <sub>18</sub>
1360	VW, sh	1359	VW	1359			v <sub>5</sub> + v <sub>12</sub>
1321	VW	1321	v	1321			v <sub>6</sub> + v <sub>7</sub>
1302	VVW	1302	VW	1302			v <sub>20</sub> + v <sub>24</sub>
1261	VW	1261	w	1261			v <sub>11</sub> + v <sub>12</sub>
1242 1239	m sh	1243 1239 1235	m m w	1242 1239 1236	m m sh	1245 1240 1237	v <sub>19</sub>
1201	VS	1203	VW	1203			v <sub>21</sub> + v <sub>24</sub>
1145 1141 1138 1135	VS sh VS VS	1146 1144 1139 1135	VVS sh VS VS	1145 1143 1138 1133	sh s sh s	1143 1141	v <sub>5</sub>
							... cont'd.

Table XXV - cont'd.

1130	sh	1131	sh	1129	vw		v <sub>6</sub> + v <sub>8</sub>
1120	sh	1120	sh				
1111	sh	1110	sh				
1035	sh	1037	vw				
1031	w	1035	vw	1036	sh		v <sub>20</sub>
		1032	w	1032	w		
		1030	w	1030	sh		
1028	sh	1028	w				
930	vw	929	vw	932	sh		v <sub>21</sub>
				930	sh		
				928	m		
818	sh	818	w	816	m		v <sub>7</sub> + v <sub>8</sub>
812	m	813	m	812	s		
803	m	803	m	802	s		v <sub>6</sub>
800	m	799	m	798	s		
758	vw	760	vw				v <sub>7</sub> + v <sub>12</sub>
603	vw	604	vw				2v <sub>8</sub>
579	vw	580	vw				2v <sub>23</sub>
559	vw	560	vw				v <sub>23</sub> + v <sub>24</sub>
516	s	516	s	515	s		v <sub>7</sub>
510	vs	510	vs	508	vs		...

210.

... cont'd.

Table XXV - cont'd.

501	sh	501	w	501	w	2 <sup>v</sup> 12
397	vw	396	w	404 400 397	sh m sh	v22
300 297	sh s	301 296	sh s	300 296	vs vvs	v8
288	sh	287 281	sh vw	288	sh	v23
273	w	274 270 267	w sh sh	274 270 267	s sh sh	v24

a5% of t-butyl bromide-h<sub>9</sub> in t-butyl bromide-d<sub>9</sub>

Table XXVI - cont'd.

2142	sh	2142	sh					$v_3 + v_{18}$
2131	sh	2134	sh					$2v_4$
2114	w	2114	m					$v_2$
2108	sh	2107	sh					$v_3 + v_4$
2095	sh	2094	sh					$2v_{17}$
2081	sh	2082	sh					$v_{17} + v_{18}$
2070	m	2069	m					$2v_{18}$
2052	w	2051	w					$v_4 + v_5$
2044	w	2044	w					$v_5 + v_{18}$
1305	vw	1305	vw					$v_3 + v_{24}$
1287	w	1287	w					$v_4 + v_{23}$
		1279	sh					$v_{17} + v_{23}$
		1221	s				1221	
1219	sh	1217	s				1219	
1217	s	1214	w				1217	
		1193	w				1214	
1193	w							$v_7 + 21$
								...
								cont'd.

Table XXVI

Frequencies and assignment of the features observed in the infrared and Raman spectra of t-butyl bromide-d<sub>9</sub> in the solid Phase III.

195°K		90°K				Assignment
Pure Solid		Pure Solid		Dilute <sup>a</sup> Solution		
IR		IR		Raman		
$\nu$ -1 cm <sup>-1</sup>	Inten- sity	$\nu$ -1 cm <sup>-1</sup>	Inten- sity	$\Delta\nu$ -1 cm <sup>-1</sup>	Inten- sity	$\nu$ -1 cm <sup>-1</sup>
		2245	sh	2245	sh	$\nu_{16} + \nu_{18}$
2240	sh	2240	s	2239	m	$\nu_{13}$
2238	s	2237	s	2236	sh	$2\nu_3$
2232	sh	2232	w	2231	w	$\nu_9$
2222	w	2222	w	2221	sh	$\nu_{1'}$ , $\nu_{14}$
2214	s	2214	s	2213	s	$\nu_5 + \nu_{16}$
2203	sh	2204	w	2204	w	$\nu_3 + \nu_4$
2159	sh	2159	sh			$\nu_3 + \nu_{17}$
2150	m	2148	m			... cont'd.

Table XXVI - cont'd.

1157	VW	1157	w				$v_{20} + v_{22}$
1148	VW	1148	w				$v_6 + v_7$
1119	w	1119	w				$v_3$
1113	s	1113	s				$v_8 + v_{20}$
		1110	sh				$v_{21} + v_{22}$
		1107	sh				$v_4$
1092	w	1092	w				$v_{17}$
1074	w	1074	w				$v_{18}, v_{19}$
1063	sh	1063	w				$v_{10}, v_6, v_{22}$
		1058	sh				$v_5$
1052	s	1052	s				...
1049	sh	1049	m				cont'd.
1045	sh	1045	m				
1037	sh	1035	sh				
1029	w	1029	w				
		1026	sh				
1000	vs	1000	vs	1000	w	1000	
		997	sh	997	sh	997	
		992	sh	992	sh	995	
989	vs	988	vs	988	w		

Table XXVI - cont'd.

980	sh	980	sh				$v_6 + v_8$
922	vvw	923	w				$v_{21} + v_{12}$
903	vvw	904	vw				$v_6 + v_{24}$
891	vvw	890	w				$2v_7$
		882	vw				$v_6 + v_{12}$
838	vvw	838	vw				$3v_8$
826	sh	828	w				
824	w	826	w				$v_{20}$
821	sh	824	w				
		821	w				
760	vw	760	w				$v_{11}$
739	vw	739	vw				
		736	w				$v_{21}$
		734	sh				
709	m	709	w	709	sh		$v_7 + v_8$
		707	w				
704	s	704	s	703	m	703	$v_6$
		700	sh				
		697	sh	697	sh		
							... cont'd.



Table XXVI - cont'd.

519	sh	529	sh						$2\nu_{8'}$ $\nu_{8} + \nu_{23}$
513	w	522	sh						
		518	vW						
		512	w						
		508	vW						
463	sh	476	vW	466	w	454	454	454	$\nu_{23} + \nu_{24}$
		466	w	460	w	446	446	446	
		460	w						
454	s	454	s	454	s				$\nu_{7}$
447	vs	446	vs	446	vs				
335	w	335	w						$\nu_{22}$
277	sh	276	sh	276	sh	276	276	276	$\nu_{8}$
271	s	271	s	271	s	270	270	270	
244	w	252	vW	249	sh	245	245	245	$\nu_{23}$
241	sh	245	w	237	m	237	237	237	
		238	vW		w				
214	vW	219	vW						$\nu_{24}$

a 5% of t-butyl bromide-d<sub>9</sub> in t-butyl bromide-h<sub>9</sub>.

The frequencies of the features observed are given in Tables XXV and XXVI for the light and heavy isotopes respectively.

The far-infrared spectra of  $C_4H_9Br$  and  $C_4D_9Br$  at 195°K and 90°K are shown in Figure 51. The nominal sample thickness was 0.2 mm in all cases. The spectra were recorded in two halves, between 10 and 50  $cm^{-1}$  and between 20 and 110  $cm^{-1}$ . Four or more spectra were averaged to reduce the noise level, and averaged spectra were obtained for the two halves. The agreement between the two halves in the overlap region was excellent, and enabled the composite spectra shown in the Figure 51 to be drawn essentially without smoothing. The width of the lines in Figure 51 exceeds the noise level. The spectra were recorded at a resolution of 1  $cm^{-1}$  for the spectra at 90°K. The nominal sample thickness was 0.2 mm for all far-infrared samples. The frequencies of the features are given in Table XXIV along with the ratios of the frequencies of corresponding features in the spectra of the light and heavy isotopes at 90°K. The far-infrared spectrum of the light compound was recorded at several temperatures between 195°K and 90°K. The changes in the spectrum in going from 195°K to 90°K were gradual and all of the features observed at 90°K could be discerned at 120°K.

The far-infrared spectrum of  $C_4H_9Br$  at 83°K has

pletes in about 30 minutes if the sample is kept at 195°K, as indicated by the splitting observed in the  $\nu_6$  and  $\nu_7$  bands of the light compound, Figs. 43 and 44. On the other hand, the reverse transition, III to II, is fast and is complete in less than 5 minutes. The samples were always kept at 195°K for at least half an hour before recording the spectra of phase III. For the light compound, spectra were also recorded at several temperatures between 195°K and 90°K. It was found that the resolution of the bands into components improved steadily, with no abrupt changes, as the temperature was lowered.

The infrared spectra of phase III formed from a 5% solution of  $C_4H_9Br$  in  $C_4D_9Br$  and of  $C_4D_9Br$  in  $C_4H_9Br$  were also recorded. Only the more intense bands of the guest isotope which do not overlap with host lattice absorptions could be studied. These are shown in Figures 32-42 along with the corresponding bands in the pure solid. To study the spectra of these mixed crystals the samples had to be thicker than for the study of the pure isotopes. In spite of this added difficulty, the bands of interest, that is the strong bands of the solute isotope, were recorded with approximately the same noise level and resolution as for the pure compound, although significant light scattering was evident from the low background transmission.

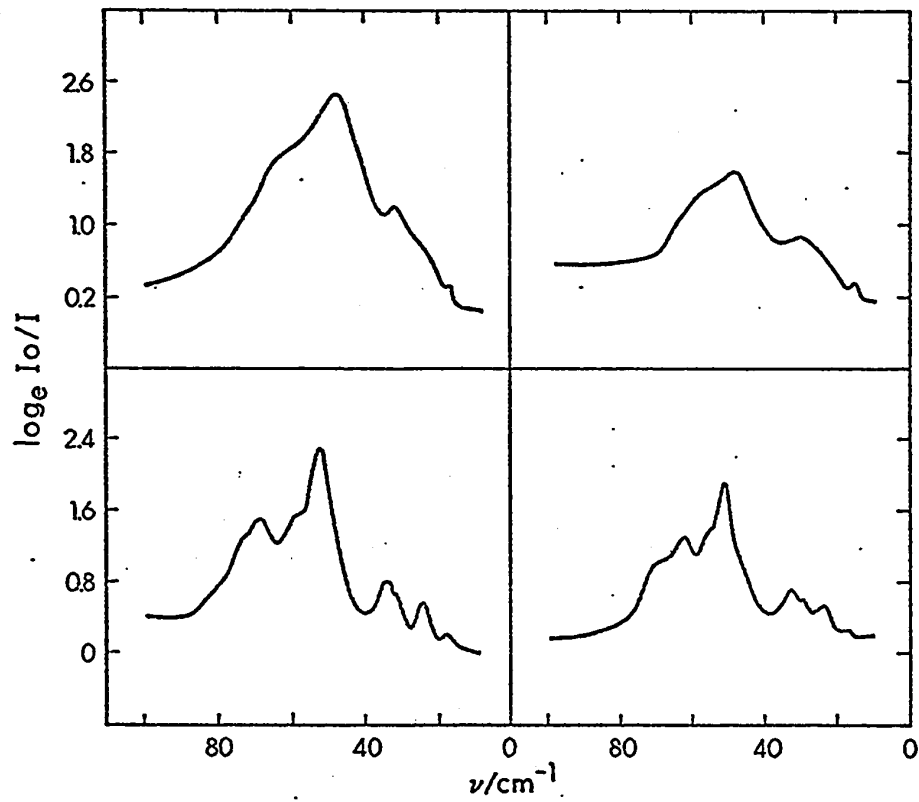


Figure 51

Far-infrared spectra of t-butyl bromide- $\text{h}_9$  (left boxes) and - $\text{d}_9$  (right boxes) in phase III; at 90°K (lower boxes) and 195°K (upper boxes).

been reported earlier by Durig et al (113). They report only two features, in contrast to eight features reported in this present work (see Figure 51, and Table XXIV). The four low frequency features occur below  $34 \text{ cm}^{-1}$  and were not accessible to Durig et al. The other two features not previously reported were clearly visible on all spectra recorded on the interferometer and have been confirmed by recording the interferogram using different beam splitters and two kinds of mirror drives (Section 3.2).

The Raman spectra of  $\text{C}_4\text{H}_9\text{Br}$  and  $\text{C}_4\text{D}_9\text{Br}$  at  $90^\circ\text{K}$  are shown on expanded frequency scales in Figures 32-39, 42-47, and 50 along with the corresponding bands in the infrared. Since the different Raman bands shown in the above Figures were obtained under different conditions, relative band intensities cannot be obtained from the Figures. Approximate relative intensities of the strongest peaks in each band were obtained from separate spectra in which several bands were recorded under identical conditions. The relative intensities are given in Tables XXV and XXVI. The bands of  $\text{C}_4\text{H}_9\text{Br}$  due to  $\nu_3$  (Figure 36),  $\nu_{18}$  (Figure 35),  $\nu_{19}$  (Figure 34),  $\nu_{20}$  (Figure 45),  $\nu_{21}$  and  $\nu_{22}$  (Figure 50) and  $\nu_6$  of  $\text{C}_4\text{D}_9\text{Br}$  (Figure 38) were recorded at high gain settings and high resolution was not obtained.

These bands were recorded at  $2 \text{ cm}^{-1}$  resolution and have been smoothed to show only the reproducible features. All of the other bands, shown in Figures 32 to 50, were recorded at a resolution of  $1 \text{ cm}^{-1}$ . The frequencies of the observed features in the Raman spectra are given in Tables XXV and XXVI. The relative intensities of the features in the bands due to the  $\nu_6$ ,  $\nu_7$ , and  $\nu_8$  modes of  $\text{C}_4\text{H}_9\text{Br}$  (Figures 44, 43 and 32) and  $\nu_6$  and  $\nu_7$  modes of  $\text{C}_4\text{D}_9\text{Br}$  (Figures 38 and 37) in the Raman spectra are very similar to those seen in the infrared spectra. For most other modes they are quite different.

The Raman spectrum of the light compound below  $100 \text{ cm}^{-1}$  largely confirms the results of Durig et al (113), except that a very strong indication of an additional feature at  $34 \text{ cm}^{-1}$  was obtained. This region of the spectrum is not reproduced in this thesis. Only one feature, at  $50 \pm 2 \text{ cm}^{-1}$  could be located in the Raman spectrum of  $\text{C}_4\text{D}_9\text{Br}$  at  $90^\circ\text{K}$  below  $100 \text{ cm}^{-1}$ . However the fluorescence problem for  $\text{C}_4\text{D}_9\text{Br}$  was much more severe in this region than for  $\text{C}_4\text{H}_9\text{Br}$ .

### 6.1.3 X-Ray Measurements on Phase III

The crystal structures of t-butyl bromide- $\text{h}_9$  and  $\text{-d}_9$  were studied at  $120 \pm 10^\circ\text{K}$  using powder methods. Both isotopes were maintained at  $195^\circ\text{K}$  for at least forty min-

utes before being cooled to 120°K, to ensure that the II to III transition was complete. No evidence of residual phase II was ever observed on the photographs.

Table XXVII contains the interplanar spacings (d-values) calculated from the measurements of the observed lines in the X-ray powder photographs of t-butyl bromide-h<sub>9</sub> at 120 ±10°K, as well as the approximate relative intensities of these lines. These d-values are designated the 'observed' values in the Table and are the averages of the values obtained from several photographs taken using copper and cobalt X-ray lines. The number of measurements included in the average is shown in the Table for each line, along with the mean deviation from the average.

One photograph of t-butyl bromide-d<sub>9</sub> was also taken and it was found to be identical with those obtained for the light compound, which confirms that the two isotopes crystallize in the same structure.

The Hesse-Lipson procedure was used to deduce the unit cell dimensions (173). All of the lines could be indexed on an orthorhombic unit cell very similar to the one specified at the bottom of Table XXVII. The indices for each line are given in Table XXVII. The unit cell parameters were refined by least squares. The computer program used in the refinement minimized the sum of

Table XXVII

Observed and calculated d-spacings for the first 28 lines of the X-ray pattern of t-butyl bromide in phase III at 120°K.

Line	Inten- sity	d-spacing (Å)		Observed d - Calculated d (Å)	Number of photo- graphs used	hkl
		Observed	Calculated			
1	vw	9.424 ± 0.185	9.460	-0.034	7	001
2	w	5.447 ± 0.037	5.400	+0.047	9	020
3	m	5.068 ± 0.029	5.016	+0.052	7	201
4	s	4.886 ± 0.012	4.912	-0.028	6	120
5	vs	4.742 ± 0.015	4.730	+0.012	8	002
6	s	4.446 ± 0.025	4.392	+0.054	8	102
7	vw	4.231 ± 0.017	4.231	0.000	5	012
8	s	3.952 ± 0.018	3.944	+0.008	8	300
9	w	3.592 ± 0.016	3.600	-0.008	7	030
10	w	3.460 ± 0.013	3.500	-0.040	7	311
					...	cont'd.



Table XXVII - cont'd.

11	m	3.334 ± 0.014	3.365	-0.031	7	031
12	m	3.159 ± 0.010	3.153	+0.006	7	003
13	w	3.029 ± 0.010	3.029	0.000	7	302
14	VW	2.909 ± 0.006	2.917	-0.008	6	312
15	m	2.736 ± 0.012	2.731	+0.005	7	411
16	VW	2.627 ± 0.007	2.633	-0.006	5	140
17	w	2.515 ± 0.007	2.508	+0.007	5	402
18	VW	2.432 ± 0.003	2.443	-0.011	4	412
19	VW	2.364 ± 0.006	2.365	-0.001	4	004
20	w	2.222 ± 0.002	2.222	0.000	3	431
21	VW	2.167 ± 0.002	2.166	0.001	3	024
22	VW	2.108 ± 0.008	2.106	0.002	2	051
23	VW	2.052 ± 0.008	2.051	0.001	2	043
24	VVW	2.017 ± 0.008	2.016	0.001	1	342
25	VW	1.970 ± 0.003	1.970	0.000	2	522
					.	. cont'd.

Table XXVII - cont'd.

26	W	1.923 ± 0.002	1.934	0.011	3	243
27	VVW	1.883 ± 0.010	1.878		1	234
28	VVW	1.785 ± 0.010	1.785		1	523

Unit Cell Dimensions:

$a = 11.832 \pm 0.014 \text{ \AA}$

$b = 10.801 \pm 0.012 \text{ \AA}$

$c = 9.460 \pm 0.012 \text{ \AA}$

$\alpha = 90^\circ$

$\beta = 90^\circ$

$\gamma = 90^\circ$

$Z = 8 \text{ molecules}$

Density:  $1.5055 \text{ gm cm}^{-3}$  (from X-ray data at 120°K)

Possible space groups:  $P222-D_2^1$ ,  $Pmm2-C_2^1$ , or  $Pmmm-D_2^1$ .

the squares of the deviations of the calculated and observed d-spacings, assuming the indices supplied to be correct (174). The problem converged quickly to yield the unit cell parameters listed at the bottom of the Table XXVII. The calculated d-values and their differences from the observed values are shown in Table XXVII. The agreement between the calculated and observed d-values is as good as can be expected from the present data. Thus the unit cell parameters given in the Table satisfactorily explain the observed diffraction pattern.

Schwartz et al (128) determined the unit cell dimensions of t-butyl bromide at 238°K in phase I. According to their data there are four molecules per unit cell with a unit cell volume of  $676.8 \text{ \AA}^3$ . The unit cell volume of t-butyl bromide at 120°K obtained from the parameters given under Table XXVII is  $1208.9 \text{ \AA}^3$ . This corresponds to 7.2 molecules per unit cell if one assumes that there is no change in the density on cooling from 238°K to 120°K. Because disorder-to-order transitions are normally accompanied by an increase in density, it seems reasonable to assume that there are 8 molecules per unit cell at 120°K. The increase in density obtained for t-butyl bromide under this assumption is 10% and is consistent with values found for other cases by Rudman and Post (175). An inspection

The spectra of solid phases I and II (Figures 21 and 22) do not show any fine structure due to intramolecular coupling. This could result simply from the lack of translational symmetry in the plastic phases, but it undoubtedly also results from the rapid molecular reorientation. The breadth of the bands due to the intramolecular modes can be attributed, in general, to a combination of the three factors discussed in Section 1.2.3. Briefly these are (a) coupling between the vibrations of neighbouring molecules (intermolecular coupling), (b) variation in the local fields experienced by the molecules (site effects), and (c) the reorientational motions of the molecules. The spectral results reported in this thesis do not provide a quantitative measure of the broadening caused by these three factors, but they do permit a qualitative discussion to be presented. The following discussion assumes that the infrared halfwidths can be compared with the Raman halfwidths to obtain meaningful information about the range of vibrational frequencies which arises from each intramolecular mode, because of the site and intermolecular coupling effects, and about the influence of orientational motion. This assumption implies that, in the absence of reorientational contributions, the shapes and widths of the infrared and Raman bands are the same,

since they are determined only by the number of vibrations at a particular frequency. It is supported by the fact that the magnitude of the splittings observed in the spectra of the ordered phases of t-butyl bromide- $h_9$  and  $-d_9$  is the same in the infrared and the Raman spectra. The reorientational contributions to the Raman bandwidth are different from those to the infrared bandwidth and are therefore not compared.

Figures 23 and 24 show the halfwidths of some of the strong, well-separated, infrared bands of the liquid and solid phases, plotted against temperature. In the liquid and high temperature solid phases the halfwidths show a gradual decrease with decreasing temperature, with no sharp changes at the L to I and I to II transitions, but they do decrease sharply at the II to III transition. The gradual decrease must result from smaller contributions from molecular reorientation, as well as smaller effects due to the decreasing influence of anharmonicity at lower temperatures. The last effect also occurs in ordered crystals (176, 177), but is usually small and will be neglected. Since the intermolecular distances in solids are not strongly temperature-dependent, the line-width contributions due to intermolecular coupling and site effects are not expected to vary significantly over

of the indices of the observed lines shows that there are no systematic absences, which indicates that the unit cell is not centered and the crystal does not contain any glide planes or screw axes (47). The lattice is orthorhombic and these data therefore indicate that phase III of *t*-butyl bromide crystallizes in one of the three space groups  $P222-D_2^1$ ,  $Pmm2-C_{2v}^1$ , or  $Pmmm-D_{2h}^1$ .

## 6.2 DISCUSSION OF THE SPECTRA OF THE PLASTIC PHASES

### 6.2.1 INTRAMOLECULAR MODES

The existing literature on the solid state of *t*-butyl bromide, as summarized in Section 1.3.2, indicates that the solid phases I and II are orientationally disordered, and that the molecules reorient at frequencies greater than  $10^9 \text{ sec}^{-1}$  in these phases and in the liquid. The only difference between the two plastic phases and the liquid is that in the solids the molecules occupy regularly-spaced lattice sites, while in the liquid they are randomly arranged with no long range order in their positions. They can presumably undergo translational diffusion in the liquid more readily than in the plastic solids. The similarity between the mid-infrared spectra of the liquid and those of the solid phases I and II indicates that translational diffusion does not have a pronounced effect on the mid-infrared spectra.

the temperature range employed in the experiments reported here. The temperature dependence of the linewidths is therefore ascribed to the contribution from molecular reorientation.

Approximate but independent support for the above conclusion is obtained from the study of the bandwidths of two  $A_1$  modes,  $\nu_7$  and  $\nu_8$  of  $C_4H_9Br$ , in the Raman spectra of the liquid and solid phase II. The halfwidths of these bands were found to be essentially the same in the Raman spectra of the liquid recorded without a polarizer and in that recorded with a polarizer parallel to the direction of incident polarization, Figure 28. This arises because these two bands are strongly polarized, their depolarization ratios being 0.1 and 0.15 respectively. These observations imply that the  $\nu_7$  and  $\nu_8$  bands are determined mainly by the isotropic Raman scattering (81-82) which is not affected by molecular reorientation. Therefore the observed halfwidths of these Raman bands arise principally from intermolecular coupling of the vibrations and site effects. It was found that the bandwidths of the  $\nu_7$  and  $\nu_8$  Raman bands remain constant, at values of  $9.0 \text{ cm}^{-1}$  and  $7.0 \text{ cm}^{-1}$  respectively, in going from the liquid phase, at  $25^\circ\text{C}$ , to the solid at  $-45^\circ\text{C}$ , while the corresponding infrared bands decrease in halfwidth by  $1.0 \text{ cm}^{-1}$  over this tem-

perature range.

It must be emphasized that the above arguments based on the Raman spectra are only qualitative. Bartoli and Litovitz (81) have pointed out that the observed bandwidths should be corrected for the influence of the finite slit widths before any conclusions are drawn. They also point out that the anisotropic scattering does contribute to the observed bandwidths, even for polarized Raman bands. But in the present case the slit width was  $1 \text{ cm}^{-1}$  compared to band halfwidths of  $9 \text{ cm}^{-1}$  and  $7 \text{ cm}^{-1}$  for these two strongly polarized bands. Hence it seems certain that the conclusions drawn would not be significantly altered by the above corrections. The halfwidth of the infrared bands at  $273^\circ\text{K}$  are  $10.5 \text{ cm}^{-1}$  for both  $\nu_7$  and  $\nu_8$ , compared to  $9$  and  $7 \text{ cm}^{-1}$  for the Raman bands. From the arguments presented, the differences,  $1.5$  and  $3.5 \text{ cm}^{-1}$  for  $\nu_7$  and  $\nu_8$  respectively, must be the widths contributed by the molecular reorientation to the infrared bands.

Comparison of the bandwidths in the spectra of the 5% solutions of  $\text{C}_4\text{H}_9\text{Br}$  in  $\text{C}_4\text{D}_9\text{Br}$  and of  $\text{C}_4\text{D}_9\text{Br}$  in  $\text{C}_4\text{H}_9\text{Br}$  with those of the pure isotopes gives an indication of the importance of the intermolecular coupling contributions. In the dilute solutions, each solute molecule is



surrounded by solvent molecules; consequently, those vibrations of the solute molecule whose frequencies are well removed from frequencies of the solvent, do not couple significantly with vibrations of neighbouring molecules. Intermolecular coupling will therefore not effect the shape and breadth of the absorption bands due to these modes in the dilute solution. Figures 25-27 show the bands of the solute molecules in phases I and II, and their halfwidths are listed in Tables XXII and XXIII, which contain data only for the stronger, non-overlapping bands. The bandwidths are smaller in the spectra of the solution than in those of the pure phase. In general, this proves that intermolecular coupling does contribute significantly to the observed band width. The difference between the half-width of a band in the spectrum of the pure phase and in 5% solution is a measure of the line broadening caused by intermolecular coupling. It can be seen that this difference in widths is not constant for all bands, but ranges from about  $1 \text{ cm}^{-1}$  to  $4 \text{ cm}^{-1}$ . In most cases the larger value is associated with bands which occur in regions of quite extensive absorption by combination and overtone bands, in addition to the fundamentals.

All three sources of line broadening can contribute to the observed bandwidth in the infrared spectrum of

The above discussion shows that intermolecular coupling, site-effects and molecular reorientations, all contribute significantly to the observed linewidths in the infrared spectra of the liquid and the plastic crystal phases of t-butyl bromide. Furthermore, the small gradual decreases in the halfwidths, with decreasing temperature, observed in the liquid and plastic crystal phases are mainly caused by the decreased contributions of the reorientational motions.

No differences in the structures of phase I and II are apparent from the spectral studies reported here. A first order phase transition separates these phases and previous studies have given very little information about the differences between them. The infrared spectra do not improve this situation because the spectra of the phases are essentially identical.

#### 6.2.2 FAR-INFRARED

The similarity between the far-infrared spectra of the two plastic phases and the liquid phase of t-butyl bromide is consistent with observations on other systems (94-96). These similarities indicate that the translational diffusion of the molecules has little influence upon the spectrum, and that the spectrum arises from the same or similar processes in both liquid and plastic phases.

a pure phase, while only site effects and molecular reorientation can contribute to the observed bandwidth in the infrared spectrum of a dilute solution, and only intermolecular coupling and site effects contribute to the width of the isotropic Raman scattering (81, 82). If one assumes that the contributions of the three sources to the linewidth are linearly additive, one can estimate the individual contributions from the values of the halfwidths in the infrared spectra of the pure phase and of the dilute solution, and from the halfwidth of the band due to isotropic Raman scattering by the pure phase. Such complete data is available for the  $\nu_8$  mode of  $C_4H_9Br$  from the results reported in this thesis. The halfwidths of the  $\nu_8$  bands are  $9.5\text{ cm}^{-1}$  and  $5.0\text{ cm}^{-1}$  in the infrared spectra of phase II, Table XXII, while the halfwidth of the band in the Raman spectrum is  $7.0\text{ cm}^{-1}$ . Therefore the contribution due to intermolecular coupling is  $4.5\text{ cm}^{-1}$ , the contribution from site effects is  $2.5\text{ cm}^{-1}$ , and that due to molecular reorientation is  $2.5\text{ cm}^{-1}$ . These values are undoubtedly approximate because, as Bartoli and Litovitz (81) have pointed out, the various contributions to the width are not strictly additive and the line shapes from each term should be convoluted to derive the actual spectrum.

It was shown in Chapters 4 and 5 that intramolecular vibrations occur at frequencies greater than  $180\text{ cm}^{-1}$  both for t-butyl bromide- $\text{h}_9$  and  $-\text{d}_9$ . Hence the far-infrared absorption cannot be attributed to any intramolecular vibration. This absorption cannot be attributed to difference bands arising from intramolecular energy levels because the absorption intensity does not decrease with decrease in temperature as the intensity of a difference band would. Furthermore, the frequency of maximum absorption increases with decreasing temperature (Figure 29) while the frequency of a difference band would be essentially temperature-independent. Thus it is clear that the observed far-infrared absorption cannot arise from intramolecular vibrations.

T-butyl bromide and t-butyl chloride are very similar molecules and show similar far-infrared spectra in their liquid and plastic solid phases. The reported (106) far-infrared spectra of solutions of t-butyl chloride in nonabsorbing solvents are similar to the spectrum of the pure liquid. One can therefore rule out intermolecular complex formation as a source of far-infrared absorption. It seems reasonable to assume that no significant intermolecular bonding exists in t-butyl bromide. Consequently the far-infrared absorption in the plastic solid and

liquid phases of t-butyl bromide can only arise from intermolecular relaxation processes and intermolecular resonance processes.

Specific evidence has been obtained in this work to indicate that the absorption maximum is determined by resonance processes for which the force field is supplied by the intermolecular forces. In the language of the quasi-harmonic treatment of lattice vibrations and potentials, the intermolecular forces increase in strength as the temperature decreases, and therefore the frequencies of resonance processes, which are controlled by the intermolecular forces, increase as the temperature decreases (63). Relaxation processes, and free molecular rotation cause the frequency of maximum absorption to decrease as the temperature decreases (3). The frequency of maximum absorption in the liquid and plastic phases of t-butyl bromide increases as the temperature decreases (Figure 29) and therefore the absorption must arise from resonance processes controlled by the intermolecular forces, that is, from rotational vibrations and translational vibrations.

Relaxation processes probably also contribute to the far-infrared absorption, but they cannot control the frequency of maximum absorption, and therefore the

is approximately proportional to the square of the molecular dipole moment, which indicates that the intensity arises from rotational vibrations. Earlier, Kroon and Van Der Elsken (182) also attributed the temperature dependence of the absorption maximum to the absorption by the translational vibrations. These workers incorrectly assumed that rotational vibrations do not increase in frequency as the temperature decreases, whereas it is well known from studies of ordered solids that both rotational and translational vibrations increase their frequency as the temperature is lowered (63-65).

Although the intensity of the absorption originates predominantly from the rotational vibrations of the molecules, it does seem certain that the translational vibrations influence the distribution of the far-infrared absorption in plastic crystals and liquids. Rotational and translational vibrations in condensed phases can couple and borrow intensity from one another if they have similar frequencies, unless the coupling is forbidden by symmetry. Symmetry forbids coupling between vibrations belonging to different irreducible representations of the factor group, as is the case for the rotational and translational vibrations of benzene (Figure 3). In plastic crystals and liquids, however, there are no elements of

absorption by relaxation processes must be weaker, or much broader, than that by the vibrations. Several workers have applied the Debye theory for orientational relaxation, modified to take account of inertial effects, to the far-infrared and microwave absorption in liquids and plastic crystals (106, 108, 178-181) and have shown that the theory can reproduce the microwave absorption, and the far-infrared absorption up to about  $10\text{ cm}^{-1}$ , rather well. It seems probable, therefore, that the relaxation process determines the shape of the absorption at these low frequencies. At higher frequencies the calculations based on this modified Debye model underestimate the intensity of the absorption band.

On the basis of these calculations, it seems apparent that the far-infrared absorption involves some intermolecular vibration or resonance process (102-105). Some workers have studied the temperature dependence of the frequency of maximum absorption (96, 180, 182-183) and found that the frequency of the maximum absorption increases with decreasing temperature, as is observed for *t*-butyl bromide (see Table XXIV). Jain and Walker (183) used this temperature dependence to deduce that translational vibrations determine the frequency of maximum absorption, even though they also proved that the intensity of absorption

symmetry and therefore no symmetry restrictions on the coupling. The translational and rotational vibrations can couple and both are expected to influence the shape of the far-infrared absorption. Support for this conclusion comes from the spectra of phase III of t-butyl bromide in which both the rotational and the translational vibrations are found to occur at similar frequencies and have comparable intensities (see Section 6.3.3).

One can conclude from the above discussion that both rotational and translational vibrations, as well as the relaxation processes, contribute to the far-infrared absorption in plastic crystals and the liquid. The intensity and the frequency of the maximum absorption are determined by the intermolecular vibrations, while the relaxation processes contribute mainly to the absorption at frequencies below about  $10 \text{ cm}^{-1}$ .

### 6.3 DISCUSSION OF THE SPECTRA AND STRUCTURE OF PHASE III

#### 6.3.1 GENERAL

Dielectric relaxation studies of phase III of t-butyl bromide clearly show that the molecular dipoles are fixed in this phase (4, 129-130). Calorimetric (129-130), dielectric relaxation (4, 129-130), and PMR studies (5) have shown that no phase transition occurs between 77°K



and 209°K, but the PMR studies indicate that the degree of molecular mobility does change in this temperature range. PMR second moment calculations (5) indicate that at 77°K the molecules are essentially static but, on warming, first the methyl groups reorient about the C-C bonds, and then the whole C-C<sub>3</sub> unit reorients about the C-Br bond. The rates of these reorientations are not known, but far-infrared spectra at 195°K provide some evidence that the molecular rotation about the C-Br bond is not very fast. A broad band with four definite features upon it is seen in the far-infrared spectrum of phase III at 195°K, Figure 51. This is characteristic of the far-infrared spectra of orientationally disordered solids in which molecular reorientation is slow, while a broad featureless band would be expected for very fast reorientation.

The vibrational spectra and the X-ray studies in the present work indicate that the molecules in phase III are ordered at temperatures below about 120°K. Although many of the features seen in the spectra at 90°K have halfwidths of about 3 cm<sup>-1</sup>, it is clear that this halfwidth is due to the superposition of unresolved lines of smaller halfwidth, because, in several instances, features one to two cm<sup>-1</sup> apart are clearly resolved. Furthermore,

some of the bands of the pure t-butyl bromide in phase III at 90°K differ significantly from the corresponding bands in the corresponding phase made from an isotopically dilute solution. Both of these observations are typical of ordered solids, but not of disordered ones. The far-infrared spectra at 90°K consist of basically sharp line absorptions. The absorption near  $65\text{ cm}^{-1}$  is not particularly sharp but the features to low frequency of it have half-widths typical of those found in ordered solids at 90°K (63-64, 91). The X-ray powder photographs at 120°K show a large number of distinct lines. Such behaviour is far more consistent with an ordered arrangement of the atoms than with a disordered one, although disorder in the hydrogen atom positions would probably not have influenced the X-ray photographs.

The above discussion shows that the C-Br bonds become fixed and ordered at the transition from phase II to phase III, because, (a) the C-Br bonds ('molecular dipoles') are fixed below the II to III transition, (b) the structure is ordered below 120°K, and (c) there is no transition between 209°K and 77°K.

The infrared absorption bands due to the degenerate, E, intramolecular modes change more than those due to the totally symmetric  $A_1$  modes as the sample tempera-

ture is raised from 90°K to 195°K. The fine structure observed in the spectrum of an ordered solid is expected to become less distinct as the sample temperature is raised from 90°K to 195°K, because anharmonic effects contribute significantly to the linewidths at higher temperatures (176-177). The small changes observed in the bands due to the  $A_1$  modes (Figures 32, 33, 37, 43, 44 and 47) are consistent with those expected in the spectrum of an ordered solid for such an increase in temperature. But the changes in the bands due to the E modes are much greater than would be expected from the effect of anharmonicity alone. This is particularly marked in the bands due to  $\nu_{20}$ , the degenerate methyl rocking modes, of  $C_4H_9Br$  (Figure 45) and  $C_4D_9Br$ , (Figure 48), but is also observed in the bands due to  $\nu_{13}$  (Figure 46),  $\nu_{18}$  (Figure 35) and  $\nu_{19}$  (Figure 34) bands of  $C_4H_9Br$  and the  $\nu_{16}$  (Figure 41) band of  $C_4D_9Br$ .

The greater loss of fine structure by the bands due to the degenerate modes, between 90°K and 195°K, is consistent with the conclusions drawn earlier, that the C-Br bonds of the molecules are fixed in an ordered arrangement at all temperatures in phase III but the molecules can reorient around them at the higher temperatures, if it is assumed that the reorientation introduces orien-

tational disorder into the crystal. In an isolated *t*-butyl bromide molecule the transition moment for an  $A_1$  mode is parallel to the C-Br bond, while that for an E mode is perpendicular to this bond. The symmetry of the molecules in the solid phase III is certainly less than the  $C_{3v}$  symmetry of an isolated molecule, as discussed later, but to a first approximation, the direction of the transition moment of an intramolecular mode of a molecule in phase III should be essentially the same as for a free molecule (100). This arises because the reduced symmetry is caused by the intermolecular forces which are much weaker than the intramolecular forces. Therefore, the transition moments on different molecules should transform as one of the irreducible representations of the space group during a crystal vibration in which each molecule executes the same,  $A_1$ , intramolecular vibration. This means that crystal vibrations based on  $A_1$  intramolecular vibrations should approximately obey the factor group selection rules at the higher temperatures, even though the crystal is disordered by the rotation about the C-Br bond. This result assumes that the  $A_1$  intramolecular modes cannot couple with the E intramolecular modes during a crystal vibration. The transition moments for the E modes are perpendicular to the C-Br bonds, and their direc-

tions in the crystal depend on the orientations of the molecules about the C-Br bond, and these orientations are disordered at the higher temperatures. Therefore, the transition moments on different molecules are disordered during a crystal vibration based on a degenerate mode of the free molecule. The factor group selection rules do not apply in this case, and all such crystal modes should be infrared active, yielding broad absorption. The above discussion rationalizes the difference in the behaviour of the bands due to two types of intramolecular modes on warming phase III, and provides evidence that the C-Br bonds are fixed in an ordered manner in phase III, but the atomic arrangement about the C-Br bond is ordered only at low temperatures.

### 6.3.2 X-RAY RESULTS

The X-ray powder pattern of phase III was indexed on an orthorhombic lattice with 8 molecules per unit cell. The three possible space groups indicated by the X-ray powder pattern of t-butyl bromide at about 123°K are  $P222-D_2^1$ ,  $Pmm2-C_{2v}^1$ , or  $Pmmm-D_{2h}^1$ . In an ordered solid, the site group of a molecule must be a sub-group of the molecular point group and of the space group of the solid. The molecular point group for t-butyl bromide is  $C_{3v}$  which

has  $C_3$ ,  $C_s$ , or the trivial  $C_1$ , as its subgroups. None of the possible space groups contains sites of symmetry  $C_{3v}$  or  $C_3$ . The space group  $D_2^1$  does not contain sites of symmetry  $C_s$ , so the molecules must be on general positions (sites of symmetry  $C_1$ ) in this space group. The number of equivalent general positions in this space group is four and, since the unit cell contains 8 molecules, two distinct sets or two orbits (4l) of site symmetry  $C_1$  must be occupied. The space groups  $C_{2v}^1$  and  $D_{2h}^1$  contain sites of symmetry  $C_1$  as well as  $C_s$ . There are 8 equivalent sites of symmetry  $C_1$  and 4 equivalent sites of symmetry  $C_s$  in space group  $D_{2h}^1$ . Therefore, molecules can either occupy one orbit of general sites or two orbits of sites of symmetry  $C_s$ . In space group  $C_{2v}^1$ , the number of equivalent sites is four for general positions and two for sites of symmetry  $C_s$ . Thus there are three combinations of occupied sites possible in the space group  $C_{2v}^1$ , as shown in Table XXVIII, p. 259. The X-ray data alone therefore yields six combinations of site and space groups. The analysis of the vibrational spectra of phase III at 90°K can supply evidence which may allow certain of these possible structures to be ruled out. This analysis is presented next, but it should be pointed out that the spectra were recorded at 90°K while the X-ray data were collected at 129°K. The

two sets of data can be considered to relate to the same structure because all of the spectral features observed at 90°K were also visible at 120°K.

### 6.3.3 VIBRATIONAL SPECTRA AT 90°K

All molecular vibrational modes belonging to the same symmetry species in the isolated molecule must show the same pattern of unit cell group splittings and of site group splittings in an ordered solid. Therefore, the  $A_1$  molecular modes of t-butyl bromide should all show the same pattern of splittings in the spectra of phase III at 90°K. The magnitude of the splittings may vary from mode to mode but the pattern should not, if all of the features are resolved. Similarly, all of the degenerate molecular modes should show the same pattern of splittings, but these should differ from those of the  $A_1$  modes. The first task is to identify these characteristic splittings in the spectra, and to separate them from features which may be due to combination or overtone transitions. The site group splittings are considered first, by studying the spectra of the isotopically dilute samples of phase III (Section 6.1.2).

#### (A) Infrared Spectra of Isotopically Dilute Solutions

The bands due to the guest molecule are only useful

for the identification of the site group splitting pattern if they occur at frequencies which are removed from host absorption bands. A further practical limitation was that only the intense bands of the guest could be studied, because the sample thickness required to study the weaker bands was sufficient to cause excessive loss of energy by scattering from the finely-divided samples of phase III. Therefore it was only possible to study a few of the bands of the guest molecules. In the analysis below, certain bands are included, even though they are quite close to bands of the host molecules, because their shape is simple and interaction with the host would be expected to complicate their shape.

The  $A_1$  modes of  $C_4H_9Br$  in  $C_4D_9Br$  are considered first. The band due to the  $\nu_8$  mode (Figure 32) is a single, asymmetric band with a halfwidth of  $4\text{ cm}^{-1}$ . Both the halfwidth and the asymmetry indicate that more than one line contributes to the band. The band due to  $\nu_5$ , (Figure 33), consists of a peak at  $1143\text{ cm}^{-1}$  with a shoulder to low frequency of it as well as a weaker peak at  $1145\text{ cm}^{-1}$ . The  $\nu_3$  mode, (Figure 36) shows a peak with a slight but definite, indication of asymmetry or a low frequency shoulder, as well as a very weak shoulder to high frequency. The bands due to  $A_1$  modes of  $C_4D_9Br$ , in its 5% solution in



$C_4H_9Br$ , show similar characteristics and variations. The band due to  $\nu_7$ , (Figure 37), shows a peak with a halfwidth of about  $3.5 \text{ cm}^{-1}$ , with a weaker peak about  $7 \text{ cm}^{-1}$  to high frequency. The band due to  $\nu_6$ , (Figure 38), appears as a single, asymmetric peak with a halfwidth of about  $3 \text{ cm}^{-1}$ , and a very weak shoulder at about  $6 \text{ cm}^{-1}$  to high frequency of the peak. The  $\nu_5$  band, Figure 39, shows two peaks  $2 \text{ cm}^{-1}$  apart and a third, weaker peak  $3 \text{ cm}^{-1}$  away on the high frequency side, while  $\nu_1$  (Figure 42) shows a single asymmetric peak, with a halfwidth of about  $3 \text{ cm}^{-1}$ , with weak features about  $8 \text{ cm}^{-1}$  away.

The very weak shoulders seen for some of the bands are assigned to some phenomenon other than site group splitting. Site group splitting can be seen for non-degenerate modes only if the molecules occupy more than one orbit, and the intensity of each component of the site group multiplet is, to a first approximation, proportional to the multiplicity of the site occupied. Thus very weak features would have to be regarded as due to molecules on sites with a multiplicity that is about one tenth of that of the sites causing the main peaks. This is impossible because there are only 8 molecules per unit cell and the minimum multiplicity of any site is 2 (Table XXVIII). Further, the band due to the  $\nu_5$  mode of  $C_4D_9Br$  (Figure 39)

must be treated with caution, because there are many fundamentals in this region and they have not been assigned unambiguously (Section 4.5). The halfwidth of this band is about  $8 \text{ cm}^{-1}$  while those of most of the other bands discussed above are between 3 and  $4 \text{ cm}^{-1}$ , and this suggests that this band is complicated by factors other than site group effects. The presence of  $\text{C}_4\text{D}_8\text{HBr}$  impurity in the  $\text{C}_4\text{D}_9\text{Br}$  could also cause complications for the bands due to the  $\nu_5$  and  $\nu_6$  modes of  $\text{C}_4\text{D}_9\text{Br}$ . The frequency of these modes is shifted by about  $10 \text{ cm}^{-1}$  by the replacement of one deuterium with one hydrogen atom, and this perhaps explains the weak features seen at 6 to  $7 \text{ cm}^{-1}$  above the main absorption. Therefore the only common factor in the bands due to the  $A_1$  modes in the spectra of the isotopically dilute solutions is that the bands have a halfwidth of about  $3 \text{ cm}^{-1}$ , and are asymmetric. This indicates that the site group splitting of the  $A_1$  modes yields at least two bands which are not well resolved.

It is necessary to explain the appearance of two side peaks of significant intensity. The peak at  $1145 \text{ cm}^{-1}$  in the spectrum of 5%  $\text{C}_4\text{H}_9\text{Br}$  (Figure 33) is extremely close to a weak feature at  $1148 \text{ cm}^{-1}$  in the spectrum of  $\text{C}_4\text{D}_9\text{Br}$  and, because similar features are not reliably seen in the other bands, it is believed to arise from interaction with

this transition of the host lattice. The peak at  $454 \text{ cm}^{-1}$  in the spectrum of 5%  $\text{C}_4\text{D}_9\text{Br}$  (Figure 37) is assigned to the combination band  $\nu_{23} + \nu_{24}$ .

The degenerate modes show more complex site splitting than that found for the  $A_1$  modes. In the spectrum of 5%  $\text{C}_4\text{D}_9\text{Br}$  in  $\text{C}_4\text{H}_9\text{Br}$  there are two definite features due to the  $\nu_{13}$  degenerate mode (Figure 42) while there are 4 definite features in the  $\nu_{16}$  band (Figure 41). In the spectrum of 5%  $\text{C}_4\text{H}_9\text{Br}$  in  $\text{C}_4\text{D}_9\text{Br}$ , there are three definite features in the band due to  $\nu_{19}$  (Figure 34) while the  $\nu_{16}$  and  $\nu_{17}$  bands (Figure 36) and  $\nu_{18}$  band (Figure 35) show two features. The weak shoulder at  $1439 \text{ cm}^{-1}$  is seen in the liquid and plastic phases and is assigned to the combination  $\nu_5 + \nu_8$  and is, therefore, not due to  $\nu_{17}$ . The appearance of the bands due to  $\nu_{16}$ ,  $\nu_{17}$ , and  $\nu_{18}$  suggests that not all of the components have been resolved. For example, the  $\nu_{16}$  band has a halfwidth of  $6 \text{ cm}^{-1}$  and the resolved features are  $2 \text{ cm}^{-1}$  apart. If the resolved features were single bands their halfwidths would be  $4 \text{ cm}^{-1}$ , but then they would not have been resolved. Therefore it appears that at least four site group components exist for each degenerate mode, and there could easily be more than four.

#### (B) Infrared Spectra of Pure Solid

The analysis of the spectra of the pure solids

can yield the factor group splitting pattern. Again, the bands due to  $A_1$  modes in the infrared spectrum of  $C_4H_9Br$  are considered first. The band due to  $\nu_8$  (Figure 32) shows two, distinct, strong features. It is believed that each of them corresponds to more than one line since the overall halfwidth of the band is about  $9\text{ cm}^{-1}$ . The weak shoulder seen on the low frequency side of the strong peak is assigned to  $\nu_{23}$ , as discussed in Section 4.3. Similar behaviour is seen in the  $\nu_7$  band (Figure 43) which has two, strong, distinct features, each with a halfwidth of about  $3\text{ cm}^{-1}$ . The extremely weak feature,  $7\text{ cm}^{-1}$  lower than the main peak, may be due to the overtone,  $2\nu_{12}$ . The band due to  $\nu_3$  shows two weak but separate peaks between 1470 and  $1480\text{ cm}^{-1}$  (Figure 36). The band due to  $\nu_6$  (Figure 44) shows two strong distinct peaks, which are accompanied by another pair of peaks to high frequency. These latter peaks can definitely be assigned to the combination transition  $\nu_7 + \nu_8$ , because a shoulder is seen on the high frequency side of the  $\nu_6$  band in the spectra of the liquid and plastic solids. The intensity of the pair of peaks due to the combination transition is probably due to interaction with the fundamental through Fermi resonance (15). Similar effects due to Fermi resonance are seen in the spectrum of solid methyl iodide (184). Each of the two peaks as-

signed to  $\nu_6$  is quite broad, and the overall halfwidth of the band is about  $9 \text{ cm}^{-1}$ , so it seems clear that more than two components contribute to this band. The absorption by  $\nu_4$  is very weak, but two features were seen (Table XXV). The intense band due to  $\nu_5$  shows four features (Figure 33) which can be grouped into two pairs. In addition there are three shoulders on its low frequency side which probably arise from the combination  $\nu_6 + \nu_8$ . One expects a similar splitting pattern for the  $A_1$  modes in the infrared spectrum of pure  $C_4D_9Br$ .  $\nu_3$  to  $\nu_6$  have different atomic displacements in the heavy and light compounds (Appendix II) and consequently the magnitude of the splittings may be different from that seen for the light compound. The band due to  $\nu_8$  in  $C_4D_9Br$  (Figure 47) shows the same pattern as seen for  $\nu_8$  in  $C_4H_9Br$  (Figure 32). The band due to  $\nu_7$  is shown in Figure 37. The two, weak, high frequency features are assigned to the combination  $\nu_{23} + \nu_{24}$ , because a shoulder is also observed in the spectra of the liquid and plastic phases. The remaining two peaks are strong and distinct, very similar to those seen for  $\nu_7$  of  $C_4H_9Br$ . The  $\nu_5$  band at about  $1000 \text{ cm}^{-1}$  (Figure 39) is similar to that seen for  $\nu_5$  of the light compound. The bands due to  $\nu_3$  and  $\nu_6$  (Figures 40, 38) are similar to each other but quite different from those seen for the corresponding modes of the light

compound. This is not really understood but could be related to the different intramolecular displacements which occur in these modes for the two molecules. Thus the analysis of the bands due to  $\nu_3$ ,  $\nu_4$ ,  $\nu_5$ ,  $\nu_6$ ,  $\nu_7$ , and  $\nu_8$  of  $C_4H_9Br$  and to  $\nu_5$ ,  $\nu_7$ , and  $\nu_8$  of  $C_4D_9Br$  shows that factor group splitting yields two bands for each mode and each of these bands contains at least two components. Therefore, at least four factor group components are seen in the infrared spectra for the  $A_1$  modes. The bands due to  $\nu_1$  and  $\nu_2$  of  $C_4H_9Br$  and to  $\nu_1$ ,  $\nu_2$  and  $\nu_4$  of  $C_4D_9Br$  have not been discussed because they occur in regions which contain complicated absorption due to several fundamentals, overtones and combinations. The probable assignment of the different features in these modes is given in Tables XXV and XXVI, and they do not add to the conclusion derived from the  $A_1$  modes discussed above.

The bands due to the E modes are more complex than those of the  $A_1$  modes. Thus in  $C_4H_9Br$ ,  $\nu_{20}$  (Figure 45) shows five definite peaks while the band due to  $\nu_{18}$  (Figure 35) shows four features. The very weak feature at  $1359\text{ cm}^{-1}$  in Figure 35 is probably due to the combination  $\nu_5 + \nu_{12}$ . The band due to  $\nu_{16}$  (Figure 36, Table XXV) also shows four features which are assigned to factor group components. But the strongest features in

the  $\nu_{16}$  and  $\nu_{18}$  bands have halfwidths of about  $3 \text{ cm}^{-1}$  and therefore are probably due to more than one line. The bands due to  $\nu_{19}$  (Figure 34) and  $\nu_{24}$  (Figure 32) show three features each. But the features are not very sharp and each feature can contain more than one line. In the infrared spectrum of  $\text{C}_4\text{D}_9\text{Br}$   $\nu_{20}$  (Figure 48) shows four distinct peaks. The bands due to  $\nu_{16}$  and  $\nu_{23}$  show three features each and, again, the features are not sharp and could contain more than one line. The analysis of the absorption by the remaining E modes is not discussed here, because they are either very weak in the infrared spectrum or occur in a region which is complicated by the presence of other fundamentals or combination bands. The probable assignment of the features in these bands is given in Tables XXV and XXVI and they do not add to the information obtained from the bands discussed above. From this data it is concluded that each degenerate molecular mode causes at least five lines in the infrared spectra of phase III.

(C) Raman Spectra

The Raman spectra of  $\text{C}_4\text{H}_9\text{Br}$  show all of the features seen in the infrared spectra (Tables XXV and XXVI Figures 32-39 and 42-47). The apparent exceptions arise because the Raman spectra were recorded at lower resolution due to experimental difficulties. On the other hand,

the Raman bands due to  $\nu_{21}$  and  $\nu_{22}$  of  $C_4H_9Br$ , Figure 50, and to  $\nu_{22}$ , Table XXVI, of  $C_4D_9Br$  each showed three definite features which could not be resolved in the infrared spectrum. The band due to  $\nu_8$  of  $C_4D_9Br$  shows three features in the Raman while only two were seen in the infrared (Figure 47). The Raman spectrum of this band was recorded at a resolution of less than  $1\text{ cm}^{-1}$ , while for the infrared spectrum the resolution was slightly greater than  $1\text{ cm}^{-1}$ . At lower resolution, the Raman spectrum also shows only the two features seen in the infrared. The two strong peaks at  $272\text{ cm}^{-1}$  and  $270\text{ cm}^{-1}$  in the Raman correspond to the strong band at  $271\text{ cm}^{-1}$  in the infrared. This supports the earlier conclusion that each of the two features seen in the bands due to the  $A_1$  modes arises from two or more unresolved lines.

#### (D) Far-Infrared Spectra

The far-infrared spectra of an ordered solid show absorption due to the intermolecular vibrations or lattice modes. The ratio of the frequencies of a lattice mode in the spectra of two isotopic molecules can be used to assign it as a rotational or a translational vibration, or some mixture of the two. Theoretically, the isotopic frequency



ratio for a pure translational vibration is given by the square root of the reciprocal of the ratio of the molecular weights, that is

$$v_1/v_2 = (M_1/M_2)^{1/2} \quad 36$$

where  $v_i$  and  $M_i$  are the frequency and molecular weight of the  $i$ th isotope. The isotopic frequency ratio for a pure rotational vibration is given by the square root of the inverse ratio of the appropriate moments of inertia. Using the moments of inertia of *t*-butyl bromide- $h_9$  and  $-d_9$  given in Table V, and their masses, one obtains

$$(v_H/v_D)_T = 1.032,$$

$$(v_H/v_D)_{R_{\perp}} = 1.081$$

and  $(v_H/v_D)_{R_{\parallel}} = 1.146$

where  $v_H$  and  $v_D$  refer to the vibrational frequencies in  $C_4H_9Br$  and  $C_4D_9Br$  respectively, the symbol T stands for the translational vibrations, and  $R_{\perp}$  and  $R_{\parallel}$  stand for the rotational vibrations with the axis of rotation perpendicular and parallel to the three-fold axis of the molecule, respectively. Comparing these calculated values with the experimental values one is led to the assignment given in Table XXIV. Thus the features at 16.8, 24.1,

31.3, and 52.2  $\text{cm}^{-1}$  in  $\text{C}_4\text{H}_9\text{Br}$  and at 16.3, 23.5, 30.3, and 50.7  $\text{cm}^{-1}$  in  $\text{C}_4\text{D}_9\text{Br}$  can be assigned to translational vibrations. The features at 58.5 and 73.5  $\text{cm}^{-1}$  in  $\text{C}_4\text{H}_9\text{Br}$  and at 55.0 and 69.6  $\text{cm}^{-1}$  in  $\text{C}_4\text{D}_9\text{Br}$  can be assigned to rotational vibrations about the axes perpendicular to the threefold axis of the molecule, and the features at 68.5  $\text{cm}^{-1}$  in  $\text{C}_4\text{H}_9\text{Br}$  and at 62.1  $\text{cm}^{-1}$  in  $\text{C}_4\text{D}_9\text{Br}$  are assigned to rotational vibrations about the symmetry axis. The feature at 34.0  $\text{cm}^{-1}$  in the light and 32.6  $\text{cm}^{-1}$  in the heavy compound has a frequency ratio of about 1.04, slightly higher than is expected for a pure translational vibration. It can be assigned to a mixed rotational and translational vibration.

#### 6.3.4 STRUCTURE OF PHASE III AT 90°K

The information obtained from the spectra can now be used, along with packing considerations and the X-ray results, to attempt to determine the most probable structure for phase III. The X-ray powder data shows very definitely that the symmetry of the lattice is not higher than orthorhombic, but one cannot be completely certain that the symmetry is not lower than orthorhombic with a smaller unit cell. One can, however, put a limit on this uncertainty from the information obtained from the vibrational spectra. The bands due to the  $A_1$  molecular modes

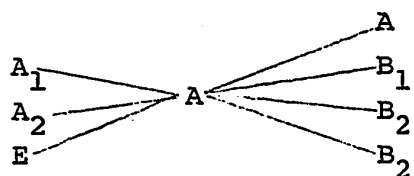
can only be explained by postulating that at least four factor group components occur. This indicates that at least four molecules occur in the unit cell. The degenerate molecular modes yield at least five factor group components, so that at least three, or more probably four, molecules are in each unit cell. The cell deduced from the X-ray data contains eight molecules. The observed spectra can be consistent with this unit cell and the following discussion is based on the assumption that the space groups and the number of molecules per unit cell indicated by the X-ray data are correct. The conclusions reached in this section must be treated with caution until a complete structure-analysis is carried out.

Figure 52 shows the correlation diagrams for a molecule with  $C_{3v}$  symmetry on sites of symmetry  $C_1$  and  $C_s$  for the three space groups deduced from the X-ray data. The number of infrared and Raman active factor group components, and the infrared active site group components and lattice modes are given in Table XXVIII for the six possible combinations of site groups and space groups. One cannot eliminate any of the six possible structures on the basis of the far-infrared evidence, because the number of bands predicted by theory is greater than the number of observed features (Tables XXIV and XXVIII). The structure

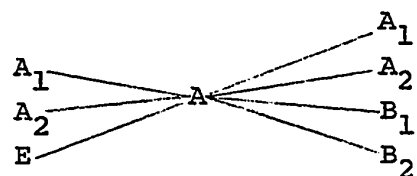
Table XXVIII  
Site group and factor analysis for phase III of t-butyl bromide.

Space Group	Possible Site Symmetry	Number of Equivalent Positions in One Orbit	Number of Site Group Components per Orbit		Possible Orbits	Total Number of Site Group Components		Number of Factor Group Components				IR Active Lattice Modes	
			A <sub>1</sub>	E		A <sub>1</sub>	E	A <sub>1</sub>	E	A <sub>1</sub>	E	Rotational	Translational
D <sub>2</sub>	C <sub>1</sub>	4	1	2	2C <sub>1</sub>	2	4	6	12	8	16	18	15
	C <sub>1</sub> C <sub>S</sub>	4 2	1 1	2 2	2C <sub>1</sub> C <sub>1</sub> + 2C <sub>S</sub> 4C <sub>S</sub>	2 3 4	4 6 8	6 7 8	12 12 12	8 8 8	16 16 16	18 15 12	15 16 17
D <sub>2h</sub>	C <sub>1</sub>	8	1	2	C <sub>1</sub>	1	2	3	6	4	8	9	6
	C <sub>S</sub>	4	1	2	2C <sub>S</sub>	2	4	4	6	4	8	8	7

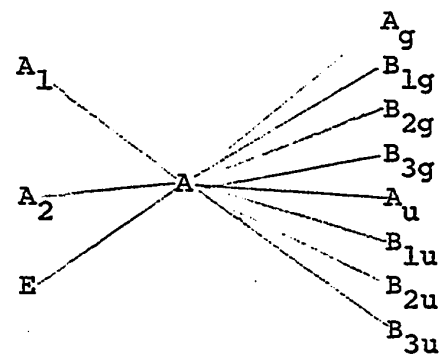
Molecular Group    Site Group    Point Group of Crystal Class

 $C_{3v}$  $C_1$  $D_2$ 

c  $R_z$   $\alpha_{xx'}$   $\alpha_{yy'}$   $\alpha_{zz}$   
 b  $R_y$   $\alpha_{xy}$   
 a  $R_x$   $\alpha_{zx}$   $\alpha_{yz}$

 $C_{3v}$  $C_1$  $C_{2v}$ 

c  $R_z$   $\alpha_{xx'}$   $\alpha_{yy'}$   $\alpha_{zz}$   
 a  $R_y$   $\alpha_{xy}$   $\alpha_{zx}$   
 b  $R_x$   $\alpha_{yz}$

 $C_{3v}$  $C_1$  $D_{2h}$ 

$R_z$   $\alpha_{xx'}$   $\alpha_{yy'}$   $\alpha_{zz}$   
 $R_y$   $\alpha_{xy}$   $\alpha_{zx}$   
 $R_x$   $\alpha_{yz}$   
 a  
 b  
 c

. . . cont'd.

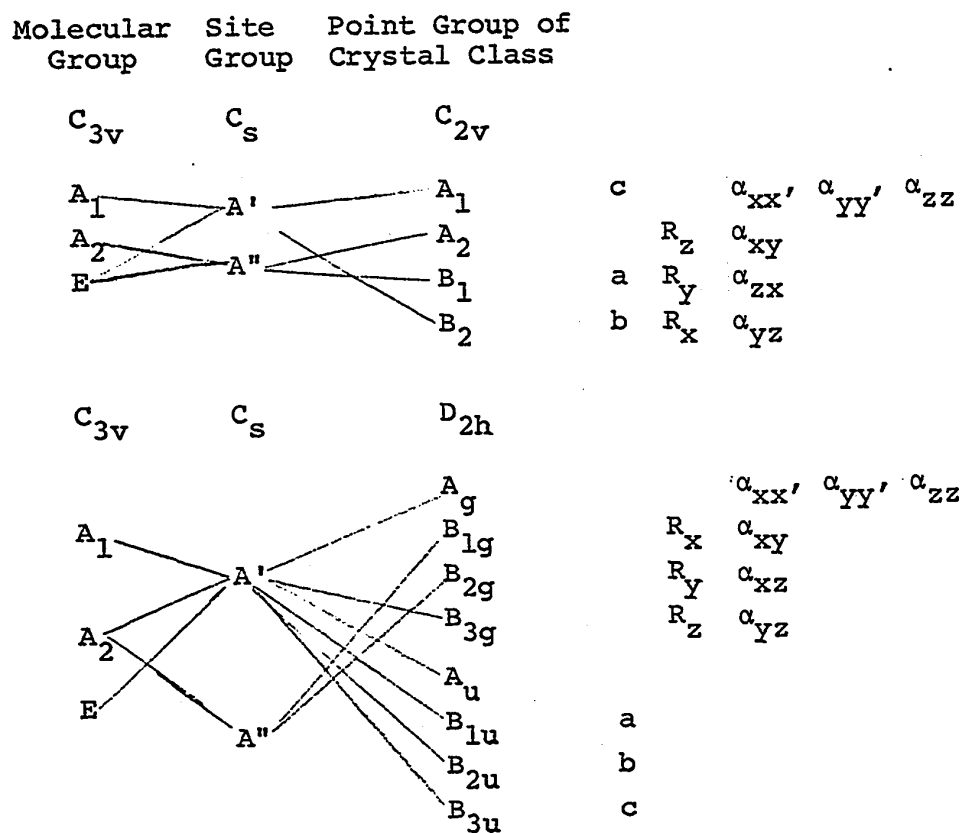


Figure 52

The correlation diagrams for the six possible combinations of the space groups and site groups indicated by X-ray data.

with eight molecules on  $C_1$  sites in the space group  $D_{2h}^1$  can definitely be ruled out on the basis of the spectra of the intramolecular modes. If this structure were correct, the spectra of the dilute isotopic solutions should show one line for the  $A_1$  modes and two lines for the E modes, while at least two components are observed for the  $A_1$  modes and at least four for the E modes. Further, this structure predicts that three factor group components should be seen for each  $A_1$  mode in the infrared spectrum of the pure solid, while at least four are seen. The coincidence of the frequencies of the bands in the Raman and infrared spectra argues against both of the structures in the centro-symmetric space group  $D_{2h}^1$ . A further argument against these two structures, and against the structure with all the molecules on  $C_1$  sites in the space group  $C_{2v}^1$ , is that in these structures the bromine atoms would be next to other bromine atoms, which is unlikely due to the electric dipolar repulsion forces. The proximity of the bromine atoms in the above three structures is required by the orthogonal mirror planes.

There remain three possible structures: space group  $C_{2v}^1$  with four orbits of  $C_s$  sites occupied; space group  $C_{2v}^1$  with two orbits of  $C_s$  sites and one orbit of  $C_1$  sites occupied; and space group  $D_2^1$  with two orbits of  $C_1$

sites occupied. The number of factor group components predicted for each of these three structures is greater than the minimum number indicated by the spectra. Therefore the observed factor group components sheds no new light on the structural possibilities. The site group splitting does lead to a unique choice of structure if the assumption is made that all of the site group components were seen in the spectra of the isotopic solutions. Two components from the  $A_1$  modes and four components from the E modes are needed to explain the observed bands. These are exactly the numbers predicted for the structure in space group  $D_2^1$  with two orbits of  $C_1$  sites occupied (Table XXVIII).

The reliability of this structure must now be briefly discussed. Of the three possible structures postulated above, this one involves the smallest number of occupied orbits. This is sometimes considered to be a favourable criterion for structures of molecular crystals, but this need not always be true, because the low temperature phases of carbon tetrabromide (185) and carbon tetrachloride (175) are known to crystallize with 32 molecules in a monoclinic unit cell, and at least 8 orbits must be occupied. The factor group splitting observed in the infrared spectra of the pure solids is consistent with



this structure but does not positively argue in favour of it. Similar comments apply to the comparison of the infrared and Raman spectra. The totally symmetric modes under  $D_2$  are inactive in the infrared and active in the Raman spectra. The bands due to the  $A_1$  molecular modes show essentially identical relative intensities and frequencies in the two types of spectra while those due to the E molecular modes show the same frequencies, but do show differences in the relative intensities, in the two types of spectra. The bands observed are, in general, rather broad for factor group components in a solid at  $90^\circ\text{K}$ , (53, 176), so these results are consistent with the proposed structure if one assumes that the frequencies of the totally symmetric crystal modes lie very close to those of the unresolved infrared active modes.

In summary, the X-ray studies and the site group splitting observed in the infrared spectra indicate that phase III of t-butyl bromide crystallizes in space group  $D_2^1$  with eight molecules on two orbits of general positions.

REFERENCES

1. Timmermans, J.; *J. Phys. Chem. Solids*, 18, 1 (1961).
2. Aston, J. G.; *Physics and Chemistry of the Organic Solid State*, Ed. Fox, D., Labes, M., and Weisserberger, A.; Interscience Publishers, New York, Vol I, 543 (1963).
3. Smyth, C. P.; *Dielectric Behaviour and Structure*, McGraw-Hill Book Co., Inc., New York, 132 (1955).
4. Powles, J. G., Williams, D. E., and Smyth, C. P.; *J. Chem. Phys.*, 21, 136 (1953).
5. Powles, J. G., and Gutowsky, H. S.; *J. Chem. Phys.*, 21, 1695 (1953).
6. Stejskal, E. E., Woessner, D. E., Farrar, T. C., and Gutowsky, H. S.; *J. Chem. Phys.*, 31, 55 (1959).
7. Andrew, E. E.; *J. Phys. Chem. Solids*, 18, 9 (1961).
8. Zimm, B. H., Orliceni, R. A., and Hoffman, J. D.; *Ann. Rev. of Phys. Chem.*, 4, 207 (1953).
9. Westrum, E. F., Jr.; *J. Chem. Ed.*, 39, 443 (1962).
10. Staveley, L. A. K.; *Ann. Rev. of Phys. Chem.*, 13, 351 (1962).
11. McClure, D. W.; *J. Chem. Phys.*, 49, 1830 (1968).
12. *Steady State Processes Involving Lattice Rearrangements*, *Discussions of Faraday Soc.*, 23, 171 (1957).

13. Plastic Crystals and Rotation in the Solid State, *Phys. and Chem. Solids*, 18, 1 (1961).
14. Thermodynamic Transitions in Condensed States, *Pure and Applied Chemistry*, 2, 207 (1961).
15. Herzberg, G.; *Molecular Spectra and Molecular Structure II. Infrared and Raman Spectra of Polyatomic Molecules*, D. Van Nostrand Company, Inc., New York (1945).
16. Wilson, E. B., Jr., Decius, J. C., and Cross, P. C.; *Molecular Vibrations*, McGraw-Hill Book Company, Inc., New York (1955).
17. Silverstein, R. M., and Bassler, G. C.; *Spectrometric Identification of Organic Compounds*, John Wiley and Sons, Inc., New York (1968).
18. Nakanishi, K; *Infrared Absorption Spectroscopy*, Nankodo Company Limited, Tokyo (1962).
19. Nakamoto, K; *Infrared Spectra of Inorganic and Coordination Compounds*, John Wiley and Sons, Inc., New York (1963).
20. Bellamy, L. J.; *Infrared Spectra of Complex Organic Molecules*, John Wiley and Sons, Inc., New York (1958).
21. Badger, R. M. and Zumwalt, L. R.; *J. Chem. Phys.*, 6, 711 (1938).

- ecular Crystals, Theory and Applications, W. A. Benjamin Inc., New York (1968).
34. Kittel, C.; Introduction to Solid State Physics, John Wiley and Sons, Inc., New York (1967).
  35. Bhagayantum, S., and Benkatarayudu, T.; Proc. Indian Ac. Sc., 9A, 224 (1939).
  36. Halford, R. H.; J. Chem. Phys., 14, 8 (1946).
  37. Hornig, D. F.; J. Chem. Phys., 16, 1063 (1948).
  38. Winston, H. and Halford, R. S.; J. Chem. Phys., 17, 607 (1949).
  39. Vedder, W., and Hornig, D. F.; Advances in Spect., 2, 189 (1961).
  40. Mitra, S. S.; Solid State Phys., 13, 1 (1962).
  41. Kopelman, R.; J. Chem. Phys., 47, 2631 (1967).
  42. Chen, S. H. and Dvorak, V.; J. Chem. Phys., 48, 4060 (1968).
  43. Fateley, W. G., McDevitt, N. T., and Bentley, F. F.; App. Spect., 25, 155 (1971).
  44. Bertie, J. E., and Bell, J. W.; J. Chem. Phys., 54, 160 (1971).
  45. Bertie, J. E., and Kopelman, R.; J. Chem. Phys., 55, 3613 (1971).
  46. Zachariason, W. H.; Theory of X-ray Diffraction in Crystals, John Wiley and Sons, Inc., New York (1945).

22. Cotton, F. A.; Chemical Applications of Group Theory, John Wiley and Sons, Inc., New York (1963).
23. Margenau, H. and Murphy, G. M.; The Mathematics of Physics and Chemistry, D. Van Nostrand Company, Inc., Princeton, New Jersey (1956).
24. Schachtschneider, J. H.; Technical Reports No. 231-64 and 57-65 Shell Development Company, Emeryville, California.
25. Shimanouchi, T.; Pure and Appl. Chem., 7, 131 (1963).
26. Brillouin, L.; Wave Propagation in Periodic Structure, Dover Publications, Inc., New York (1953).
27. Born, M., and Huang, K.; Dynamical Theory of Crystal Lattices, Clardon Press, Oxford (1954).
28. Born, M., and von Karman, T.; Physic. Z., 13, 297 (1912).
29. Frech, R., and Decius, J. C.; J. Chem. Phys., 52, 5494 (1970).
30. Buerger, M. J.; Elementary Crystallography, John Wiley and Sons, Inc., New York (1956).
31. Collin, R. L.; Acta. Cryst., 5, 431 (1952); 9, 537 (1956).
32. Davydov, A. S.; Theory of Molecular Excitons, McGraw-Hill Book Company, Inc., New York (1962).
33. Craig, D. P., and Walmsley, S. H.; Excitons in Mol-

- Califano, S.; J. Chem. Phys., 49, 5438 (1968).
59. Pace, E. L., and Noe, L. J.; J. Chem. Phys., 49, 5317 (1968).
60. Holmes, R. R., and Fild, M.; J. Chem. Phys., 50, 4161 (1970).
61. Durig, J. R., Hennum, S. E., and Baglin, F. G.; J. Chem. Phys., 54, 2367 (1971).
62. Shurvell, H. F., and Faniran, J. A.; J. Mol. Spect., 33, 436 (1970).
63. Harada, I., and Shimanouchi, T.; J. Chem. Phys., 55, 3605 (1971).
64. Logan, K. W., Trevino, S. F., Prask, H. J., and Gault, J. D.; J. Chem. Phys., 53, 3417 (1970).
65. Ito, M., and Shigeoka, T.; Spectrochim. Acta, 22, 1029 (1966).
66. Hong, H. K., and Kopelman, R.; J. Chem. Phys., 55, 3491 (1971).
67. Rebane, K. K.; Impurity Spectra of Solids, Plenum Press, New York (1970).
68. Whalley, E., and Bertie, J. E.; J. Chem. Phys., 46, 1264 (1967).
69. Dows, D. A.; Phys. and Chem. of the Organic Solid State, Vol. I, 658, Ed. Fox, D., Labes, M., and Weisserberger, A.; Interscience Publishers, New York (1963).

47. Henry, N. F. M., and Lonsdale, K.; International Tables for X-ray Crystallography, Volume I, Kynoch Press, Birmingham (1965).
48. Cox, E. G.; Rev. Mod. Phys., 3, 159 (1958).
49. Krostowski, H. J., and Pimentel, G. C.; J. Chem. Phys., 19, 661 (1951).
50. Hilbert, G. L., and Hornig, D. F.; J. Chem. Phys., 20, 918 (1952).
51. Pimentel, G. C.; Spectrochim. Acta., 12, 94 (1958).
52. Bernstein, E. R.; J. Chem. Phys., 50, 82 (1969).
53. Bernstein, E. R., Colson, S. D., Kopelman, R., and Robinson, G. W.; J. Chem. Phys., 48, 5596 (1968).  
The author is grateful to Dr. Bernstein and J. Chem. Phys. for the kind permission to reproduce Figures 4-6.
54. Hornig, D. F., and Osberg, W. E.; J. Chem. Phys., 23, 662 (1955).
55. Savoie, R., and Anderson, A.; J. Chem. Phys., 44, 548 (1965).
56. Ito, M., Suzuk, M., and Yokoyama, T.; J. Chem. Phys., 50, 2949 (1969).
57. Hornig, D. F.; Discussions of Faraday Soc., 9, 115 (1950).
58. Marzocchi, M.P., Manzelli, P., Schettino, V., and

70. Quist, A. S., Bates, J. B., and Boyd, G. E.; J. Chem. Phys., 55, 2836 (1971).
71. Hornig, D. F.; J. Chem. Phys., 17, 1346 (1949).
72. Veddar, W., and Hornig, D. F.; Adv. in Spect., 2, 189 (1961).
73. Wu, P. J., Hsu, L., and Dows, D. A.; J. Chem. Phys., 54, 2715 (1971).
74. Ito, M.; Spectrochim. Acta., 21, 2063 (1965).
75. Obremski, R. J., Brown, C.W., and Lippincott, E. R.; J. Chem. Phys., 49, 185 (1968).
76. Brown, C.W., Obremski, R.J., and Lippincott, E. R.; J. Chem. Phys., 52, 2253 (1970).
77. Gordon, R. G.; J. Chem. Phys., 39, 2788 (1963); 41, 1819 (1964); 43, 1307 (1965).
78. Rakov, A.V.; Opt. Spectrosc. 7, 128 (1959); 13, 203 (1962).
79. McClintock, M., Jennings, D. A., and Mizushima, M.; Phys. Rev. Lett., 21, 276 (1968).
80. McClung, R. E. D.; J. Chem. Phys., 51, 3842 (1969); 55, 3459 (1971).
81. Bartoli, F. J., and Litovitz, T. A.; J. Chem. Phys., 56, 404 (1972); 56, 413 (1972).
82. Buyon, G. P., Kondilenko, I. I. and Pogorelov, V. E.; Opt. Spectrosc. 27, 132 (1969).



83. Ewing, G. E.; J. Chem. Phys., 37, 2250 (1962).
84. Ewing, G. E.; J. Chem. Phys., 40, 179 (1964).
85. LeRoy, M. A.; C. R. Acad. Sc. Paris, 260, 6079 (1965).
86. Steinhardt, T. G., Jr., Neilsen, W., Margan, H. W.,  
and Staats, P.; J. de Chim Phys., 63, 176 (1966).
87. Fournier, R. P., Savoie, R., Bessette, F., and Cabana,  
A.; J. Chem. Phys., 49, 1159 (1968).
88. Pace, E. L.; Spectrochim. Acta., 27A, 491 (1971).
89. Fournier, R. P., Savoie, R., The, W. N., Belzile, R.,  
and Cabana, A.; Can. J. Chem., 50, 35 (1972).
90. Savitsky, M. F., and Hornig, D. F.; J. Chem. Phys.,  
36, 2634 (1962).
91. Bertie, J. E.; Appl. Spect., 22, 634 (1968).  
The author is thankful to Dr. J. E. Bertie for kind  
permission to reproduce Figure 7.
92. Schwartz, Y. A., Ron, A., Kimel, S.; J. Chem. Phys.,  
51, 1666 (1969).
93. Arnold, G. M., Heastie, R.; Chem. Phys. Letters, 1,  
51 (1967).
94. Brot, C., Lassier, B., Chantry, G. W., and Gebbie,  
H. A.; Spectrochimica Acta. 24A, 295 (1968).
95. Savoie, R., and Fournier, R.; Chem. Phys. Lett., 7,  
1 (1970).
96. Pourprix, B., Abbar, C., and Decoster, D.; C. R. Acad.

- Sc. (Paris), 272B, 1418 (1971).
97. Bertie, J. E., and Whalley, E.; J. Chem. Phys., 40, 1637 (1964); 46, 1271 (1967).
  98. Davies, M.; Dielectric Properties and Molecular Behaviour, Ed. Hill, N. E., Vaughan, W. E., Price, A. H., and Davies, M., Van Nostrand Reinhold Company, London (1968).
  99. Durig, J. R., and Antion, D. J.; J. Chem. Phys., 51, 3639 (1969).
  100. Whalley, E.; J. Chem. Phys., 51, 4040 (1969).
  101. Lassier, B., and Brot, C.; Chem. Phys. Lett., 1, 581 (1968).
  102. Lassier, B. and Brot, C.; J. Chim. Physique, 65, 1723 (1968).
  103. Hill, N. E.; Proc. of Phys. Soc., 82, 723 (1963).
  104. Hill, N. E.; Chem. Phys. Lett., 2, 5 (1968).
  105. Hill, N. E.; J. of Phys., A, 2, 398 (1969).
  106. LeRoy, Y., Constant, E., Abbar, C., and Desplanques, P.; Advances in Mol. Relax. Proc., 1, 273 (1967).
  107. Datta, P., and Barrow, G. M.; J. Chem. Phys., 48, 4662 (1968).
  108. Birnbaum, G., and Cohen, R.; J. Chem. Phys., 53, 2885 (1970).
  109. Harkin, W. D., and Bowers, H. E.; Phys. Rev., 38, 1845 (1931).

110. Dadieu, A., Pongratz, A., and Kohlrausch, K. W. F.; Montash, 61, 369 (1932).
111. Wagner, J.; Z. Physik. Chem. B., 45, 341 (1940).
112. Zeil, W., Buchert, H., Heel, H., and Pfortner, H.; Z. Electrochem., 64, 575 (1960).
113. Durig, J. R., Craven, S. M., and Bragin, J.; J. Chem. Phys., 51, 5663 (1969).
114. Mortimer, F. S., Blodgett, R. B., and Daniels, F.; J.A.C.S., 69, 822 (1947).
115. Sheppard, N.; Trans. Faraday Soc., 46, 527 (1950).
116. Bentley, F. F., McDevitt, N. T., and Rozek, A. L.; Spectrochimica Acta, 20, 105 (1964).
117. McDevitt, N. T., Rozek, A. L., Bentley, F. F., and Davidson, A. D.; J. Chem. Phys., 42, 1173 (1965).
118. Huttner, W., and Zeil, W.; Spectrochimica Acta, 22, 1007 (1966).
119. Möller, K. D., Demeo, A. R., Smith, D. R., and London, L. H.; J. Chem. Phys., 47, 2609 (1967).
120. Tobin, M. C.; J.A.C.S., 75, 1788 (1953).
121. Mann, D. E., Acquista, N., and Lide, D. R., Jr.; J. Mol. Spect., 2, 575 (1958).
122. Hayashi, M; Chem. Abs., 52, 5063e (1958).
123. Hirshmann, R. P., and Kinseley, R. N.; U.S. At. Energy Commission publication No. IS641 (1963).

124. Pauling, L.; Nature of the Chemical Bond, Cornell Univ. Press, Ithaca, New York (1940).
125. Dornet, R. W.; J. Chem. Phys., 1, 630, (1933).
126. Beach, J. Y., and Stevenson, D. P.; J.A.C.S., 60, 475 (1938).
127. Bowen, H. J. M., Gilchrish, A., and Sutton, L. E.; Trans. Faraday Soc., 51, 1341 (1955).
128. Williams, J. Q., and Gordy, W.; J. Chem. Phys., 18, 994 (1950).
129. Baker, W. O., and Smyth, C. P.; J.A.C.S., 61, 798 (1939).
130. Kushner, L. M., Crove, R. W., and Smyth, C. P.; J. A.C.S., 72, 1091 (1950).
131. Schwartz, R. S., Post, B., and Fankuchen, I.; J.A. C.S., 73, 4490 (1951).
132. Higgins, R. F., Ivor, R. A. B., Staveley, L. A. K., and Des C. Virden, J. J.; J. Chem. Soc., Supp. No. 1, 5762 (1964).
133. Richards, P. L.; Proceedings of the Aspen International Conference on Fourier Spectroscopy, 117, (1970).
134. Loewenstein, E. V.; Proceedings of the Aspen International Conference on Fourier Spectroscopy, 3, (1970).
135. Proceedings of the Aspen International Conference on Fourier Spectroscopy (1970).

136. Richards, P. L.; J. Opt. Soc. Am., 54, 1474 (1964).
137. Gebbie, H. A.; Far-Infrared Properties of Solids, Ed. S. S. Mitra and S. Nudelman, Plenum Press, New York (1970).
138. Mertz, L.; App. Optics, 10, 386 (1971).
139. Martin, A. E., Infrared Instrumentation and Techniques, Elsevier Publishing Company, Amsterdam (1966).
140. Rank, K. E., and Genzel, L.; Appl. Opt. 1, 643 (1962).
141. Moller, K. D., and Rothschild, W. G.; Far-Infrared Spectroscopy, Wiley-Interscience, New York (1971).
142. Michelson, A. A.; Studies in Optics, University of Chicago Press, Chicago (1927).
143. Connes, J. J.; Phys. Radium, 19, 197 (1958).
144. Jacquinet, P.; Rept. Prog. Phys., 23, 267 (1960).
145. Strong, J., and Vanasse, G. A.; J. Chem. Phys., 49, 844 (1959).
146. Sakai, H., Vanasse, G. A., and Forman, M. L.; J. Opt. Soc. Am., 58, 84 (1968).
147. Thorpe, L. W.; Proceedings of the Aspen International Conference on Fourier Spectroscopy, 341 (1970).
148. Goldman, S., Information Theory, Prentice Hall, Inc., Englewood Cliffs, New Jersey (1953).
149. Gebbie, H. A., Advances in Quantum Electronics, Ed.

- J. R. Singer, Columbia University Press, New York (1961).
150. Sanderson, R. B., and Scott, H. E.; Proceedings of the Aspen International Conference on Fourier Spectroscopy, 167 (1970).
  151. Curbelo, R., and Rosbett, C.; Proceedings of the Aspen International Conference on Fourier Spectroscopy, 221 (1970).
  152. Dowling, J. M.; Proceedings of the Aspen International Conference on Fourier Spectroscopy, 55 (1970).
  153. Handbook of Chemistry and Physics, Chemical Rubber Co., Cleveland (1970).
  154. I.U.P.A.C., Tables of Wavenumbers for the Calibration of Infrared Spectrometers, Butterworths, London (1961).
  155. Bertie, J. E., Brooks, W. L., Sunder, S., and Othen, D.; Program to Process the Output from a Far-Infrared Interferometer, Chemistry Dept., U. of Alberta, Edmonton (1968).
  156. Rao, R. N., DeVore, R. V., and Plyler, E. K.; J. of Research, N.B.S. (U.S.A.), A, Phys. and Chem., 67, 351 (1963).
  157. Loader, J.; Basic Laser Raman Spectroscopy, 19, Heyden Sadtler,

- J. R. Singer, Columbia University Press, New York (1961).
150. Sanderson, R. B., and Scott, H. E.; Proceedings of the Aspen International Conference on Fourier Spectroscopy, 167 (1970).
  151. Curbelo, R., and Rosbett, C.; Proceedings of the Aspen International Conference on Fourier Spectroscopy, 221 (1970).
  152. Dowling, J. M.; Proceedings of the Aspen International Conference on Fourier Spectroscopy, 55 (1970).
  153. Handbook of Chemistry and Physics, Chemical Rubber Co., Cleveland (1970).
  154. I.U.P.A.C., Tables of Wavenumbers for the Calibration of Infrared Spectrometers, Butterworths, London (1961).
  155. Bertie, J. E., Brooks, W. L., Sunder, S., and Othen, D.; Program to Process the Output from a Far-Infrared Interferometer, Chemistry Dept., U. of Alberta, Edmonton (1968).
  156. Rao, R. N., DeVore, R. V., and Plyler, E. K.; J. of Research, N.B.S. (U.S.A.), A, Phys. and Chem., 67, 351 (1963).
  157. Loader, J.; Basic Laser Raman Spectroscopy, 19, Heyden Sadtler,

171. Bertie, J. E., and Sunder, S., *Can. J. Chem.*, 50, 765 (1972).
172. Leroy, Y., and Constant, E.; *C. R. Acad. Sc. Paris*, 262, (Ser. B), 1391 (1966).
173. Azaroff, L. V., and Buerger, M. J.; *Powder Method in X-ray Crystallography*, McGraw Hill Book Company, Inc., New York (1958).
174. Elder, M.; Appendix in the Ph.D. thesis of Simpson, K., University of Alberta, Edmonton (1972).  
The author is thankful to Dr. M. J. Bennett for the loan of the program DREF.
175. Rudman, R., and Post, B.; *Molecular Crystals*, 5, 95 (1968).
176. Park, K.; *Physics Letters*, 22, 39 (1966); *ibid.*, 25A, 490 (1967).
177. Klemens, P. G.; *Phys. Rev.*, 148, 845 (1966).
178. Leroy, Y., Constant, E., and Desplanques, P.; *J. de Chim. Physique*, 64, 1499 (1967).
179. Constant, E., Galatry, L., Leroy, Y., and Robbert, D.; *J. de Chim. Phys.*, 65, 1022 (1968).
180. Davies, M., Pardoe, G. W. F., Chamberlain, J. E., and Gebbie, H. A.; *Trans. Farad. Soc.*, 64, 847 (1968).
181. Mansingh, A.; *J. Chem. Phys.*, 52, 5896 (1970).
182. Kroon, S. G., and Van Der Elskens, J.; *Chem. Phys. Lett.*, 1, 285 (1967).



183. Jain, R. S., and Walker, S.; J. Phys. Chem., 25, 2942 (1971).
184. Kopelman, R.; J. Chem. Phys., 44, 3547 (1966).
185. Hutcheon, W. L., and Bennett, M. J.; Chemistry Department, University of Alberta, Edmonton, unpublished work.







$G$  matrix for t-butyl bromide-h<sub>9</sub> - cont'd.

ROW 35	0.0510	-0.0510	-0.0510	0.0	0.0	0.0255	-0.0510	0.0255	0.0255	-0.0510	-0.0836	-0.0226
0.0226	0.0	0.0	0.0330	-0.0660	0.0330	0.0330	-0.0660	-0.0468	0.0234	0.0234	-0.0492	0.0985
-0.0492	-0.0492	-0.0492	0.0985	-0.0176	-0.0176	0.0	-0.1767	0.1767				
ROW 36	0.0510	-0.0510	0.0255	-0.0510	0.0	0.0	0.0	0.0255	-0.0510	0.0255	-0.0226	-0.0836
-0.0226	0.0330	0.0330	0.0	0.0	0.0330	-0.0660	0.0330	-0.0492	-0.0492	0.0985	-0.0468	0.0234
0.0234	-0.0492	0.0985	-0.0492	-0.0176	0.1639	-0.0176	0.1767	0.0	-0.1767			
ROW 37	0.0510	-0.0510	0.0255	-0.0510	0.0255	0.0255	-0.0510	0.0	0.0	0.0	-0.0226	-0.0226
-0.0836	0.0330	-0.0660	0.0330	0.0330	-0.0660	0.0	0.0	-0.0492	0.0985	-0.0492	-0.0492	-0.0492
0.0985	-0.0468	0.0234	0.0234	-0.0176	0.1639	-0.1767	0.1767	-0.0				
ROW 38	0.0	0.1573	-0.1573	0.0	0.0468	-0.0468	0.0	0.0	0.0	0.0	-0.0	-0.1301
0.1301	0.0000	0.0606	-0.0606	0.0	0.0	0.0	0.0	0.0	-0.0	-0.1557	0.1557	0.0722
-0.0361	0.0361	0.0361	-0.0722	0.0	0.1767	-0.1767	3.3201	-0.2390	-0.2390			
ROW 39	-0.1573	0.0	0.1573	0.0	0.0	0.0	0.0468	-0.0468	0.0	0.0	0.1301	0.0
-0.1301	0.0	0.0	-0.0	0.0606	-0.0606	0.0	0.0	0.0	0.0361	-0.0722	0.0	-0.1557
0.1557	-0.0361	0.0722	-0.0361	-0.1767	0.0	0.1767	-0.2390	3.3202	-0.2390			
ROW 40	0.1573	-0.1573	-0.0	0.0	0.0	0.0	0.0	0.0	0.0	0.0468	-0.0468	-0.1301
0.0	0.0	0.0	0.0	0.0	0.0	0.0000	0.0606	-0.0606	-0.0361	0.0722	-0.0361	0.0361
-0.0722	0.0	-0.1557	0.1557	0.1767	-0.1767	-0.0	-0.2390	-0.2390	3.3202			

The order of the internal coordinate is shown in Table IX.

B.  $G$  matrix for t-butyl bromide-d<sub>9</sub>.<sup>a</sup>

ROW 1	0.0960	-0.0278	-0.0278	0.0	0.0	0.0	0.0	0.0	0.0	0.0	0.0	0.0	0.0	-0.0510	-0.0510	0.0255	-0.0510	0.0255	
	-0.0510	0.0	0.0	0.0	0.0	0.0	0.0	0.0	0.0	0.0	0.0	0.0	0.0	-0.0510	0.0255	0.0255	-0.0510	0.0255	
	0.0255	-0.0510	0.0255	0.0510	0.0510	0.0510	0.0	0.0	0.0	0.0	0.0	0.0	0.0	0.0	0.0	0.0	0.0	0.0	
ROW 2	-0.0278	0.1666	-0.0278	-0.0278	-0.0278	0.0	0.0	0.0	0.0	0.0	0.0	0.0	0.0	0.0	0.0	0.0	-0.0719	-0.0719	0.0401
	0.0455	0.0719	0.0719	0.0	0.0	0.0	0.0	0.0	0.0	0.0	0.0	0.0	0.0	0.0	0.0	0.0	-0.0719	-0.0719	0.0255
	-0.0510	0.0255	-0.0510	0.0510	-0.0510	0.0510	0.0	0.0	0.0	0.0	0.0	0.0	0.0	0.0	0.0	0.0	-0.0719	-0.0719	0.0255
ROW 3	-0.0278	-0.0278	0.1666	-0.0278	0.0	0.0	-0.0278	-0.0278	-0.0278	0.0	0.0	0.0	0.0	0.0	0.0	0.0	0.0	0.0	0.0455
	0.0455	0.0	0.0	0.0719	0.0719	0.0	0.0	0.0	0.0	0.0	0.0	0.0	0.0	0.0	0.0	0.0	0.0255	-0.0719	-0.0719
	-0.0719	0.0255	-0.0719	-0.0510	0.0510	-0.0510	0.0510	0.1573	0.0	0.0	0.0	0.0	0.0	0.0	0.0	0.0	0.0255	-0.0719	-0.0719
ROW 4	-0.0278	-0.0278	-0.0278	0.1666	0.0	0.0	0.0	0.0	0.0	0.0	0.0	0.0	0.0	0.0	0.0	0.0	-0.0278	-0.0278	0.0455
	-0.0401	0.0	0.0	0.0	0.0	0.0	0.0	0.0719	0.0719	0.0	0.0	0.0	0.0	0.0	0.0	0.0	0.0255	-0.0510	-0.0719
	0.0255	-0.0719	-0.0719	-0.0510	-0.0510	-0.0510	0.0510	-0.1573	0.1573	0.0	0.0	0.0	0.0	0.0	0.0	0.0	0.0255	-0.0510	-0.0719
ROW 5	-0.0278	0.0	0.0	0.5798	-0.0278	-0.0278	0.0	0.0	0.0	0.0	0.0	0.0	0.0	0.0	0.0	0.0	0.0	0.0	0.0455
	0.0	0.0719	-0.0719	-0.0719	0.0	0.0	0.0	0.0	0.0719	0.0719	0.0	0.0	0.0	0.0	0.0	0.0	0.0	0.0	0.0255
	0.0	0.0	0.0	0.0	0.0	0.0	0.0255	0.0255	0.0	0.0	0.0	0.0	0.0	0.0	0.0	0.0	0.0	0.0	-0.0510
ROW 6	-0.0278	0.0	0.0	-0.0278	-0.0278	0.0	0.0	0.0	0.0	0.0	0.0	0.0	0.0	0.0	0.0	0.0	0.0	0.0	0.0255
	0.0	0.0719	-0.0719	-0.0719	0.0	0.0	0.0	0.0	0.0	0.0	0.0	0.0	0.0	0.0	0.0	0.0	0.0	0.0	0.0
	0.0	0.0	0.0	0.0	0.0	0.0	0.0255	0.0255	0.0	0.0	0.0	0.0	0.0	0.0	0.0	0.0	0.0	0.0	0.0
ROW 7	-0.0278	0.0	0.0	-0.0278	-0.0278	0.5798	0.0	0.0	0.0	0.0	0.0	0.0	0.0	0.0	0.0	0.0	0.0	0.0	0.0255
	0.0	0.0719	-0.0719	-0.0719	0.0719	0.0	0.0	0.0	0.0	0.0	0.0	0.0	0.0	0.0	0.0	0.0	0.0	0.0	0.0
	0.0	0.0	0.0	0.0	0.0	0.0	-0.0510	0.0255	-0.0468	0.0	0.0	0.0	0.0	0.0	0.0	0.0	0.0614	-0.0510	0.0
ROW 8	0.0	0.0	-0.0278	0.0	0.0	0.0	0.5798	-0.0278	0.0	0.0	0.0	0.0	0.0	0.0	0.0	0.0	0.0	0.0	0.0255
	0.0	0.0	0.0	0.0	0.0	0.0	0.0	0.0	0.0	0.0	0.0	0.0	0.0	0.0	0.0	0.0	0.0	0.0	0.0
	0.0614	0.0	0.0	0.0	0.0255	0.0	0.0255	0.0	0.0	0.0	0.0	0.0	0.0	0.0	0.0	0.0	0.0	0.0	0.0
ROW 9	0.0	0.0	-0.0278	0.0	0.0	0.0	-0.0278	0.5798	-0.0278	0.0	0.0	0.0	0.0	0.0	0.0	0.0	0.0	0.0	0.0255
	0.0	0.0	0.0	0.0	0.0	0.0	-0.0719	-0.0719	0.0	0.0	0.0	0.0	0.0	0.0	0.0	0.0	0.0	0.0	0.0
	0.0614	0.0	0.0	0.0	0.0	0.0	0.0255	0.0	0.0468	0.0	0.0	0.0	0.0	0.0	0.0	0.0	0.0	0.0	0.0
ROW 10	0.0	0.0	-0.0278	0.0	0.0	0.0	-0.0278	-0.0278	0.5798	-0.0278	0.0	0.0	0.0	0.0	0.0	0.0	0.0	0.0	0.0255
	0.0	0.0	0.0	0.0	0.0	0.0	-0.0719	-0.0719	0.0	0.0	0.0	0.0	0.0	0.0	0.0	0.0	0.0	0.0	0.0
	-0.0510	0.0	0.0	0.0	0.0	0.0	-0.0719	-0.0719	0.0	0.0	0.0	0.0	0.0	0.0	0.0	0.0	0.0	0.0	0.0

... cont'd.



g matrix for t-butyl bromide-d<sub>9</sub> - cont'd.

ROW 23	0.0	0.0	0.0	0.0719	0.0	0.0	0.0	0.0	0.0	0.0	0.0	0.0719	-0.0719	-0.0719	0.0	0.0	0.0	0.0
	-0.0660	0.0	0.0	0.0	0.0	0.0	1.0172	-0.2078	-0.2078	0.0	0.0	0.0	0.0	0.0	0.0	0.0	0.0	0.0
	0.0	-0.1590	-0.2213	-0.2213	0.0330	0.0330	0.0	0.0	0.0	0.0	0.0	0.0	0.0	0.0	0.0	0.0	0.0	0.0
ROW 24	0.0	0.0	0.0	0.0719	0.0	0.0	0.0	0.0	0.0	0.0	0.0	-0.0719	0.0719	-0.0719	0.0	0.0	0.0	0.0
	0.0330	0.0	0.0	0.0	0.0	0.0	-0.2078	1.0172	-0.2078	0.0	0.0	0.0	0.0	0.0	0.0	0.0	0.0	0.0
	0.0	-0.2213	-0.1590	-0.2213	0.0330	-0.0660	0.0	0.0	0.0	0.0	0.0	0.0	0.0	0.0	0.0	0.0	0.0	0.0
ROW 25	0.0	0.0	0.0	0.0719	0.0	0.0	0.0	0.0	0.0	0.0	0.0	-0.0719	0.0719	-0.0719	0.0	0.0	0.0	0.0
	0.0330	0.0	0.0	0.0	0.0	0.0	-0.2078	-0.2078	1.0172	0.0	0.0	0.0	0.0	0.0	0.0	0.0	0.0	0.0
	0.0	-0.2213	-0.1590	-0.2213	-0.0660	0.0330	0.0	0.0	-0.0660	0.0	0.0	0.0	0.0	0.0	0.0	0.0	0.0	0.0
ROW 26	-0.0510	-0.0719	0.0255	0.0255	-0.0510	0.0614	0.0	0.0	0.0	0.0	0.0	0.0	0.0	0.0	0.0	0.0959	0.0247	0.0234
	0.0247	-0.1590	-0.2213	-0.2213	0.0	0.0	0.0	0.0	0.0	0.0	0.0	0.5886	0.0065	0.0065	0.0065	0.0293	-0.0234	0.0234
	-0.0059	0.0293	-0.0059	-0.0234	-0.0468	-0.0492	-0.0492	0.0	0.0361	-0.0361	0.0	0.0	0.0	0.0	0.0	0.0959	0.0247	0.0234
ROW 27	0.0255	-0.0719	0.0255	0.0255	0.0614	-0.0510	0.0614	0.0	0.0	0.0	0.0	0.0	0.0	0.0	0.0	-0.0480	0.0171	0.0059
	-0.0418	-0.2213	-0.1590	-0.2213	0.0	0.0	0.0	0.0	0.0	0.0	0.0	0.0065	0.5886	0.0065	0.0065	-0.0059	-0.0059	-0.0059
	0.0117	-0.0234	-0.0059	0.0293	0.0234	-0.0492	0.0985	-0.1557	0.0361	0.0722	0.0722	0.0	0.0	0.0	0.0	0.0	0.0	0.0
ROW 28	-0.0510	-0.0719	0.0255	0.0255	0.0614	-0.0510	0.0614	0.0	0.0	0.0	0.0	0.0	0.0	0.0	0.0	-0.0480	0.0171	0.0059
	0.0247	0.0	0.0	-0.1590	-0.2213	-0.2213	0.0	0.0	0.0	0.0	0.0	0.0	0.0	0.0	0.0	-0.0480	0.0171	0.0059
	-0.0059	-0.0059	0.0117	-0.0059	0.0234	0.0985	-0.0492	0.1557	-0.0722	-0.0361	0.0	0.0	0.0	0.0	0.0	-0.0480	0.0171	0.0059
ROW 29	-0.0510	0.0255	-0.0719	0.0255	0.0	0.0	-0.0510	0.0614	0.0614	0.0614	0.0	0.0	0.0	0.0	0.0	0.0247	0.0959	0.0065
	0.0247	0.0	0.0	0.0	-0.1590	-0.2213	-0.2213	0.0	0.0	0.0	0.0	0.0	0.0	0.0	0.0	0.0247	0.0959	0.0065
	0.0065	0.0293	-0.0234	-0.0059	-0.0468	-0.0492	-0.0361	0.0	0.0361	0.0	0.0	0.0	0.0	0.0	0.0	0.0247	0.0959	0.0065
ROW 30	0.0255	0.0255	-0.0719	0.0255	0.0	0.0	0.0614	-0.0510	0.0614	0.0614	0.0	0.0	0.0	0.0	0.0	-0.0418	-0.0480	0.5886
	0.0171	0.0	0.0	0.0	-0.2213	-0.1590	-0.2213	0.0	0.0	0.0	0.0	0.0	0.0	0.0	0.0	-0.0418	-0.0480	0.5886
	0.0065	-0.0059	-0.0059	0.0117	0.0985	0.0234	-0.0492	-0.0361	0.0	0.0361	0.0	0.0	0.0	0.0	0.0	-0.0418	-0.0480	0.5886
ROW 31	0.0255	-0.0510	-0.0719	0.0255	0.0	0.0	0.0614	0.0614	0.0614	0.0614	0.0	0.0	0.0	0.0	0.0	0.0171	-0.0480	0.0065
	-0.0418	0.0	0.0	0.0	-0.2213	-0.2213	-0.1590	0.0	0.0	0.0	0.0	0.0	0.0	0.0	0.0	0.0171	-0.0480	0.0065
	0.5886	-0.0234	0.0293	-0.0059	-0.0492	0.0234	0.0985	-0.0361	0.1557	-0.0722	0.0722	0.0	0.0	0.0	0.0	0.0171	-0.0480	0.0065
ROW 32	-0.0510	0.0255	-0.0719	0.0255	0.0	0.0	0.0	0.0	0.0	0.0	0.0	-0.0510	0.0614	0.0614	0.0247	0.0247	0.0059	0.0059
	0.0959	0.0	0.0	0.0	0.0	0.0	0.0	0.0	0.0	0.0	0.0	0.0	0.0	0.0	0.0247	0.0247	0.0059	0.0059
	-0.0234	0.5886	0.0065	-0.0065	-0.0492	-0.0468	0.0361	-0.0361	0.0	0.0	0.0	0.0	0.0	0.0	0.0247	0.0247	0.0059	0.0059
ROW 33	0.0255	-0.0510	0.0255	-0.0719	0.0	0.0	0.0	0.0	0.0	0.0	0.0	0.0614	-0.0510	0.0614	0.0247	0.0247	0.0059	0.0059
	-0.0480	0.0	0.0	0.0	0.0	0.0	-0.2213	-0.1590	-0.2213	-0.2213	0.0293	-0.0234	-0.0059	0.0293	0.0293	0.0247	0.0059	0.0059
	0.0293	0.0065	0.5886	0.0065	-0.0492	0.0985	0.0234	0.0361	0.0722	-0.1557	0.0	0.0	0.0	0.0	0.0	0.0247	0.0059	0.0059

... cont'd.



$G$  matrix for *t*-butyl bromide- $d_9$  - cont'd.

ROW 34	0.0255	0.0510	-0.0719	0.0	0.0	0.0	0.0	0.0	0.0	0.0614	-0.0510	-0.0418	0.0171
-0.0480	0.0	0.0	0.0	-0.2213	-0.2213	-0.1590	-0.0234	0.0293	-0.0059	-0.0059	0.0117		
-0.0059	0.0065	0.5886	0.0985	-0.0492	0.0234	0.1557							
ROW 35	0.0510	0.0510	-0.0510	0.0	0.0	0.0255	-0.0510	0.0255	0.0255	-0.0510	-0.0836	-0.0226	
-0.0226	0.0	0.0	0.0	0.0330	-0.0660	0.0330	0.0330	-0.0660	-0.0660	0.0234	0.0492	0.0985	
-0.0492	-0.0492	-0.0492	0.0985	0.1639	-0.0176	0.0	-0.1767	0.1767					
ROW 36	0.0510	-0.0510	0.0510	0.0255	-0.0510	0.0	0.0	0.0255	-0.0510	0.0255	-0.0226	-0.0836	
-0.0226	0.0330	0.0330	-0.0660	0.0	0.0	0.0330	-0.0660	0.0330	-0.0492	0.0985	-0.0468	0.0234	
0.0234	-0.0492	0.0985	-0.0492	-0.0176	0.1639	-0.0176	0.1767	0.0	-0.1767				
ROW 37	0.0510	-0.0510	0.0510	0.0255	-0.0510	0.0255	0.0255	-0.0510	0.0	0.0	-0.0226	-0.0226	
-0.0510	0.0330	0.0330	-0.0660	0.0	0.0	0.0330	-0.0660	0.0	0.0	0.0	-0.0492	-0.0492	
-0.0836	-0.0468	0.0234	0.0234	-0.0176	-0.0176	0.1639	-0.1767	0.1767	0.0	0.0	-0.0492	-0.0492	
0.0985	0.0	0.1573	-0.1573	0.0	0.0468	-0.0468	0.0	0.0	0.0	0.0	0.0	0.0	-0.1303
0.0	0.0	0.0606	-0.0606	0.0	0.0	0.0	0.0	0.0	0.0	0.0	-0.1557	0.1557	-0.0361
-0.1303	0.0361	0.0361	-0.0722	0.0	0.1767	-0.1767	1.9210	-0.2394	-0.2394				0.0722
ROW 39	0.0	-0.1573	0.0	0.1573	0.0	0.0	0.0	0.0468	-0.0468	0.0	0.0	0.1303	0.0
0.0	0.0	0.0	0.0	0.0	0.0606	-0.0606	0.0	0.0	0.0	0.0361	-0.0722	0.0	-0.1557
-0.1557	-0.0361	0.0722	-0.0361	-0.1767	0.0	0.1767	-0.2394	1.9210	-0.2394				
ROW 40	0.0	0.1573	-0.1573	0.0	0.0	0.0	0.0	0.0	0.0	0.0	0.0468	-0.0468	-0.1303
0.0	0.0	0.0	0.0	0.0	0.0	0.0	0.0	0.0606	-0.0606	-0.0361	0.0722	-0.0361	0.0361
0.0	0.0	0.0	0.0	0.0	0.0	0.0	0.0	0.0	0.0	0.0	0.0	0.0	0.0
-0.0722	0.0	-0.1557	0.1557	0.1767	-0.1767	0.0	-0.2394	-0.2394	1.9210				

The order of the internal coordinate is shown in Table IX.

## APPENDIX II

A. Eigenvectors for t-butyl bromide-h<sub>9</sub> using force field I.<sup>a</sup>

Symmetry	Frequency Eigenvector									
A <sub>1</sub>	FREQUENCY = 2980.6 CM-1									
	0.0032	-0.0012	-0.0012	-0.0012	0.4956	-0.2467	-0.2467	0.4956	-0.2467	-0.2467
	0.4956	-0.2467	-0.2467	-0.0381	-0.0381	-0.0381	0.0817	-0.0409	-0.0409	0.0817
	-0.0409	-0.0409	0.0817	-0.0409	-0.0409	-0.0581	0.0292	0.0292	-0.0581	0.0292
	0.0292	-0.0581	0.0292	0.0292	0.0381	0.0381	0.0381	0.0	0.0	0.0
	FREQUENCY = 2547.5 CM-1									
	0.0010	-0.0313	-0.0313	-0.0313	0.3354	0.3371	0.3371	0.3354	0.3371	0.3371
	0.3354	0.3371	0.3371	-0.0007	-0.0007	-0.0007	-0.0316	-0.0312	-0.0312	-0.0316
	-0.0312	-0.0312	-0.0316	-0.0312	-0.0312	0.0306	0.0317	0.0317	0.0306	0.0317
	0.0317	0.0306	0.0317	0.0317	0.0007	0.0007	0.0007	0.0	0.0	0.0
	FREQUENCY = 1463.7 CM-1									
	0.0345	-0.0137	-0.0137	-0.0137	0.0085	-0.0047	-0.0047	0.0085	-0.0047	-0.0047
	0.0085	-0.0047	-0.0047	-0.0044	-0.0044	-0.0044	-0.6776	0.3383	0.3383	-0.6776
	0.3383	0.3383	-0.6776	0.3383	0.3383	-0.2187	0.1099	0.1099	-0.2187	0.1099
	0.1099	-0.2187	0.1099	0.1099	0.0044	0.0044	0.0044	0.0	0.0	0.0
FREQUENCY = 1393.9 CM-1										
-0.0008	-0.0801	-0.0801	-0.0801	-0.0081	-0.0079	-0.0079	-0.0081	-0.0079	-0.0079	
-0.0081	-0.0079	-0.0079	-0.0009	-0.0009	-0.0009	-0.3314	-0.3347	-0.3347	-0.3314	
-0.3347	-0.3347	-0.3314	-0.3347	-0.3347	0.3325	0.3341	0.3341	0.3325	0.3341	
0.3341	0.3325	0.3341	0.3341	0.0009	0.0009	0.0009	0.0	0.0	0.0	
FREQUENCY = 1168.6 CM-1										
0.1556	-0.0720	-0.0720	-0.0720	-0.0147	0.0054	0.0054	-0.0147	0.0054	0.0054	
-0.0147	0.0054	0.0054	-0.1399	-0.1399	-0.1399	-0.1943	-0.0896	-0.0896	0.1943	
-0.0896	-0.0896	0.1943	-0.0896	-0.0896	-0.4233	0.2041	0.2041	-0.4233	0.2041	
0.2041	-0.4233	0.2041	0.2041	0.1399	0.1399	0.1399	0.0	0.0	0.0	
FREQUENCY = 809.2 CM-1										
0.0909	-0.1551	-0.1551	-0.1551	-0.0017	-0.0043	-0.0043	-0.0017	-0.0043	-0.0043	
-0.0017	-0.0043	-0.0043	-0.0460	-0.0460	-0.0460	-0.0079	0.0373	0.0373	-0.0079	
0.0373	0.0373	-0.0079	0.0373	0.0373	0.0828	-0.0747	-0.0747	0.0828	-0.0747	
-0.0747	0.0828	-0.0747	-0.0747	0.0460	0.0460	0.0460	0.0	0.0	0.0	
FREQUENCY = 526.8 CM-1										
0.2324	-0.0032	-0.0032	-0.0032	0.0005	0.0008	0.0008	0.0005	0.0008	0.0008	
0.0005	0.0008	0.0008	-0.1280	-0.1280	-0.1280	-0.0324	-0.0021	-0.0021	-0.0324	
-0.0021	-0.0021	-0.0324	-0.0021	-0.0021	0.0718	-0.0176	-0.0176	0.0718	-0.0176	
-0.0176	0.0718	-0.0176	-0.0176	0.1280	0.1280	0.1280	0.0	0.0	0.0	
FREQUENCY = 300.4 CM-1										
-0.0875	0.0139	0.0139	0.0139	-0.0012	0.0006	0.0006	-0.0012	0.0006	0.0006	
-0.0012	0.0006	0.0006	-0.0583	-0.0583	-0.0583	0.0078	0.0078	0.0078	-0.0081	
0.0078	0.0078	-0.0081	0.0078	0.0078	0.0109	-0.0092	-0.0092	0.0109	-0.0092	
-0.0092	0.0109	-0.0092	-0.0092	0.0583	0.0583	0.0583	0.0	0.0	0.0	
A <sub>2</sub>	FREQUENCY = 2978.2 CM-1									
	0.0	0.0	0.0	0.0	0.0	0.4286	-0.4286	0.0	0.4286	-0.4286
	0.0	0.4286	-0.4286	0.0	0.0	0.0	0.0	0.0700	-0.0700	0.0
	0.0700	-0.0700	0.0	0.0700	-0.0700	0.0	-0.0478	0.0478	0.0	-0.0478
	0.0478	0.0	-0.0478	0.0478	0.0	0.0	0.0	0.0381	0.0381	0.0381
	FREQUENCY = 1456.3 CM-1									
	0.0	0.0	0.0	0.0	0.0	0.0084	-0.0084	0.0	0.0084	-0.0084
	0.0	0.0084	-0.0084	0.0	0.0	0.0	0.0	-0.5966	0.5966	0.0
	-0.5966	0.5966	0.0	-0.5966	0.5966	0.0	-0.1579	0.1579	0.0	-0.1579
	0.1579	0.0	-0.1579	0.1579	0.0	0.0	0.0	-0.0200	-0.0200	-0.0200
	FREQUENCY = 1021.0 CM-1									
	0.0	0.0	0.0	0.0	0.0	0.0085	-0.0085	0.0	0.0085	-0.0085
	0.0	0.0085	-0.0085	0.0	0.0	0.0	0.0	-0.1272	0.1272	0.0
	-0.1272	0.1272	0.0	-0.1272	0.1272	0.0	0.3608	-0.3608	0.0	0.3608
	-0.3608	0.0	0.3608	-0.3608	0.0	0.0	0.0	-0.0507	-0.0507	-0.0507
FREQUENCY = 266.7 CM-1										
0.0	0.0	0.0	0.0	0.0	0.0001	-0.0001	0.0	0.0001	-0.0001	
0.0	0.0001	-0.0001	0.0	0.0	0.0	0.0	0.0009	-0.0009	0.0	
0.0009	-0.0009	0.0	0.0009	-0.0009	0.0	-0.0012	0.0012	0.0	-0.0012	
0.0012	0.0	-0.0012	0.0012	0.0	0.0	0.0	-0.9711	-0.9711	-0.9711	

. . . cont'd.

A. Eigenvectors for t-butyl bromide-h<sub>9</sub> using  
force field I - cont'd.

Sym- metry	Frequency Eigenvector									
E (a)	FREQUENCY = 2981.7 CM-1									
	0.0	-0.0032	0.0016	0.0016	0.2750	-0.1344	-0.1344	-0.1375	0.5505	-0.4161
	-0.1375	-0.4161	0.5505	-0.0178	0.0629	0.0099	0.0453	-0.0230	-0.0230	-0.0226
	0.0918	-0.0689	-0.0226	-0.0689	0.0918	-0.0301	0.0153	0.0153	0.0150	-0.0643
	0.0490	0.0150	0.0490	-0.0643	-0.0835	0.0418	0.0418	0.0	0.0499	-0.0499
	FREQUENCY = 2979.1 CM-1									
	0.0	0.0022	-0.0011	-0.0011	0.6431	-0.3237	-0.3237	-0.3215	-0.0429	0.3665
	-0.3215	0.3665	-0.0429	-0.0481	0.0241	0.0241	0.1059	-0.0528	-0.0528	-0.0530
	-0.0072	0.0599	-0.0530	0.0599	-0.0072	-0.0728	0.0362	0.0362	0.0364	0.0060
	-0.0422	0.0364	-0.0422	0.0060	0.0081	-0.0040	-0.0040	0.0	-0.0225	0.0225
FREQUENCY = 2946.3 CM-1										
0.0	-0.0456	0.0228	0.0228	0.4767	0.4755	0.4755	-0.2383	-0.2405	-0.2350	
-0.2383	-0.2350	-0.2405	0.0023	-0.0011	-0.0011	-0.0430	-0.0432	-0.0432	0.0215	
0.0211	0.0221	0.0215	0.0221	0.0211	0.0439	0.0428	0.0428	-0.0219	-0.0229	
-0.0199	-0.0219	-0.0199	-0.0229	-0.0025	0.0012	0.0012	0.0	0.0062	-0.0062	
FREQUENCY = 1462.6 CM-1										
0.0	-0.0475	0.0237	0.0237	-0.0041	0.0003	0.0003	0.0020	0.0027	-0.0050	
0.0020	-0.0090	0.0087	0.0235	-0.0117	-0.0117	0.2452	-0.1335	-0.1335	-0.1226	
-0.6237	0.7572	-0.1226	0.7572	-0.6237	0.0925	-0.0354	-0.0354	-0.0462	-0.2033	
0.2387	-0.0462	0.2387	-0.2033	-0.0041	0.0021	0.0021	0.0	0.0616	-0.0616	
FREQUENCY = 1457.4 CM-1										
0.0	0.0067	-0.0034	-0.0034	0.0138	-0.0067	-0.0067	-0.0069	0.0069	-0.0001	
-0.0069	-0.0001	0.0068	0.0217	-0.0109	-0.0109	-0.9376	0.4705	0.4705	0.4688	
-0.4335	-0.0370	0.4688	-0.0370	-0.4335	-0.2466	0.1226	0.1226	0.1243	-0.1047	
-0.0179	0.1243	-0.0179	-0.1047	0.0309	-0.0154	-0.0154	0.0	-0.0197	0.0197	
FREQUENCY = 1377.8 CM-1										
0.0	-0.1185	0.0592	0.0592	-0.0097	-0.0102	-0.0102	0.0049	0.0041	0.0061	
0.0049	0.0061	0.0041	0.0123	-0.0061	-0.0061	-0.4837	-0.4661	-0.4661	0.2419	
0.2542	0.2120	0.2419	0.2120	0.2542	0.4766	0.4697	0.4697	0.2583	-0.2491	
-0.2207	-0.2353	-0.2207	-0.2491	-0.0176	0.0638	0.0088	0.0	0.0358	-0.0358	
FREQUENCY = 1257.2 CM-1										
0.0	-0.2613	0.1306	0.1306	-0.0009	-0.0065	-0.0065	0.0005	-0.0099	0.0164	
0.0005	0.0164	-0.0099	0.1661	-0.0831	-0.0831	-0.0541	0.0769	0.0769	0.0270	
0.1390	-0.2158	0.0270	-0.2158	0.1390	0.0793	-0.0895	-0.0895	-0.0396	-0.2752	
0.3647	-0.0396	0.3647	-0.2752	-0.2525	0.1262	0.1262	0.0	0.4963	-0.4963	
FREQUENCY = 1030.5 CM-1										
0.0	0.0140	-0.0070	-0.0070	-0.0140	0.0074	0.0074	0.0070	-0.0074	0.0001	
0.0070	0.0001	-0.0074	-0.0709	0.0354	0.0354	0.1927	-0.0974	-0.0974	-0.0564	
0.0877	0.0057	-0.0564	0.0097	0.0877	-0.5635	0.2828	0.2828	0.2818	-0.2706	
-0.0122	0.2818	-0.0122	-0.2706	-0.0571	0.0285	0.0285	0.0	0.0003	-0.0003	
FREQUENCY = 929.8 CM-1										
0.0	-0.2009	0.1005	0.1005	-0.0061	-0.0022	-0.0022	0.0030	0.0068	-0.0046	
0.0030	-0.0046	0.0068	0.0706	-0.0353	-0.0353	0.0507	-0.0135	-0.0135	-0.0253	
-0.0832	0.0967	-0.0253	0.0967	-0.0832	-0.1404	0.0584	0.0584	0.0702	0.2554	
-0.3138	0.0702	-0.3138	0.2554	-0.0432	0.0216	0.0216	0.0	0.2123	-0.2123	
FREQUENCY = 395.8 CM-1										
0.0	-0.0460	0.0230	0.0230	-0.0001	-0.0011	-0.0011	0.0000	0.0024	-0.0013	
0.0000	-0.0013	0.0024	-0.0348	0.0174	0.0174	0.0067	-0.0017	-0.0017	-0.0033	
0.0210	-0.0194	-0.0033	-0.0194	0.0210	-0.0067	0.0017	0.0017	0.0034	-0.0334	
0.0316	0.0034	0.0316	-0.0334	0.2021	-0.1011	-0.1011	0.0	-0.4287	0.4287	
FREQUENCY = 282.6 CM-1										
0.0	0.0115	-0.0058	-0.0058	0.0012	-0.0003	-0.0003	-0.0006	0.0006	-0.0003	
-0.0006	-0.0003	0.0006	0.1183	-0.0592	-0.0592	0.0090	-0.0049	-0.0049	-0.0045	
0.0060	-0.0011	-0.0045	-0.0011	0.0060	-0.0129	0.0068	0.0068	0.0064	-0.0068	
-0.0001	0.0064	-0.0001	-0.0068	0.0540	-0.0270	-0.0270	0.0	0.8698	-0.8698	
FREQUENCY = 244.4 CM-1										
0.0	0.0095	-0.0047	-0.0047	0.0009	-0.0002	-0.0002	-0.0004	0.0002	0.0001	
-0.0004	0.0001	0.0002	0.1183	-0.0591	-0.0591	0.0067	-0.0037	-0.0037	-0.0032	
0.0018	0.0018	-0.0033	0.0018	0.0018	-0.0056	0.0051	0.0051	0.0048	-0.0013	
-0.0038	0.0048	-0.0038	-0.0013	-0.0046	0.0023	0.0023	0.0	-0.7345	0.7345	

. . . cont'd.

A. Eigenvectors for t-butyl bromide-h<sub>9</sub> using  
force field I - cont'd.

Sym- metry	Frequency Eigenvector									
E (b)	FREQUENCY = 2981.7 CM-1									
	0.0	0.0	-0.0028	0.0028	0.0	-0.5580	0.5580	0.2393	0.1025	-0.3555
	-0.2383	0.3955	-0.1625	0.0	-0.0154	0.0154	0.0	-0.0928	0.0926	0.0393
	0.0265	-0.0663	-0.0393	0.0663	-0.0265	0.0	0.0654	-0.0654	-0.0260	-0.0194
	0.0460	0.0260	-0.0460	0.0154	0.0	-0.0724	0.0724	-0.0577	0.0288	0.0288
	FREQUENCY = 2979.1 CM-1									
	0.0	0.0	-0.0019	0.0019	0.0	-0.2365	0.2365	-0.5569	0.3985	0.1620
	0.5569	-0.1620	-0.3985	0.0	0.0417	-0.0417	0.0	-0.0387	0.0387	-0.0917
	0.0651	0.0263	0.0917	-0.0263	-0.0651	0.0	0.0275	-0.0275	0.0631	-0.0453
	-0.0175	-0.0631	0.0175	0.0453	0.0	-0.0070	0.0070	-0.0260	0.0130	0.0130
	FREQUENCY = 2946.4 CM-1									
	0.0	0.0	0.0395	-0.0395	0.0	-0.0032	0.0032	-0.4128	-0.4102	-0.4134
	0.4128	0.4134	0.4102	0.0	-0.0020	0.0020	0.0	-0.0006	0.0006	0.0372
	0.0377	0.0371	-0.0372	-0.0371	-0.0377	0.0	-0.0017	0.0017	-0.0380	-0.0362
	-0.0379	0.0360	0.0379	0.0362	0.0	0.0021	-0.0021	0.0072	-0.0036	-0.0036
	FREQUENCY = 1462.6 CM-1									
	0.0	0.0	-0.0411	0.0411	0.0	-0.0102	0.0102	-0.0035	0.0054	-0.0048
	0.0035	0.0048	-0.0054	0.0	0.0203	-0.0203	0.0	0.7972	-0.7972	0.2124
	-0.5142	0.2830	-0.2124	-0.2830	0.5142	0.0	0.2551	-0.2551	0.0801	-0.1582
	0.0969	-0.0801	-0.0969	0.1582	0.0	-0.0036	0.0036	-0.0711	0.0356	0.0356
FREQUENCY = 1457.4 CM-1										
0.0	0.0	-0.0058	0.0058	0.0	0.0040	-0.0040	-0.0120	0.0038	0.0078	
0.0120	-0.0078	-0.0038	0.0	-0.0188	0.0188	0.0	-0.2289	0.2289	0.8120	
-0.2929	-0.5219	-0.8120	0.5219	0.2929	0.0	-0.0501	0.0501	0.2152	-0.0812	
-0.1313	-0.2152	0.1313	0.0812	0.0	-0.0267	0.0267	-0.0228	0.0114	0.0114	
FREQUENCY = 1377.8 CM-1										
0.0	0.0	0.1026	-0.1026	0.0	-0.0011	0.0011	0.0084	0.0094	0.0083	
-0.0084	-0.0094	-0.0083	0.0	-0.0106	0.0106	0.0	0.0244	-0.0244	0.4189	
0.3915	0.4159	-0.4189	-0.4159	-0.3915	0.0	-0.0164	0.0164	-0.4127	-0.3586	
-0.4150	0.4127	0.4150	0.3586	0.0	0.0152	-0.0152	0.0413	-0.0206	-0.0206	
FREQUENCY = 1257.2 CM-1										
0.0	0.0	-0.2263	0.2263	0.0	0.0152	-0.0152	-0.0008	-0.0132	0.0020	
0.0008	-0.0020	0.0132	0.0	0.1439	-0.1439	0.0	-0.2049	0.2049	-0.0468	
0.1690	-0.0358	0.0468	0.0358	-0.1690	0.0	0.3695	-0.3695	0.0687	-0.2622	
0.1072	-0.0687	-0.1072	0.2622	0.0	-0.2187	0.2187	-0.5730	0.2865	0.2865	
FREQUENCY = 1030.5 CM-1										
0.0	0.0	0.0121	-0.0121	0.0	0.0043	-0.0043	-0.0121	0.0042	0.0025	
0.0121	-0.0042	-0.0025	0.0	-0.0614	0.0614	0.0	-0.0451	0.0451	0.1669	
-0.0618	-0.1069	-0.1669	0.1069	0.0618	0.0	0.1492	-0.1492	-0.4880	0.1703	
0.3195	0.4880	-0.3195	-0.1703	0.0	-0.0494	0.0494	-0.0004	0.0002	0.0002	
FREQUENCY = 929.8 CM-1										
0.0	0.0	-0.1740	0.1740	0.0	-0.0066	0.0066	-0.0052	0.0014	-0.0052	
0.0052	0.0052	-0.0014	0.0	0.0612	-0.0612	0.0	0.1038	-0.1038	0.0439	
-0.0636	0.0402	-0.0439	-0.0402	0.0636	0.0	-0.3286	0.3286	-0.1216	0.2148	
-0.1138	0.1216	0.1138	-0.2148	0.0	-0.0374	0.0374	-0.2451	0.1225	0.1225	
FREQUENCY = 395.8 CM-1										
0.0	0.0	-0.0399	0.0399	0.0	-0.0021	0.0021	-0.0001	0.0001	-0.0020	
0.0001	0.0020	-0.0001	0.0	-0.0302	0.0302	0.0	-0.0233	0.0233	0.0058	
0.0102	-0.0131	-0.0058	0.0131	-0.0102	0.0	0.0375	-0.0375	-0.0058	-0.0173	
0.0203	0.0058	-0.0203	0.0173	0.0	0.1751	-0.1751	0.4951	-0.2475	-0.2475	
FREQUENCY = 282.6 CM-1										
0.0	0.0	0.0100	-0.0100	0.0	-0.0005	0.0005	0.0010	-0.0000	-0.0005	
-0.0010	0.0005	0.0000	0.0	0.1025	-0.1025	0.0	-0.0041	0.0041	0.0078	
-0.0022	-0.0063	-0.0078	0.0063	0.0022	0.0	0.0039	-0.0039	-0.0111	0.0040	
0.0078	0.0111	-0.0078	-0.0040	0.0	0.0468	-0.0468	-1.0043	0.5021	0.5021	
FREQUENCY = 244.4 CM-1										
0.0	0.0	0.0082	-0.0082	0.0	-0.0001	0.0001	0.0003	-0.0002	-0.0002	
-0.0008	0.0002	0.0002	0.0	0.1024	-0.1024	0.0	0.0000	-0.0000	0.0058	
-0.0032	-0.0032	-0.0058	0.0032	0.0032	0.0	-0.0014	0.0014	-0.0083	0.0051	
0.0037	0.0083	-0.0037	-0.0051	0.0	-0.0040	0.0040	0.3481	-0.4241	-0.4241	

<sup>a</sup>The 40 entries for each frequency, k, give the L<sub>ik</sub> values (equation 37) in the same order of internal coordinates as in Table IX.

B. Eigenvectors for t-butyl bromide-d<sub>9</sub> using  
force field I.<sup>a</sup>

Sym- metry	Frequency Eigenvector										
A <sub>1</sub>	FREQUENCY = 2227.4 CM-1										
	0.0085	-0.0033	-0.0033	-0.0033	0.3675	-0.1824	-0.1824	0.3675	-0.1824	-0.1824	
	0.3675	-0.1824	-0.1824	-0.0556	-0.0556	-0.0556	0.1108	-0.0558	-0.0558	0.1108	
	-0.0558	-0.0558	0.1108	-0.0558	-0.0558	-0.0831	0.0420	0.0420	-0.0831	0.0420	
	0.0420	-0.0831	0.0420	0.0420	0.0556	0.0556	0.0556	0.0	0.0	0.0	
	FREQUENCY = 2125.2 CM-1										
	0.0034	-0.0495	-0.0495	-0.0495	0.2392	0.2415	0.2415	0.2392	0.2415	0.2415	
	0.2392	0.2415	0.2415	-0.0023	-0.0023	-0.0023	-0.0450	-0.0483	-0.0483	-0.0490	
	-0.0483	-0.0483	-0.0490	-0.0483	-0.0483	0.0461	0.0495	0.0458	0.0461	0.0498	
	0.0458	0.0461	0.0498	0.0458	0.0023	0.0023	0.0023	0.0	0.0	0.0	
	FREQUENCY = 1122.8 CM-1										
	-0.0617	-0.1383	0.1383	0.1383	0.0204	0.0146	0.0146	0.0204	0.0146	0.0146	
	0.0204	0.0146	0.0146	0.0458	0.0458	0.0458	0.2600	0.2197	0.2197	0.2600	
	0.2197	0.2197	0.2600	0.2197	0.2197	-0.1454	-0.2770	-0.2770	-0.1454	-0.2770	
	-0.2770	-0.1454	-0.2770	-0.2770	-0.0458	-0.0458	-0.0458	0.0	0.0	0.0	
	FREQUENCY = 1054.3 CM-1										
	0.0700	-0.0118	-0.0118	-0.0118	0.0167	-0.0034	-0.0034	0.0107	-0.0034	-0.0034	
	0.0107	-0.0034	-0.0034	-0.0248	-0.0248	-0.0248	-0.4267	0.2738	0.2738	-0.4267	
	0.2738	0.2738	-0.4267	0.2738	0.2738	-0.2167	0.0479	0.0479	-0.2167	0.0479	
	0.0479	-0.2167	0.0479	0.0479	0.0248	0.0248	0.0248	0.0	0.0	0.0	
	FREQUENCY = 1001.8 CM-1										
	0.1875	-0.0564	-0.0564	-0.0564	-0.0215	0.0116	0.0116	-0.0215	0.0116	0.0116	
	-0.0215	0.0116	0.0116	-0.1580	-0.1580	-0.1580	0.2678	-0.0319	-0.0319	0.2678	
	-0.0319	-0.0319	0.2678	-0.0319	-0.0319	-0.3537	0.0748	0.0748	-0.3537	0.0748	
	0.0748	-0.3537	0.0748	0.0748	0.1580	0.1580	0.1580	0.0	0.0	0.0	
	FREQUENCY = 687.2 CM-1										
	0.0492	-0.1093	-0.1093	-0.1093	0.0007	-0.0061	-0.0061	0.0007	-0.0061	-0.0061	
	0.0007	-0.0061	-0.0061	-0.0107	-0.0107	-0.0107	0.0372	0.0709	0.0709	0.0372	
	0.0709	0.0709	0.0372	0.0709	0.0709	0.0630	-0.1210	-0.1210	0.0630	-0.1210	
	-0.1210	0.0630	-0.1210	-0.1210	0.0107	0.0107	0.0107	0.0	0.0	0.0	
	FREQUENCY = 467.5 CM-1										
	0.2133	-0.0072	-0.0072	-0.0072	0.0021	0.0003	0.0003	0.0021	0.0003	0.0003	
	0.0021	0.0003	0.0003	-0.0921	-0.0921	-0.0921	-0.0369	-0.0087	-0.0087	-0.0369	
	-0.0087	-0.0087	-0.0369	-0.0087	-0.0087	0.0952	-0.0205	-0.0205	0.0952	-0.0205	
	-0.0205	0.0952	-0.0205	0.0921	0.0921	0.0921	0.0921	0.0	0.0	0.0	
	FREQUENCY = 273.6 CM-1										
	0.0642	-0.0111	-0.0111	-0.0111	0.0016	-0.0009	-0.0009	0.0016	-0.0009	-0.0009	
	0.0016	-0.0009	-0.0009	0.0597	0.0597	0.0597	0.0148	-0.0094	-0.0094	0.0148	
	-0.0094	-0.0094	0.0148	-0.0094	-0.0094	-0.0209	0.0125	0.0125	-0.0209	0.0125	
	0.0125	-0.0209	0.0125	0.0125	-0.0598	-0.0598	-0.0598	0.0	0.0	0.0	
	A <sub>2</sub>	FREQUENCY = 2220.9 CM-1									
		0.0	0.0	0.0	0.0	0.0	0.3178	-0.3178	0.0	0.3178	-0.3178
		0.0	0.3178	-0.3178	0.0	0.0	0.0	0.0	0.0944	-0.0944	0.0
		0.0944	-0.0944	0.0	0.0944	-0.0944	0.0	-0.0655	0.0655	0.0	-0.0655
		0.0655	0.0	-0.0655	0.0655	0.0	0.0	0.0	0.0524	0.0524	0.0524
		FREQUENCY = 1044.9 CM-1									
		0.0	0.0	0.0	0.0	0.0	-0.0122	0.0122	0.0	-0.0122	0.0122
		0.0	-0.0122	0.0122	0.0	0.0	0.0	0.0	0.4370	-0.4370	0.0
		0.4370	-0.4370	0.0	0.4370	-0.4370	0.0	0.0797	-0.0797	0.0	0.0797
		-0.0797	0.0	0.0797	-0.0797	0.0	0.0	0.0	0.0281	0.0281	0.0281
		FREQUENCY = 772.2 CM-1									
		0.0	0.0	0.0	0.0	0.0	0.0109	-0.0109	0.0	0.0109	-0.0109
		0.0	0.0109	-0.0109	0.0	0.0	0.0	0.0	-0.0655	0.0655	0.0
		-0.0655	0.0655	0.0	-0.0655	0.0655	0.0	0.2786	-0.2786	0.0	0.2786
		-0.2786	0.0	0.2786	-0.2786	0.0	0.0	0.0	-0.0556	-0.0556	-0.0556
	FREQUENCY = 189.1 CM-1										
	0.0	0.0	0.0	0.0	0.0	-0.0001	0.0001	0.0	-0.0001	0.0001	
	0.0	-0.0001	0.0001	0.0	0.0	0.0	0.0	-0.0010	0.0010	0.0	
	-0.0010	0.0010	0.0	-0.0010	0.0010	0.0	0.0013	-0.0013	0.0	0.0013	
	-0.0013	0.0	0.0013	-0.0013	0.0	0.0	0.0	0.6886	0.6886	0.6886	

. . . cont'd.

B. Eigenvectors for t-butyl bromide-d<sub>9</sub> using  
force field I - cont'd.

Sym- metry	Frequency Eigenvector
E (a)	FREQUENCY = 2230.1 CM-1
	0.0 -0.0097 0.0049 0.0049 0.1859 -0.0888 -0.0888 -0.0930 0.4081 -0.3193
	-0.0930 -0.3193 0.4081 -0.0188 0.0094 0.0094 0.0553 -0.0291 -0.0291 -0.0277
	0.1258 -0.0967 -0.0277 -0.0967 0.1258 -0.0359 0.0194 0.0194 0.0179 -0.0921
	0.0727 0.0179 0.0727 -0.0921 -0.1258 0.0604 0.0604 0.0 0.0800 -0.0800
	FREQUENCY = 2223.3 CM-1
	0.0 -0.0060 0.0030 0.0030 -0.4E36 0.2445 0.2445 0.2418 0.0150 -0.2595
	0.2418 -0.2595 0.0150 0.0655 -0.0348 -0.0348 -0.1460 0.0721 0.0721 -0.0730
	0.0049 -0.0770 0.0730 -0.0770 0.0049 0.1029 -0.0505 -0.0505 -0.0514 -0.0062
	0.0568 -0.0514 0.0568 -0.0062 -0.0090 0.0045 0.0045 0.0 0.0341 -0.0341
FREQUENCY = 2122.0 CM-1	
0.0 -0.0755 0.0377 0.0377 0.3418 0.3359 0.3359 -0.1709 -0.1743 -0.1656	
-0.1709 -0.1656 -0.1743 0.0078 -0.0039 -0.0039 -0.0656 -0.0656 -0.0656 0.0325	
0.0316 0.0340 0.0325 0.0340 0.0316 0.0679 0.0642 0.0642 -0.0340 -0.0375	
-0.0267 -0.0340 -0.0267 -0.0375 -0.0087 0.0044 0.0044 0.0 0.0215 -0.0215	
FREQUENCY = 1215.0 CM-1	
0.0 0.3274 -0.1637 -0.1637 0.0175 0.0221 0.0221 -0.0088 0.0051 -0.0272	
-0.0088 -0.0272 0.0051 -0.1687 0.0843 0.0843 0.1199 0.1537 0.1537 -0.0600	
-0.0754 -0.0784 -0.0600 -0.0784 -0.0754 -0.2292 -0.0591 -0.0991 0.1146 0.2594	
-0.1603 0.1146 -0.1603 0.2594 0.2315 -0.1157 -0.1157 0.0 -0.4898 0.4898	
FREQUENCY = 1050.5 CM-1	
0.0 0.0020 -0.0010 -0.0010 0.0102 -0.0044 -0.0044 -0.0051 0.0182 -0.0138	
-0.0051 -0.0138 0.0182 0.0190 -0.0095 -0.0095 -0.2818 0.1579 0.1579 0.1409	
-0.5687 0.4108 0.1409 0.4108 -0.5687 -0.0554 0.0107 0.0107 0.0277 -0.0834	
0.0727 0.0277 0.0727 -0.0834 0.0646 -0.0323 -0.0323 0.0 -0.0321 0.0321	
FREQUENCY = 1047.2 CM-1	
0.0 0.0168 -0.0084 -0.0084 -0.0129 0.0133 0.0133 0.0065 -0.0029 -0.0104	
0.0065 -0.0104 -0.0029 -0.0147 0.0074 0.0074 0.7323 -0.1882 -0.1882 -0.3661	
-0.1035 0.3084 0.0425 0.3084 0.1067 0.2990 0.3081 0.3081 -0.1495 -0.0467	
0.1544 -0.0001 0.1544 0.0236 -0.0223 0.0112 0.0112 0.0 0.0394 -0.0394	
FREQUENCY = 1034.8 CM-1	
0.0 0.0008 -0.0004 -0.0004 -0.0178 -0.0058 -0.0058 0.0089 0.0136 -0.0078	
0.0089 -0.0078 0.0136 -0.0827 0.0413 0.0413 -0.0851 -0.4150 -0.4150 0.0425	
0.1067 0.3084 0.0425 0.3084 0.1067 0.2990 0.3081 0.3081 -0.1495 -0.0467	
-0.2614 -0.1495 -0.2614 -0.0467 0.1125 -0.0562 -0.0562 0.0 -0.2184 0.2184	
FREQUENCY = 788.4 CM-1	
0.0 -0.0231 0.0116 0.0116 0.0178 -0.0057 -0.0057 -0.0089 0.0114 -0.0016	
-0.0089 -0.0016 0.0114 0.0792 -0.0396 -0.0396 -0.0738 0.0510 0.0510 0.0369	
-0.0403 -0.0107 0.0369 -0.0107 -0.0403 0.4102 -0.2192 -0.2192 -0.2051 0.2395	
-0.0203 -0.2051 -0.0203 0.2395 0.0702 -0.0351 -0.0351 0.0 0.0011 -0.0011	
FREQUENCY = 736.4 CM-1	
0.0 -0.1196 0.0598 0.0598 -0.0090 -0.0002 -0.0002 0.0045 0.0097 -0.0096	
0.0045 -0.0096 0.0097 0.0181 -0.0091 -0.0091 0.0807 0.0218 0.0218 -0.0403	
-0.0583 0.0365 -0.0403 0.0365 -0.0583 -0.2063 0.0410 0.0410 0.1031 0.2237	
-0.2647 0.1031 -0.2647 0.2237 0.0197 -0.0058 -0.0058 0.0 0.0737 -0.0737	
FREQUENCY = 338.6 CM-1	
0.0 0.0361 -0.0180 -0.0180 0.0002 0.0014 0.0014 -0.0001 -0.0027 0.0014	
-0.0001 0.0014 -0.0027 0.0400 -0.0200 -0.0200 -0.0133 -0.0038 -0.0038 0.0067	
-0.0237 0.0275 0.0067 0.0275 -0.0237 0.0129 0.0041 0.0041 -0.0064 0.0412	
-0.0452 -0.0064 -0.0452 0.0412 -0.1674 0.0837 0.0837 0.0 0.3126 -0.3126	
FREQUENCY = 241.9 CM-1	
0.0 0.0123 -0.0061 -0.0061 0.0019 -0.0005 -0.0005 -0.0010 0.0009 -0.0004	
-0.0010 -0.0004 0.0009 0.1386 -0.0653 -0.0653 0.0132 -0.0100 -0.0100 -0.0066	
0.0098 0.0001 -0.0066 0.0001 0.0098 -0.0200 0.0134 0.0134 0.0100 -0.0105	
-0.0029 0.0100 -0.0029 -0.0105 0.0426 -0.0213 -0.0213 0.0 0.3630 -0.3630	
FREQUENCY = 181.7 CM-1	
0.0 0.0022 -0.0011 -0.0011 0.0004 -0.0001 -0.0001 -0.0001 0.0000 0.0001	
-0.0001 0.0000 0.0000 0.0466 -0.0233 -0.0233 0.0030 -0.0021 -0.0021 -0.0015	
0.0003 0.0018 -0.0015 0.0018 0.0003 -0.0044 0.0028 0.0028 0.0022 0.0001	
-0.0029 0.0022 -0.0029 0.0001 -0.0131 0.0066 0.0066 0.0 -0.7357 0.7357	

. . . cont'd.

B. Eigenvectors for t-butyl bromide-d<sub>9</sub> using  
force field I - cont'd.

Sym- metry	Frequency Eigenvector									
E (b)	FREQUENCY = 2230.1 CM-1									
	0.0	0.0	-0.0084	0.0084	0.0	-0.4199	0.4199	0.1611	0.1331	-0.2869
	-0.1611	0.2869	-0.1331	0.0	-0.0163	0.0163	0.0	-0.1254	0.1254	0.0479
	0.0390	-0.0894	-0.0479	0.0894	-0.0390	0.0	0.0951	-0.0951	-0.0311	-0.0308
	0.0643	0.0311	-0.0643	0.0308	0.0	-0.1047	0.1047	-0.0924	0.0462	0.0462
	FREQUENCY = 2223.3 CM-1									
	0.0	0.0	0.0052	-0.0052	0.0	0.1585	-0.1585	0.4188	-0.2910	-0.1325
	-0.4188	0.1325	0.2910	0.0	-0.0602	0.0602	0.0	0.0473	-0.0473	0.1264
	-0.0861	-0.0368	-0.1264	0.0368	0.0861	0.0	-0.0364	0.0364	-0.0891	0.0620
	0.0256	0.0891	-0.0256	-0.0620	0.0	0.0078	-0.0078	0.0394	-0.0197	-0.0197
FREQUENCY = 2122.0 CM-1										
0.0	0.0	0.0654	-0.0654	0.0	-0.0050	0.0050	-0.2960	-0.2918	-0.2969	
0.2960	0.2969	0.2918	0.0	-0.0068	0.0068	0.0	-0.0014	0.0014	0.0563	
0.0576	0.0561	-0.0563	-0.0561	-0.0576	0.0	-0.0063	0.0063	-0.0528	-0.0525	
-0.0587	0.0588	0.0587	0.0525	0.0	0.0076	-0.0076	0.0249	-0.0124	-0.0124	
FREQUENCY = 1215.0 CM-1										
0.0	0.0	0.2835	-0.2835	0.0	-0.0187	0.0187	0.0152	0.0285	0.0092	
-0.0152	-0.0098	-0.0285	0.0	-0.1461	0.1461	0.0	-0.0017	0.0017	-0.1039	
0.1340	0.1323	-0.1039	-0.1323	-0.1340	0.0	-0.2423	0.2423	-0.1985	0.0353	
-0.2070	0.1985	0.2070	-0.0353	0.0	0.2005	-0.2005	0.5656	-0.2828	-0.2828	
FREQUENCY = 1050.5 CM-1										
0.0	0.0	-0.0018	0.0018	0.0	0.0185	-0.0185	-0.0089	-0.0054	0.0131	
0.0089	-0.0131	0.0054	0.0	-0.0165	0.0165	0.0	-0.5653	0.5653	0.2445	
0.1458	-0.4196	-0.2445	0.4196	-0.1458	0.0	-0.0901	0.0901	0.0430	0.0357	
-0.0544	-0.0430	0.0544	-0.0357	0.0	-0.0559	0.0559	-0.0371	0.0185	0.0185	
FREQUENCY = 1047.3 CM-1										
0.0	0.0	-0.0145	0.0145	0.0	0.0044	-0.0044	0.0112	-0.0137	-0.0093	
-0.0112	0.0093	0.0137	0.0	0.0127	-0.0127	0.0	-0.2286	0.2286	-0.6340	
0.2772	0.0486	0.6340	-0.0486	-0.2772	0.0	-0.0757	0.0757	-0.0001	0.1920	
0.1164	0.0001	-0.1164	-0.1920	0.0	0.0193	-0.0193	0.0455	-0.0227	-0.0227	
FREQUENCY = 1034.8 CM-1										
0.0	0.0	0.0007	-0.0007	0.0	-0.0123	0.0123	-0.0154	0.0011	-0.0112	
0.0154	0.0112	-0.0011	0.0	-0.0716	0.0716	0.0	0.1165	-0.1165	-0.0736	
-0.4177	-0.3012	0.0736	0.3012	0.4177	0.0	-0.1239	0.1239	0.2590	0.3267	
0.2048	-0.2590	-0.2048	-0.3267	0.0	0.0974	-0.0974	0.2522	-0.1261	-0.1261	
FREQUENCY = 788.4 CM-1										
0.0	0.0	0.0200	-0.0200	0.0	0.0075	-0.0075	-0.0154	0.0047	0.0122	
0.0154	-0.0122	-0.0047	0.0	-0.0686	0.0686	0.0	-0.0171	0.0171	0.0639	
-0.0356	-0.0527	-0.0639	0.0527	0.0356	0.0	0.1500	-0.1500	-0.3552	0.1148	
0.2648	0.3552	-0.2648	-0.1148	0.0	-0.0608	0.0608	0.0012	-0.0006	-0.0006	
FREQUENCY = 736.4 CM-1										
0.0	0.0	0.1035	-0.1035	0.0	0.0111	-0.0111	0.0078	-0.0054	0.0057	
-0.0078	-0.0057	0.0054	0.0	-0.0157	0.0157	0.0	-0.0547	0.0547	-0.0699	
0.0085	-0.0462	0.0699	0.0462	-0.0085	0.0	0.2520	-0.2520	0.1786	-0.1765	
0.1055	-0.1765	-0.1055	0.1765	0.0	-0.0170	0.0170	0.0651	-0.0425	-0.0425	
FREQUENCY = 338.6 CM-1										
0.0	0.0	0.0312	-0.0312	0.0	0.0024	-0.0024	0.0002	-0.0000	0.0024	
-0.0002	-0.0024	0.0000	0.0	0.0347	-0.0347	0.0	0.0255	-0.0295	-0.0116	
-0.0181	0.0114	0.0116	-0.0114	0.0181	0.0	-0.0499	0.0499	0.0112	0.0285	
-0.0214	-0.0112	0.0214	-0.0285	0.0	0.1450	-0.1450	-0.3610	0.1805	0.1805	
FREQUENCY = 241.9 CM-1										
0.0	0.0	0.0106	-0.0106	0.0	-0.0005	0.0005	0.0017	-0.0000	-0.0008	
-0.0017	0.0008	0.0000	0.0	0.1201	-0.1201	0.0	-0.0056	0.0056	0.0114	
-0.0058	-0.0114	-0.0114	0.0114	0.0058	0.0	0.0044	-0.0044	-0.0173	0.0054	
0.0138	0.0173	-0.0138	-0.0054	0.0	0.0369	-0.0369	-0.4191	0.2096	0.2096	
FREQUENCY = 181.7 CM-1										
0.0	0.0	0.0019	-0.0019	0.0	0.0001	-0.0001	0.0004	-0.0001	-0.0001	
-0.0004	0.0001	0.0001	0.0	0.0403	-0.0403	0.0	0.0009	-0.0009	0.0026	
-0.0023	-0.0014	-0.0026	0.0014	0.0023	0.0	-0.0018	0.0018	-0.0038	0.0033	
0.0016	0.0038	-0.0016	-0.0033	0.0	-0.0114	0.0114	0.8541	-0.4271	-0.4271	

<sup>a</sup>The 40 entries for each frequency, k, give the L<sub>ik</sub> values (equation 37) in the same order of internal coordinates as in Table IX.

C. Eigenvectors for t-butyl bromide-h<sub>9</sub> using  
force field II.<sup>a</sup>

Sym- metry	Frequency Eigenvector									
A <sub>1</sub>	FREQUENCY = 2984.0 CM-1									
	0.0039	-0.0014	-0.0014	-0.0014	0.4956	-0.2467	-0.2467	0.4956	-0.2467	-0.2467
	0.4956	-0.2467	-0.2467	-0.0384	-0.0384	-0.0384	0.0819	-0.0410	-0.0410	0.0819
	-0.0410	-0.0410	0.0819	-0.0410	-0.0410	-0.0522	0.0292	0.0292	-0.0582	0.0292
	0.0292	-0.0582	0.0292	0.0292	0.0384	0.0384	0.0384	0.0	0.0	0.0
	FREQUENCY = 2941.2 CM-1									
	0.0013	-0.0312	-0.0312	-0.0312	0.3354	0.3371	0.3371	0.3354	0.3371	0.3371
	0.3354	0.3371	0.3371	-0.0008	-0.0008	-0.0008	-0.0314	-0.0311	-0.0311	-0.0314
	-0.0311	-0.0311	-0.0314	-0.0311	-0.0311	0.0304	0.0317	0.0317	0.0304	0.0317
	0.0317	0.0304	0.0317	0.0317	0.0008	0.0008	0.0008	0.0	0.0	0.0
	FREQUENCY = 1463.3 CM-1									
	0.0323	-0.0136	-0.0136	-0.0136	0.0088	-0.0049	-0.0049	0.0088	-0.0049	-0.0049
	0.0088	-0.0049	-0.0049	-0.0025	-0.0025	-0.0025	-0.6835	0.3378	0.3378	-0.6835
	0.3378	0.3378	-0.6835	0.3378	0.3378	-0.2080	0.1079	0.1079	-0.2080	0.1079
	0.1079	-0.2080	0.1079	0.1079	0.0025	0.0025	0.0025	0.0	0.0	0.0
	FREQUENCY = 1391.7 CM-1									
	0.0035	-0.0796	-0.0796	-0.0796	-0.0081	-0.0076	-0.0076	-0.0081	-0.0076	-0.0076
	-0.0081	-0.0076	-0.0076	-0.0036	-0.0036	-0.0036	-0.3250	-0.3383	-0.3383	-0.3250
-0.3383	-0.3383	-0.3250	-0.3383	-0.3383	0.3293	0.3261	0.3361	0.3293	0.3261	
0.3361	0.3293	0.3361	0.3361	0.0036	0.0036	0.0036	0.0	0.0	0.0	
FREQUENCY = 1179.8 CM-1										
0.1740	-0.0793	-0.0793	-0.0793	-0.0150	0.0053	0.0053	-0.0150	0.0053	0.0053	
-0.0150	0.0053	0.0053	-0.1494	-0.1494	-0.1494	0.1829	-0.0773	-0.0773	0.1829	
-0.0773	-0.0773	0.1829	-0.0773	-0.0773	-0.4213	0.1965	0.1965	-0.4213	0.1965	
0.1965	-0.4213	0.1965	0.1965	0.1494	0.1494	0.1494	0.0	0.0	0.0	
FREQUENCY = 804.6 CM-1										
0.1109	-0.1501	-0.1501	-0.1501	-0.0012	-0.0041	-0.0041	-0.0012	-0.0041	-0.0041	
-0.0012	-0.0041	-0.0041	-0.0540	-0.0540	-0.0540	-0.0220	0.0375	0.0375	-0.0220	
0.0375	0.0375	-0.0220	0.0375	0.0375	0.1203	-0.0867	-0.0867	0.1203	-0.0867	
-0.0867	0.1203	-0.0867	-0.0867	0.0540	0.0540	0.0540	0.0	0.0	0.0	
FREQUENCY = 541.5 CM-1										
0.1990	0.0238	0.0238	0.0238	0.0003	0.0013	0.0013	0.0003	0.0013	0.0013	
0.0003	0.0013	0.0013	-0.1193	-0.1193	-0.1193	-0.0349	0.0021	0.0021	-0.0349	
0.0021	0.0021	-0.0349	0.0021	0.0021	0.0775	-0.0234	-0.0234	0.0775	-0.0234	
-0.0234	0.0775	-0.0234	-0.0234	0.1193	0.1193	0.1193	0.0	0.0	0.0	
FREQUENCY = 259.0 CM-1										
-0.1115	0.0116	0.0116	0.0116	-0.0009	0.0004	0.0004	-0.0009	0.0004	0.0004	
-0.0009	0.0004	0.0004	-0.0445	-0.0445	-0.0445	-0.0049	0.0060	0.0060	-0.0049	
0.0060	0.0060	-0.0049	0.0060	0.0060	0.0064	-0.0068	-0.0068	0.0064	-0.0068	
-0.0068	0.0064	-0.0068	-0.0068	0.0445	0.0445	0.0445	0.0	0.0	0.0	
A <sub>2</sub>	FREQUENCY = 2981.5 CM-1									
	0.0	0.0	0.0	0.0	0.0	0.4286	-0.4286	0.0	0.4286	-0.4286
	0.0	0.4286	-0.4286	0.0	0.0	0.0	0.0	0.0702	-0.0702	0.0
	0.0702	-0.0702	0.0	0.0702	-0.0702	0.0	-0.0475	0.0475	0.0	-0.0475
	0.0475	0.0	-0.0475	0.0475	0.0	0.0	0.0	0.0381	0.0381	0.0381
	FREQUENCY = 1456.9 CM-1									
	0.0	0.0	0.0	0.0	0.0	0.0086	-0.0086	0.0	0.0086	-0.0086
	0.0	0.0086	-0.0086	0.0	0.0	0.0	0.0	-0.5983	0.5983	0.0
	-0.5983	0.5983	0.0	-0.5983	0.5983	0.0	-0.1527	0.1527	0.0	-0.1527
	0.1527	0.0	-0.1527	0.1527	0.0	0.0	0.0	-0.0208	-0.0208	-0.0208
	FREQUENCY = 1005.0 CM-1									
	0.0	0.0	0.0	0.0	0.0	0.0081	-0.0081	0.0	0.0081	-0.0081
	0.0	0.0081	-0.0081	0.0	0.0	0.0	0.0	-0.1187	0.1187	0.0
	-0.1187	0.1187	0.0	-0.1187	0.1187	0.0	0.3630	-0.3630	0.0	0.3630
	-0.3630	0.0	0.3630	-0.3630	0.0	0.0	0.0	-0.0509	-0.0509	-0.0509
	FREQUENCY = 276.4 CM-1									
	0.0	0.0	0.0	0.0	0.0	0.0001	-0.0001	0.0	0.0001	-0.0001
	0.0	0.0001	-0.0001	0.0	0.0	0.0	0.0	0.0010	-0.0010	0.0
0.0010	-0.0010	0.0	0.0010	-0.0010	0.0	-0.0013	0.0013	0.0	-0.0013	
0.0013	0.0	-0.0013	0.0013	0.0	0.0	0.0	-0.9711	-0.9711	-0.9711	

. . . cont'd.



C. Eigenvectors for t-butyl bromide-h<sub>9</sub> using  
force field II - cont'd.

Sym- metry	Frequency Eigenvector									
E (a)	FREQUENCY = 2984.9 CM-1									
	0.0	-0.0031	0.0016	0.0016	0.2793	-0.1373	-0.1373	-0.1396	0.5504	-0.4131
	-0.1396	-0.4131	0.5504	-0.0182	0.0091	0.0091	0.0462	-0.0234	-0.0234	-0.0231
	0.0919	-0.0686	-0.0231	-0.0686	0.0919	-0.0305	0.0155	0.0155	0.0152	-0.0638
	0.0483	0.0152	0.0483	-0.0638	-0.0834	0.0417	0.0417	0.0	0.0496	-0.0496
	FREQUENCY = 2982.4 CM-1									
	0.0	-0.0021	0.0011	0.0011	-0.6414	0.3223	0.3223	0.3207	0.0471	-0.3694
	0.3207	-0.3694	0.0471	0.0480	-0.0240	-0.0240	-0.1058	0.0527	0.0527	0.0529
	0.0078	-0.0606	0.0529	-0.0606	0.0078	0.0722	-0.0359	-0.0359	-0.0361	-0.0064
	0.0423	-0.0361	0.0423	-0.0064	-0.0037	0.0043	0.0043	0.0	0.0229	-0.0229
FREQUENCY = 2940.3 CM-1										
0.0	-0.0456	0.0228	0.0228	0.4765	0.4756	0.4756	-0.2382	-0.2400	-0.2357	
-0.2382	-0.2357	-0.2400	0.0023	-0.0011	-0.0011	-0.0431	-0.0433	-0.0433	0.0216	
0.0213	0.0220	0.0216	0.0220	0.0213	0.0440	0.0429	-0.0429	-0.0220	-0.0230	
-0.0199	-0.0220	-0.0199	-0.0230	-0.0025	0.0013	0.0013	0.0	0.0063	-0.0063	
FREQUENCY = 1462.4 CM-1										
0.0	0.0417	-0.0209	-0.0209	0.0036	-0.0003	-0.0003	-0.0018	-0.0054	0.0057	
-0.0018	0.0097	-0.0094	-0.0207	0.0103	0.0103	-0.2107	0.1156	0.1156	0.1053	
0.6452	-0.7608	0.1053	-0.7608	0.6452	-0.0785	0.0290	0.0290	0.0392	0.1568	
-0.2258	0.0392	-0.2258	0.1968	-0.0033	0.0016	0.0016	0.0	-0.0499	0.0499	
FREQUENCY = 1458.2 CM-1										
0.0	0.0079	-0.0039	-0.0039	0.0144	-0.0069	-0.0069	-0.0072	0.0066	0.0003	
-0.0072	0.0003	0.0066	0.0222	-0.0111	-0.0111	-0.9496	0.4768	0.4768	0.4748	
-0.4091	-0.0677	0.4748	-0.0677	-0.4091	-0.2434	0.1197	0.1197	0.1217	-0.0937	
-0.0259	0.1217	-0.0259	-0.0937	0.0311	-0.0156	0.0156	0.0	-0.0210	0.0210	
FREQUENCY = 1379.5 CM-1										
0.0	-0.1187	0.0593	0.0593	-0.0058	-0.0103	-0.0103	0.0049	0.0042	0.0061	
0.0049	0.0061	0.0042	0.0123	-0.0062	-0.0062	-0.4829	-0.4666	-0.4666	0.2415	
0.2525	0.2140	0.2415	0.2140	0.2525	0.4767	0.4697	0.4697	-0.2384	-0.2490	
-0.2206	-0.2384	-0.2206	-0.2490	-0.0175	0.0068	0.0068	0.0	0.0360	-0.0360	
FREQUENCY = 1248.8 CM-1										
0.0	-0.2660	0.1330	0.1330	-0.0011	-0.0065	-0.0065	0.0005	-0.0093	0.0158	
0.0005	0.0158	-0.0093	0.1687	-0.0843	-0.0843	-0.0459	0.0724	0.0724	0.0229	
0.1216	-0.1939	0.0229	-0.1939	0.1216	0.0816	-0.0902	-0.0902	-0.0408	-0.2747	
0.3650	-0.0408	0.3650	-0.2747	-0.2526	0.1268	0.1268	0.0	0.5047	-0.5047	
FREQUENCY = 1014.8 CM-1										
0.0	0.0143	-0.0072	-0.0072	-0.0134	0.0071	0.0071	0.0067	-0.0072	0.0001	
0.0067	0.0001	-0.0072	-0.0707	0.0354	0.0354	0.1756	-0.0904	-0.0904	-0.0893	
0.0822	0.0082	-0.0893	0.0082	0.0822	-0.5658	0.2840	0.2840	0.2829	-0.2746	
-0.0093	0.2829	-0.0093	-0.2746	-0.0575	0.0288	0.0288	0.0	0.0005	-0.0005	
FREQUENCY = 919.7 CM-1										
0.0	-0.1955	0.0977	0.0977	-0.0059	-0.0021	-0.0021	0.0030	0.0067	-0.0046	
0.0030	-0.0046	0.0067	0.0673	-0.0336	-0.0336	0.0503	-0.0133	-0.0133	-0.0252	
-0.0799	0.0532	-0.0252	0.0532	-0.0799	-0.1467	0.0615	0.0615	0.0734	0.2608	
-0.3223	0.0734	-0.3223	0.2608	-0.0388	0.0194	0.0194	0.0	0.2043	-0.2043	
FREQUENCY = 396.5 CM-1										
0.0	-0.0471	0.0236	0.0236	-0.0001	-0.0011	-0.0011	0.0001	0.0023	-0.0013	
0.0001	-0.0013	0.0023	-0.0361	0.0181	0.0181	0.0065	-0.0015	-0.0015	-0.0032	
0.0208	-0.0193	-0.0032	-0.0193	0.0208	-0.0067	0.0016	0.0016	0.0033	-0.0345	
0.0329	0.0033	0.0329	-0.0345	0.1999	-0.0999	-0.0999	0.0	-0.4542	0.4542	
FREQUENCY = 289.9 CM-1										
0.0	0.0111	-0.0055	-0.0055	0.0012	-0.0003	-0.0003	-0.0006	0.0007	-0.0003	
-0.0006	-0.0003	0.0007	0.1112	-0.0556	-0.0556	0.0091	-0.0049	-0.0049	-0.0046	
0.0065	-0.0015	-0.0046	-0.0015	0.0065	-0.0135	0.0672	0.0072	0.0069	-0.0078	
0.0006	0.0068	0.0006	-0.0078	0.0597	-0.0258	-0.0258	0.0	0.8904	-0.8904	
FREQUENCY = 251.2 CM-1										
0.0	0.0107	-0.0053	-0.0053	0.0010	-0.0002	-0.0002	-0.0005	0.0002	0.0000	
-0.0005	0.0000	0.0002	0.1236	-0.0618	-0.0618	0.0073	-0.0040	-0.0040	-0.0037	
0.0021	0.0020	-0.0037	0.0020	0.0021	-0.0110	0.0059	0.0059	0.0055	-0.0016	
-0.0043	0.0055	-0.0043	-0.0016	-0.0035	0.0017	0.0017	0.0	-0.6905	0.6905	

. . . cont'd.

C. Eigenvectors for t-butyl bromide-h<sub>9</sub> using  
force field II. - cont'd.

Sym- metry	Frequency Eigenvector									
	E (b)	FREQUENCY = 2984.9 CM-1								
	0.0	0.0	-0.0027	0.0027	0.0	-0.5563	0.5563	0.2419	0.1592	-0.3971
	-0.2419	0.3971	-0.1592	0.0	-0.0158	0.0158	0.0	-0.0927	0.0927	0.0400
	0.0261	-0.0666	-0.0400	0.0666	-0.0261	0.0	0.0648	-0.0648	-0.0264	-0.0190
	0.0458	0.0264	-0.0458	0.0190	0.0	-0.0722	0.0722	-0.0573	0.0267	0.0287
	FREQUENCY = 2982.4 CM-1									
	0.0	0.0	0.0019	-0.0019	0.0	0.2406	-0.2406	0.5554	-0.3994	-0.1589
	-0.5554	0.1589	0.3994	0.0	-0.0415	0.0415	0.0	0.0395	-0.0395	0.0916
	-0.0654	-0.0259	-0.0916	0.0259	0.0654	0.0	-0.0281	0.0281	-0.0625	0.0452
	0.0171	0.0625	-0.0171	-0.0452	0.0	0.0075	-0.0075	0.0264	-0.0132	-0.0132
	FREQUENCY = 2940.3 CM-1									
	0.0	0.0	0.0395	-0.0395	0.0	-0.0025	0.0025	-0.4127	-0.4107	-0.4131
	0.4127	0.4131	0.4107	0.0	-0.0020	0.0020	0.0	-0.0005	0.0005	0.0373
	0.0377	0.0373	-0.0373	-0.0377	0.0	0.0	-0.0018	0.0018	-0.0381	-0.0362
	-0.0380	0.0381	0.0380	0.0362	0.0	0.0022	-0.0022	0.0073	-0.0036	-0.0036
	FREQUENCY = 1462.4 CM-1									
	0.0	0.0	0.0361	-0.0361	0.0	0.0111	-0.0111	0.0031	-0.0058	0.0053
	-0.0031	-0.0053	0.0058	0.0	-0.0179	0.0179	0.0	-0.8117	0.8117	-0.1827
	0.5061	-0.3056	0.1827	0.3056	-0.5061	0.0	-0.2440	0.2440	-0.0680	0.1471
	-0.0968	0.0680	0.0968	-0.1471	0.0	-0.0028	0.0028	0.0577	-0.0288	-0.0288
	FREQUENCY = 1458.2 CM-1									
	0.0	0.0	-0.0068	0.0068	0.0	0.0037	-0.0037	-0.0125	0.0042	0.0078
	0.0125	-0.0078	-0.0042	0.0	-0.0192	0.0192	0.0	-0.1974	0.1974	0.8223
	-0.3142	-0.5116	-0.8223	0.5116	0.3142	0.0	-0.0392	0.0392	-0.2108	-0.0640
	-0.1233	-0.2108	0.1233	0.0840	0.0	-0.0269	0.0269	-0.0242	0.0121	0.0121
	FREQUENCY = 1379.5 CM-1									
	0.0	0.0	0.1028	-0.1028	0.0	-0.0011	0.0011	0.0085	0.0094	0.0084
	-0.0085	-0.0084	-0.0094	0.0	-0.0107	0.0107	0.0	0.0222	-0.0222	0.4182
	0.3930	0.4152	-0.4182	-0.4152	-0.3930	0.0	-0.0164	0.0164	-0.4129	-0.3985
	-0.4149	0.4129	0.4149	0.3985	0.0	0.0152	-0.0152	0.0416	-0.0208	-0.0208
	FREQUENCY = 1248.8 CM-1									
	0.0	0.0	-0.2303	0.2303	0.0	0.0145	-0.0145	-0.0009	-0.0129	0.0016
	0.0009	-0.0016	0.0129	0.0	0.1461	-0.1461	0.0	-0.1822	0.1822	-0.0397
	0.1538	-0.0284	0.0397	0.0284	-0.1538	0.0	0.3693	-0.3693	0.0707	-0.2628
	0.1065	-0.0707	-0.1065	0.2628	0.0	-0.2197	0.2197	-0.5828	0.2914	0.2914
	FREQUENCY = 1014.8 CM-1									
	0.0	0.0	0.0124	-0.0124	0.0	0.0042	-0.0042	-0.0116	0.0040	0.0083
	0.0116	-0.0083	-0.0040	0.0	-0.0613	0.0613	0.0	-0.0427	0.0427	0.1547
	-0.0569	-0.0996	-0.1547	0.0996	0.0569	0.0	0.1532	-0.1532	-0.4500	0.1693
	0.3225	0.4900	-0.3225	-0.1693	0.0	-0.0498	0.0498	-0.0006	0.0003	0.0003
	FREQUENCY = 919.7 CM-1									
	0.0	0.0	-0.1693	0.1693	0.0	-0.0065	0.0065	-0.0051	0.0015	-0.0051
	0.0051	0.0051	-0.0015	0.0	0.0583	-0.0583	0.0	0.0999	-0.0999	0.0436
	-0.0615	0.0384	-0.0436	-0.0384	0.0615	0.0	-0.3367	0.3367	-0.1271	0.2216
	-0.1151	0.1271	0.1151	-0.2216	0.0	-0.0336	0.0336	-0.2359	0.1180	0.1180
	FREQUENCY = 396.5 CM-1									
	0.0	0.0	-0.0408	0.0408	0.0	-0.0021	0.0021	-0.0001	0.0001	-0.0020
	0.0001	-0.0020	-0.0001	0.0	-0.0313	0.0313	0.0	-0.0231	0.0231	0.0056
	0.0103	-0.0128	-0.0056	0.0128	-0.0103	0.0	0.0389	-0.0389	-0.0058	-0.0181
	0.0208	0.0058	-0.0208	0.0181	0.0	0.1731	-0.1731	0.5245	-0.2623	-0.2623
	FREQUENCY = 289.9 CM-1									
	0.0	0.0	0.0096	-0.0096	0.0	-0.0006	0.0006	0.0010	0.0000	-0.0006
	-0.0010	0.0006	-0.0000	0.0	0.0963	-0.0963	0.0	-0.0046	0.0046	0.0079
	-0.0020	-0.0066	-0.0079	0.0066	0.0020	0.0	0.0049	-0.0049	-0.0117	0.0038
	0.0086	0.0117	-0.0086	-0.0038	0.0	0.0517	-0.0517	-1.0281	0.5140	0.5140
	FREQUENCY = 251.2 CM-1									
	0.0	0.0	0.0092	-0.0092	0.0	-0.0001	0.0001	0.0009	-0.0002	-0.0003
	-0.0009	0.0003	0.0002	0.0	0.1070	-0.1070	0.0	-0.0001	0.0001	0.0053
	-0.0035	-0.0035	-0.0063	0.0035	0.0035	0.0	-0.0015	0.0015	-0.0095	0.0058
	0.0043	0.0095	-0.0043	-0.0058	0.0	-0.0030	0.0030	0.7974	-0.3987	-0.3987

<sup>a</sup>The 40 entries for each frequency, k, give the L<sub>ik</sub> values (equation 37) in the same order of internal coordinates as in Table IX.

D. Eigenvectors for t-butyl bromide-d<sub>9</sub> using  
force field II - cont'd.

Sym- metry	Frequency Eigenvector									
	E (a)	FREQUENCY = 2232.3 CM-1								
	0.0	-0.0094	0.0047	0.0047	0.1893	-0.0909	-0.0909	-0.0947	0.4081	-0.3172
	-0.0947	-0.3172	0.4081	-0.0195	0.0097	0.0097	0.0566	-0.0296	-0.0296	-0.0283
	0.1259	-0.0963	-0.0283	-0.0563	0.1259	-0.0366	0.0196	0.0196	0.0183	-0.0914
	0.0718	0.0183	0.0718	-0.0914	-0.1205	0.0603	0.0603	0.0	0.0793	-0.0793
	FREQUENCY = 2225.7 CM-1									
	0.0	-0.0060	0.0030	0.0030	-0.4824	0.2437	0.2437	0.2412	0.0181	-0.2618
	0.2412	-0.2618	0.0181	0.0653	-0.0347	-0.0347	-0.1458	0.0720	0.0720	0.0729
	0.0058	-0.0778	0.0729	-0.0778	0.0058	0.1021	-0.0502	-0.0502	-0.0510	-0.0069
	0.0570	-0.0510	0.0570	-0.0069	-0.0059	0.0049	0.0049	0.0	0.0347	-0.0347
	FREQUENCY = 2117.7 CM-1									
	0.0	-0.0755	0.0377	0.0377	0.3417	0.3359	0.3399	-0.1708	-0.1740	-0.1659
	-0.1708	-0.1659	-0.1740	0.0078	-0.0039	-0.0039	-0.0652	-0.0658	-0.0658	0.0326
	0.0318	0.0340	0.0326	0.0340	0.0318	0.0681	0.0643	0.0643	-0.0340	-0.0376
	-0.0267	-0.0340	-0.0267	-0.0376	-0.0088	0.0044	0.0044	0.0	0.0215	-0.0215
	FREQUENCY = 1210.3 CM-1									
	0.0	0.3283	-0.1641	-0.1641	0.0176	0.0223	0.0223	-0.0088	0.0046	-0.0269
	-0.0088	-0.0269	0.0046	-0.1683	0.0842	0.0842	0.1271	0.1579	0.1579	-0.0636
	-0.0811	-0.0769	-0.0636	-0.0769	-0.0811	-0.2325	-0.1050	-0.1050	0.1164	0.2577
	-0.1526	0.1164	-0.1526	0.2577	0.2303	-0.1151	-0.1151	0.0	-0.4891	0.4891
	FREQUENCY = 1052.1 CM-1									
	0.0	-0.0011	0.0005	0.0005	0.0103	-0.0055	-0.0055	-0.0052	0.0191	-0.0136
	-0.0052	-0.0136	0.0191	0.0183	-0.0092	-0.0092	-0.3206	0.1514	0.1514	0.1604
	-0.5569	0.4075	0.1604	0.4075	-0.5569	-0.0409	0.0294	0.0294	0.0204	-0.0846
	0.0551	0.0204	0.0551	-0.0846	0.0689	-0.0345	-0.0345	0.0	-0.0389	0.0389
	FREQUENCY = 1048.3 CM-1									
	0.0	0.0127	-0.0064	-0.0064	-0.0145	0.0126	0.0126	0.0072	-0.0009	-0.0116
	0.0072	-0.0116	-0.0009	-0.0194	0.0097	0.0097	0.7088	-0.2168	-0.2168	-0.3544
	-0.1193	0.3360	-0.3544	0.3360	-0.1193	0.0203	-0.1478	-0.1478	-0.0102	0.0130
	0.1348	-0.0102	0.1348	0.0130	-0.0127	0.0064	0.0064	0.0	0.0253	-0.0253
	FREQUENCY = 1035.0 CM-1									
	0.0	0.0051	-0.0026	-0.0026	-0.0170	-0.0064	-0.0064	0.0085	0.0129	-0.0064
	0.0085	-0.0064	0.0129	-0.0051	0.0426	0.0426	-0.1218	-0.4023	-0.4023	0.0659
	0.1370	0.2653	0.0659	0.2653	0.1370	0.2900	0.3203	0.3203	-0.1480	-0.0444
	-0.2759	-0.1480	-0.2759	-0.0444	0.1143	-0.0572	-0.0572	0.0	-0.2284	0.2284
	FREQUENCY = 776.4 CM-1									
	0.0	-0.0239	0.0119	0.0119	0.0169	-0.0094	-0.0094	-0.0085	0.0111	-0.0018
	-0.0085	-0.0018	0.0111	0.0789	-0.0394	-0.0394	-0.0653	0.0465	0.0465	0.0327
	-0.0369	-0.0096	0.0327	-0.0096	-0.0369	0.4091	-0.2184	-0.2184	-0.2045	0.2435
	-0.0251	-0.2045	-0.0251	0.2435	0.0714	-0.0357	-0.0357	0.0	0.0004	-0.0004
	FREQUENCY = 726.7 CM-1									
	0.0	-0.1171	0.0586	0.0586	-0.0089	-0.0001	-0.0001	0.0044	0.0094	-0.0093
	0.0044	-0.0093	0.0094	0.0153	-0.0076	-0.0076	0.0772	0.0202	0.0202	-0.0386
	-0.0540	0.0338	-0.0386	0.0338	-0.0540	-0.2111	0.0469	0.0468	0.1056	0.2221
	-0.2689	0.1056	-0.2689	0.2221	0.0215	-0.0108	-0.0108	0.0	0.0682	-0.0682
	FREQUENCY = 338.8 CM-1									
	0.0	0.0369	-0.0184	-0.0184	0.0003	0.0014	0.0014	-0.0001	-0.0027	0.0013
	-0.0001	0.0013	-0.0027	0.0416	-0.0208	-0.0208	-0.0130	-0.0042	-0.0042	0.0065
	-0.0232	0.0274	0.0065	0.0274	-0.0232	0.0126	0.0044	0.0044	-0.0003	0.0427
	-0.0471	-0.0063	-0.0471	0.0427	-0.1655	0.0828	0.0828	0.0	0.3237	-0.3237
	FREQUENCY = 246.8 CM-1									
	0.0	0.0126	-0.0063	-0.0063	0.0020	-0.0005	-0.0005	-0.0010	0.0009	-0.0005
	-0.0010	-0.0005	0.0009	0.1364	-0.0662	-0.0662	0.0137	-0.0103	-0.0103	-0.0069
	0.0104	-0.0001	-0.0069	-0.0001	0.0104	-0.0218	0.0143	0.0143	0.0109	-0.0118
	-0.0025	0.0109	-0.0025	-0.0118	0.0461	-0.0231	-0.0231	0.0	0.3658	-0.3658
	FREQUENCY = 187.8 CM-1									
	0.0	0.0026	-0.0013	-0.0013	0.0005	-0.0001	-0.0001	-0.0002	0.0000	0.0001
	-0.0002	0.0001	0.0000	0.0488	-0.0244	-0.0244	0.0033	-0.0023	-0.0023	-0.0017
	0.0003	0.0020	-0.0017	0.0020	0.0003	-0.0051	0.0032	0.0032	0.0025	0.0002
	-0.0034	0.0025	-0.0034	0.0002	-0.0141	0.0071	0.0071	0.0	-0.7318	0.7318

. . . cont'd.

D. Eigenvectors for t-butyl bromide-d<sub>9</sub> using  
force field II.<sup>a</sup>

Sym- metry	Frequency Eigenvector	
A <sub>1</sub>	FREQUENCY = 2230.1 CM-1 0.0102 -0.0039 -0.0039 -0.0039 0.3676 -0.1822 -0.1822 0.3676 -0.1822 -0.1822 0.3676 -0.1822 -0.1822 -0.0565 -0.0565 -0.0565 0.1109 -0.0560 -0.0560 0.1109 -0.0560 -0.0560 0.1109 -0.0560 -0.0560 -0.0837 0.0424 0.0424 -0.0837 0.0424 0.0424 -0.0837 0.0424 0.0424 0.0565 0.0565 0.0565 0.0565 0.0 0.0 0.0	
	FREQUENCY = 2120.0 CM-1 0.0043 -0.0452 -0.0452 -0.0452 0.2389 0.2417 0.2417 0.2389 0.2417 0.2417 0.2389 0.2417 0.2417 -0.0027 -0.0027 -0.0027 -0.0478 -0.0478 -0.0478 0.1109 -0.0478 -0.0478 -0.0478 -0.0478 -0.0478 0.0452 0.0496 0.0496 0.0452 0.0496 0.0456 0.0452 0.0496 0.0496 0.0027 0.0027 0.0027 0.0 0.0 0.0	
	FREQUENCY = 1122.2 CM-1 -0.1033 0.1454 0.1454 0.1454 0.0231 0.0121 0.0121 0.0231 0.0121 0.0121 0.0231 0.0121 0.0121 0.0749 0.0749 0.0749 0.2424 0.2062 0.2062 0.2424 0.2062 0.2062 0.2424 0.2062 0.2062 -0.0616 -0.2866 -0.2866 -0.0816 -0.2866 -0.2866 -0.0816 -0.2866 -0.2866 -0.0749 -0.0749 -0.0749 0.0 0.0 0.0	
	FREQUENCY = 1053.6 CM-1 0.0707 -0.0061 -0.0061 -0.0061 0.0111 -0.0025 -0.0025 0.0111 -0.0025 -0.0025 0.0111 -0.0025 -0.0025 -0.0259 -0.0259 -0.0259 -0.4045 0.2875 0.2875 -0.4045 0.2875 0.2875 -0.4045 0.2675 0.2675 -0.2300 0.0298 0.0298 -0.2300 0.0298 0.0298 -0.2300 0.0298 0.0298 0.0259 0.0259 0.0259 0.0259 0.0 0.0 0.0	
	FREQUENCY = 1026.3 CM-1 0.1849 -0.0393 -0.0393 -0.0393 -0.0200 0.0135 0.0135 -0.0200 0.0135 0.0135 -0.0200 0.0135 0.0135 -0.1536 -0.1536 -0.1536 0.3153 -0.0026 -0.0026 0.3153 -0.0026 -0.0026 0.3153 -0.0026 -0.0026 -0.3566 0.0232 0.0232 -0.3566 0.0232 0.0232 -0.3566 0.0232 0.0232 0.1536 0.1536 0.1536 0.1536 0.0 0.0 0.0	
	FREQUENCY = 676.9 CM-1 0.0576 -0.1076 -0.1076 -0.1076 0.0014 -0.0060 -0.0060 0.0014 -0.0060 -0.0060 0.0014 -0.0060 -0.0060 -0.0109 -0.0109 -0.0109 0.0248 0.0650 0.0650 -0.0109 0.0650 0.0650 0.0248 0.0650 0.0650 0.0937 -0.1243 -0.1243 0.0937 -0.1243 -0.1243 0.0937 -0.1243 -0.1243 0.0109 0.0109 0.0109 0.0109 0.0 0.0 0.0	
	FREQUENCY = 469.2 CM-1 0.1835 0.0130 0.0130 0.0130 0.0017 0.0009 0.0009 0.0017 0.0009 0.0009 0.0017 0.0009 0.0009 -0.0877 -0.0877 -0.0877 -0.0432 -0.0044 -0.0044 -0.0432 -0.0044 -0.0044 -0.0432 -0.0044 -0.0044 0.1050 -0.0265 -0.0265 -0.1050 -0.0265 -0.0265 0.1050 -0.0265 -0.0265 0.0877 0.0877 0.0877 0.0877 0.0 0.0 0.0	
	FREQUENCY = 240.2 CM-1 0.0948 -0.0105 -0.0105 -0.0105 0.0015 -0.0007 -0.0007 0.0015 -0.0007 -0.0007 0.0015 -0.0007 -0.0007 0.0452 0.0452 0.0452 0.0095 -0.0077 -0.0077 0.0095 -0.0077 -0.0077 0.0095 -0.0077 -0.0077 -0.0125 0.0094 0.0094 -0.0125 0.0094 0.0094 -0.0125 0.0094 0.0094 -0.0452 -0.0452 -0.0452 0.0 0.0 0.0	
	A <sub>2</sub>	FREQUENCY = 2223.2 CM-1 0.0 0.0 0.0 0.0 0.0 0.3178 -0.3178 0.0 0.3178 -0.3178 0.0 0.3178 -0.3178 0.0 0.0 0.0 0.0945 -0.0945 0.0 0.0945 -0.0945 0.0 0.0945 -0.0945 0.0 -0.0652 0.0652 0.0 -0.0652 0.0652 0.0 -0.0652 0.0652 0.0 0.0 0.0 0.0523 0.0523 0.0523
		FREQUENCY = 1046.3 CM-1 0.0 0.0 0.0 0.0 0.0 -0.0125 0.0125 0.0 -0.0125 0.0125 0.0 -0.0125 0.0125 0.0 0.0 0.0 0.4377 -0.4377 0.0 0.4377 -0.4377 0.0 0.4377 -0.4377 0.0 0.0764 -0.0764 0.0 0.0764 -0.0764 0.0 0.0764 -0.0764 0.0 0.0 0.0 0.0288 0.0288 0.0288
		FREQUENCY = 759.5 CM-1 0.0 0.0 0.0 0.0 0.0 0.0104 -0.0104 0.0 0.0104 -0.0104 0.0 0.0104 -0.0104 0.0 0.0 0.0 0.0 0.0603 0.0603 0.0 -0.0603 0.0603 0.0 -0.0603 0.0603 0.0 0.2796 -0.2796 0.0 0.2796 -0.2796 0.0 0.2796 -0.2796 0.0 0.0 0.0 -0.0557 -0.0557 -0.0557
		FREQUENCY = 196.0 CM-1 0.0 0.0 0.0 0.0 0.0 -0.0001 0.0001 0.0 -0.0001 0.0001 0.0 -0.0001 0.0001 0.0 0.0 0.0 0.0 -0.0010 0.0010 0.0 -0.0010 0.0010 0.0 -0.0010 0.0010 0.0 0.0014 -0.0014 0.0 0.0014 -0.0014 0.0 0.0014 -0.0014 0.0 0.0 0.0 0.6885 0.6885 0.6885

. . . cont'd.

D. Eigenvectors for t-butyl bromide-d<sub>9</sub> using  
force field II - cont'd.

Sym- metry	Frequency Eigenvector
E (b)	FREQUENCY = 2232.3 CM-1
	0.0 0.0 -0.0082 0.0082 0.0 -0.4188 0.4188 0.1639 0.1308 -0.2880
	-0.1639 0.2880 -0.1308 0.0 0.0 -0.0168 0.0168 0.0 -0.1283 0.1283 0.0490
	0.0385 -0.0898 -0.0490 0.0898 -0.0385 0.0 0.0942 -0.0942 -0.0317 -0.0301
	0.0641 0.0317 -0.0641 0.0301 0.0 -0.1044 0.1044 -0.0916 0.0458 0.0458
	FREQUENCY = 2225.7 CM-1
	0.0 0.0 0.0052 -0.0052 0.0 0.1615 -0.1615 0.4178 -0.2919 -0.1303
	-0.4178 0.1303 0.2919 0.0 -0.0600 0.0600 0.0 0.0483 -0.0483 0.1263
	-0.0265 -0.0382 -0.1263 0.0382 0.0855 0.0 -0.0369 0.0369 -0.0284 0.0619
	0.0250 0.0884 -0.0250 -0.0619 0.0 0.0085 -0.0085 0.0400 -0.0200 -0.0200
FREQUENCY = 2117.7 CM-1	
0.0 0.0 0.0653 -0.0653 0.0 -0.0046 0.0046 -0.2959 -0.2921 -0.2967	
0.2959 0.2967 0.2921 0.0 -0.0067 0.0067 0.0 -0.0013 0.0013 0.0565	
0.0576 0.0563 -0.0565 -0.0563 -0.0576 0.0 -0.0063 0.0063 -0.0590 -0.0526	
-0.0589 0.0590 0.0589 0.0526 0.0 0.0076 -0.0076 0.0248 -0.0124 -0.0124	
FREQUENCY = 1210.3 CM-1	
0.0 0.0 0.2843 -0.2843 0.0 -0.0181 0.0181 0.0153 0.0284 0.0102	
-0.0153 -0.0102 -0.0284 0.0 -0.1458 0.1458 0.0 0.0024 -0.0024 0.1101	
0.1356 0.1380 -0.1101 -0.1380 -0.1356 0.0 -0.2369 0.2369 -0.2017 0.0275	
-0.2094 0.2017 0.2094 -0.0275 0.0 0.1994 -0.1994 0.5647 -0.2824 -0.2824	
FREQUENCY = 1052.1 CM-1	
0.0 0.0 0.0010 -0.0010 0.0 0.0189 -0.0189 -0.0089 -0.0047 0.0142	
0.0089 -0.0142 0.0047 0.0 -0.0159 0.0159 0.0 -0.5578 0.5578 0.2781	
0.1477 -0.4101 -0.2781 0.4101 -0.1477 0.0 -0.0806 0.0806 0.0354 0.0148	
-0.0659 0.0354 0.0659 -0.0148 0.0 -0.0597 0.0597 -0.0449 0.0225 0.0225	
FREQUENCY = 1048.3 CM-1	
0.0 0.0 -0.0110 0.0110 0.0 0.0062 -0.0062 0.0125 -0.0140 -0.0078	
-0.0125 0.0078 0.0140 0.0 0.0168 -0.0168 0.0 -0.2631 0.2631 -0.6137	
0.3192 0.0561 0.6137 -0.0561 -0.3192 0.0 -0.0704 0.0704 -0.0176 0.1632	
0.0928 0.0176 -0.0928 -0.1632 0.0 0.0110 -0.0110 0.0292 -0.0146 -0.0146	
FREQUENCY = 1035.0 CM-1	
0.0 0.0 0.0044 -0.0044 0.0 -0.0111 0.0111 -0.0147 -0.0000 -0.0111	
0.0147 0.0111 0.0000 0.0 -0.0737 0.0737 0.0 0.0741 -0.0741 -0.1142	
-0.3855 -0.3114 0.1142 0.3114 0.3855 0.0 -0.1336 0.1336 0.2563 0.3442	
0.2105 -0.2563 -0.2105 -0.3442 0.0 0.0990 -0.0990 0.2637 -0.1319 -0.1319	
FREQUENCY = 776.4 CM-1	
0.0 0.0 0.0207 -0.0207 0.0 0.0074 -0.0074 -0.0147 0.0044 0.0118	
0.0147 -0.0118 -0.0044 0.0 -0.0683 0.0683 0.0 -0.0158 0.0158 0.0566	
-0.0324 -0.0482 -0.0566 0.0482 0.0324 0.0 0.1551 -0.1551 -0.3543 0.1116	
0.2667 0.3543 -0.2667 -0.1116 0.0 -0.0619 0.0619 0.0005 -0.0002 -0.0002	
FREQUENCY = 726.7 CM-1	
0.0 0.0 0.1014 -0.1014 0.0 0.0108 -0.0108 0.0077 -0.0053 0.0055	
-0.0077 -0.0055 0.0053 0.0 -0.0132 0.0132 0.0 -0.0507 0.0507 -0.0669	
0.0078 -0.0428 0.0669 0.0428 -0.0078 0.0 0.2835 -0.2835 0.1829 -0.1822	
0.1012 -0.1829 -0.1012 0.1822 0.0 -0.0127 0.0127 0.0787 -0.0394 -0.0394	
FREQUENCY = 338.8 CM-1	
0.0 0.0 0.0320 -0.0320 0.0 0.0023 -0.0023 0.0003 0.0000 0.0023	
-0.0003 -0.0023 -0.0000 0.0 0.0360 -0.0360 0.0 0.0292 -0.0292 -0.0112	
-0.0182 0.0110 0.0112 -0.0110 0.0182 0.0 -0.0518 0.0518 0.0109 0.0297	
-0.0221 -0.0109 0.0221 -0.0297 0.0 -0.1433 0.1433 -0.3738 0.1869 0.1869	
FREQUENCY = 246.8 CM-1	
0.0 0.0 0.0109 -0.0109 0.0 -0.0008 0.0008 0.0017 -0.0000 -0.0008	
-0.0017 0.0008 0.0000 0.0 0.1181 -0.1181 0.0 -0.0061 0.0061 0.0119	
-0.0059 -0.0120 -0.0119 0.0120 0.0059 0.0 0.0054 -0.0054 -0.0159 0.0097	
0.0151 0.0189 -0.0151 -0.0097 0.0 0.0400 -0.0400 -0.4223 0.2112 0.2112	
FREQUENCY = 187.8 CM-1	
0.0 0.0 0.0022 -0.0022 0.0 0.0001 -0.0001 0.0004 -0.0002 -0.0001	
-0.0004 0.0001 0.0002 0.0 0.0423 -0.0423 0.0 0.0010 -0.0010 0.0029	
-0.0025 -0.0016 -0.0029 0.0016 0.0025 0.0 -0.0020 0.0020 -0.0044 0.0036	
0.0018 0.0044 -0.0018 -0.0036 0.0 -0.0122 0.0122 0.8450 -0.4225 -0.4225	

<sup>a</sup>The 40 entries for each frequency, k, give the L<sub>ik</sub> values (equation 37) in the same order of internal coordinates as in Table IX.

















